

UNIVERSIDAD DE CANTABRIA

PROGRAMA DE DOCTORADO EN INGENIERÍA QUÍMICA, DE LA
ENERGÍA Y DE PROCESOS



TESIS DOCTORAL

**Integración de procesos basada en preconcentración con
membranas y oxidación electroquímica de sustancias poli- y
perfluoroalquílicas en tratamiento de aguas industriales**

PhD THESIS

**Process integration based on membrane preconcentration
and electrochemical oxidation of poly- and perfluoroalkyl
substances in industrial water treatment**

Realizada por:

Álvaro Soriano Portilla

Dirigida por:

Prof. Dra. Ana María Urtiaga Mendía

Prof. Dr. Eugenio Daniel Gorri Cirella

Escuela de Doctorado de la Universidad de Cantabria

Santander 2019

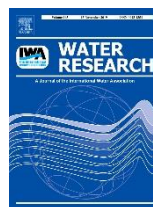
Programa de Doctorado en Ingeniería Química, de la Energía de y Procesos (BOE núm. 16 de 19 de Enero de 2015. RUCT: 5601000)

The research described in this thesis has been conducted at the Environmental Technologies and Bioprocesses (ETB) group of the Department of Chemical and Biomolecular Engineering of the University of Cantabria.

This research has been financially supported by the Spanish Ministry of Economy and Competitiveness, Spanish State Research Agency and the European Regional Development Fund through the projects: CTM2013-44081-R (MINECO/FEDER, UE) “Desarrollo de tecnologías innovadoras para el tratamiento de contaminantes perfluorados en aguas” and CTM2016-75509-R (AEI/FEDER, UE) “Estrategias avanzadas de integración de membranas y procesos electrocatalíticos y fotocatalíticos para la eliminación de contaminantes persistentes”.

This PhD thesis has been performed as a compendium of interrelated scientific publications. The scientific articles that enable this dissertation modality are published in international journals indexed in the Journal Citation Reports (JCR):

- Á. Soriano, D. Gorri, and A. Urriaga, “Efficient treatment of perfluorohexanoic acid by nanofiltration followed by electrochemical degradation of the NF concentrate” *Water Research*, 112, pp. 147–156, 2017.



Q1, IF (2017): 7.051. Environmental Engineering (2/50).

- A. Urriaga, Á. Soriano, and J. Carrillo-Abad, “BDD anodic treatment of 6:2 fluorotelomer sulfonate (6:2 FTSA). Evaluation of operating variables and by-product formation” *Chemosphere*, 201, pp. 571–577, 2018.



Q1, IF (2018): 5.108. Environmental Sciences (32/250).

- Á. Soriano, D. Gorri, and A. Urriaga, “Membrane preconcentration as an efficient tool to reduce the energy consumption of perfluorohexanoic acid electrochemical treatment” *Separation and Purification Technology*, 208, pp. 160–168, 2019.



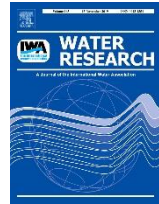
Q1, IF (2018): 5.107. Chemical Engineering (14/138)

- Á. Soriano, D. Gorri, and A. Urtiaga, “Selection of High Flux Membrane for the Effective Removal of Short-Chain Perfluorocarboxylic Acids” *Industrial & Engineering Chemistry Research*, 58, 8, pp. 3329 – 3338, 2019



Q1, IF (2018): 3.375. Chemical Engineering (33/138)

- Á. Soriano, D. Gorri, L.T. Biegler and A. Urtiaga, “An optimization model for the treatment of perfluorocarboxylic acids considering membrane preconcentration and BDD electrooxidation” *Water Research*, 164, 114959, 2019.



Q1, IF (2018): 7.913. Environmental Engineering (3/52).

Agradecimientos

En primer lugar, me gustaría expresar mi más sincero agradecimiento a mis directores de tesis, la profesora Ane Urtiaga y el profesor Daniel Gorri, por haberme dado la oportunidad de llevar a cabo mi labor investigadora en el Departamento de Ingenierías Química y Biomolecular, por la confianza depositada en mí, por su inmensa labor en forma de innumerables horas de trabajo dedicadas a esta tesis doctoral, y por compartir conmigo su conocimiento y experiencia, que tan valiosos han sido para mi formación.

I would also like to thank Prof. L.T. Biegler for giving me the opportunity to work in the Department of Chemical Engineering of the Carnegie Mellon University, surrounded by all the great people who are part of the department. His help and advice have hugely contributed to the last part of this thesis.

Me gustaría también agradecer a todos los compañeros del Departamento de Ingeniería Química y Biomolecular. Especialmente a todos los/as compañero/as que han pasado por el seminario 458, y los que están en la escalera A. Sois demasiados para nombraros, pero, a todos/as vosotros/as, muchas gracias por contribuir a crear un excelente ambiente de trabajo y compañerismo. Agradecimientos especiales también para los técnicos, en particular Sonia Gómez y Gema Pérez, por su valioso trabajo y asistencia diaria.

Mis más especiales agradecimientos a mis amigos, a mi familia, especialmente a mis padres, y a Sara, por vuestro continuo apoyo durante esta etapa.

Table of contents

<i>Summary / Resumen</i>	XI
<hr/>	
<i>Introduction</i>	1
<hr/>	
1.1. Poly- and perfluoroalkyl substances	3
1.2. PFASs occurrence, health risks and regulation	8
1.3. Advanced technologies for PFASs treatment	11
1.4. Integration of electrochemical oxidation and membrane separation	33
1.5. Thesis scope and outline	35
<i>Materials and methods</i>	53
<hr/>	
2.1. Chemicals	55
2.2. Nanofiltration/reverse osmosis experiments	56
2.3. Electrochemical oxidation experiments	65
2.4. Analytical methods	69
2.5. Design, modelling and optimization of the integrated membrane – electrooxidation system	71
2.6. References	77
<i>Results summary</i>	81
<hr/>	
3.1. Nanofiltration/reverse osmosis treatment	83
3.2. Electrochemical oxidation treatment	106
3.3. Design, simulation and optimization of the integrated membrane – electrooxidation system	124

3.4 Nomenclature	146
3.5 References	148
<i>Conclusions</i>	155
<hr/>	
4.1. Conclusions and perspective	157
4.2. Conclusiones y perspectiva futura	163
<i>Scientific publications</i>	171
<hr/>	
<i>Appendices</i>	241
<hr/>	

Summary / Resumen

In this doctoral thesis a novel process for the treatment of poly- and perfluoroalkyl substances (PFASs) has been developed. The importance of this work with respect to previous research also lies in the focus on short chain PFASs used as substitutes of regulated long-chain PFASs. Long-chain PFASs exhibit toxic, persistence and bioaccumulation properties. Consequently, several restrictions and recommendations have emerged around the world in last years about their use, manufacture, and presence in drinking water and water bodies. The on-going industrial transition from long-chain PFASs have led to a wide number of fluorinated alternatives, such as their shorter-chained homologues and 6:2 fluorotelomers and derived substances. Although less bioaccumulative, the present alternatives are equally persistent. The main source of emission of PFASs to environmental media are the industrial processes involved in PFASs synthesis, transformation and use, together with the precursors transformation products in water bodies.

Lately, intensive research efforts have been directed to develop new advanced technologies for the treatment of PFASs. Among them, electrochemical oxidation (ELOX) has proved to completely degrade and mineralize PFASs, when using the appropriate electrode materials. However, many challenges of this technology should be addressed before its large-scale implementation as standard technology for the treatment of PFASs. Mass transfer limitations due to the low concentration of PFASs typically found in impacted waters, and the high energy consumption of the ELOX treatment are some of the main constraints. Pressure-driven membrane separation technologies have also proved to be effective in the

removal of PFASs. However, separation technologies are not enough since they transfer the pollutant to a concentrated phase that needs further treatment. Therefore, research efforts must be directed towards the integration of destructive/separation technologies as a way to overcome their individual limitations in the treatment of persistent organic pollutants.

On the basis of the foregoing, this thesis aims to develop new advanced technologies for the treatment of PFASs in industrial process waters and effluents, with a particular focus on short-chain and substitutive PFASs. Most of the thesis work has been carried out with perfluorohexanoic acid (PFHxA) and the applied methodology combined experiments that were carried out at laboratory scale with the use of process design, simulation and optimization tools. First, nanofiltration (NF) and reverse osmosis (RO) were evaluated in the treatment of PFHxA from real and simulated industrial effluents. From these studies, it was possible to identify the most suitable membrane/s for the design of the envisaged NF/RO – ELOX integrated process. On the other hand, the use of electrochemical oxidation by means of boron-doped diamond (BDD) anodes was studied to degrade PFHxA from NF/RO concentrated industrial effluents and also for the treatment of 6:2 fluorotelomer sulfonic acid in model aqueous solutions. Finally, the design, simulation and optimization of the novel integrated NF/RO – ELOX process was carried out. First, a preliminary simulation study focused on reducing the energy consumption of PFHxA electrochemical treatment from industrial effluents was reported. Taking as starting point the limitations and challenges raised from this preliminary study, we carried out a more rigorous optimization study of a multistage NF/RO – ELOX integrated approach. The optimization model and techno-economic assessment were aimed to minimize the total costs (capital and operating expenses) of the integrated process.

En esta tesis doctoral se ha desarrollado un proceso novedoso para el tratamiento de sustancias poli- y perfluoralquílicas. La importancia de este trabajo respecto a trabajos anteriores también radica en el enfoque en PFASs de cadena corta actualmente utilizados como sustitutos de PFASs de cadena larga regulados. Los PFASs de cadena larga muestran propiedades de toxicidad, persistencia y potencial de bioacumulación. Como consecuencia, han surgido en todo el mundo diversas restricciones y recomendaciones acerca de su uso, fabricación, presencia en el agua potable y en diferentes cuerpos de agua. La progresiva transición desde los PFASs de cadena larga y sus precursores han llevado a un gran número de alternativas fluoradas, como sus homólogos de cadena corta o los compuestos 6:2 fluorotelómeros y sustancias derivadas. Aunque muestran menor potencial de bioacumulación, son igualmente persistentes. La principal fuente de emisión de PFASs al medio ambiente son los procesos industriales involucrados en la síntesis de PFASs, uso y transformación, así como los productos de transformación de precursores en cuerpos de agua.

En los últimos años los esfuerzos de investigación han sido dirigidos hacia el desarrollo de nuevas tecnologías avanzadas para el tratamiento de estas sustancias. Entre ellas, la oxidación electroquímica (ELOX) ha demostrado ser capaz de la completa destrucción y mineralización de los PFASs, cuando se utilizan los materiales de electrodo apropiados. Sin embargo, hay muchos retos de esta tecnología que aún deben ser abordados antes de su implementación a gran escala como la tecnología estándar en el tratamiento de PFASs. Algunas restricciones importantes son, las

limitaciones de transferencia de materia debido a las bajas concentraciones de PFASs típicamente encontradas en aguas impactadas y el alto consumo energético. Los procesos de membrana impulsados por gradiente de presión también han demostrado ser efectivos en la recuperación de PFASs. Sin embargo, las tecnologías de separación no son suficientes ya que transfieren el contaminante a una fase concentrada que necesita tratamiento adicional. Por lo tanto, los esfuerzos de investigación deben estar dirigidos hacia la integración de tecnologías de destrucción y separación como una manera de superar sus limitaciones tecnológicas individuales en el tratamiento de PFASs.

En base a lo anterior, esta tesis tiene como objetivo desarrollar nuevas tecnologías avanzadas para el tratamiento de PFASs en aguas de proceso y efluentes industriales, con especial enfoque en compuestos sustitutivos de PFASs de cadena larga. La mayor parte del trabajo se ha llevado a cabo con ácido perfluorohexanoico (PFHxA) y la metodología empleada combinó experimentos a escala de laboratorio con la utilización de herramientas de diseño de procesos, simulación y optimización. Para este propósito, primero se ha evaluado el uso de nanofiltración (NF) y ósmosis inversa en el tratamiento de PFHxA a partir de efluentes industriales reales y simulados. A partir de estos estudios, fue posible identificar aquellas membranas más adecuadas para el diseño del sistema novedoso integrado NF/OI – ELOX previsto. Se ha estudiado el uso de oxidación electroquímica por medio de ánodos de diamante dopado con boro (DDB) para degradar, por un lado, PFHxA procedente de efluentes reales concentrados con NF, y por el otro, ácido 6:2 fluorotelomero sulfónico (6:2 FTSA) procedente de disoluciones modelo. Por último, se llevó a cabo el diseño, simulación y optimización del proceso integrado NF/OI – ELOX. En primer lugar, se reporta el estudio preliminar con herramientas de

simulación enfocado en la reducción del consumo energético del tratamiento electroquímico de PFHxA mediante su integración con preconcentración con membranas. A partir de las limitaciones, retos y cuestiones surgidas de este estudio preliminar, se llevó a cabo una optimización rigurosa de un proceso integrado multietapa de membranas y electrooxidación. El modelo de optimización y el análisis tecno económico tuvo como objetivo la minimización de los costes totales (de operación y de capital) del proceso integrado.

1. Introduction

1.1. Poly- and perfluoroalkyl substances (PFASs)

Water demand worldwide has increased by a 1% rate per year in the last decades and is expected to increase up to 30% above the current consumption volume until 2050, principally by the increasing demands in industrial and domestic sectors in emerging economies. Nowadays, more than 2 billion people are experiencing high water stress and the arising use of water resources will contribute to continue growing physical water stress levels in the next few years [1]. Water quality is also a major 21st century challenge to be faced in developing and developed countries. Goal number six of the 2030 Agenda and Sustainable Development Goals (SDGs) adopted in 2015 by worldwide countries in a United Nations summit aims to “*ensure availability and sustainable management of water and sanitation for all*” [2]. In order to meet this goal, it is mandatory to reduce the release of pollutants and hazardous substances. A major emphasis on new emerging pollutants should be made [3], such as surfactants, additives, pharmaceuticals, personal care products, pesticides or industrial chemicals, as a consequence of their potential high risks on the environment and human health [4]. Among them, emerging persistent organic pollutants (POPs) are of major concern due to their ubiquity in the environment, bioaccumulation potential, wide spatial distribution and resistance to degradation by traditional wastewater treatment techniques [5].

An important group of emerging POPs is a family called poly and perfluoroalkyl substances (PFASs). PFASs are man-made organic compounds, commercially synthesized since the 1950s, with unique physico-chemical properties. PFASs are chemically and thermally stable, lipophobic and hydrophobic [6]. For that reason they have been extensively

used as processing aid in the fabrication of surfactants, emulsifiers, additives for polymers, paper and cardboard coatings in the food packaging industry, water repellent textiles or leather and aqueous firefighting foams (AFFFs), among others [7]–[9].

These organofluorinated compounds consist of a fully or partially fluorinated alkyl chain attached to a hydrophilic end group, which can differ. Generally, we consider *per*fluoroalkyl substances those compounds where the alkyl chain is fully fluorinated and *poly*fluorinated substances those with partially fluorinated alkyl chains, having at least one perfluoroalkyl moiety C_nF_{2n+1} [10], [11]. Nowadays, there are at least 42 subfamilies of PFASs. Some of the most important are perfluoroalkyl carboxylic acids (PFCAs), perfluoroalkyl sulfonic acids (PFSAs), perfluoroalkyl sulfamido substances (FASAs), fluorotelomer alcohols (FTOHs), polyfluoroalkyl phosphoric acid esters (PAPs), perfluoroalkyl phosphinic acids (PFPIAs), fluorotelomer sulfonic acids (FTSs) and polyfluoropolyethers (PFPEs) [6]. It is also needed to distinguish between “long-chain” PFASs (generally $n \geq 7$, where n refers to the number of carbon units in the fully fluorinated chain) and “short-chain” PFASs ($n < 7$) [12], with different toxicological and bioaccumulative properties that will be discussed in the next section.

Perfluorocarboxylic acids (PFCAs) are one of the most important PFASs subfamilies. They consist on a fully fluorinated alkyl chain attached to a carboxylic acid end group. Their general chemical formula is $C_nF_{2n+1}COOH$ [13]. The most relevant PFCA is perfluorooctanoic acid (PFOA), which have been extensively used in the last decades by diverse industrial sectors including aerospace, automotive, building, chemical processing, electronics, semiconductors, textile industries, and production

of fluoropolymers and fluorinated telomers. Short-chain PFCAs can also be formed in the environment by degradation of fluorinated precursors such as fluorotelomer alcohols [14]. Among perfluoroalkyl substances, perfluoroalkyl sulfonic acids (PFSAs) ($C_nF_{2n+1}SO_3H$) are also of special relevance. The most important PFSA in terms of scientific attention received in the last years is perfluorooctane sulfonic acid (PFOS) [12]. The third most important category of perfluoroalkyl substances are perfluoroalkyl sulfamido substances (FASAs), being the most representative perfluorooctane sulfonamide (PFOSA) [15]. Table 1.1 lists some of the most relevant per- and polyfluorinated alkyl substances.

Among polyfluoroalkyl substances, fluorotelomers are of major importance as they are some of the most used PFASs in products [16]. Their antiwetting and antistaining properties make them attractive for the fabrication of several consumer products such as clothing, carpeting, painting surfaces or food containers [17]. Saturated fluorotelomer carboxylic acids ($C_nF_{2n+1}CH_2CH_2COOH$) contain two unfluorinated carbons (ethyl group, CH_2-CH_2) between the perfluoroalkyl chain and the carboxylic acid group, while, on the other hand, unsaturated fluorotelomer carboxylic acids ($C_nF_{2n+1}CF=CHCOOH$) are characterized by the double bond between the last CF unit of the perfluoroalkyl chain and the unfluorinated carbon unit, CH [18]. Fluorotelomer alcohols ($C_nF_{2n+1}CH_2CH_2OH$), with a hydroxyl end group, and fluorotelomer sulfonic acids ($C_nF_{2n+1}CH_2CH_2SO_3H$), with a sulfonic end group, are also relevant fluorotelomers widely used in fluorotelomer-based polymeric materials, surfactant products and as stabilizers in the formulation of AFFFs [19], [20].

Table 1.1 Most relevant PFASs and their abbreviations. Adapted from Voogt and Sáez (2006) [21] and Buck et al (2011) [12].

Compound	Abbreviation	CAS No.	Mol weight	Structural formula
Perfluorobutane sulfonic acid	PFBS	29420-49-3	299.21	$C_4F_9SO_3^-$
Perfluorohexane sulfonic acid	PFHxS	355-46-4	399.22	$C_6F_{13}SO_3^-$
Perfluorooctane sulfonic acid	PFOS	2795-39-3;	499.23	$C_8F_{17}SO_3^-$
6:2 fluorotelomer sulfonic acid	6:2 FTSA	29420-49-3	428.16	$C_8H_4F_{13}SO_3^-$
6:2 fluorotelomer alcohol	6:2 FTOH	647-42-7	364.11	$C_8H_5F_{13}O$
8:2 fluorotelomer alcohol	8:2 FTOH	865-86-1	464.12	$C_{10}H_5F_{17}O$
Perfluorooctane sulfonamide	PFOSA	754-91-6	499.14	$C_8H_2F_{17}SO_2N$
N- methyl perfluorooctane sulfonamidoethanol	N-MeFOSE	24448-09-7	557.23	$C_{11}H_8F_{17}NO_3S$
N-ethyl perfluorooctane sulfonamidoethanol	N-EtFOSE	1691-99-2	571.26	$C_{12}H_{10}F_{17}NO_3S$

Table 1.1 (cont.)

Compound	Abbreviation	CAS No.	Mol weight	Structural formula
N-ethyl perfluooctane sulfonamido ethylacrylate	N-EtFOSEA	423-82-5	625.3	C ₁₅ H ₁₀ F ₁₇ NO ₄ S
Perfluorohexanoic acid	PFHxA	307-24-4	314.05	C ₆ HF ₁₁ O ₂
Perfluoroheptanoic acid	PFHpA	375-85-9	364.06	C ₇ HF ₁₃ O ₂
Perfluorooctanoic acid	PFOA	335-67-1	414.07	C ₈ HF ₁₅ O ₂
Perfluorononanoic acid	PFNA	375-95-1	464.08	C ₉ HF ₁₇ O ₂
Perfluorodecanoic acid	PFDA	335-76-2	514.09	C ₁₀ HF ₁₉ O ₂
Perfluoroundecanoic acid	PFUnA	2058-94-8	654.09	C ₁₁ HF ₂₁ O ₂
Perfluorododecanoic acid	PFDoA	307-55-1	614.1	C ₁₂ HF ₂₃ O ₂
Perfluorotetradecanoic acid	PFTeDA	376-06-7	714.12	C ₁₄ HF ₂₇ O ₂

1.2. PFASs occurrence, health risks and regulation

Release sources of poly- and perfluoroalkyl substances into the environment can be classified as (i) direct emissions, where PFASs are released throughout their complete product cycle (production, supply chains and disposal of consumer and industrial products), and (ii), indirect emissions, as a consequence of transformation of their precursors [22].

From 1951 to 2004, historical total global emissions of PFCAs, considering both direct and indirect emissions, are estimated in 3200 – 7300 tons. The major contribution to total source emissions were direct PFASs sources. The total estimated global production of PFCAs was 4400 – 8000 tons, 470 – 900 of these were released into the environmental media as direct emissions. Another important focus of PFCAs releases were fluoropolymer processing and manufacture, consumer and industrial products and AFFSs. On the other hand, indirect emissions, either by transformation of perfluorooctanesulfonyl fluoride (POSF) based precursors or fluorotelomer-based precursors, or by PFCAs residual impurities, were estimated in 30 – 350 tons [23]. Notable among the PFASs manufacturing worldwide is the annual production of PFOS and related substances, which was estimated at 4500 tons per year until the year 2000, according to the Organization for Economic Co-operation and Development (OECD) [24]. From 1995 to 2004, the production of fluorotelomer products was also very high, estimated in 5000 – 6250 tons per year [25].

Major PFASs manufacturers are already ceasing the production of long-chain PFASs in Europe and North America due to increasing public awareness and stricter regulations. In 2006, the United States

Environmental Protection Agency (EPA) invited some of the major worldwide leading companies in the PFASs industry to join a global stewardship program to commit to achieve, no later than 2010, a 95% reduction of PFOA emissions, its precursors, related higher homologue chemicals and product level content of these chemicals. Total elimination of these products was planned to 2015 [26]. According to the final progress report, all participating companies have satisfactorily met the PFOA Stewardship Program goals [27]. However, the issue still persists as China has rapidly increased the production of PFOS from year 2000 onwards, currently estimated in 100-200 tons per year, as well as the production of long-chain PFCAs, exceeding the North America and Europe levels before the action plans [28].

Due to the high energy of the carbon-fluorine bond, PFASs are extremely persistent and extremely resistant to chemical, physical and biological degradation [29]. Indeed, their occurrence in river and human drinking water resources has been extensively reported around the globe [30]–[33], as well as their presence in soils [34], [35], fire-fighting training areas [36], [37], landfills [38] or wastewater treatment plants (WWTP) [15], [39], among others. Figure 1.1 shows an outline of PFASs pathways from their production and use until their fate on the aquatic and terrestrial ecosystem.

As a consequence of their extreme persistence and high mobility through water bodies, PFASs can be easily assimilated by organisms through bioaccumulation in the food chain [40]. Scientific evidences about the toxicological properties of long-chain PFASs on humans (e.g. immunological damage effects, cancer, infertility, etc...[41]–[43]), have led to several restrictions around their use and manufacture. In 2013, PFOS and its derivatives were classified as priority hazardous substances by the

European water policy [44]. More recently, the European Regulation concerning Registration, Evaluation and Authorization of Chemicals (REACH), has established severe restrictions around the manufacturing and usage of perfluorooctanoic acid (PFOA), its salts and PFOA-related substances. Additionally, the United States Environmental Protection Agency has recently set guideline health levels for PFOA and PFOS in drinking water at $0.07 \mu\text{g L}^{-1}$, both individually or combined [45]. The National Food Agency of Sweden have also suggested an action limit value of 90 ng L^{-1} for the sum of eleven PFASs and a health limit, where water consumption must be completely avoided, of 900 ng L^{-1} [46].

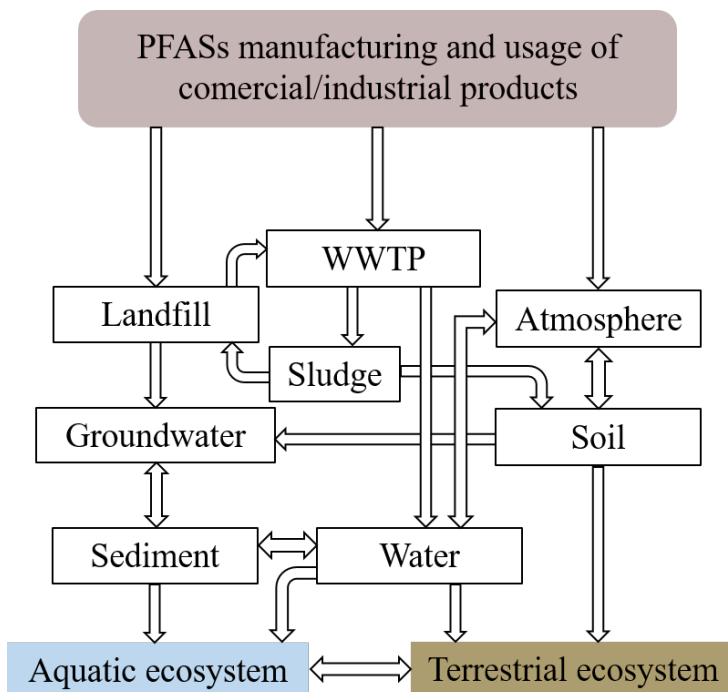


Figure 1.1. Global scheme of PFASs transport and fate in the environment. Adapted from Ahrens and Bundschuh (2014) [47]

As a result, manufacturers are progressively phasing-out long-chain PFASs and substituting them with their short-chain alternative homologues and fluorotelomers (e.g. 6:2 fluorotelomers) [48]. Although 6:2 fluorotelomers can be biologically degraded, its degradation products (short-chain perfluorocarboxylic acids [49]) are as extremely persistent as their longer-chained homologues, are more water-soluble, have weaker adsorption onto solids, and thus, can be more easily transported through water bodies [50]. On the contrary, short-chain PFASs are less bioaccumulative in humans and animals but may show higher uptake on plants and their fruits. Overall, shorter-chain PFASs have shorter elimination half-life in small mammals than longer PFASs. [51]. As the volume of production of these fluorinated alternatives is expected to increase in the next years, concentrations of extremely persistent short-chain perfluorocarboxylic acids in the environment, such as PFHxA, would likely increase. The scientific attention in the last years have been mostly focused on recently phased-out long-chain PFASs, therefore, this thesis research was focused on currently implemented short-chain PFASs and other substitutive compounds such as 6:2 fluorotelomers.

1.3. Advanced technologies for PFASs treatment

Conventional sewage wastewater treatment methods have proven to be ineffective to remove PFASs from water [47]. Therefore, research efforts are being directed towards the development of different physicochemical techniques focused on the removal and/or destruction of these substances. Some of the most relevant are adsorption, advanced oxidation processes and hyperfiltration processes (nanofiltration and reverse osmosis) [52].

The most extensively studied adsorbent for the removal of PFASs is activated carbon, either by granular activated carbon (GAC) or by powder activated carbon (PAC), but other options include the use of anion exchange resins, zeolite or carbon nanotubes [52], [53]. A great disadvantage of the adsorption technology for the treatment of PFASs is that the sorption efficiency significantly declines for short-chain PFASs [53] and may be diminished by the presence of other organic compounds with similar molecular weights that compete for the active sites and have higher adsorption potential [54]. Some other disadvantages of this technology are its low regeneration efficiency, the need of a large amount of organic solvents such as methanol or ethanol, and the large generation of wastes [55]. The most common treatment of PFASs adsorption media is an economically costly incineration at very high temperatures ($>1000\text{ }^{\circ}\text{C}$) [56]. Membrane separation technologies, in particular nanofiltration and reverse osmosis have also showed great PFASs removal efficiencies. Overall, nanofiltration removal rates range from 90 to 99%, while reverse osmosis generally achieves more than 99% removal of the PFASs originally present in water, at the expense of lower water productivity [57], [58]. However, the main disadvantage of these membrane processes is that they transfer the pollutants to a concentrated phase which needs further treatment in order to destroy them [59].

Among advanced oxidation processes, some recent studies have reported the high reactivity of sulfate radical anions ($\text{SO}_4^{\bullet-}$), produced from the photolysis of persulfate ions ($\text{S}_2\text{O}_8^{2-}$) [14]. Heat activated $\text{S}_2\text{O}_8^{2-}$ [60] or electrochemically activated $\text{S}_2\text{O}_8^{2-}$ [61] are other interesting options. Some other oxidants such as ozone, ozone combined with UV or with hydrogen peroxide or even Fenton have been proved to be ineffective to destroy PFOA or PFOS [40]. Additionally, some promising results are being

obtained with photocatalytic oxidation technologies using innovative photocatalysts such as TiO₂-rGO [62], β-Ga₃O₃ or In₂O₃ catalysts [63]. The main problem with this technique is the high energy consumption needed to power the UV lamps [62], [64]. Finally, electrochemical oxidation has showed excellent results in the mineralization of PFASs to fluoride and carbon dioxide, in particular by means of boron-doped diamond electrodes (BDD) [64]–[66]. Some available technologies considered for the treatment of PFASs are represented in Figure 1.2, according to the work published by Ross et al. (2018) [54], whose authors belong to an international consultancy company specialized in PFASs treatment.

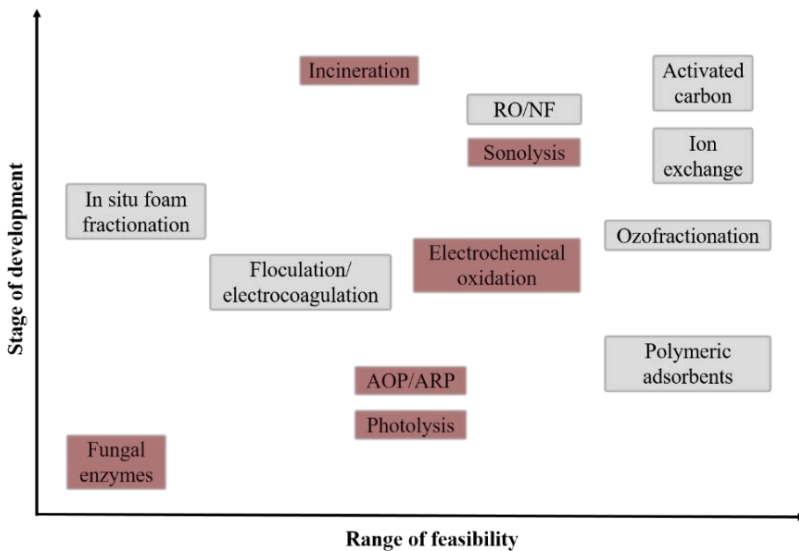


Figure 1.2. Summary of PFASs treatment technologies for water and their stage of development and feasibility. In red: destructive technologies. In grey: separation and adsorptive technologies. Adapted from Ross et al. (2018) [54]

1.3.1 Electrochemical oxidation

Electrochemical oxidation, or anodic oxidation, is a new technology that has attracted a lot of attention for the last years, where electric energy is used in the mineralization of organic pollutants. It is particularly interesting for the treatment of diluted wastewater (chemical oxygen demand (COD) < 5 g/L) [67]. Two main applications of the electrochemical treatment can be differentiated: (i) electrochemical conversion, where non-biodegradable organics are transformed into biocompatible organics suitable to be degraded by biological treatment [68] and (ii), complete electrochemical combustion of the organics to carbon dioxide and water [69].

The main advantages of electrochemical oxidation are that simple equipment is needed, its ease of operation and control, capability to adjust to variations in the inlet composition and flow rate, mild conditions (ambient temperature and pressure), no auxiliary chemicals needed to be added, and that generally no wastes are produced [70]–[72]. In contrast to its numerous advantages, the electrochemical oxidation has also some drawbacks. When treating low concentrated organic pollutants, low overall kinetics are obtained, that results from mass transfer limitations [59], [72]. This low concentration of organics may also lead to low current efficiencies, promoting undesirable secondary reactions that compete with the main reaction of interest [73]. High energy consumption of the electrochemical oxidation technology is usually reported [74], [75]. Another bottleneck for its large-scale implementation is the high economical investment needed, particularly when expensive electrodes, such as boron doped diamond (BDD), are used [76].

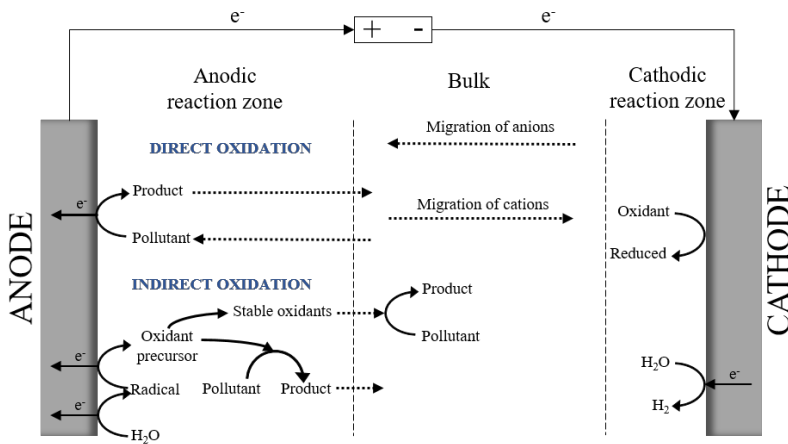
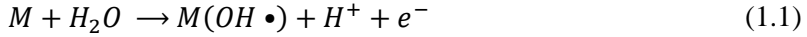


Figure 1.3. Main processes considered in the anodic and cathodic zones of the electrochemical reactor. Adapted from Cañizares et al. (2009) [79], Sirés et al. (2014) [80] and Anglada (2011) [81].

In electrochemical oxidation, pollutants can be destroyed by two main oxidation mechanisms (Figure 1.3), that can occur both individually or coexist [71], [77], [78]:

- Direct oxidation, which involves direct electron transfer from the pollutant to the anode surface, which generally yields poor decontamination.
- Indirect oxidation, where other species exchange electrons with the anode to form electroactive species to carry out the pollutants oxidation.

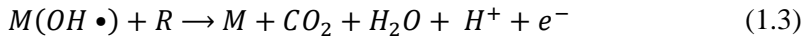
The first step in the oxidation of organic pollutants by means of hydroxyl radicals is their generation from the discharge of water molecules and adsorption at the active site of the anode surface (M) [82]:



From this step, the reactivity of the physisorbed OH• depends on the nature of the electrode material. Therefore, two types of electrodes have been proposed in literature, classified as active and nonactive electrodes [67], [71], [82]. In active electrodes, a strong interaction is established between the hydroxyl radicals and the active surface. A higher oxide is then formed, which can act as a mediator in the oxidation of organic pollutants:



On the contrary, nonactive electrodes show a much weaker interaction between the electrode surface and the hydroxyl radicals. The formed physisorbed hydroxyl radicals (also called physisorbed active oxygen) contributes to the complete mineralization or combustion of the organic pollutants (R) to carbon dioxide.



Energy consuming secondary reactions, such as the oxygen evolution reaction (OER), also occur simultaneously. On nonactive electrodes, the undesirable OER occurs between the physisorbed hydroxyl radical and water to form a O₂ molecule, although the exact mechanism is not totally well understood yet, and it has been speculated that the production of intermediate H₂O₂ may play a role on BDD electrodes [83]:



In general, it can be considered that active anodes (carbon, graphite IrO₂, RuO₂ or Pt) which are good catalysts for the OER (low OER overpotential), as a consequence of the strong interaction between the anode surface and OH•, allows the partial oxidation of pollutants, while, nonactive anodes (bad catalysts for the OER and high OER overpotential), such as PbO₂, SnO₂ or BDD, may allow the complete combustion of organic pollutants to CO₂, which makes them attractive for wastewater treatment [67], [77]. For example, in the case of BDD electrodes, the interaction BDD anode surface-hydroxyl radical is so weak, that the very reactive generated hydroxyl radicals are considered “quasi-free”, which certainly strongly contributes to achieve complete combustion of organics [84]. Table 1.2 lists different electrode materials according to their oxidation power and catalytic activity towards OER.

Table 1.2. Oxidation potential and overpotential for OER of different anode materials in acidic media. Adapted from Comninellis et al. (2008) [84]

Anode material	Oxidation potential (V)	Overpotential for OER (V)	Adsorption enthalpy of M-OH•
RuO ₂ -TiO ₂ (DSA [®] -Cl ₂)	1.4-1.7	0.18	Chemisorption of OH•
Ir - Ta ₂ O ₅ (DSA [®] - O ₂)	1.5-1.8	0.25	
Ti/Pt	1.7-1.9	0.3	
Ti/PbO ₂	1.8-2.0	0.5	↑
Ti/SnO ₂ - Sb ₂ O ₅	1.9-2.2	0.7	
p-Si/BDD	2.2-2.6	0.3	Physisorption of OH•

When treating an effluent naturally containing different anion species, several oxidative species, such as persulfate, hypochlorite, hydrogen peroxide, chlorine or ozone can be electrogenerated and may also contribute to oxidize organic pollutants [85]. When chloride is present in the water it can be converted into active chlorine (chlorine, hypochlorous acid and hypochlorite) [86]. These species can be further oxidized to undesired and toxic chlorate (ClO_3^-) and perchlorate anions (ClO_4^-) [66], [87], [88]. When sulfate is present in the effluent to be electrolyzed, generation of other oxidative species such as persulfate also play an important role in the oxidation of organic pollutants. Its generation is particularly favored by high O_2 overvoltage anodes such as BDD and PbO_2 [89]. Sulfate oxidation mechanisms on BDD anodes are not totally well understood yet and research is still ongoing with different proposals available in literature [90]–[92].

BDD electrodes are very promising and widely studied electrodes for electrochemical oxidation of persistent organic pollutants. From Table 1.2, it can be seen that is the electrode with the loosest interaction with largely produced hydroxyl radicals, what makes it the electrode with the highest oxidation power. Some of the main advantages of this material are its high chemical inertness and low adsorption of species (which prevents fouling), extended lifespan, superior stability and corrosion resistivity, low background current and very efficient generation of secondary oxidations [93]–[95]. Another very important feature is its very high overpotential for both oxygen and hydrogen evolution in aqueous electrolytes [96], [97]. All these features contribute to its high reactivity for organics oxidation, extensively reported in literature, leading to complete mineralization of a wide range of pollutants, such as ammonia, cyanide, phenols, aniline, hydrocarbons, dyes, surfactants, drugs and pesticides, including refractory

pollutants [71]. However, some major limitations of the BDD electrodes have to be overcome. One of the most important is the difficulty to find an appropriate substrate on which to deposit the BDD film. The price of niobium, tantalum and tungsten substrates is very high. Silicon substrate shows poor mechanical strength and has lower conductivity. Titanium substrate is very interesting (good electrical conductivity, mechanical strength and chemical inertness) but its service lifetime is relatively short [72], [98], [99].

The promising application of electrochemical oxidation for the degradation of PFASs is currently an ongoing research. The efficiency of electrochemical oxidation of PFASs have been proved to be strongly dependent on the type of anode material as it influences the electron transfer, the $\text{OH}\cdot$ generation and the oxygen evolution potential [64]. Electrochemical oxidation of PFASs is particularly effective when using electrodes where the OER potential is high as it enables the generation of large quantities of $\text{OH}\cdot$ when using low potential values, as in the case of BDD anodes.

Cartell and Farrell (2008) [100] firstly explored the use of BDD electrodes to investigate the oxidation of PFOS at initial concentration of 0.4 mM (200 mg L^{-1}) and current density that ranged from 10 to 200 A m^{-2} using two different reactor configurations (a rotating disk electrode (RDE) and a flow through reactor). Very fast pseudo first order kinetics were obtained in the flow through reactor at 20 A m^{-2} (0.12 min^{-1}). Next work by Liao and Farrell (2009) [101] studied the oxidation of PFBS with a RDE reactor and BDD anodes, and concluded that the zeroth-order kinetics obtained were an indicator that it was a reaction limited by the availability of active sites. Ochiai et al. (2011) [102] studied the decomposition of highly concentrated

(8 mM) PFOA solutions using a commercial BDD anode, reporting increasing concentrations of CO₂ and F⁻ ions during the course of the experiment, which manifested its successfully mineralization. Zhuo et al. (2012) [103] investigated the BDD electrochemical oxidation of PFBA, PFH_xA, PFOA, PFDeA, PFBS, PFH_xS, which followed first order degradation kinetics that increased with the alkyl chain length. It was justified with the decreasing water solubility and hydrophobicity properties of longer-chained PFCAs, which facilitated the adsorption on the hydrophobic BDD surface. Very high degradation ratio (97.5% after 2 h) for PFOA was obtained at 59 A m⁻². More recently, Gómez-Ruiz et al. (2018) [104] compared the effect of the chemical and structural features of two commercial BDD anodes on the decomposition of PFOA: a microcrystalline coating on silicon and a ultrananocrystalline coating on niobium. Results were significantly better in terms of both PFOA removal and TOC removal when using the microcrystalline BDD anode, which was explained by its higher sp³ carbon content, lower boron content and H-terminated carbon content which clearly favored a much more efficient PFOA mineralization, as revealed by Raman and XPS spectroscopy techniques.

Another explored anodic material for the destruction of PFASs is SnO₂ using different combinations of antimony, cerium, bismuth or fluoride as dopants to enhance its conductivity [99], [105]–[107]. Most works have been conducted using antimony as dopant. Degradation ratios using these electrodes hugely differ in the literature, depending on the specific electrode, the compound studied, cell configuration, type of electrolyte and current density used etc. However, the main problems of SnO₂ electrodes are their short service life, lack of commercial availability, and the possible release of antimony to the water, which is a very toxic substance with an

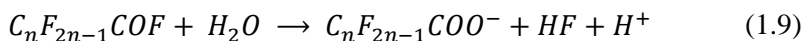
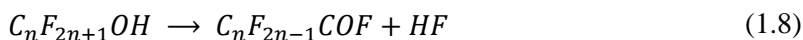
EPA drinking water threshold of $6 \mu\text{g L}^{-1}$ [83]. PbO_2 based electrodes have also been explored to the removal of PFASs with reasonably good results [108]–[111]. Similar to SnO_2 electrodes, kinetics information and degradation ratios vastly differ in the literature. Also, although various efforts are being carried out in order to improve PbO_2 electrodes stability, very toxic lead ions leaching into the solution is an important drawback, and thus, water treatment applications with PbO_2 should be carefully considered [83], [108]. Other electrodes materials considered were active anodes, such as Pt, Ti/Ru– IrO_2 , and Ti/ SnO_2 –Sb/ MnO_2 electrodes, which showed poor catalytic activity towards PFOA [64]. With the exception of very few works carried out with real water matrixes [66], [112], most of the information available in literature have been obtained working with synthetic solutions doped with PFASs. In the same way, most studies have been focused on PFOA and PFOS removal, two of the main long-chain PFASs that are currently being phased out by chemical manufacturers.

The electrooxidation mechanisms of PFASs involves a combination of both direct oxidation (electron transfer to the anode) and indirect oxidation through interaction with hydroxyl radicals in a step by step degradation pathway. For both PFCAs and PFASs the reaction begins with a direct electron transfer from the carboxyl or sulfonic group to the anode to form a highly unstable $\text{C}_n\text{F}_{2n+1}\text{COO}\cdot$ or $\text{C}_n\text{F}_{2n+1}\text{SO}_3\cdot$ radical which undergoes Kolbe decarboxylation or desulfonated reaction to form perfluoroalkyl radicals ($\text{C}_n\text{F}_{2n+1}$) [64]. The initiation reaction mechanism, for perfluorocarboxylic acids, is the following:





In a widely proposed PFASs reaction mechanism [99], [103], [113], [114], the newly formed $C_nF_{2n+1} \bullet$ radical reacts with a hydroxyl radical to form a perfluoroalcohol $C_nF_{2n+1}OH$, which, due to its thermally unstable nature, forms $C_nF_{2n+1}COF$ releasing one fluoride molecule. This finally reacts with a water molecule, to form a shorter-chained perfluorocarboxylic acid, $C_{n-1}F_{2n-1}COO^-$. The complete cycle is then repeated, losing a CF_2 unit each time until complete mineralization to CO_2 . The detailed degradation pathway is the following:



A degradation mechanism for 6:2 FTSA have also been proposed [19]. In this case, the reaction mechanism starts with a hydroxyl radical attack to the unfluorinated carbon following H-atom abstraction mechanism, which results in substitution of hydrogen by alcohol groups. This intermediate would simultaneously form both PFHxA and PFHpA, although PFHxA was found in much higher proportion. The degradation of the perfluorocarboxylates would follow the exact mechanism previously described until complete defluorination and mineralization to CO_2 .

At present, the vast majority of published works dealing with the electrochemical degradation of PFASs have been conducted with synthetic solutions. The study of the electrochemical treatment of these substances

needs to be extended to real wastewater. Real effluents usually contain different salts in concentrations that may be lower than those used as electrolyte in electrochemical experiments conducted in the laboratory. The presence of different ionic species or organic matter may lead to electrode passivation inhibiting the electrolytic process. The PFASs degradation efficiency observed in real wastewater may also strongly differ to synthetic aqueous solutions if there are presence of other organic compounds that lead to competing side reactions. On the other hand, energy consumption and costs of the PFASs electrochemical treatment should be reduced. The energy consumption of the PFASs electrochemical degradation reported in literature [64], [66] is still excessively high for its adoption at high scale as the main PFASs treatment option. Given that these compounds are generally present at very low concentrations, mass transfer limitations need to be avoided. In that sense, research efforts should be directed towards the combination of the ELOX technology with different separation and destructive technologies in order to minimize energy consumption and costs.

Many other challenges should be addressed. The cost of the electrode materials is still very high, specially the cost of BDD electrodes. Due to the extremely high recalcitrance of these substances, very harsh oxidative conditions are needed as those achieved by BDD electrodes. Thus, research efforts should be directed towards the optimization of the BDD manufacturing process or towards the development of new cheaper but equally effective electrocatalytic materials. The improvement of the long-term stability, electrocatalytic performance, control of toxic byproducts, optimization of operating parameters and design and optimization of new reactor configurations are also other important challenges to be faced in the development of the ELOX technology [72].

1.3.1. Pressure-driven membrane processes: nanofiltration and reverse osmosis

Pressure-driven membrane processes, are used for a wide range of industrial applications since the 1960s [115]. These processes can be used to purify or concentrate a dilute aqueous solution [116]. In pressure-driven membrane processes treating aqueous solutions, the membranes are selective barriers (polymeric, ceramic/metal, solid or liquid, neutral or electrically charged, homogeneous or heterogeneous, symmetric or asymmetric, etc...) which separates two phases in order to selectively restrict the transport of one or more components [117]. The pressure difference between the feed and the permeate side is used as the driving force to drive the transport of the solvent (typically water) through the membrane, being retained in the process particles and dissolved components based on diverse properties such as their size, shape and charge [118].

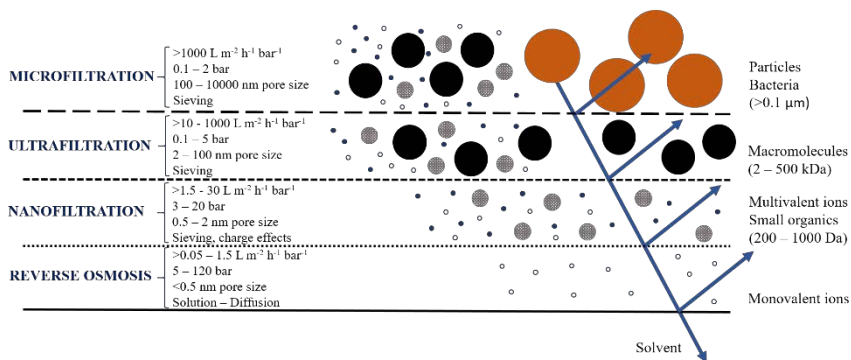


Figure 1.4. Pressure-driven membrane separation processes and their main characteristics. Adapted from Van der Bruggen et al. (2003) [118] and Jye and Ismail (2016) [119].

Pressure-driven membrane processes can be divided into four major groups, considering the pore size of the membranes and the required operating pressure [120]: microfiltration (MF), ultrafiltration (UF), nanofiltration (NF) and reverse osmosis (RO). Figure 1.4 shows an overview of the main characteristics of the different groups of pressure-driven membrane processes. Given the large pore size of both microfiltration and ultrafiltration and the range of molecular weight of PFASs (Table 1.1) it is clear that these compounds would not be effectively retained by these membranes [121]. Therefore, membranes with lowest pore sizes such as nanofiltration, aided by surface charge rejection, or nonporous membranes based on separation-diffusion mechanisms, such as reverse osmosis, are needed for the separation of these compounds.

Nanofiltration membranes are placed between ultrafiltration and reverse osmosis membranes, achieve high rejection of organic compounds (>90%) with molecular weight higher than the molecular weight cut off of the membrane, very high rejection of multivalent ions (>99%) and moderate rejection of monovalent ions (0 – 70%) [122]. When compared to reverse osmosis, a great advantage of nanofiltration is that for some applications very demanding separations can be achieved, at the same time high water fluxes are obtained at lower operating pressures [123]. Another interesting feature of nanofiltration membranes are their electrical properties or surface charge, which not only makes possible the very high rejection of multivalent ionic species [124]–[126], but also the high retention of negatively charged organic species by electrostatic repulsion mechanisms [127]. In the case of uncharged solutes, retention mechanisms are probably a combination of size exclusion and non-electrostatic interactions between the membrane and the solute (e.g. Van der Waals forces) [128], so solute size and polarity of the solute and pore size and membrane material play

an important role [129]. Polarity may also influence the retention of neutrally charged solutes, as it seems that a higher dipole moment of a molecule is associated with lower overall retentions, probably explained by electrostatic attraction of opposite charged side of the dipole with the charged membrane that orientates the dipole towards the pore [130].

Nanofiltration uses in diverse industrial applications have progressively increased in last decades. Nanofiltration have been used for desalting applications or removal of total dissolved solids (TDS) (saline surface water, brackish groundwater, tertiary treated wastewater, seawater and industrial process water) [131], purification of pharmaceuticals, biotechnology, food engineering (beverage industries, dairy industries) [132], [133], production of ultrapure water for the semiconductor industry, removal of heavy metals for the metalworking industry, paper mill waste treatment or removal of sulphate [134]. Nanofiltration is also able to successfully remove from water a wide variety of organic compounds such as pesticides, dyes, endocrine disruptors, natural organic matter (NOM) [135], pharmaceutical active compounds [136] and persistent organic pollutants [137].

Reverse osmosis needs to operate at the highest pressures among all pressure driven membrane processes. Although reverse osmosis membranes polymer network has been traditionally considered as a “nonporous” film where the solvent is dissolved, in reality it can be considered that the polymer network is “dynamic” and allows water molecules to enter, being the “pores” transient channels in the dense film [117]. Therefore, solute transport through reverse osmosis membranes could be explained by solution-diffusion across the membrane (dissolution of the solvent and water into the water – swollen polymer matrix, diffusion

through the membrane and desorption from the downstream membrane surface [134]) and diffusion/advection through a membrane pore [138]. The main application of reverse osmosis is water desalination, being a less costly alternative to the highly energy demanding thermal evaporation by means of multiple-stage flash or multiple effect distillation [139]. Moreover, it has been also considered for the removal of recalcitrant NOM (such as humic acid [140]), removal of arsenic from groundwater [141], pharmaceutical active compounds [142], [143], pesticides [144], a wide range of contaminants of emerging concern [145] or even for bioethanol purification [146].

Nanofiltration and reverse osmosis are of special interest for the separation of PFASs from different water sources. Table 1.3 shows some bibliographic references regarding PFASs removal by pressure-driven membrane processes. Tang and coworkers [58] first reported the use of commercial reverse osmosis to remove PFOS from a wastewater generated from photolithographic processes. The concentration of PFOS in the original wastewater was 1650 mg L^{-1} , but tests were conducted with concentrations that ranged from 1 mg L^{-1} to 1650 mg L^{-1} . PFOS rejections were higher than 99% and the permeate flux was found to be stable along the filtration run for low concentrated solutions but declined at increasing the PFOS concentration.

In a later work, Tang and coworkers [147] also studied the use of nanofiltration membranes in the treatment of PFOS spiked in ultrapure water at 10 mg L^{-1} . PFOS rejection by nanofiltration ranged from 90 to 99%. They observed that water flux declined with time, especially for the more permeable membranes (NF270, NF90 and ESPA3). Steinle and Reinhard [57] studied the nanofiltration separation of a wide variety of

PFASs (PFPA, PFBS, PFHxA, PFHpA, PFHxS, PFOA, 6:2 FtS, PFNA, PFOS, FOSA, PFDA, PFA, PFDS, PFDoA and PFTA) at very low concentrations (150 – 400 ng L⁻¹). Rejection was estimated in more than 95% for the majority of the compounds. They also observed a negative influence of membrane fouling on membrane rejection. Rejection was clearly influenced by the pH of the solution. Acid pH decreased PFASs rejection as the electrostatic repulsion between the charged membrane surface and the negatively charged dissociated compounds was weakened.

Later works, such as the one published by Zhao and coworkers [148] working with a NF270 membrane in the removal of PFOS and Chen and coworkers [149] using low-pressure reverse osmosis (LPRO) membranes for the removal of a variety of PFASs in the solution, confirmed that the increase of pH from acidic to basic conditions was favourable for achieving higher rejections.

The presence of counter ion species in the solution was found to exert different effects on PFASs rejection, depending on their chain length. Zhao and coworkers [148] and Wang and coworkers [153] found that the increasing concentration of calcium cations (Ca²⁺) in the solution improved the PFOS rejection by nanofiltration membranes. Different explanations were proposed. While Zhao and coworkers explained this behaviour by the formation of potential bridges between PFOS and calcium cations that increased the molecular size, Wang and coworkers explained it by the possible blockage of membranes pores by deposition of calcium cations that prevented PFOS filtration. More recently, a work by Wang and coworkers [154] confirmed the positive correlation between the addition of calcium cations and the increase of PFOS rejection but observed a completely different behaviour (decrease of rejection with the increase of

calcium concentration in the solution) for the shorter-chained PFBS. This was explained by different dominant retention mechanism of the NF membrane for these two target PFASs. Further studies with other PFASs, specially with PFCAs, are needed to confirm this behaviour.

Overall, nanofiltration membranes achieve lower PFASs rejections (90 – 99%) than reverse osmosis (>99%), which are strongly influenced by the solution pH, ionic strength or initial PFASs concentration, but higher water permeate fluxes are obtained. The vast majority of previous works have been focused on PFOS and PFOA, two compounds that are being currently phased-out. Research should now be focused on the evaluation of NF or RO for the retention of currently implemented short-chain PFASs used as substitutive compounds or being degradation products of also substitutive 6:2 fluorotelomers. Also, very few studies have evaluated PFASs membrane separation at high concentrations relevant in industrial process water streams, and even fewer works have evaluated PFASs retention mechanisms in real water matrixes that may have different salts or other organic dissolved, as most of them have used just ultrapure water samples spiked with PFASs. In that sense, it is needed to understand the effect of the presence of ionic species in the solution as in the case of real industrial effluents and also the impact of increasing the ionic strength in the retention by NF and RO of short-chain PFASs. The use of LPRO membranes should be also evaluated as they are suitable for medium-high salinity feed waters as in the case of real industrial effluents and achieves high fluxes and organic retention while requiring less energy as they can be operated at lower pressures. [155]

Table 1.3. Some relevant published works regarding the use of pressure-driven membrane processes for PFASs removal. Results attained in the present thesis are also included for comparison.

Reference	PFASs studied	Synthetic or real water	Membrane/s	Initial concentration	Rejection
Tang et al. (2006) [58]	PFOS	Real	ESPA3, LFC3, BW30, SG	1650 mg L ⁻¹	>99%
Tang et al. (2007) [147]	PFOS	Synthetic	BW30, ESPA3, LFC1, LFC3, SG, DK, NF90, NF270	10 mg L ⁻¹	90 – 99%
Steinle et al. (2008) [57]	PFPhA, PFBS, PFHxA, PFHpA, PFHxS, PFOA, 6:2 FTSA, PFNA, PFOS, FOSA, PFDA, PFUnA, PFDS, PFDoA, PFTA	Synthetic	NF270, NF200, DK, DL	800 mg L ⁻¹	>95%.
Lipp et al. (2010) [150]	PFBA, PFBS, PFOA, PFOS	Real and synthetic	NF90, NF270, NF200	600-4200 ng L ⁻¹	95 – 99.9%

Table 1.3 (cont.)

Rattanaoudo m al. (2011) [151]	PFOA	Synthetic	XN45	0.1, 10, 1000 mg L ⁻¹	60 – 85%
Zhao et al. (2013) [148]	PFOS	Synthetic	NF270	10,100,200,300,400,500 µg L ⁻¹	93 – 96%
Appleman et al. (2013) [7]	PFBA,PFHxA, PFOA, PFNA, PFDA, PFBS,PFHxS, PFOS	Synthetic	NF270	1 µg L ⁻¹	>93%.
Chen et al. (2014) [149]	PFPeA, PFBS, PFHxA, PFOA, PFOS	Synthetic	ES-20, NTR- 759HR, NTR- 729HF, NTR- 7450, UTC-60	1000 mg L ⁻¹	>98%
Hang et al. (2015) [152]	PFOA	Synthetic	NF270 , NF90	10, 100, 10000 mg L ⁻¹	NF270: 94 – 98% NF90: 99%
Wang et al. (2015) [153]	PFOS	Synthetic	Synthetic PMIA membrane	100 µg L ⁻¹	88 – >99%

Table 1.3 (cont.)

Zhao et al. (2016)	PFOS	Synthetic	NF270	100 µg L ⁻¹	94 – 99%
Yu et al. (2016)	PFOS	Synthetic	HYDRACORE, NF270	100 µg L ⁻¹	NF270: 95 – 97% HYDRACORE: 40-85%
Soriano et al. (2017)	PFHxA	Real	NF270	S1: 204 mg L ⁻¹ S2: 64 mg L ⁻¹	93.9 – 97.1%
Wang et al. (2018)	PFOS, PFBS	Synthetic	Poly(piperazineamide) synthetic membrane	25 – 150 µg L ⁻¹	PFOS: 88 – 92% PFBS: 20 – 50%
Soriano et al. (2019)	PFHxA	Synthetic / synthetic emulating real solution (SERS)	NF270, NF90, XLE, BW30, SW30XLE	100 mg L ⁻¹	In SERS: NF270: 89.3 – 92.5%; NF90: 98.1 – 99.6%; XLE: 99.0 – 99.4%.

1.4. Integration of electrochemical oxidation and membrane separation

A great disadvantage of pressure-driven membrane processes is that the pollutants are retained in the concentrate stream, that needs further treatment before its disposal [68]. Due to the concerning properties of PFASs mentioned above, an appropriate treatment technology should be the one that allows complete destruction and mineralization of these substances. In spite of the excellent ability of the ELOX technology to degrade and mineralize PFASs, its practical implementation is still hindered by its slow overall kinetics that results from mass transfer limitations. In particular, the high energy consumption of the ELOX technology is one of the main challenges that should be overcome [72]. The synergy and integration of these two technologies could help to overcome their individual limitations in the treatment of persistent organic pollutants [68].

Typically, membrane separation is used as a pre-treatment process to concentrate the pollutant and then, ELOX is used as a post-treatment of the concentrate stream [142], [156]–[158]. The use of this strategy was previously reported by Pérez et al. (2010) [143], who applied BDD electrodes to treat the concentrate stream of a reverse osmosis unit used for water reclamation and industrial reuse of the secondary effluent of a WWTP. Another study by Urriaga et al. (2013) [142] proposed the use of an integrated tertiary water treatment train for the removal of a wide variety of pharmaceutical compounds from the influent and the effluent of a WWTP. The treatment train consisted in an ultrafiltration unit followed by a two-stages reverse osmosis unit and an ELOX unit to treat the concentrate from the RO process. The strategy was proven to be successful as RO

managed to retain more than 99% of the inlet target compounds and the application of ELOX with BDD electrodes removed more than 95% of the studied compounds from the RO effluent.

However, almost all the studies published so far have been exclusively focused on the evaluation and applicability of the ELOX technology just as a post-treatment process to degrade pollutants from a concentrate process of a membrane separation unit. Very little information about the energetic and economic advantages of the synergetic membrane/ELOX approaches is provided in literature. A remarkable exception is the work published by Madsen et al. (2015) [74] that evaluated the use of NF and RO membranes followed by ELOX to degrade a pesticide (BAM) and found that the total energy required could be reduced up to a 95% through the coupled process strategy. Still, rigorous methodologies should be developed to design and optimize an integrated membrane/ELOX based on a complete techno-economic analysis as a way to explore all the potential benefits of this strategy.

In that sense, in this PhD thesis an integrated membrane separation - ELOX process was proposed to separate and degrade persistent short-chain perfluorocarboxylic acids. The designed process was optimized based on a complete techno-economic analysis. Further information is provided in Chapter 2 of the present thesis document. A basic scheme of the integrated strategy is depicted in Figure 1.5.

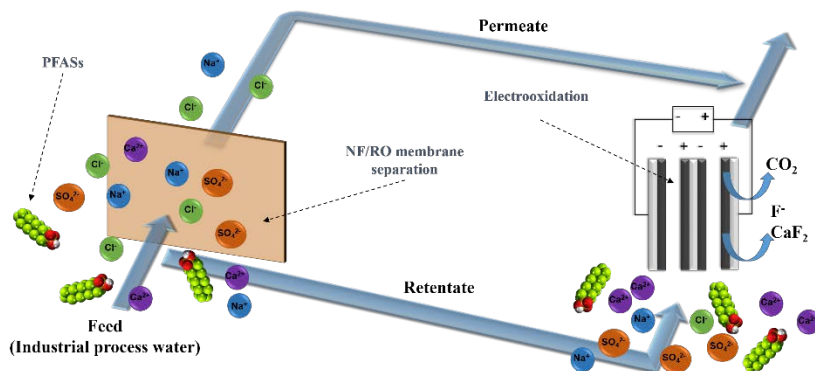


Figure 1.5. Basic scheme of the integration of NF/RO and ELOX for the treatment of PFASs.

1.5. Thesis scope and outline

This thesis was developed in the Environmental and Bioprocess Technologies (EBT) Research Group at the Department of Chemical and Biomolecular Engineering of the University of Cantabria. The main objective of this thesis is to develop advanced technologies for the treatment of PFASs in industrial wastewater treatment, especially those substances that are progressively being used in the industry as alternative to regulated PFASs. For that reason, most of the published results of this thesis corresponds to the treatment of real process industrial effluents. The industrial wastewater samples were obtained with the collaboration of ANSES - National Laboratory for Hydrology from France, which made possible to contact one of the leading companies in the fluorochemicals manufacturing industry, which supplied the samples under a confidentiality agreement framework. The main goal has been addressed by the following specific thesis objectives:

- Study of the removal efficiency of short-chain PFASs from real industrial effluents by nanofiltration and reverse osmosis membranes.
- Evaluation of the electrochemical oxidation by means of BDD anodes of alternative short-chain PFASs from NF/RO concentrated industrial streams and synthetic water mixtures.
- Overcome membrane separation and electrochemical oxidation individual limitations by the integration of both technologies.
- Use of process system engineering and optimization tools for the design and scaling-up of the integrated process.

These objectives resulted in the publication of five articles, as depicted in Figure 1.6.

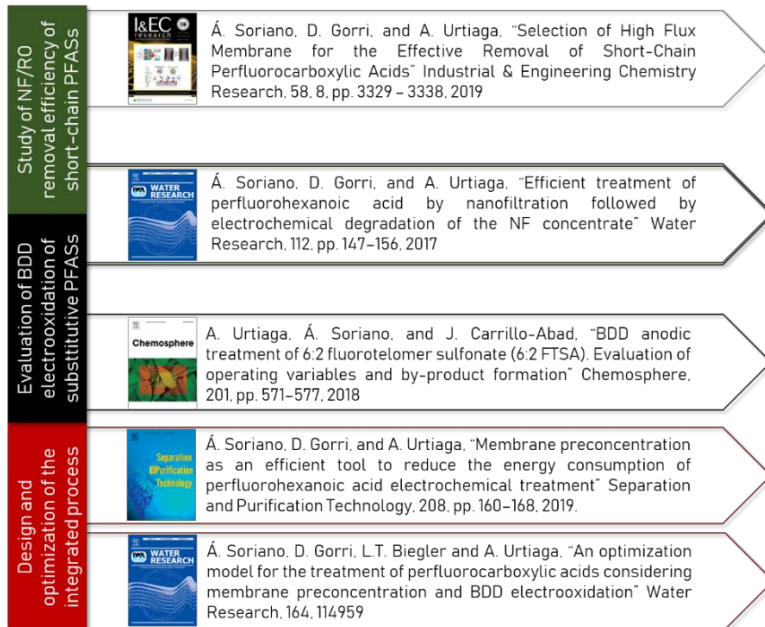


Figure 1.6. Overall objectives of this thesis and their connection with the published articles included in Chapter 5.

Based on the above mentioned specific goals and the regulation framework of the University of Cantabria regarding the development of a PhD thesis document “*as a compendium*” of interrelated scientific publications (*Regulations of the academic management of Doctoral Studies regulated by the Royal Legislative Decree 99/2011*), this document has been structured in five chapters:

- **Chapter 1:** Introduction. This chapter contains an overview of PFASs, their definition and concerning properties, alternative treatment technologies and a brief description about the fundamentals of pressure-driven membrane processes and electrochemical oxidation and the state-of-the-art of these technologies in the treatment of PFASs.
- **Chapter 2:** Materials and methods. This chapter describes chemicals, materials, analytical methods, experimental procedures and optimization tools used in the present thesis.
- **Chapter 3:** Results summary. This chapter comprises the main results that have been published in scientific journals during the development of this thesis. It shows the most relevant results of the electrochemical oxidation of short-chain PFASs by means of BDD anodes and of the removal of short-chain PFASs using nanofiltration and reverse osmosis. Finally, it also contains the discussion about the main results of the design, integration and optimization of a hybrid membrane separation – electrooxidation process for the treatment of short-chain perfluorocarboxylic acids.
- **Chapter 4:** General conclusions and prospective. This chapter contains the main conclusions and remarks of this thesis, as well as the prospection for future progress.

- **Chapter 5:** Scientific publications. This section includes all the scientific publications published in JCR journals during the doctoral period.

1.6. References

- [1] WWAP (UNESCO World Water Assessment Programme), “The United Nations World Water Development Report 2019: Leaving No One Behind,” UNESCO, Paris, 2019.
- [2] UN General Assembly, “Transforming our world: the 2030 Agenda for Sustainable Development,” 2015.
- [3] UN-Water, “Un-Water SDG 6: public dialogue report 2018,” 2018.
- [4] UNESCO, “International Initiative on Water Quality: promoting scientific research, knowledge sharing, effective technology and policy approaches to improve water quality for sustainable development,” 2015.
- [5] S. Harrad, “Beyond the Stockholm Convention: An Introduction to Current Issues and Future Challenges in POPs Research,” in *Persistent Organic Pollutants*, S. Harrad, Ed. John Wiley & Sons, Inc., 2009.
- [6] N. . Cheremisinoff, *Perfluorinated Chemicals (PFCs): Contaminants of Concern*. John Wiley & Sons, Inc., 2017.
- [7] T. D. Appleman, E. R. V Dickenson, C. Bellona, and C. P. Higgins, “Nanofiltration and granular activated carbon treatment of perfluoroalkyl acids,” *J. Hazard. Mater.*, vol. 260, pp. 740–746, 2013.
- [8] M. F. Rahman, S. Peldszus, and W. B. Anderson, “Behaviour and fate of perfluoroalkyl and polyfluoroalkyl substances (PFASs) in drinking water treatment: A review,” *Water Res.*, vol. 50, no. 0, pp. 318–340, Jan. 2014.
- [9] P. Mccleaf, S. Englund, A. Ostlund, K. Lindegren, K. Wiberg, and L. Ahrens, “Removal efficiency of multiple poly- and perfluoroalkyl substances (PFASs) in drinking water using granular activated carbon (GAC) and anion exchange (AE) column tests,” *Water Res.*, vol. 120, pp. 77–87, 2017.
- [10] A. B. Lindstrom, M. J. Strynar, and E. L. Libelo, “Polyfluorinated compounds: Past, present, and future,” *Environ. Sci. Technol.*, vol. 45, no. 19, pp. 7954–7961, 2011.
- [11] N. A. Fernandez, L. Rodriguez-Freire, M. Keswani, and R. Sierra-Alvarez, “Effect

- of chemical structure on the sonochemical degradation of perfluoroalkyl and polyfluoroalkyl substances (PFASs),” *Environ. Sci. Water Res. Technol.*, vol. 2, no. 6, pp. 975–983, 2016.
- [12] R. C. Buck *et al.*, “Perfluoroalkyl and polyfluoroalkyl substances in the environment: Terminology, classification, and origins,” *Integr. Environ. Assess. Manag.*, vol. 7, no. 4, pp. 513–541, 2011.
- [13] S. C. Panchangam, A. Y. C. Lin, K. L. Shaik, and C. F. Lin, “Decomposition of perfluorocarboxylic acids (PFCAs) by heterogeneous photocatalysis in acidic aqueous medium,” *Chemosphere*, vol. 77, no. 2, pp. 242–248, 2009.
- [14] H. Hori *et al.*, “Efficient decomposition of environmentally persistent perfluorocarboxylic acids by use of persulfate as a photochemical oxidant,” *Environ. Sci. Technol.*, vol. 39, no. 7, 2005.
- [15] O. S. Arvaniti, E. I. Ventouri, A. S. Stasinakis, and N. S. Thomaidis, “Occurrence of different classes of perfluorinated compounds in Greek wastewater treatment plants and determination of their solid-water distribution coefficients,” *J. Hazard. Mater.*, vol. 239–240, pp. 24–31, 2012.
- [16] S. Posner and N. C. of Ministers, *Per and Polyfluorinated Substances in the Nordic Countries: Use, Occurrence and Toxicology*. Nordic Council of Ministers, 2013.
- [17] J. W. Washington, J. E. Naile, T. M. Jenkins, and D. G. Lynch, “Characterizing fluorotelomer and polyfluoroalkyl substances in new and aged fluorotelomer-based polymers for degradation studies with GC/MS and LC/MS/MS,” *Environ. Sci. Technol.*, vol. 48, no. 10, pp. 5762–5769, 2014.
- [18] M. M. Phillips, M. J. A. Dinglasan-Panlilio, S. A. Mabury, K. R. Solomon, and P. K. Sibley, “Fluorotelomer acids are more toxic than perfluorinated acids,” *Environ. Sci. Technol.*, vol. 41, no. 20, pp. 7159–7163, 2007.
- [19] J. Carrillo-Abad, V. Pérez-Herranz, and A. Urtiaga, “Electrochemical oxidation of 6:2 fluorotelomer sulfonic acid (6:2 FTSA) on BDD: electrode characterization and mechanistic investigation,” *J. Appl. Electrochem.*, vol. 48, no. 6, pp. 589–596, 2018.
- [20] L. Zhao, P. W. Folsom, B. W. Wolstenholme, H. Sun, N. Wang, and R. C. Buck, “6:2 Fluorotelomer alcohol biotransformation in an aerobic river sediment system,” *Chemosphere*, vol. 90, no. 2, pp. 203–209, 2013.
- [21] P. De Voogt and M. Sáez, “Analytical chemistry of perfluoroalkylated substances,” *TrAC - Trends Anal. Chem.*, vol. 25, no. 4, pp. 326–342, 2006.
- [22] L. Ahrens, “Polyfluoroalkyl compounds in the aquatic environment : a review of

- their occurrence and fate,” *J. Environ. Monit.*, vol. 13, no. 20, pp. 20–31, 2011.
- [23] S. H. Prevedouros, Konstantinos; Cousins, Ian T.; Buck, Robert C., Korzeniowski, “Critical Review Sources , Fate and Transport of Fate,” *Environ. Sci. Technol.*, vol. 40, no. 1, pp. 32–44, 2006.
- [24] S. P. J. van Leeuwen and J. de Boer, “Extraction and clean-up strategies for the analysis of poly- and perfluoroalkyl substances in environmental and human matrices,” *J. Chromatogr. A*, vol. 1153, no. 1–2, pp. 172–185, 2007.
- [25] R. Van Zelm, M. A. J. Huijbregts, M. H. Russell, T. Jager, and D. Van De Meent, “Modeling the environmental fate of perfluorooctanoate and its precursors from global fluorotelomer acrylate polymer use,” *Environ. Toxicol. Chem.*, vol. 27, no. 11, pp. 2216–2223, 2008.
- [26] USEPA, “Risk Management for Per- and Polyfluoroalkyl Substances (PFASs) under TSCA.” [Online]. Available: <https://www.epa.gov/assessing-and-managing-chemicals-under-tsca/risk-management-and-polyfluoroalkyl-substances-pfass#tab-3>. [Accessed: 05-Sep-2019].
- [27] USEPA, “EPA’s Non-CBI Summary Tables for 2015 Company Progress Reports (Final Progress Reports).” [Online]. Available: <https://www.epa.gov/assessing-and-managing-chemicals-under-tsca/epas-non-cbi-summary-tables-2015-company-progress>.
- [28] T. Wang, R. Vestergren, D. Herzke, J. Yu, and I. T. Cousins, “Levels, Isomer Profiles, and Estimated Riverine Mass Discharges of Perfluoroalkyl Acids and Fluorinated Alternatives at the Mouths of Chinese Rivers,” *Environ. Sci. Technol.*, vol. 50, no. 21, pp. 11584–11592, 2016.
- [29] M. F. Rahman, S. Peldszus, and W. B. Anderson, “Behaviour and fate of perfluoroalkyl and polyfluoroalkyl substances (PFASs) in drinking water treatment: A review,” *Water Res.*, vol. 50, no. 0, pp. 318–340, Jan. 2014.
- [30] O. Quiñones and S. A. Snyder, “Occurrence of perfluoroalkyl carboxylates and sulfonates in drinking water utilities and related waters from the United States,” *Environ. Sci. Technol.*, vol. 43, no. 24, pp. 9089–9095, 2009.
- [31] J. Thompson, G. Eaglesham, and J. Mueller, “Concentrations of PFOS, PFOA and other perfluorinated alkyl acids in Australian drinking water,” *Chemosphere*, vol. 83, no. 10, pp. 1320–1325, 2011.
- [32] T. G. Schwanz, M. Llorca, M. Farré, and D. Barceló, “Perfluoroalkyl substances assessment in drinking waters from Brazil, France and Spain,” *Sci. Total Environ.*, vol. 539, pp. 143–152, 2016.

- [33] S. Castiglioni *et al.*, “Sources and fate of perfluorinated compounds in the aqueous environment and in drinking water of a highly urbanized and industrialized area in Italy,” *J. Hazard. Mater.*, vol. 282, pp. 51–60, 2015.
- [34] E. F. Houtz, C. P. Higgins, J. A. Field, and D. L. Sedlak, “Persistence of perfluoroalkyl acid precursors in AFFF-impacted groundwater and soil,” *Environ. Sci. Technol.*, vol. 47, no. 15, pp. 8187–8195, 2013.
- [35] V. Boiteux *et al.*, “Analysis of 29 per- and polyfluorinated compounds in water, sediment, soil and sludge by liquid chromatography-tandem mass spectrometry,” *Int. J. Environ. Anal. Chem.*, vol. 96, no. 8, pp. 705–728, 2016.
- [36] M. M. Schultz, D. F. Barofsky, and J. A. Field, “Quantitative Determination of Fluorotelomer Sulfonates in Groundwater by LC MS/MS,” *Environ. Sci. Technol.*, vol. 38, no. 6, pp. 1828–1835, 2004.
- [37] C. A. Moody and J. A. Field, “Determination of Perfluorocarboxylates in Groundwater Impacted by Fire-Fighting Activity Determination of Perfluorocarboxylates in Groundwater Impacted by Fire-Fighting Activity,” *Environ. Sci. Technol.*, vol. 33, no. 16, pp. 2800–2806, 1999.
- [38] H. Hamid, L. Y. Li, and J. R. Grace, “Review of the fate and transformation of per- and polyfluoroalkyl substances (PFASs) in landfills,” *Environ. Pollut.*, vol. 235, pp. 74–84, 2018.
- [39] J. Thompson *et al.*, “Removal of PFOS, PFOA and other perfluoroalkyl acids at water reclamation plants in South East Queensland Australia,” *Chemosphere*, vol. 82, no. 1, pp. 9–17, 2011.
- [40] S. Fujii, C. Polprasert, S. Tanaka, N. P. H. Lien, and Y. Qiu, “New POPs in the water environment: Distribution, bioaccumulation and treatment of perfluorinated compounds - A review paper,” *J. Water Supply Res. Technol. - AQUA*, vol. 56, no. 5, pp. 313–326, 2007.
- [41] P. Grandjean, E. Andersen, and E. Budtz-Jørgensen, “Serum vaccine antibody concentrations in children exposed to perfluorinated compounds,” *JAMA*, vol. 307, no. 4, pp. 391–397, 2012.
- [42] M. P. Velez, T. E. Arbuckle, and W. D. Fraser, “Maternal exposure to perfluorinated chemicals and reduced fecundity: the MIREC study,” *Hum. Reprod.*, vol. 30, no. 3, pp. 701–709, 2015.
- [43] E. C. Bonefeld-Jørgensen *et al.*, “Perfluorinated compounds are related to breast cancer risk in Greenlandic Inuit: A case control study,” *Environ. Heal.*, vol. 10, p. 88, 2011.

- [44] The European Commission, “Directive 2013/39/EU of the European Parliament and of the council, amending Directives 2000/60/EC and 2008/105/EC as regards priority substances in the field of water policy,” 2013.
- [45] USEPA, “Drinking Water Health Advisories for PFOA and PFOS,” 2016. [Online]. Available: <https://www.epa.gov/ground-water-and-drinking-water/drinking-water-health-advisories-pfoa-and-pfos>. [Accessed: 16-Mar-2018].
- [46] L. Gobelius *et al.*, “Per- and Polyfluoroalkyl Substances in Swedish Groundwater and Surface Water: Implications for Environmental Quality Standards and Drinking Water Guidelines,” *Environ. Sci. Technol.*, vol. 52, no. 7, pp. 4340–4349, 2018.
- [47] L. Ahrens and M. Bundschuh, “Fate and effects of poly- and perfluoroalkyl substances in the aquatic environment: A review,” *Environ. Toxicol. Chem.*, vol. 33, no. 9, pp. 1921–1929, 2014.
- [48] Z. Wang, I. T. Cousins, M. Scheringer, and K. Hungerbühler, “Fluorinated alternatives to long-chain perfluoroalkyl carboxylic acids (PFCAs), perfluoroalkane sulfonic acids (PFASs) and their potential precursors,” *Environ. Int.*, vol. 60, no. 2013, pp. 242–248, 2013.
- [49] L. A. D’Agostino and S. A. Mabury, “Aerobic biodegradation of two fluorotelomer sulfonamide-based Aqueous Film Forming Foam components produces perfluoroalkyl carboxylates,” *Environ. Toxicol. Chem.*, vol. 36, no. 8, pp. 2012–2021, 2017.
- [50] S. Brendel, É. Fetter, C. Staude, L. Vierke, and A. Biegel-Engler, “Short-chain perfluoroalkyl acids: environmental concerns and a regulatory strategy under REACH,” *Environ. Sci. Eur.*, vol. 30, no. 1, p. 9, 2018.
- [51] Z. Wang, I. T. Cousins, M. Scheringer, and K. Hungerbuehler, “Hazard assessment of fluorinated alternatives to long-chain perfluoroalkyl acids (PFAAs) and their precursors: Status quo, ongoing challenges and possible solutions,” *Environ. Int.*, vol. 75, pp. 172–179, 2015.
- [52] O. S. Arvaniti and A. S. Stasinakis, “Review on the occurrence, fate and removal of perfluorinated compounds during wastewater treatment,” *Sci. Total Environ.*, vol. 524–525, pp. 81–92, 2015.
- [53] Z. Du *et al.*, “Adsorption behavior and mechanism of perfluorinated compounds on various adsorbents—A review,” *J. Hazard. Mater.*, vol. 274, pp. 443–454, 2014.
- [54] I. Ross *et al.*, “A review of emerging technologies for remediation of PFASs,”

- Remediat. J.*, vol. 28, no. 2, pp. 101–126, 2018.
- [55] F. Li *et al.*, “Short-chain Per- and Polyfluoroalkyl Substances in Aquatic Systems: Occurrence, Impacts and Treatment,” *Chem. Eng. J.*, vol. 380, no. June 2019, p. 122506, 2019.
- [56] T. Pancras, G. Schrauwen, T. Held, K. Baker, I. Ross, and H. Slenders, “Environmental fate and effects of poly- and perfluoroalkyl substances (PFAS),” 2016.
- [57] E. Steinle-Darling and M. Reinhard, “Nanofiltration for trace organic contaminant removal: Structure, solution, and membrane fouling effects on the rejection of perfluorochemicals,” *Environ. Sci. Technol.*, vol. 42, no. 14, pp. 5292–5297, 2008.
- [58] C. Y. Tang, Q. S. Fu, A. P. Robertson, C. S. Criddle, and J. O. Leckie, “Use of Reverse Osmosis Membranes to Remove Perfluorooctane Sulfonate (PFOS) from Semiconductor Wastewater,” *Environ. Sci. Technol.*, vol. 40, no. 23, pp. 7343–7349, Dec. 2006.
- [59] Z. Pan *et al.*, “Membrane technology coupled with electrochemical advanced oxidation processes for organic wastewater treatment: recent advances and future prospects,” *Chem. Eng. J.*, 2019.
- [60] T. A. Bruton and D. L. Sedlak, “Treatment of Aqueous Film-Forming Foam by Heat-Activated Persulfate under Conditions Representative of in Situ Chemical Oxidation,” *Environ. Sci. Technol.*, vol. 51, no. 23, pp. 13878–13885, 2017.
- [61] K. Serrano, P. A. Michaud, C. Comninellis, and A. Savall, “Electrochemical preparation of peroxodisulfuric acid using boron doped diamond thin film electrodes,” *Electrochim. Acta*, vol. 48, no. 4, pp. 431–436, 2002.
- [62] B. Gomez-Ruiz, P. Ribao, N. Diban, M. J. Rivero, I. Ortiz, and A. Urriaga, “Photocatalytic degradation and mineralization of perfluorooctanoic acid (PFOA) using a composite TiO₂-rGO catalyst,” *J. Hazard. Mater.*, vol. 344, pp. 950–957, 2018.
- [63] T. Shao, P. Zhang, L. Jin, and Z. Li, “Photocatalytic decomposition of perfluorooctanoic acid in pure water and sewage water by nanostructured gallium oxide,” *Appl. Catal. B Environ.*, vol. 142–143, pp. 654–661, 2013.
- [64] J. Niu, Y. Li, E. Shang, Z. Xu, and J. Liu, “Electrochemical oxidation of perfluorinated compounds in water,” *Chemosphere*, vol. 146, pp. 526–538, 2016.
- [65] A. Urriaga, C. Fernández-González, S. Gómez-Lavín, and I. Ortiz, “Kinetics of the electrochemical mineralization of perfluorooctanoic acid on ultrananocrystalline boron doped conductive diamond electrodes,” *Chemosphere*, vol. 129, pp. 20–26,

- 2015.
- [66] B. Gomez-Ruiz *et al.*, “Efficient electrochemical degradation of poly- and perfluoroalkyl substances (PFASs) from the effluents of an industrial wastewater treatment plant,” *Chem. Eng. J.*, vol. 322, pp. 196–204, 2017.
- [67] A. Kapałka, G. Fóti, and C. Comninellis, “Basic Principles of the Electrochemical Mineralization of Organic Pollutants for Wastewater Treatment,” in *Electrochemistry for the Environment*, C. Comninellis and G. Chen, Eds. New York, NY: Springer New York, 2010, pp. 1–23.
- [68] A. M. Urriaga, R. Ibañez, M. J. Rivero, and I. Ortiz, “Integration of Electrochemical Advanced Oxidation With Membrane Separation and Biodegradation,” *Electrochem. Water Wastewater Treat.*, pp. 495–510, 2018.
- [69] C. Comninellis, “Electrocatalysis in the electrochemical conversion/ combustion of organic pollutants for waste water treatment.,” *Electrochim. Acta*, vol. 39, no. 11–12, pp. 1857 – 1862, 1994.
- [70] C. Zhang, L. Wang, J. Li, P. Su, and C. Peng, “Removal of perfluorinated compounds in wastewater treatment plant effluents by electrochemical oxidation,” *Water Sci. Technol.*, vol. 71, no. 12, pp. 1783–1789, 2015.
- [71] C. A. C. A. Martínez-Huitle, M. A. M. A. Rodrigo, I. Sirés, and O. Scialdone, “Single and Coupled Electrochemical Processes and Reactors for the Abatement of Organic Water Pollutants: A Critical Review,” *Chem. Rev.*, vol. 115, no. 24, pp. 13362–13407, 2015.
- [72] J. Radjenovic and D. L. Sedlak, “Challenges and Opportunities for Electrochemical Processes as Next-Generation Technologies for the Treatment of Contaminated Water,” *Environ. Sci. Technol.*, vol. 49, no. 19, pp. 11292–11302, 2015.
- [73] M. Panizza, P. A. Michaud, G. Cerisola, and C. Comninellis, “Anodic oxidation of 2-naphthol at boron-doped diamond electrodes,” *J. Electroanal. Chem.*, vol. 507, no. 1, pp. 206–214, 2001.
- [74] H. T. Madsen, E. G. Søgaaard, and J. Muff, “Reduction in energy consumption of electrochemical pesticide degradation through combination with membrane filtration,” *Chem. Eng. J.*, vol. 276, pp. 358–364, 2015.
- [75] A. Anglada, D. Ortiz, A. M. Urriaga, and I. Ortiz, “Electrochemical oxidation of landfill leachates at pilot scale: Evaluation of energy needs,” *Water Sci. Technol.*, vol. 61, no. 9, pp. 2211–2217, 2010.
- [76] C. Fang, M. Megharaj, and R. Naidu, “Electrochemical Advanced Oxidation

- Processes (EAOP) to degrade per- and polyfluoroalkyl substances (PFASs),” *J. Adv. Oxid. Technol.*, vol. 0, no. 0, 2017.
- [77] M. Panizza and G. Cerisola, “Direct and mediated anodic oxidation of organic pollutants,” *Chem. Rev.*, vol. 109, no. 12, 2009.
- [78] A. Anglada, A. Urtiaga, and I. Ortiz, “Contributions of electrochemical oxidation to waste-water treatment: Fundamentals and review of applications,” *J. Chem. Technol. Biotechnol.*, vol. 84, no. 12, pp. 1747–1755, 2009.
- [79] O. Simond *et al.*, “Modeling of wastewater electro-oxidation processes part II. Application to active electrodes,” *Electrochim. Acta*, vol. 43, no. 4, pp. 13362–13407, 2009.
- [80] I. Sirés, E. Brillas, M. A. Oturan, M. A. Rodrigo, and M. Panizza, “Electrochemical advanced oxidation processes: Today and tomorrow. A review,” *Environ. Sci. Pollut. Res.*, vol. 21, no. 14, pp. 8336–8367, 2014.
- [81] Á. Anglada, “Eliminación de amoníaco y materia orgánica de lixiviados de vertedero mediante electro-oxidación en ánodos de diamante dopado con boro,” Universidad de Cantabria, 2011.
- [82] B. Marselli, J. Garcia-Gomez, P.-A. Michaud, M. A. Rodrigo, and C. Comninellis, “Electrogeneration of Hydroxyl Radicals on Boron-Doped Diamond Electrodes,” *J. Electrochem. Soc.*, vol. 150, no. 3, p. D79, 2003.
- [83] B. P. Chaplin, “Critical review of electrochemical advanced oxidation processes for water treatment applications,” *Environ. Sci. Process. Impacts*, vol. 16, no. 6, pp. 1182–1203, 2014.
- [84] C. Comninellis, A. Kapalka, S. Malato, S. . Parsons, I. Poulios, and D. Mantzavinos, “Perspective Advanced oxidation processes for water treatment: advances and trends for R&D,” *J. Chem. Technol. Biotechnol.*, vol. 83, pp. 769–776, 2008.
- [85] F. Sopaj, M. A. Rodrigo, N. Oturan, F. I. Podvorica, J. Pinson, and M. A. Oturan, “Influence of the anode materials on the electrochemical oxidation efficiency. Application to oxidative degradation of the pharmaceutical amoxicillin,” *Chem. Eng. J.*, vol. 262, pp. 286–294, 2015.
- [86] M. Panizza and G. Cerisola, “Electrochemical oxidation of 2-naphthol with in situ electrogenerated active chlorine,” *Electrochim. Acta*, vol. 48, no. 11, pp. 1515–1519, 2003.
- [87] A. Anglada, A. Urtiaga, and I. Ortiz, “Pilot Scale Performance of the Electro-Oxidation of Landfill Leachate at Boron-Doped Diamond Anodes,” *Environ. Sci.*

- Technol.*, vol. 43, no. 6, pp. 2035–2040, Mar. 2009.
- [88] G. Pérez, J. Saiz, R. Ibañez, A. M. Urriaga, and I. Ortiz, “Assessment of the formation of inorganic oxidation by-products during the electrocatalytic treatment of ammonium from landfill leachates,” *Water Res.*, vol. 46, no. 8, pp. 2579–2590, 2012.
- [89] S. Garcia-Segura, J. Keller, E. Brillas, and J. Radjenovic, “Removal of organic contaminants from secondary effluent by anodic oxidation with a boron-doped diamond anode as tertiary treatment,” *J. Hazard. Mater.*, vol. 283, pp. 551–557, 2015.
- [90] J. Carrillo-Abad, V. Pérez-Herranz, and A. Urriaga, “Electrochemical oxidation of 6:2 fluorotelomer sulfonic acid (6:2 FTSA) on BDD: electrode characterization and mechanistic investigation,” *J. Appl. Electrochem.*, vol. 0, no. 0, p. 0, 2018.
- [91] J. Davis, J. C. Baygents, and J. Farrell, “Understanding persulfate production at boron doped diamond film anodes,” *Electrochim. Acta*, vol. 150, pp. 68–74, 2014.
- [92] H. Song *et al.*, “Electrochemical activation of persulfates at BDD anode: Radical or nonradical oxidation?,” *Water Res.*, vol. 128, pp. 393–401, 2018.
- [93] A. Cabeza, A. M. Urriaga, and I. Ortiz, “Electrochemical treatment of landfill leachates using a boron-doped diamond anode,” *Ind. Eng. Chem. Res.*, vol. 46, no. 5, pp. 1439–1446, 2007.
- [94] S. Liang, R. “David” Pierce, H. Lin, S.-Y. D. Chiang, and Q. “Jack” Huang, “Electrochemical oxidation of PFOA and PFOS in concentrated waste streams,” *Remediat. J.*, vol. 28, no. 2, pp. 127–134, 2018.
- [95] Y. He, H. Lin, Z. Guo, W. Zhang, H. Li, and W. Huang, “Recent developments and advances in boron-doped diamond electrodes for electrochemical oxidation of organic pollutants,” *Sep. Purif. Technol.*, vol. 212, no. December 2017, pp. 802–821, 2018.
- [96] J. H. T. Luong, K. B. Male, and J. D. Glennon, “Boron-doped diamond electrode: Synthesis, characterization, functionalization and analytical applications,” *Analyst*, vol. 134, no. 10, pp. 1965–1979, 2009.
- [97] P. A. Michaud, M. Panizza, L. Ouattara, T. Diaco, G. Foti, and C. Comninellis, “Electrochemical oxidation of water on synthetic boron-doped diamond thin film anodes,” *J. Appl. Electrochem.*, vol. 33, no. 2, pp. 151–154, 2003.
- [98] X. Chen and G. Chen, “Proper Hot Filament CVD Conditions for Fabrication of Ti-Boron Doped Diamond Electrodes,” *J. Electrochem. Soc.*, vol. 151, no. 4, p. B214, 2004.

- [99] H. Lin, J. Niu, S. Ding, and L. Zhang, "Electrochemical degradation of perfluorooctanoic acid (PFOA) by Ti/SnO₂-Sb, Ti/SnO₂-Sb/PbO₂ and Ti/SnO₂-Sb/MnO₂ anodes," *Water Res.*, vol. 46, no. 7, pp. 2281–2289, 2012.
- [100] K. E. Carter and J. Farrell, "Oxidative destruction of perfluorooctane sulfonate using boron-doped diamond film electrodes," *Environ. Sci. Technol.*, vol. 42, no. 16, pp. 6111–6115, 2008.
- [101] Z. Liao and J. Farrell, "Electrochemical oxidation of perfluorobutane sulfonate using boron-doped diamond film electrodes," *J. Appl. Electrochem.*, vol. 39, pp. 1993–1999, 2009.
- [102] T. Ochiai *et al.*, "Efficient electrochemical decomposition of perfluorocarboxylic acids by the use of a boron-doped diamond electrode," *Diam. Relat. Mater.*, vol. 20, no. 2, pp. 64–67, 2011.
- [103] Q. Zhuo *et al.*, "Degradation of perfluorinated compounds on a boron-doped diamond electrode," *Electrochim. Acta*, vol. 77, pp. 17–22, 2012.
- [104] B. Gomez-Ruiz, N. Diban, and A. Urriaga, "Comparison of microcrystalline and ultrananocrystalline boron doped diamond anodes: Influence on perfluorooctanoic acid electrolysis," *Sep. Purif. Technol.*, vol. 208, no. March, pp. 169–177, 2018.
- [105] B. Yang *et al.*, "Highly efficient electrochemical degradation of perfluorooctanoic acid (PFOA) by F-doped Ti/SnO₂ electrode," *J. Hazard. Mater.*, vol. 299, pp. 417–424, 2015.
- [106] Q. Zhuo, S. Deng, B. Yang, J. Huang, and G. Yu, "Efficient electrochemical oxidation of perfluorooctanoate using a Ti/SnO₂-Sb-Bi anode," *Environ. Sci. Technol.*, vol. 45, no. 7, pp. 2973–2979, 2011.
- [107] B. Yang *et al.*, "Electrochemical mineralization of perfluorooctane sulfonate by novel F and Sb co-doped Ti/SnO₂ electrode containing Sn-Sb interlayer," *Chem. Eng. J.*, vol. 316, pp. 296–304, 2017.
- [108] J. Niu, H. Lin, J. Xu, H. Wu, and Y. Li, "Electrochemical mineralization of perfluorocarboxylic acids (PFCAs) by Ce-doped modified porous nanocrystalline PbO₂ film electrode," *Environ. Sci. Technol.*, vol. 46, no. 18, pp. 10191–10198, 2012.
- [109] Z. Xu, Y. Yu, H. Liu, and J. Niu, "Highly efficient and stable Zr-doped nanocrystalline PbO₂ electrode for mineralization of perfluorooctanoic acid in a sequential treatment system," *Sci. Total Environ.*, vol. 579, pp. 1600–1607, 2017.
- [110] H. Lin *et al.*, "Highly efficient and mild electrochemical mineralization of long-chain perfluorocarboxylic acids (C₉-C₁₀) by Ti/SnO₂-Sb-Ce, Ti/SnO₂-Sb/Ce-

- PbO₂, and Ti/BDD electrodes,” *Environ. Sci. Technol.*, vol. 47, no. 22, pp. 13039–13046, 2013.
- [111] Q. Zhuo *et al.*, “Electrochemical oxidation of PFOA in aqueous solution using highly hydrophobic modified PbO₂ electrodes,” *J. Electroanal. Chem.*, vol. 801, no. July, pp. 235–243, 2017.
- [112] C. E. Schaefer, C. Andaya, A. Urriaga, E. R. McKenzie, and C. P. Higgins, “Electrochemical treatment of perfluorooctanoic acid (PFOA) and perfluorooctane sulfonic acid (PFOS) in groundwater impacted by aqueous film forming foams (AFFFs),” *J. Hazard. Mater.*, vol. 295, pp. 170–175, 2015.
- [113] Q. Zhuo, S. Deng, B. Yang, J. Huang, and G. Yu, “Efficient electrochemical oxidation of perfluorooctanoate using a Ti/SnO₂-Sb-Bi anode,” *Environ. Sci. Technol.*, vol. 45, no. 7, pp. 2973–2979, 2011.
- [114] Q. Zhuo *et al.*, “Electrochemical oxidation of 1H,1H,2H,2H-perfluorooctane sulfonic acid (6:2 FTS) on DSA electrode: Operating parameters and mechanism,” *J. Environ. Sci. (China)*, vol. 26, no. 8, pp. 1733–1739, 2014.
- [115] R. Singh, *Membrane Technology and Engineering for Water Purification*. 2015.
- [116] M. Mulder, *Basic Principles of Membrane Technology*, 2nd ed. Dordrecht: Kluwer Academic Publishers, 1996.
- [117] A. . Fane, R. Wang, and Y. Jia, “Membrane Technology: Past, Present and Future,” in *Membrane and Desalination Technologies*, L. K. Wang, P. Chen, Y.-T. Hung, and N. K. Shammam, Eds. Humana Press, 2011, pp. 1–38.
- [118] B. Van Der Bruggen, C. Vandecasteele, T. Van Gestel, W. Doyen, and R. Leysen, “A review of pressure-driven membrane processes in wastewater treatment and drinking water production,” *Environmental Progress*, vol. 22, no. 1. pp. 46–56, 2003.
- [119] L. W. Jye and A. F. Ismail, *Nanofiltration Membranes: synthesis, characterization, and application*. CRC Press, 2016.
- [120] Z. F. Cui, Y. Jiang, and R. W. Field, *Membrane Technology: A Practical Guide to Membrane Technology and Applications in Food and Bioprocessing*. 2010.
- [121] T. D. Appleman *et al.*, “Treatment of poly- and perfluoroalkyl substances in U.S. full-scale water treatment systems,” *Water Res.*, vol. 51, no. 0, pp. 246–255, 2014.
- [122] B. Van Der Bruggen and J. Geens, “Nanofiltration,” in *Advanced Membrane Technology and Applications*, New Jersey: John Wiley & Sons, Inc., 2008, pp. 271–295.
- [123] M. Nyström, L. Kaipia, and S. Luque, “Fouling and retention of nanofiltration

- membranes,” *J. Memb. Sci.*, vol. 98, no. 3, pp. 249–262, 1995.
- [124] X. L. Wang, T. Tsuru, S. I. Nakao, and S. Kimura, “The electrostatic and steric-hindrance model for the transport of charged solutes through nanofiltration membranes,” *J. Memb. Sci.*, vol. 135, no. 1, pp. 19–32, 1997.
- [125] A. Pérez-González, R. Ibáñez, P. Gómez, A. M. Urriaga, I. Ortiz, and J. A. Irabien, “Nanofiltration separation of polyvalent and monovalent anions in desalination brines,” *J. Memb. Sci.*, vol. 473, pp. 16–27, 2015.
- [126] P. Ortiz-albo, R. Ibáñez, A. Urriaga, and I. Ortiz, “Separation and Purification Technology Phenomenological prediction of desalination brines nanofiltration through the indirect determination of zeta potential,” *Sep. Purif. Technol.*, vol. 210, no. April 2018, pp. 746–753, 2019.
- [127] L. D. Nghiem, A. I. Schäfer, and M. Elimelech, “Role of electrostatic interactions in the retention of pharmaceutically active contaminants by a loose nanofiltration membrane,” *J. Memb. Sci.*, vol. 286, no. 1–2, pp. 52–59, 2006.
- [128] M. R. Teixeira, M. J. Rosa, and M. Nyström, “The role of membrane charge on nanofiltration performance,” *J. Memb. Sci.*, vol. 265, no. 1–2, pp. 160–166, 2005.
- [129] H. M. Krieg, S. J. Modise, K. Keizer, and H. W. J. P. Neomagus, “Salt rejection in nanofiltration for single and binary salt mixtures in view of sulphate removal,” *Desalination*, vol. 171, no. 2, pp. 205–215, 2005.
- [130] B. Van Der Bruggen, J. Schaep, D. Wilms, and C. Vandecasteele, “Influence of molecular size, polarity and charge on the retention of organic molecules by nanofiltration,” *J. Memb. Sci.*, vol. 156, no. 1, pp. 29–41, 1999.
- [131] R. Bergman, *Reverse Osmosis and Nanofiltration: Manual of Water Supply Practices M46*. 2007.
- [132] A. W. Mohammad, Y. H. Teow, W. L. Ang, Y. T. Chung, D. L. Oatley-Radcliffe, and N. Hilal, “Nanofiltration membranes review: Recent advances and future prospects,” *Desalination*, vol. 356, pp. 226–254, 2015.
- [133] F. Salehi, “Current and future applications for nanofiltration technology in the food processing,” *Food Bioprod. Process.*, vol. 92, no. 2, pp. 161–177, 2014.
- [134] A. Bhattacharya and P. Ghosh, “Nanofiltration and Reverse Osmosis Membranes: Theory and Application in Separation of Electrolytes,” *Rev. Chem. Eng.*, vol. 20, no. 1–2, pp. 111–173, 2004.
- [135] L. Braeken, R. Ramaekers, Y. Zhang, G. Maes, B. Van Der Bruggen, and C. Vandecasteele, “Influence of hydrophobicity on retention in nanofiltration of aqueous solutions containing organic compounds,” *J. Memb. Sci.*, vol. 252, no. 1–

- 2, pp. 195–203, 2005.
- [136] I. Vergili, “Application of nanofiltration for the removal of carbamazepine, diclofenac and ibuprofen from drinking water sources,” *J. Environ. Manage.*, vol. 127, pp. 177–187, 2013.
- [137] S.-D. D. Eva, L. Eric, and R. Martin, “Effects of sorption on the rejection of trace organic contaminants during nanofiltration,” *Environ. Sci. Technol.*, vol. 44, no. 7, pp. 2592–2598, 2010.
- [138] C. Bellona, J. E. Drewes, P. Xu, and G. Amy, “Factors affecting the rejection of organic solutes during NF/RO treatment - A literature review,” *Water Res.*, vol. 38, no. 12, pp. 2795–2809, 2004.
- [139] S. J. Judd, “Membrane technology costs and me,” *Water Res.*, vol. 122, pp. 1–9, 2017.
- [140] C. Y. Tang, Y. N. Kwon, and J. O. Leckie, “Fouling of reverse osmosis and nanofiltration membranes by humic acid-Effects of solution composition and hydrodynamic conditions,” *J. Memb. Sci.*, vol. 290, no. 1–2, pp. 86–94, 2007.
- [141] F. fang Chang, W. jun Liu, and X. mao Wang, “Comparison of polyamide nanofiltration and low-pressure reverse osmosis membranes on As(III) rejection under various operational conditions,” *Desalination*, vol. 334, no. 1, pp. 10–16, 2014.
- [142] A. Urriaga, G. Pérez, R. Ibáñez, and I. Ortiz, “Removal of pharmaceuticals from a WWTP secondary effluent by ultrafiltration/reverse osmosis followed by electrochemical oxidation of the RO concentrate,” *Desalination*, vol. 331, pp. 26–34, 2013.
- [143] G. Pérez, A. R. Fernández-Alba, A. M. Urriaga, and I. Ortiz, “Electro-oxidation of reverse osmosis concentrates generated in tertiary water treatment,” *Water Res.*, vol. 44, no. 9, pp. 2763–2772, 2010.
- [144] H. T. Madsen and E. G. Søgaard, “Applicability and modelling of nanofiltration and reverse osmosis for remediation of groundwater polluted with pesticides and pesticide transformation products,” *Sep. Purif. Technol.*, vol. 125, pp. 111–119, 2014.
- [145] S. Kim *et al.*, “Removal of contaminants of emerging concern by membranes in water and wastewater: A review,” *Chem. Eng. J.*, vol. 335, no. September 2017, pp. 896–914, 2018.
- [146] P. Kanchanalai, R. P. Lively, M. J. Realff, and Y. Kawajiri, “Cost and energy savings using an optimal design of reverse osmosis membrane pretreatment for

- dilute bioethanol purification,” *Ind. Eng. Chem. Res.*, vol. 52, no. 32, pp. 11132–11141, 2013.
- [147] C. Y. Tang, Q. S. Fu, C. S. Criddle, and J. O. Leckie, “Effect of Flux (Transmembrane Pressure) and Membrane Properties on Fouling and Rejection of Reverse Osmosis and Nanofiltration Membranes Treating Perfluorooctane Sulfonate Containing Wastewater,” *Environmental Science & Technology*, vol. 41, no. 6. American Chemical Society, pp. 2008–2014, 2007.
- [148] C. Zhao, J. Zhang, G. He, T. Wang, D. Hou, and Z. Luan, “Perfluorooctane sulfonate removal by nanofiltration membrane the role of calcium ions,” *Chem. Eng. J.*, vol. 233, no. 0, pp. 224–232, 2013.
- [149] X. Chen, H. Ozaki, R. R. Giri, S. Taniguchi, and R. Takanami, “Low-pressure reverse osmosis membrane separation of non-fluorinated and perfluorinated organic compounds in water,” *Desalin. Water Treat.*, vol. 52, no. 31–33, pp. 5796–5805, 2014.
- [150] P. Lipp, F. Sacher, and G. Baldauf, “Removal of organic micro-pollutants during drinking water treatment by nanofiltration and reverse osmosis,” *Desalin. Water Treat.*, vol. 13, no. 1–3, pp. 226–237, 2010.
- [151] R. Rattanaoudom and C. Visvanathan, “Removal of PFOA by hybrid membrane filtration using PAC and hydrotalcite,” *Desalin. Water Treat.*, vol. 32, no. 1–3, pp. 262–270, 2011.
- [152] X. Hang, X. Chen, J. Luo, W. Cao, and Y. Wan, “Removal and recovery of perfluorooctanoate from wastewater by nanofiltration,” *Sep. Purif. Technol.*, vol. 145, pp. 120–129, 2015.
- [153] T. Wang, C. Zhao, P. Li, Y. Li, and J. Wang, “Fabrication of novel poly(m-phenylene isophthalamide) hollow fiber nanofiltration membrane for effective removal of trace amount perfluorooctane sulfonate from water,” *J. Memb. Sci.*, vol. 477, no. 0, pp. 74–85, Jan. 2015.
- [154] J. Wang *et al.*, “Perfluorooctane sulfonate and perfluorobutane sulfonate removal from water by nanofiltration membrane: The roles of solute concentration, ionic strength, and macromolecular organic foulants,” *Chem. Eng. J.*, vol. 332, pp. 787–797, 2018.
- [155] T. Fujioka *et al.*, “N-nitrosamine rejection by nanofiltration and reverse osmosis membranes: The importance of membrane characteristics,” *Desalination*, vol. 316, pp. 67–75, 2013.
- [156] A. Y. Bagastyo, D. J. Batstone, I. Kristiana, W. Gernjak, C. Joll, and J. Radjenovic,

- “Electrochemical oxidation of reverse osmosis concentrate on boron-doped diamond anodes at circumneutral and acidic pH,” *Water Res.*, vol. 46, no. 18, pp. 6104–6112, 2012.
- [157] J. Radjenovic, A. Bagastyo, R. A. Rozendal, Y. Mu, J. Keller, and K. Rabaey, “Electrochemical oxidation of trace organic contaminants in reverse osmosis concentrate using RuO₂/IrO₂-coated titanium anodes,” *Water Res.*, vol. 45, no. 4, pp. 1579–1586, 2011.
- [158] G. Pérez, P. Gómez, R. Ibañez, I. Ortiz, and A. M. Urtiaga, “Electrochemical disinfection of secondary wastewater treatment plant (WWTP) effluent,” *Water Sci. Technol.*, vol. 62, no. 4, pp. 892–897, 2010.

2. Materials and methods

This chapter briefly discusses the materials, experimental, modelling and optimization methods used in this thesis. More detailed information can be found in the scientific publications gathered in Chapter 5 of the present thesis document.

2.1. Chemicals

The main chemical reagents used in this thesis are summarized in Table 2.1. All chemicals were reagent grade or higher. All solutions were prepared using ultrapure water (Milli-Q, Millipore).

Table 2.1. List of the chemicals used for the experimental work.

Reagent	Abbreviation	Formula	Supplier
Perfluorobutanoic acid	PFBA	$C_4HF_7O_2$	Sigma-Aldrich
Perfluoropentanoic acid	PFPeA	$C_5HF_9O_2$	Sigma-Aldrich
Perfluorohexanoic acid	PFHxA	$C_6HF_{11}O_2$	Sigma-Aldrich
Perfluoroheptanoic acid	PFHpA	$C_7HF_{13}O_2$	Sigma-Aldrich
6:2 Fluorotelomer sulfonic acid	6:2 FTSA	$C_8H_4F_{13}SO_3^-$	Synquest laboratories
6:2 Fluorotelomer sulfonic acid aqueous solution (CAPSTONE FS-10®)		$C_8H_4F_{13}SO_3^-$	Chemours
Calcium sulfate dyhydrate		$CaSO_4 \cdot 2H_2O$	Scharlau
Sodium sulfate		Na_2SO_4	Panreac
Sodium perchlorate		$NaClO_4$	Panreac
Sodium chloride		$NaCl$	Panreac
Sodium carbonate		Na_2CO_3	Merck Millipore
Sodium hydroxide		$NaOH$	Panreac
Hydrochloric acid		HCl	Panreac
Methanol (UHPLC-MS)		CH_3OH	Scharlau

2.2. Nanofiltration/reverse osmosis experiments

2.2.1. Feed water composition

Different feed water compositions were used for experiments with nanofiltration and reverse osmosis membranes: i) real industrial process water; and ii) synthetic aqueous solutions. The nature of the different feed water solutions is described with more detail below.

Real industrial process water. Two different process water samples were received from an industrial fluoropolymer manufacturer, located in France. Both samples were taken just before the PFHxA collecting facility that removes the contaminant before the general wastewater treatment that is applied at the industrial plant. Table 2.2 summarizes the chemical characterization of the two samples (from now on referred as S1 and S2). PFHxA in S1 sample was three times more concentrated than in S2 sample. Some common inorganic salts were also present. No other PFASs were detected by the HPLC-DAD technique used.

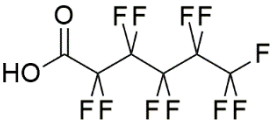
Synthetic aqueous solutions. Model solutions emulating the real industrial effluents described above with PFHxA concentration which ranged from 100 mg L⁻¹ to 500 mg L⁻¹ in aqueous solutions with or without dissolved salts. PFHxA model solutions with salts were prepared with the following salt content: 36 mg L⁻¹ of NaCl, 575 mg L⁻¹ of CaSO₄, and 98 mg L⁻¹ of NaHCO₃.

Table 2.3 shows the characteristics of PFHxA relevant to this work.

Table 2.2. Physico-chemical characterization of the industrial process waters used in membrane separation experiments

Parameter	Units	S1	S2
PFHxA	mg L ⁻¹	204	64
TOC	mg L ⁻¹	82	24
pH	-	7.7	7.4
Conductivity	mS cm ⁻¹	1.05	1.02
Chloride	mg L ⁻¹	19.8	16.9
Sulfate	mg L ⁻¹	321	360
Bicarbonate	mg L ⁻¹	98	92
Calcium	mg L ⁻¹	172	171
Sodium	mg L ⁻¹	24.9	28.7

Table 2.3. Selected PFHxA characteristics.

Perfluorohexanoic acid (PFHxA)	
Molecular formula	C ₆ HF ₁₁ O ₂
Molecular structure	
Molar mass (g mol ⁻¹)	314.05
Molecular length (nm)	1.184 ^a
Molecular width (nm)	0.415 ^a
Stokes radius at 20°C (nm)	0.349 ^b
<i>pK_a</i>	-0.16 [6]
<i>D</i> _{PFHxA} at 20°C (m ² s ⁻¹)	6.2 × 10 ⁻¹⁰ ^c

^a The molecular width was estimated using the procedure described by Kiso and coworkers [19].

^b Estimated using the Stokes–Einstein equation [20].

^c The Wilke–Chang equation [21] was used to estimate the PFHxA diffusion coefficient in water.

2.2.2. Commercial nanofiltration and reverse osmosis membranes

Three aromatic polyamide RO membranes (XLE, BW30, and SW30XLE) and four NF membranes (NF90, NF270, ESNA-LF and ESNA-LF2) were used throughout this thesis work. All the membranes have thin film composite (TFC) structures with a flat sheet configuration. A summary of the membrane characteristics reported in the literature and technical data sheets is shown in Table 2.4. The static contact angle of water on different membrane samples was determined using contact angle goniometry and the drop contact angle was captured immediately after drop deposition; measurements were repeated using three different samples for each membrane type. Finally, the contact angle was measured from the images shown in Figure 2.1, captured by using Meazure© 2.0 software (C Thing Software 2001–2004, US).

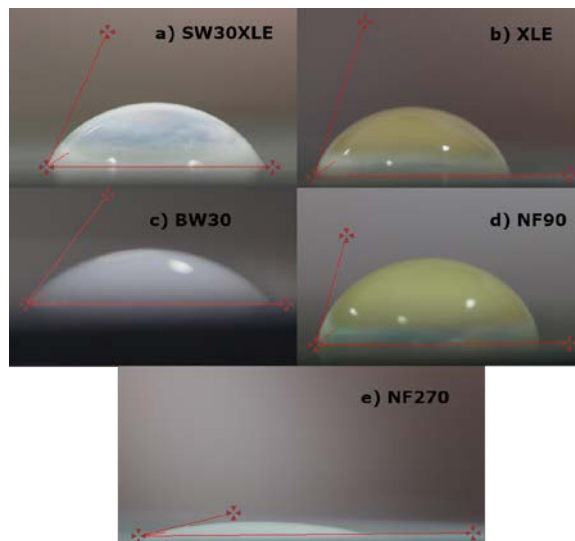


Figure 2.1. Captured images for measurement of contact angle of different nanofiltration and reverse osmosis membranes.

Table 2.4. Characteristics of the membranes used in this thesis

	NF270	NF90	XLE	SW30XLE	BW30	ESNA-LF	ESNA-LF2
Manufacturer	Dow Filmtec	Dow Filmtec	Dow Filmtec	Dow Filmtec	Dow Filmtec	Hydranautics	Hydranautics
Top layer	Semi-aromatic piperazine-based polyamide[1]	Full aromatic polyamide[1]	Full aromatic polyamide[2]	Full aromatic polyamide[3]	Full aromatic polyamide [4]	Meta-phenylene diamine TFC [5]	Meta-phenylene diamine TFC [6]
Molecular weight cut off (MWCO, Da)	300 [6]	100-200[6]	100[7]	<100[8]	98[9]	200 [10]	200 [11]
Contact angle (°)	14.4±0.8	73.5±1.9 63.2[7]	67.2±4.6	61.4±4.6 67.5±5.0[12]	43.7±10.0	60 ± 6.2 [13]	32±5 [11]
Active layer thickness (nm)	21 ± 2.4[14] 29 ± 4[15]	≈ 200[14], [16]	n.a.	n.a.	≈ 200[14], [17]	223 ± 37 [13]	n.a
Isoelectric point (mV)	≈3.5 ^a [18]	4.2 ^b [4]	≈4.4 ^a [2]	3.1 ^c [19]	4.3 ^b [4]	4.9 [5]	≈4 [20]
Zeta potential at neutral pH (mV)	≈-30 ^a [18]	≈-25 ^b [4]	≈-30 ^a [2]	≈-15 ^c [19]	≈-10 ^b [4]	-11.5 [13]	-22.7 [20]

n.a.: not available

^a *Electrolyte: NaCl 10 mM*

^b *Electrolyte: NaCl 20 mM and NaHCO₃ 1 mM*

^c *Electrolyte: KCl 10*

2.2.3. Experimental set-up

Figure 2.2 shows a schematic illustration describing the basic laboratory-scale filtration set-up used throughout the experimental runs. The flat-sheet membrane coupons were housed in a rectangular crossflow test cell (SEPA-CF, GE Osmonics) with an effective membrane area of 155 cm², a channel width of 9.5 cm, and a channel height of 1.7 mm. A hydraulic hand pump (LARZEP W00607) was used to keep the cell holder closed. The feed solution was maintained at constant temperature in a jacketed tank connected to a refrigeration system (Julabo F25-ME). The feed was circulated using a variable-speed diaphragm pump (Hydra-Cell D-03). The operating pressure was adjusted via a back-pressure valve (Swagelok, 0–40 bar) placed at the retentate port.

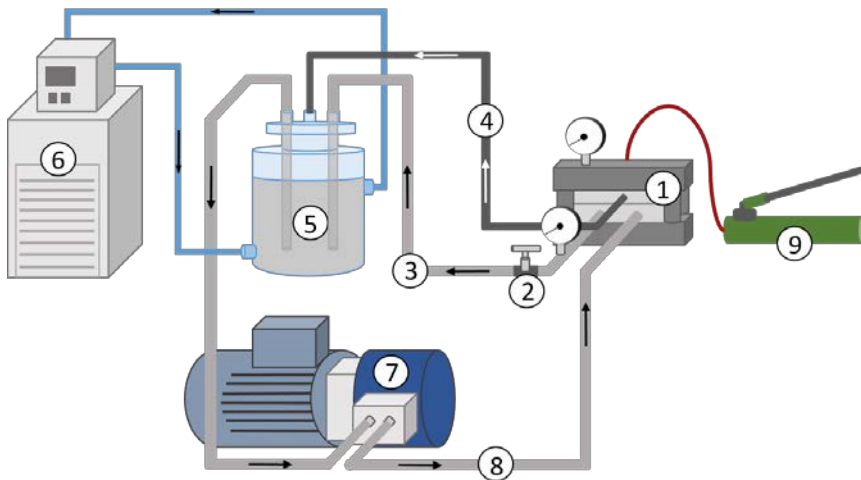


Figure 2.2. Nanofiltration/reverse osmosis experimental system working in total recirculation mode. 1: Crossflow test cell, 2: Back-pressure valve, 3: Retentate stream, 4: Permeate stream, 5: Feed tank, 6: Refrigerated circulator, 7: Diaphragm pump, 8: Feed stream, 9: Hydraulic hand pump.

2.2.4. Operation protocol

Prior to all experiments, new membrane coupons were soaked in ultrapure water for 24 – 48 h to hydrate them and remove impurities. Two distinct operation modes were used in the NF/RO experiments: (i) total recirculation experiments and (ii) concentration mode experiments. Figure 2.3 shows a schematic representation of the NF/RO operation modes.

Total recirculation experiments. The aim of this type of experiment is to characterize the membrane in terms of membrane rejection of different solutes and water permeability. The feed reservoir was maintained at atmospheric pressure at $20^{\circ}\text{C} \pm 0.1^{\circ}\text{C}$ and the membrane feed side operating liquid pressure was set at 20, 10, 5, or 2.5 bar. The permeate flux was continuously measured to ensure steady-state fluxes. Both the retentate and the permeate streams were recycled to the feed tank so that the feed concentration always remained constant.

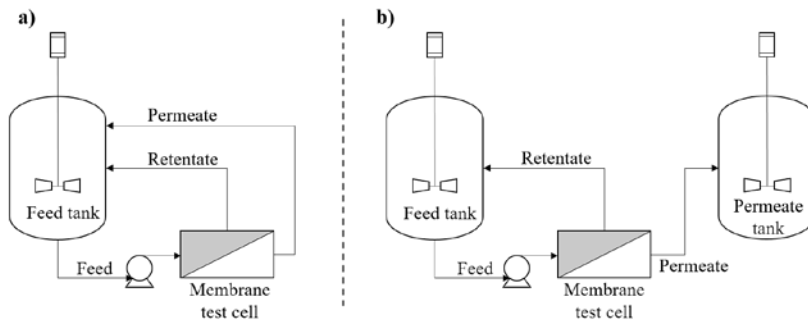


Figure 2.3. Operation modes used in NF/RO experiments: a) total recirculation mode, b) concentration mode

Concentration mode experiments. In this kind of operation mode, only the retentate stream was recycled to the feed tank. The permeate stream was collected in a separated tank. Therefore, the PFHxA concentration in the feed side continuously increased throughout the experimental run. Experiments were conducted until a volume reduction factor (VRF) of 5 (in experiments with industrial process waters) and 10 (experiments with AFFFs impacted simulated groundwater) was achieved. VRF is defined as the ratio between the initial feed volume and the final feed volume [21]. In all concentration mode experiments, the operation pressure was fixed at 10 bar.

2.2.5. Calculation of membrane performance parameters

The volumetric permeate flux (J_v , L m⁻² h⁻¹) through the membrane was determined from the permeate flowrate (Q_p , L h⁻¹) and the membrane area, as follows,

$$J_v = \frac{Q_p}{A} \quad (2.1)$$

Based on Darcy's law, the volumetric permeate flux can be related to the trans-membrane pressure (ΔP , bar) and the osmotic pressure gradient ($\Delta\pi$, bar) between the feed and the permeate [22]:

$$J_v = L_p(\Delta P - \Delta\pi) \quad (2.2)$$

where L_p is the hydraulic permeability (L m⁻² h⁻¹ bar⁻¹) which is empirically determined from the slope of the plot of the permeate flux versus the effective pressure gradient. The osmotic pressure of the solutions was calculated from the concentration of the dissolved salts [23].

The observed solute rejection (R_{obs}) was calculated as follows,

$$R_{obs,i}(\%) = \left(1 - \frac{C_{p,i}}{C_{f,i}}\right) \times 100 \quad (2.3)$$

where $C_{p,i}$ and $C_{f,i}$ are the solute i concentrations in the permeate and in the feed (mg L^{-1}), respectively.

The high retention of species promotes the accumulation of solute at the membrane surface. Because of the low diffusivity of the retained solutes in the membrane, solutes diffuse back from the boundary layer to the bulk solution. An equilibrium is then reached between the convective transport towards the membrane and the counter-flow diffusion of solute. This is the so-called concentration polarization phenomena, which can be expressed by the following steady-state, one-dimensional mass balance, based on the film theory:

$$J_v C_i - D_i \frac{dC_i}{dx} = J_v C_{p,i} \quad (2.4)$$

where C_i is the solute i concentration and D_i is the solute i diffusivity in water ($\text{m}^2 \text{s}^{-1}$). This equation can be integrated for a finite thickness boundary layer (δ), which gives the following expression:

$$\frac{C_{m,i} - C_{p,i}}{C_{f,i} - C_{p,i}} = \exp\left(\frac{J_v}{k_i}\right) \quad (2.5)$$

being $C_{m,i}$ the concentration at the membrane surface and k_i (m s^{-1}) the mass transfer coefficient. Because of concentration polarization, $C_{m,i}$ is much higher than the concentration in the bulk $C_{f,i}$. This means that the intrinsic

membrane rejection ($R_{int,i}$) is higher than the observed rejection (R_{obs}). The calculation of $R_{int,i}$ is useful for the determination of membrane characteristics. However, $C_{m,i}$ is not directly measurable. Thus, Eq. (2.5) can be expressed in terms of $R_{obs,i}$ and $R_{int,i}$ as follows:

$$\ln\left(\frac{1 - R_{obs,i}}{R_{obs,i}}\right) = \ln\left(\frac{1 - R_{int,i}}{R_{int,i}}\right) + \frac{J_v}{k_i} \quad (2.6)$$

which can be solved for $R_{int,i}$, to obtain the following expression which relates the intrinsic and the observed rejection:

$$R_{int,i} = \frac{R_{obs,i} \exp\left(\frac{J_v}{k_i}\right)}{1 + R_{obs,i} \left[\exp\left(\frac{J_v}{k_i}\right) - 1 \right]} \quad (2.7)$$

The mass transfer coefficient (m s^{-1}) for solute i in the feed side boundary layer was calculated using a correlation for laminar flow through rectangular closed channels [24]:

$$Sh = \frac{2hk}{D_{AB}} = 0.664 \cdot Re^{0.5} Sc^{0.33} \left(\frac{2h}{L}\right)^{0.33} \quad (2.8)$$

where Sh , Re , and Sc are the Sherwood, Reynolds, and Schmidt numbers, respectively; h is the membrane test cell channel height (1.7 mm) and L is the length of the path that follows the fluid inside the membrane test cell (0.13 m). D_{AB} is the diffusion coefficient of the species in water ($\text{m}^2 \text{s}^{-1}$). The diffusion coefficients reported by Samson and coworkers [25] were applied for the ionic species (sulfate, calcium, sodium, and chloride). In

the case of PFHxA, the Wilke-Chang equation [26] was used to estimate its diffusion coefficient in water, $D_{PFHxA,w}=7.05\times 10^{-10}$ m² s⁻¹, at 25°C.

2.3. Electrochemical oxidation experiments

2.3.1. Feed water composition

Different types of water matrixes were used as feed when conducting electrochemical oxidation experiments:

- Concentrates from NF experiments with high concentrations of PFHxA. The nature of these real industrial process waters was discussed in section 2.2 and the initial physico-chemical characterization (before pre-concentration by NF) is shown in Table 2.2. The PFHxA concentration in the NF concentrated S1 sample was 870 mg L⁻¹ and in the NF concentrated sample S2 (corresponding to VRF=5) was 344 mg L⁻¹. More details on the salts composition of concentrated S1 and S2 samples can be found in Chapter 5.
- Synthetic PFHxA solutions emulating the NF concentrates of real industrial process waters, with concentrations as described above.
- 6:2 FTSA aqueous solutions (100 mg L⁻¹), in experiments evaluating the electrochemical oxidation of this compound. In experiments that aimed to assess the influence of the supporting electrolyte in the electrooxidation of 6:2 FTSA, three electrolytes were tested: Na₂SO₄ (5 g L⁻¹), NaCl (3.5 g L⁻¹) and NaClO₄ (9.4 g L⁻¹), with similar background conductivity (6.9 mS cm⁻¹)
- PFHpA, PFHxA or PFPeA individual aqueous solutions with initial concentrations of 100 mg L⁻¹ and 5 g L⁻¹ of Na₂SO₄ as

supporting electrolyte in experiments aimed to evaluate the individual kinetics of short-chain perfluorocarboxylic acids electrooxidation that were obtained as 6:2 FTSA degradation products.

2.3.2. Experimental set-up

The electrochemical oxidation laboratory set-up consisted of an electrochemical cell (DiaCell 201 PP, Adamant Technologies), a power supply (Vitecom 75-HY3005D), a jacketed feed tank, and a cooling bath (Polyscience 9510). A schematic representation of the experimental set-up is shown in Figure 2.4. The cell contained two parallel flow-by compartments made of a central bipolar p-Si/BDD electrode and p-Si/BDD anode and cathode, with an interelectrode gap of 1 mm in each channel. Each electrode had a surface area of 70 cm², therefore, the total anodic area was 140 cm². The main characteristics of the electrochemical cell are summarized in Table 2.5.

Table 2.5. Main characteristics of the electrochemical cell

Diacell 201 PP	
Cathode material	p-Si/BDD (bipolar)
Anode material	p-Si/BDD
Geometry	Circular
Number of anodes	2
Total anodic area	140 cm ² (2 × 70 cm ²)
Interelectrode gap	1 mm
Cell diameter	94.4 mm

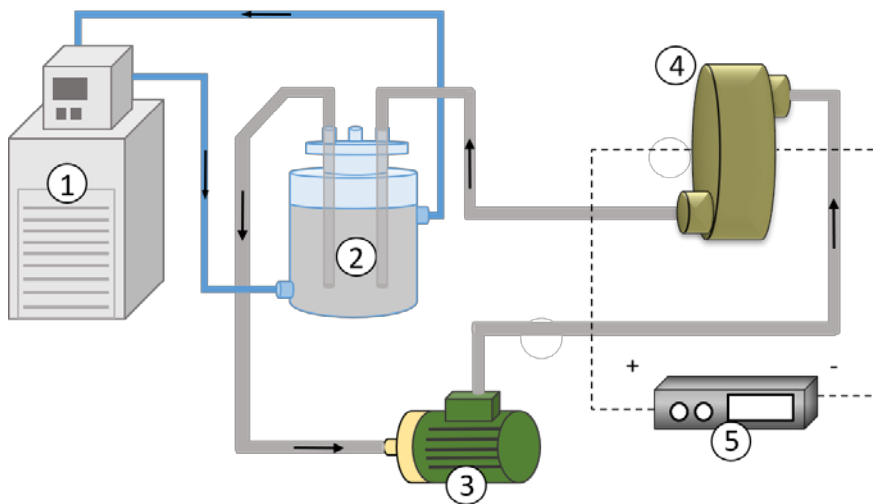


Figure 2.4. Electrochemical oxidation set-up. 1: Refrigerated circulator, 2: Feed tank, 3: Magnetic drive centrifugal pump, 4: Diacell 201 PP electrochemical cell, 5: Power supply.

2.3.3. Operation protocol

All the experiments were carried out in batch mode and under galvanostatic conditions. The applied current density was varied between 5 and 600 A m⁻². The temperature of the solution was kept constant at 20 °C. The treated volume varied between experiments: (i) 2 L for the 6:2 FTSA and short-chain perfluorocarboxylic acids (PFPeA, PFHxA, PFHpA) electrochemical treatment, (ii) approximately 1 L for the PFHxA in real process waters concentrated by nanofiltration and (iii), 1 L for the synthetic AFFFs impacted groundwaters. Sample volume differed between experiments, depending on the analysis needs. Treated samples were collected in polypropylene containers and preserved at 4 °C until analysis.

2.3.4. Calculation of the electrooxidation system performance parameters

The efficiency of the electrochemical oxidation process was calculated using the specific electrical charge (Q , $A \cdot h \cdot L^{-1}$) and the energy consumption (W , $kWh \cdot m^{-3}$) as follows [27]:

$$Q = \frac{JAt}{v} \quad (2.9)$$

$$W = QV \quad (2.10)$$

where J is the current density ($A \cdot m^{-2}$), A is the total anode area (m^2), t is the electrolysis time (h), v is the feed tank volume (L), and V is the cell voltage (V).

Cominellis group [28] firstly reported a model describing the electrochemical oxidation of organic compounds by BDD electrogenerated $OH\bullet$ radicals and/or direct electron transfer which is assumed to be a fast reaction and controlled by mass transfer of the organic towards the anode. Under those conditions the limiting current density (J_{lim}) for the organic compound mineralization can be described by the following equation:

$$J_{lim} = nFk_m C_{org} \quad (2.11)$$

where n is the number of exchanged electrons, k_m is the mass transfer coefficient ($m \ s^{-1}$), F is the Faraday constant ($96485 \ C \ mol^{-1}$) and C_{org} is the concentration of the organic compound ($mol \ m^{-3}$). Knowing the value

of J_{lim} is useful information to determine if the process kinetics is controlled either by the charge supply or by mass transfer in the liquid phase. Two different operation regimes are distinguished [29]: (i) if $J < J_{lim}$, the electrolysis is under current control and (ii) if $J > J_{lim}$, the electrolysis under mass transfer control.

2.4 Analytical methods

PFASs in water samples were quantified using different analytical methods. The appropriate method was selected according to the concentration range and salts content in the samples.

The PFHxA concentration in the feed and retentate from NF/RO experiments was generally within the range 5-900 mg L⁻¹. Moreover, these samples could have high concentrations of dissolved salts. For this type of samples, a high-performance liquid chromatography (HPLC) system with a diode array UV-visible detector (Waters 2695-DAD) was employed. The separation column was an X-Bridge C18 (5 μm, 250 × 4.6 mm). Methanol and a sodium hydrogen phosphate solution in a 65:35 volume ratio was used as a mobile phase at a 0.5 mL min⁻¹ flow rate; the detection wavelength was 205.4 nm.

PFHxA concentration in NF permeate samples from aimed to concentrate the real industrial process waters, was determined using a HPLC system (Waters 2690) equipped with a triple quadrupole mass spectrometer (TQD Detector Acquity, Waters). The column was the X-Bridge BEH C18 (2.5 μm, 2.1 × 75 mm). The eluents were: (i) an aqueous solution containing ammonium acetate (CH₃COONH₄) 2 mM and 5% of methanol, and (ii) pure methanol. The eluent flow rate was 0.15 mL min⁻¹. In this analytical method, the limit of quantification (LOQ) for PFHxA was 1 μg L⁻¹. No pre-

treatment was applied to these samples, as the high sulfate and calcium rejection of the NF membrane meant that the permeate samples had low salt concentrations.

In the rest of electrochemical oxidation and NF/RO experiments, PFASs from water samples were quantified using an ultra-performance liquid chromatography (UPLC) system (Acquity H-Class, Waters) coupled to a triple-quadrupole mass spectrometer (Acquity TQD, Waters) and an Acquity UPLC BEH C18 (1.7 μm , 2.1 \times 50 mm) column. A 2 mM ammonium acetate and 5 % methanol aqueous solution and pure methanol were used as mobile phases at a flow rate of 0.15 mL min^{-1} and the PFHxA LOQ was 1 $\mu\text{g L}^{-1}$. When needed, samples were prepared by a solid-phase extraction (SPE) procedure prior to instrumental analysis in order to eliminate dissolved salts. Non-filtered samples were diluted in 2% formic acid in order to acidify samples. Then, TELOS neoWAX SPE cartridges (200 mg, 6 mL; Kinesis, U.K.) were conditioned with methanol and subsequently equilibrated with ultrapure water (Milli-Q, Millipore) before sample loading. The total loaded sample volume was 400 μL . Two interference elution wash steps were carried out separately with 3 mL Milli-Q water each one to eliminate ionic interferences. Finally, target analytes were eluted with 2 mL of methanol: ammonium hydroxide (95:5 v/v). The extracts were further evaporated until dryness under a gentle stream of dry nitrogen gas. The final volume was adjusted to 1 mL with Milli-Q water and filtered (0.22 μm) prior to injection.

Anion species in water samples were quantified by ion chromatography (Dionex ICS-1100) via an ion-exchange resin column (Dionex AS9-HC). A 9 mM sodium carbonate solution was used as a mobile phase at a flow rate of 1 mL min^{-1} . Cations were analyzed using ion chromatography

(Dionex DX-120) with a Dionex IonPac TM CS12 column and an 18 mM methanesulfonic acid solution as a mobile phase at a flow rate of 1 mL min⁻¹.

An automatic carbon analyzer (TOC-V CPH Shimadzu) was used to measure the total organic carbon (TOC). Conductivity was measured using a portable conductivity meter (Hach sensION 5). The pH was measured using a pH meter (GLP Crison 22). Finally, free chlorine content was quantified using the N,N-Diethyl-p-phenylene diamine (DPD) Ferrous Titrimetric Method according to Standard Methods 4500-Cl [30].

2.5 Design, modelling and optimization of the integrated membrane – electrooxidation system

In this part of the PhD thesis, it was designed an integrated process considering a membrane pre-concentration followed by electrochemical oxidation of the concentrate. The techno-economic assessment of the integrated strategy included its design, modelling and optimization, and its comparison with the base case, where no membrane pre-concentration is considered, and all the feed is electrolyzed. First, it was carried out a preliminary simulation work using a single-stage membrane pre-concentration coupled to electrooxidation layout. This study aimed at evaluating the energy consumption of the hybrid process. Then, it was carried out an insightful optimization study of a multistage membrane-electrooxidation integrated approach, considering the total economy of the process (capital and operating costs), with the objective of minimizing the total costs of the integrated process.

Figure 2.5 shows a basic scheme of the proposed integration strategy. First, the feed is sent to a single or multistage membrane pre-concentration stage.

A lower volume of concentrate, which contains a high concentration of the solute to be degraded, and high concentration of electrolyte, is then sent to the electrooxidation stage. The product from the electrooxidation stage is then mixed with the permeate from the membrane pre-concentration stage, conforming the final product. Specific details about the set-up configurations and approach to each specific problem are detailed in next sections.

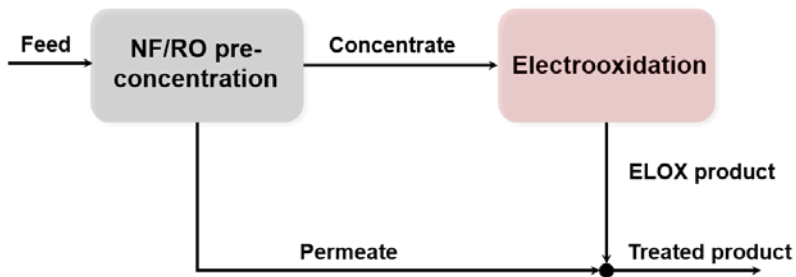


Figure 2.5. Basic integration approach.

2.5.1. Preliminary integration approach: study of the energy consumption

In this preliminary study, it was considered a single NF pre-concentration stage provided with commercial spiral wound membrane modules and a battery of serial-parallel electrochemical cells (Figure 2.6). Their characteristics were implemented in the simulations. The contribution of the two technologies to the total energy consumption was also analyzed. The characteristics of the feed waters were analogous to those described in section 2.2.1.

The composition of the resulting concentrate was considered as the feed properties in the ELOX simulation. For the ELOX simulations, the characteristics of an existing ELOX pilot plant previously used by our research group [31], [32] were considered. The pilot plant is composed of a battery of serial-parallel electrochemical cells with a total BDD anode surface of 1.05 m^2 , each one with similar characteristics to the cell used in the laboratory experiments. The current density was set at 50 A m^{-2} since it was experimentally determined to optimally degrade PFHxA from NF concentrates (section 3.2.1.1). Table 2.6 collects information about the main characteristics and operating conditions considered for the simulation of both processes.

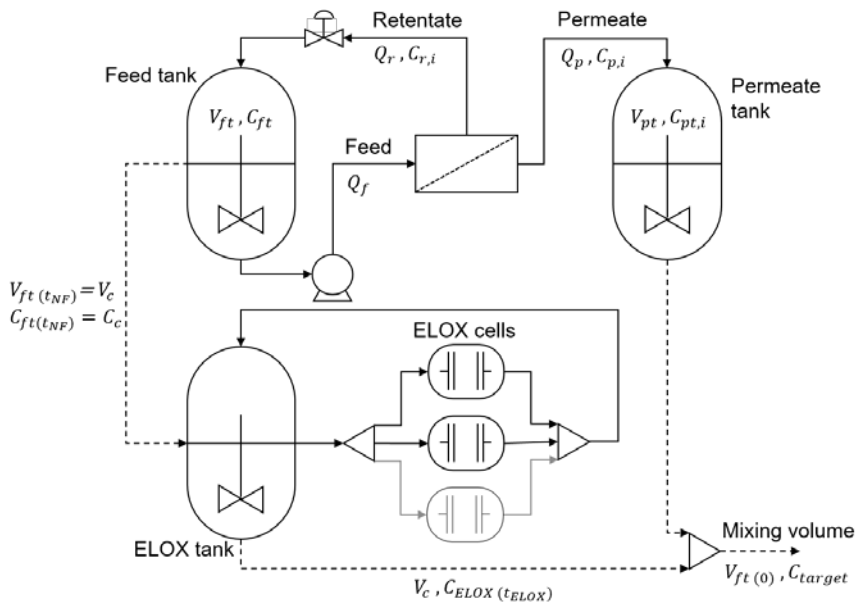


Figure 2.6. Global scheme of the NF-ELOX integrated process in the preliminary energy optimization study. NF set-up with the commercial membrane module and ELOX of the NF concentrate using serial-parallel cells

Table 2.6. Operating conditions and main characteristics of the system considered for the simulations.

Nanofiltration pilot plant	
Membrane area	7.6 m ²
Operating temperature	20°C
Operating feed pressure	10 bar
Feed flow rate	3.6 m ³ h ⁻¹
Initial feed tank volume	5 m ³
Electrooxidation pilot plant	
Total anode surface	1.05 m ²
Current density	50 A m ⁻²

2.5.2 Design and optimization of the multistage membrane pre-concentration – electrooxidation integrated process

A schematic chart of the proposed multistage membrane pre-concentration coupled to electrolysis system is illustrated in Figure 2.7. Both processes were designed to work in sequential batch mode. The feed is sent to the pre-concentration (PC) membrane unit. At the end of the pre-concentration run time (t_{PC}), the volume of retentate that remains in the feed tank is used to feed the ELOX system. After the required electrolysis time (t_{ELOX}), the electrolyzed volume is mixed with the volume of permeate that was obtained in the membrane pre-concentration, resulting in the product volume. Transfer times are neglected. Each batch is processed once the precedent one has been completed.

The proposed membrane separation consists of a multistage cascade of membrane units where the permeate stream of the k stage is pressurized to become the feed to the $k+1$ stage (Figure 2.7b). The successive filtration stages will allow to reduce the concentration of pollutants in the permeate, that is finally collected in the permeate tank. The retentate stream of each stage is recycled to the previous stage, except the retentate from the first

stage, which is recycled to the feed tank. In this way, the PFHxA concentration in the feed tank will increase over time. The ELOX system is designed as a battery of n electrochemical reactors disposed in serial-parallel arrangement, all provided with boron-doped diamond electrodes (BDD).

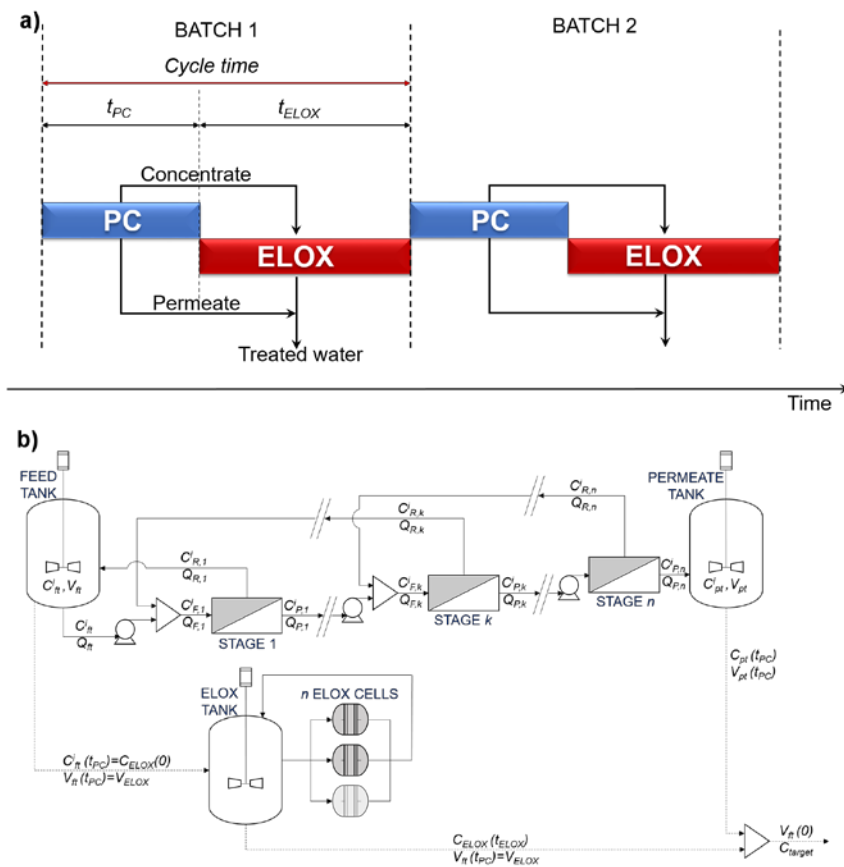


Figure 2.7. Global scheme of the multistage countercurrent cascade membrane pre-concentration (PC) coupled to electrooxidation (ELOX) system. a) Gantt-based chart for batch scheduling, b) detailed process flowsheet.

Detailed information about the integrated process modelling, the economic model and the process input parameters can be found in *Á. Soriano, D. Gorri, L. T. Biegler, and A. Urtiaga, “An optimization model for the treatment of perfluorocarboxylic acids considering membrane preconcentration and BDD electrooxidation,” Water Research, 164, 114954, 2019* in Chapter 5.

2.5.2.1. Process optimization

The integrated process was optimized by determining the minimum total annual cost (TC), accounting for the capital expenditures (CAPEX) and the operating expenditures (OPEX):

$$TC = CAPEX \frac{r(1+r)^t}{(1+r)^t - 1} + OPEX \quad (2.12)$$

The operating costs (OPEX) was on annual basis and the total capital investment (CAPEX) was annualized considering the time value of money, being t the period of time (years) and r the investment rate [33].

The optimization problem can be formulated as follows,

$$\begin{aligned} \min TC(x) \\ \text{s.t } h(x) &= 0 \\ g(x) &\geq 0 \\ L &\leq x \leq U \end{aligned} \quad (2.13)$$

where x the vector of decision variables (pre-concentration time, membrane area per stage and electrode area), h the vector of algebraic

equations from the process modelling, g the model constraints and L and U the lower and upper limits of the set of decision variables.

2.5.2.2. Optimization software

The dynamic non-linear problem (NLP) of the integrated process case of study was implemented in the General Algebraic Modelling System (GAMS). The group of ordinary differential equations describing the integrated process model were discretized by Lagrange interpolation polynomials using Runge-Kutta collocation methods in order to be solved as algebraic equations by GAMS [34]. The NLP was solved using the IPOPTH solver, an interior point optimizer for large-scale nonlinear optimization, on a 3.20 GHz Intel® Core™ i5-6500 processor. The GAMS code of the single-stage and multistage integrated process cases of study can be found in *Appendix A2* of the present thesis document.

Part of this work was developed during a short research stay at Carnegie Mellon University (2018) under the supervision of Prof. L.T. Biegler.

2.6 References

- [1] F. Fernández, B. Jastorff, R. Störman, S. Stolte, and J. Thöming, “Thinking in Terms of Structure-Activity-Relationships (T-SAR): A Tool to Better Understand Nanofiltration Membranes,” *Membranes (Basel)*, vol. 1, no. 3, pp. 162–183, 2011.
- [2] G. Hurwitz, G. R. Guillen, and E. M. V. Hoek, “Probing polyamide membrane surface charge, zeta potential, wettability, and hydrophilicity with contact angle measurements,” *J. Memb. Sci.*, vol. 349, no. 1–2, pp. 349–357, Mar. 2010.
- [3] J. T. Arena, B. McCloskey, B. D. Freeman, and J. R. McCutcheon, “Surface modification of thin film composite membrane support layers with polydopamine: Enabling use of reverse osmosis membranes in pressure retarded osmosis,” *J. Memb. Sci.*, vol. 375, no. 1–2, pp. 55–62, 2011.
- [4] L. A. Richards, M. Vuachère, and A. I. Schäfer, “Impact of pH on the removal of

- fluoride, nitrate and boron by nanofiltration/reverse osmosis,” *Desalination*, vol. 261, no. 3, pp. 331–337, Oct. 2010.
- [5] J. Tanninen, M. Mänttari, and M. Nyström, “Effect of salt mixture concentration on fractionation with NF membranes,” *J. Memb. Sci.*, vol. 283, no. 1–2, pp. 57–64, 2006.
- [6] I. Escalona, A. Fortuny, F. Stüber, C. Bengoa, A. Fabregat, and J. Font, “Fenton coupled with nanofiltration for elimination of Bisphenol A,” *Desalination*, vol. 345, pp. 77–84, 2014.
- [7] P. Xu, J. E. Drewes, T. U. Kim, C. Bellona, and G. Amy, “Effect of membrane fouling on transport of organic contaminants in NF/RO membrane applications,” *J. Memb. Sci.*, vol. 279, no. 1–2, pp. 165–175, Aug. 2006.
- [8] Y. Louis, C. Garnier, V. Lenoble, D. Omanović, S. Mounier, and I. Pižeta, “Characterisation and modelling of marine dissolved organic matter interactions with major and trace cations,” *Mar. Environ. Res.*, vol. 67, no. 2, pp. 100–107, 2009.
- [9] K. Boussu *et al.*, “Characterization of polymeric nanofiltration membranes for systematic analysis of membrane performance,” *J. Memb. Sci.*, vol. 278, no. 1–2, pp. 418–427, 2006.
- [10] K. Kimura, G. Amy, J. E. Drewes, T. Heberer, T. U. Kim, and Y. Watanabe, “Rejection of organic micropollutants (disinfection by-products, endocrine disrupting compounds, and pharmaceutically active compounds) by NF/RO membranes,” *J. Memb. Sci.*, vol. 227, no. 1–2, pp. 113–121, 2003.
- [11] E. Negaresh, A. Antony, M. Bassandeh, D. E. Richardson, and G. Leslie, “Selective separation of contaminants from paper mill effluent using nanofiltration,” *Chem. Eng. Res. Des.*, vol. 90, no. 4, pp. 576–583, 2012.
- [12] J. R. McCutcheon and M. Elimelech, “Influence of membrane support layer hydrophobicity on water flux in osmotically driven membrane processes,” *J. Memb. Sci.*, vol. 318, no. 1–2, pp. 458–466, 2008.
- [13] M. Hayatbakhsh, M. Sadrzadeh, D. Pernitsky, S. Bhattacharjee, and J. Hajinasiri, “Treatment of an in situ oil sands produced water by polymeric membranes,” *Desalin. Water Treat.*, vol. 57, no. 32, pp. 14869–14887, 2016.
- [14] A. J. C. Semião and A. I. Schäfer, “Removal of adsorbing estrogenic micropollutants by nanofiltration membranes: Part B-Model development,” *J. Memb. Sci.*, vol. 431, pp. 257–266, 2013.
- [15] C. Boo, Y. Wang, I. Zucker, Y. Choo, C. O. Osuji, and M. Elimelech, “High

- Performance Nanofiltration Membrane for Effective Removal of Perfluoroalkyl Substances at High Water Recovery,” *Environ. Sci. Technol.*, vol. 52, no. 13, pp. 7279–7288, 2018.
- [16] M. Paul and S. D. Jons, “Chemistry and fabrication of polymeric nanofiltration membranes: A review,” *Polym. (United Kingdom)*, vol. 103, pp. 417–456, 2016.
- [17] Y. Li, S. Li, and K. Zhang, “Influence of hydrophilic carbon dots on polyamide thin film nanocomposite reverse osmosis membranes,” *J. Memb. Sci.*, vol. 537, pp. 42–53, 2017.
- [18] C. Y. Tang, Y. N. Kwon, and J. O. Leckie, “Characterization of humic acid fouled reverse osmosis and nanofiltration membranes by transmission electron microscopy and streaming potential measurements,” *Environ. Sci. Technol.*, vol. 41, no. 3, pp. 942–949, 2007.
- [19] S. Azari and L. Zou, “Using zwitterionic amino acid l-DOPA to modify the surface of thin film composite polyamide reverse osmosis membranes to increase their fouling resistance,” *J. Memb. Sci.*, vol. 401–402, pp. 68–75, 2012.
- [20] A. Llansana, E. Ferrero, V. Ayala, and J. J. Malfeito, “Characterization of nanofiltration membranes and their evaluation for RO desalination pre-treatment,” in *IDA World Congress*, 2007.
- [21] M. Mulder, *Basic Principles of Membrane Technology*, 2nd ed. Dordrecht: Kluwer Academic Publishers, 1996.
- [22] A. Pérez-González, R. Ibáñez, P. Gómez, A. M. Urriaga, I. Ortiz, and J. A. Irabien, “Nanofiltration separation of polyvalent and monovalent anions in desalination brines,” *J. Memb. Sci.*, vol. 473, pp. 16–27, Jan. 2015.
- [23] T. Asano, *Wastewater Reclamation and Reuse: Water Quality Management Library*, no. v. 10. Florida: CRC Press, 1998.
- [24] G. B. Van der Berg, I. G. Rácz, and C. A. Smolders, “Mass transfer coefficients in cross-flow ultrafiltration,” *J. Memb. Sci.*, vol. 47, pp. 25–51, 1989.
- [25] E. Samson, J. Marchand, and K. A. Snyder, “Calculation of ionic diffusion coefficients on the basis of migration test results,” *Mater. Struct. Constr.*, vol. 36, no. 257, pp. 156–165, 2003.
- [26] R. H. Perry, D. W. Green, and J. O. Maloney, *Perry’s Chemical Engineers’ Handbook*, 7th ed. New York: McGraw-Hill, 1997.
- [27] A. Anglada, A. Urriaga, and I. Ortiz, “Contributions of electrochemical oxidation to waste-water treatment: Fundamentals and review of applications,” *J. Chem. Technol. Biotechnol.*, vol. 84, no. 12, pp. 1747–1755, 2009.

- [28] M. Panizza, P. A. Michaud, G. Cerisola, and C. Comminellis, "Anodic oxidation of 2-naphthol at boron-doped diamond electrodes," *J. Electroanal. Chem.*, vol. 507, no. 1, pp. 206–214, 2001.
- [29] Á. Anglada, "Eliminación de amoníaco y materia orgánica de lixiviados de vertedero mediante electro-oxidación en ánodos de diamante dopado con boro," Universidad de Cantabria, 2011.
- [30] APHA, "4500-Cl- B. Argentometric method," *Stand. Methods Exam. Water Wastewater*, vol. 20, no. 4, p. 541, 1998.
- [31] A. Anglada, A. M. Urtiaga, and I. Ortiz, "Laboratory and pilot plant scale study on the electrochemical oxidation of landfill leachate," *J. Hazard. Mater.*, vol. 181, no. 1–3, pp. 729–735, 2010.
- [32] A. Anglada, R. Ibañez, A. Urtiaga, and I. Ortiz, "Electrochemical oxidation of saline industrial wastewaters using boron-doped diamond anodes," *Catal. Today*, vol. 151, no. 1–2, pp. 178–184, Apr. 2010.
- [33] L. T. Biegler, I. E. Grossmann, and A. W. Westerberg, *Systematic methods of chemical process design*. New Jersey: Prentice Hall PTR, 1997.
- [34] L. T. Biegler, *Nonlinear Programming: Concepts, Algorithms and Applications to Chemical Processes*. Philadelphia: Society for Industrial and Applied Mathematics, 2010.

3. Results summary

The main results obtained throughout this PhD thesis are summarized in this chapter. Firstly, the experimental results of the nanofiltration and reverse osmosis treatment of short-chain PFHxA are presented. The second part presents the electrochemical oxidation results of short-chain PFASs of actual implementation in the industry. Finally, the main results of the design and optimization of integrated membrane separation coupled to electrochemical oxidation process are also presented, paying special attention to the economic benefits of the proposed integrated strategy.

3.1. Nanofiltration/reverse osmosis treatment

In this section, the main results of the nanofiltration and reverse osmosis treatment of industrially relevant PFHxA are presented. First, the research was focused on the evaluation of the nanofiltration technology to concentrate PFHxA present in industrial process waters streams. The physico-chemical characterization of these industrial waters is presented in section 2.2.1 of Chapter 2. Next, a more insightful study of different commercial nanofiltration and reverse osmosis membranes was carried out. It was analyzed the effect of PFHxA initial concentration in the solution, feed solution ionic strength and pH at different operation pressures and the performance of these membranes was compared in terms of solute rejection and permeate flux. The objective was to identify the commercial NF/RO membrane that would be most suitable for decontaminating persistent PFHxA present in industrial aqueous emissions, via the integrated membrane–electrooxidation proposed process.

3.1.1. Treatment of real industrial process waters

The results showed in this section correspond to the following published work: *Á. Soriano, D. Gorri, and A. Urtiaga, "Efficient treatment of perfluorohexanoic acid by nanofiltration followed by electrochemical degradation of the NF concentrate" Water Research, 112, pp. 147–156, 2017.*

Initially, the treatment of the real industrial process waters was made using a flat NF270 membrane, supplied by Dow Filmtec. It consists on a thin film composite of a polyester non-woven support matrix, a microporous polysulfone interlayer, and a semiaromatic piperazine-based aromatic polyamide barrier layer. At neutral pH, the NF270 membrane surface is negatively charged, a property that would improve the rejection of large negative species such as perfluorohexanoate, which is obtained by the dissociation of PFHxA at neutral pH [1]. As described in section 2.2.4 of Chapter 2, experiments were carried out using two distinct operation modes: total recirculation experiments and concentration mode experiments.

3.1.1.1 Total recirculation tests

Figure 3.1 shows the correlation between the permeate flux and the pressure gradient across the membrane. Three types of water samples were considered: ultrapure water, real industrial process waters, and the model solution. The last represents the salt composition of the real samples S1 and S2, according to Table 2.2, but without the addition of PFHxA. The membrane permeability to ultrapure water was the highest one, $L_{pw}=13.3 \pm 0.04 \text{ L m}^{-2} \text{ h}^{-1} \text{ bar}^{-1}$, a value that is similar to previously reported water permeability values for the same NF270 membrane [2]. The presence of

salts in solution decreased the membrane permeability, as it was observed for the flux data obtained with the model solution, $L_{pm}=11.7 \pm 1.2 \text{ L m}^{-2} \text{ h}^{-1} \text{ bar}^{-1}$. A similar trend was observed in previous studies dealing with the NF treatment of desalination brines, e.g.: Pérez-González and coworkers [3] found that solution permeability decreased exponentially when increasing the feed salt concentration. The membrane permeability values of the two samples of real process water S1 and S2 (which contained PFHxA) were very similar to each other ($L_{p,S1}=9.6 \text{ L m}^{-2} \text{ h}^{-1} \text{ bar}^{-1}$, and $L_{p,S2}=9.4 \text{ L m}^{-2} \text{ h}^{-1} \text{ bar}^{-1}$), and lower than the values for pure water and the model salt solution. Hang and coworkers [4] reported a similar observation after the nanofiltration of PFOA and suggested that such behavior could be attributed to adsorption of the molecule in the expanded membrane pores.

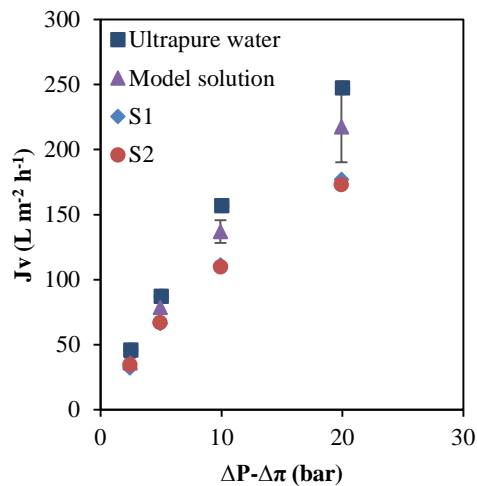


Figure 3.1. Experimental permeate volumetric flux data as a function of the effective pressure gradient. Model solution composition: NaCl (60 mg L^{-1}), CaSO_4 (600 mg L^{-1}). Averages of duplicate experiments are reported for ultrapure water and the model solution.

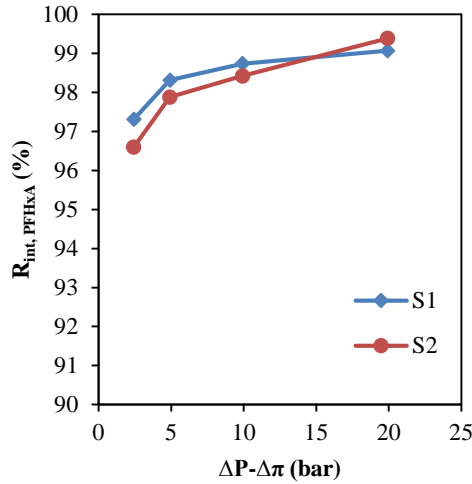


Figure 3.2 PFHxA intrinsic rejection as a function of the effective pressure for process water samples S1 and S2 using the NF270 membrane.

The dependence of the membrane PFHxA intrinsic rejection on the effective pressure is shown in Figure 3.2. As explained in Section 2.2.5 of Chapter 2, intrinsic rejection (R_{int}) characterizes the performance of the membranes after removing the effect of the concentration polarization of dilute species at the liquid boundary layer. PFHxA rejection increased from 97.3% to 99.1% when treating S1, and from 96.6% to 99.4% for S2, in the range of effective pressure gradient $2.4 < (\Delta P - \Delta \pi) < 19.9$ bar. Two main observations can be derived from data in Figure 3.2. First, the PFHxA intrinsic rejection remained high over the entire range of applied pressure. Secondly, the difference in the concentration of PFHxA, which was three times higher in S1 than in S2, did not significantly affect the rejection rate. Appleman and coworkers [5] reported PFHxA rejections higher than 95%, when using the same NF270 membrane for the treatment of artificial

groundwater spiked with a PFHxA concentration of $1 \mu\text{g L}^{-1}$. The authors revealed that PFHxA was not detected in the permeate over the limit of quantification of the analytical technique used in that work. It can be argued that the differences in the feed concentration, which in that work was 200 times lower than in sample S1 of the present study, significantly reduced the concentration gradient across the membrane and thus the permeation flux of the species. Similar observations were reported by Steinle-Darling and Reinhard [6] who studied the nanofiltration of synthetic mixtures of 15 perfluorochemicals in deionized water with concentrations in the range $150\text{--}400 \text{ ng L}^{-1}$. Past research [7] demonstrated that NF membranes achieved a high rejection of negatively charged organic compounds, through the electrostatic exclusion mechanism. However, the detection of PFHxA in the permeate observed in the present work, suggests that once the compound reached a partitioning equilibrium at the feed/membrane interface—which is enhanced by the comparatively high feed concentrations used in this work—the diffusion mechanism governs the overall solute transport through the membrane pores.

Figure 3.3 shows the intrinsic rejection of ions (sulfate, chloride, sodium, and calcium) as a function of the operating pressure for the sample S1. Similar rejections were observed when NF was applied to S2 and to the model solutions (results not shown). In the range of operating pressures studied (2.5 – 20 bar) chloride rejection increased from 6.8% to 56.4%, sodium rejection from 65.6% to 88.2%, calcium rejection from 87.3% to 97.9%, and sulfate rejection from 98.8% to 99.6%. The high values of sulfate rejection are very similar to those obtained for PFHxA because both are large negatively charged species that are easily rejected by the negatively charged membrane at neutral pH (pH=7.7 for S1 sample and pH=7.4 for S2 sample). The low value of chloride rejection can be

explained by the Donnan ion distribution between the solution and the membrane. It means that sodium and calcium cations were attracted by the negatively charged membrane and were highly distributed from the liquid phase to the membrane phase. Chloride ions, which are much smaller than sulfate anions, tended to pass through the membrane together with the small cations in order to preserve the electroneutrality [8]. Similar ion rejection behavior was observed by Pérez-González and coworkers [3], who treated brackish water desalination brines in the pressure range of 5 to 20 bar using the same NF270 membrane. The observed ions rejections were beneficial for increasing the conductivity of the concentrate to be used as an electrolyte in the electrochemical treatment.

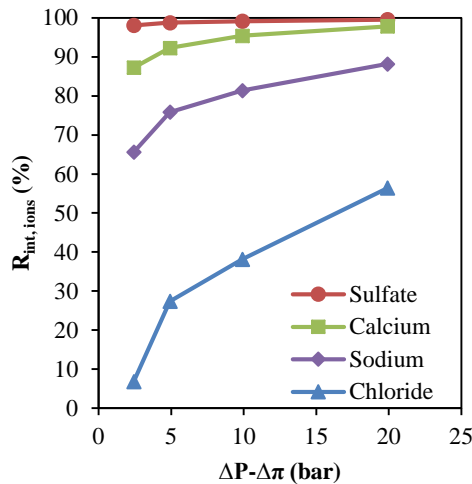


Figure 3.3. Intrinsic rejection of ions as a function of the effective pressure. Data were obtained using sample S1 and the NF270 membrane. Similar results were observed for S2 sample and the model salts solution.

3.1.1.2 Concentration mode experiments

The purpose of the concentration mode experiments was to obtain a low volume of highly concentrated PFHxA solution. In addition, these experiments allowed the evaluation of the stability of membrane performance along the time of operation in terms of PFHxA rejection and permeate flux.

Figure 3.4 shows the evolution of the permeate flux over time (for samples S1 and S2) using a feed pressure of 10 bar. In both cases, the flux slightly decreased in the first hours and then stabilized at a constant value. The membrane permeability values at constant flux were $L_{p,S1}=9.4 \text{ L m}^{-2} \text{ h}^{-1} \text{ bar}^{-1}$ and $L_{p,S2}=8.6 \text{ L m}^{-2} \text{ h}^{-1} \text{ bar}^{-1}$, which are similar or only slightly below those reported in the previous section.

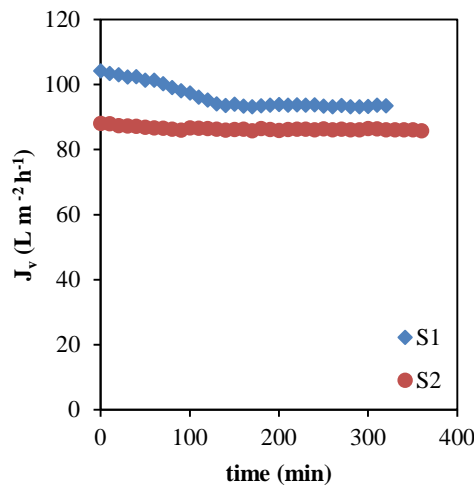


Figure 3.4. Nanofiltration operation in concentration mode. Permeate flux evolution with time for samples S1 and S2. Feed pressure = 10 bar.

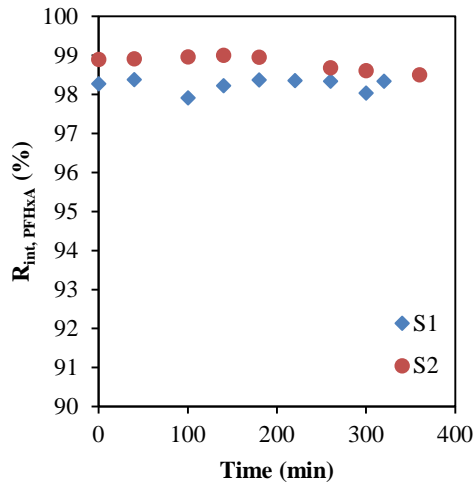


Figure 3.5. Intrinsic PFHxA rejection in concentration mode experiments. NF270 membrane. Feed pressure: 10 bar.

At the end of each experiment, the membrane was tested again with ultrapure water to evaluate whether the observed loss of permeability corresponded to reversible or irreversible fouling. For example, after the NF test with S1, the membrane permeability to pure water was $12.8 \text{ L m}^{-2} \text{ h}^{-1} \text{ bar}^{-1}$, which was only 4% less than the initial value reported in Figure 3.1. The difference was assigned to the slight variability of properties among different membrane specimens. It was concluded that the NF of PFHxA industrial solutions did not generate irreversible fouling in the NF270 membrane.

In the concentration mode experiments, the NF270 membrane showed high PFHxA intrinsic rejections that were essentially constant over time: $98.2 \pm 0.2\%$, and $98.8 \pm 0.2\%$, for S1 and S2 respectively (Figure 3.5). The volume was reduced from the 10 L initially used as feed, to a final volume

of approximately 2 L of concentrate. PFHxA concentrations of 870 mg L⁻¹ and 344 mg L⁻¹ were achieved in the final concentrates C-S1 and C-S2, respectively.

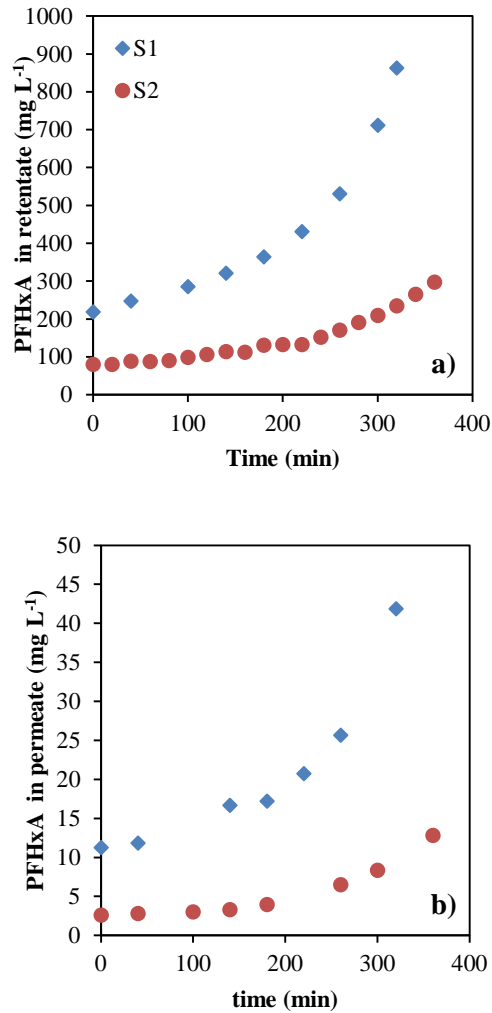


Figure 3.6. a) PFHxA concentration in the concentrate, and b) PFHxA concentration in the permeate in concentration mode experiments. NF270 membrane. Feed pressure: 10 bar.

The evolution with time of the PFHxA concentration in retentate and permeate streams is shown in Figure 3.6. Simultaneously, the conductivity of the concentrates reached 2.48 mS cm^{-1} and 2.63 mS cm^{-1} . These concentrates served as feed for the next electrooxidation step. PFHxA was detected in the permeate at concentrations of 21 mg L^{-1} for S1, and 8 mg L^{-1} for S2. These values corresponded to the composite permeates obtained throughout the duration of the concentration-mode tests.

Moreover, Figure 3.7 shows that under the conditions of the present study, PFHxA concentrations in the permeate and in the retentate matched a linear relationship ($r^2=0.97$); this observation further supports diffusion as the predominant PFHxA transport mechanism through the NF270 membrane.

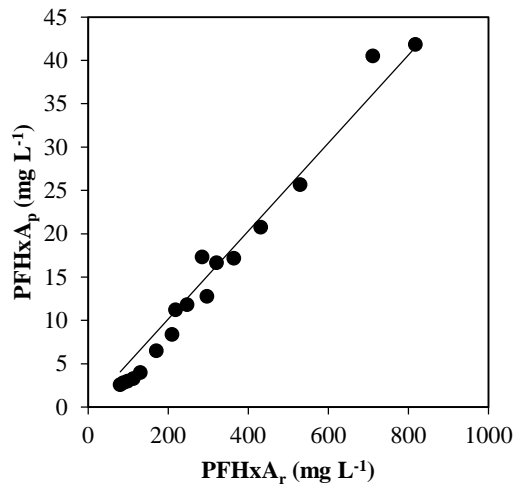


Figure 3.7. Nanofiltration operation in concentration mode. PFHxA concentration in the permeate vs. PFHxA concentration in the retentate. The NF270 membrane was operated at a feed pressure of 10 bar.

3.1.2. Evaluation and selection of NF/RO commercial membranes for the design of the integrated process

This section of the thesis dissertation presents an insightful evaluation of different NF and RO membranes, with the purpose of selecting the most suitable membrane for the treatment of PFHxA in aqueous streams derived from fluoropolymer manufacturing. The experimental data will also lead to obtain empirical parameters needed for the integration approach described in section 2.5.1 of Chapter 2. Most of the results showed in this section correspond to the following published work: *Á. Soriano, D. Gorri, and A. Urriaga, "Selection of High Flux Membrane for the Effective Removal of Short-Chain Perfluorocarboxylic Acids" Industrial & Engineering Chemistry Research, 58, 8, pp. 3329 – 3338, 2019.*

Three aromatic polyamide RO membranes (XLE, BW30, and SW30XLE) and two NF membranes (NF90 and NF270) were characterized in this work. Some additional experiments were conducted with two nanofiltration membranes (ESNA-LF and ESNA-LF2, from Hydranautics), that were not published in the previously mentioned work, although the results were disseminated in the 12th European Congress of Chemical Engineering, celebrated in September 2019. The results from these two NF membranes were added at the end of this section. The characteristics of all the membranes used throughout the development of this thesis are summarized in Table 2.4 in Chapter 2 of this thesis document.

3.1.2.1 Influence of pH on membrane performance

The volumetric fluxes of the five NF and RO membranes at acidic and neutral conditions are shown in Figure 3.8.

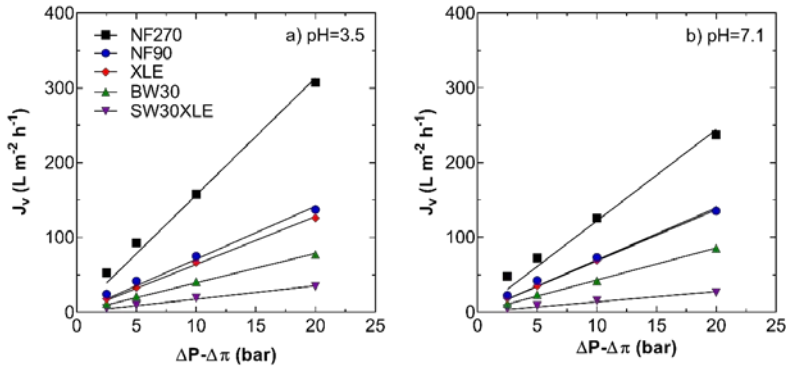


Figure 3.8. Volumetric permeate flux (J_v) as a function of the effective pressure gradient ($\Delta P - \Delta \pi$) for NF and RO membranes; 100 mg L^{-1} PFHxA. (a): $\text{pH} = 3.5 \pm 0.1$; (b) $\text{pH} = 7.1 \pm 0.1$.

Experiments were performed at $\text{pH} = 3.5$, as obtained from the dissociation of PFHxA (100 mg L^{-1}) in water, and also at neutral pH , which was obtained by adding sodium hydroxide. Membrane permeability (L_p) was calculated using Equation 2.2

In line with previous publications [3], [9], [10] (Table 3.1), the highest permeate flux was obtained for the NF270 membrane, whose permeability was approximately double that of the NF90 membrane, both in acidic and neutral pH conditions. The lower permeability of the NF90 membrane compared to the NF270 membrane can be explained by its smaller pore size ($0.34 \text{ nm} \pm 0.02$) compared to the NF270 pore diameter ($0.42 \text{ nm} \pm 0.02$) [11]. In addition, data in the literature [11] indicate that the NF270 active layer is much thinner than in the other NF and RO membranes included in this study (Table 2.3). The more hydrophilic behavior of the NF270 membrane is also suggested by its low water contact angle ($14.4 \pm 0.8^\circ$), a property that facilitates water sorption and likely

contributed to making the NF270 membrane the most water permeable of the five membranes we studied. Among the RO membranes, the XLE was the most water permeable and had a L_p value close to the permeability of the NF90. Finally, also in agreement with data reported in the literature and by the manufacturer (Table 3.1), the permeability of both the BW30 and SW30XLE membranes (designed for brackish water or sea water desalination, respectively) was much lower than that of the NF270, NF90, and XLE membranes.

Feed pH did not substantially affect the permeability of the membranes, except for the NF270 (Table 3.1) in which the permeability increased from $12.2 \text{ L m}^{-2} \text{ h}^{-1} \text{ bar}^{-1}$ at pH=7.1 to $15.3 \text{ L m}^{-2} \text{ h}^{-1} \text{ bar}^{-1}$ at pH=3.5, the latter pH being close to the membrane's isoelectric point (Table 2.4). Other authors have also noted that the maximum flux performance is attained at solution pH near the isoelectric point of NF membranes, when treating aqueous solutions containing humic acid, heavy metal ions, phenolic compounds, or atrazine [12]–[15] and proposed different explanations for this phenomena. At pH higher than the isoelectric point, the deprotonation of carboxylic acid end groups ($=\text{COO}^-$) in the active layer of the NF270 membrane could force the polymeric matrix to adopt an extended chain conformation because of electrostatic repulsion between the charged groups, therefore resulting in a reduction of the pore size (shrinking membrane material). However, at the membrane isoelectric point, and in absence of electrostatic repulsion, these pores are not reduced in size and maximum permeate flux is obtained [12].

The influence of the feed pH on the intrinsic (R_{int}) and observed (R_{obs}) PFHxA rejections, is shown in Figure 3.9 for the membranes studied. Rejection by the NF270 membrane was strongly influenced by the pH of

the solution: at $\Delta P=10$ bar, PFHxA rejection reduced from 96.2% at a neutral pH to 86.9% in acidic conditions (pH=3.5). The observed rejections for the other four membranes exceeded 99% at a neutral pH in the whole pressure range studied, and the highest rejection values were obtained for the NF90 ($R_{obs}=99.8\%$), XLE ($R_{obs}=99.7\%$), and BW30 ($R_{obs}=99.7\%$) membranes.

Table 3.1. Hydraulic permeability (L_p , $L\ m^{-2}\ h^{-1}\ bar^{-1}$) values for the studied membranes.

Membrane	Pure water ^a	Feedwater ^b	PFHxA (100 mg L ⁻¹) aqueous solutions (this study)		
			pH=3.5 ^c	pH=7.1 ^c	Model industrial effluents (pH=7.8) ^d including salts
NF270	13.3 ± 0.04 [3]	13.0	15.3 ± 0.4	12.2	12.2 ± 0.1
NF90	5.8 ± 0.3[9]	10.4	7.1	7.0	5.6 ± 0.1
XLE	5.7 ± 0.4[9]	7.8	6.4	6.9	5.4 ± 0.1
BW30	4.4[10]	3.8	3.9	4.3	-
SW30XLE	1.1[16]	1.3	1.8	1.8 ± 0.4	-

^a Pure water permeability values available in the literature.

^b Hydraulic permeability calculated based on the manufacturer's product data sheets [17] considering the applied pressure and the osmotic pressure of the feed solution; feedwater and testing conditions varied. The parameters used were the following—for the NF90 and NF270: 7.6 m² membrane module, 4.8 bar, 2000 mg L⁻¹ MgSO₄, 25°C, and 15% water recovery; XLE: 8.1 m² membrane module, 6.9 bar, 500 mg L⁻¹ NaCl, 25°C, and 15% water recovery; BW30: 7.2 m² membrane module, 15.5 bar, 2000 mg L⁻¹ NaCl, 25°C, and 15% water recovery; SW30XLE: 37 m² membrane module, 55.2 bar, 32000 mg L⁻¹ NaCl, 5 mg L⁻¹ boron, 25°C, and 8% water recovery.

^c Hydraulic permeability values for the experiments using aqueous solutions of 100 mg L⁻¹ PFHxA in ultrapure water at an acidic pH and a neutral pH.

^d Hydraulic permeability values for the experiments using model aqueous solutions of 100 mg L⁻¹ PFHxA with CaSO₄, NaCl, and NaHCO₃, as specified in section 2.2.1.

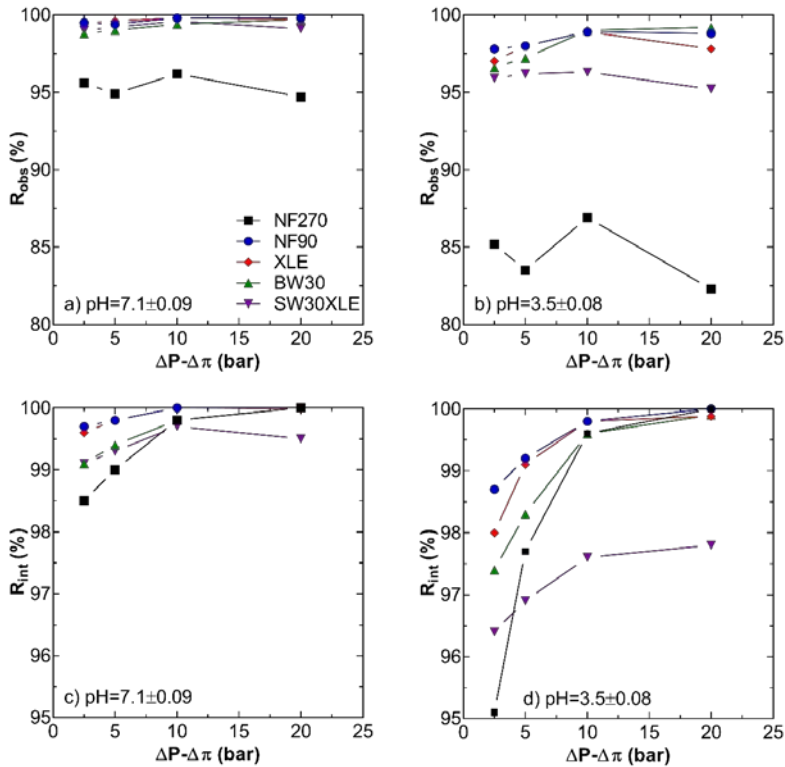


Figure 3.9. PFHxA observed rejection (R_{obs}) and intrinsic rejection (R_{int}) for the different nanofiltration (NF270, NF90) and reverse osmosis (XLE, BW30, and SW30XLE) commercial membranes with different pH solutions ($pH = 3.5 \pm 0.1$ and $pH = 7.1 \pm 0.1$), using 100 mg L^{-1} of PFHxA in MilliQ aqueous solution as the feed. (a): R_{obs} at a neutral pH and (b) R_{obs} at an acidic pH. (c) R_{int} at a neutral pH and (d) R_{int} at an acidic pH.

The permeation fluxes we measured for these membranes were used to establish the impact that concentration polarization has on R_{int} and was calculated using Equation 2.7. Comparison of R_{int} and R_{obs} values (Figure 3.9) shows that rejection by the high-flux NF270 membrane was strongly influenced by concentration polarization because R_{obs} was significantly

lower than R_{int} , in the same conditions. At a neutral pH and $\Delta P=10$ bar, the $R_{int,PFHxA}$ for all the membranes exceeded 99%; NF90, XLE, and BW30 had the best $R_{int,PFHxA}$ at 99.9%, followed by NF270 (99.8%) and SW30XLE (99.7%).

Although the accurate estimation of PFCAs dissociation constant currently remains a challenge, there is strong evidence that the pK_a of these substances is near zero [18]. Steinle and Reinhard [6] estimated that the PFHxA $pK_a=-0.16$ using the SPARC chemical reactivity model. Accordingly, PFHxA is almost completely dissociated in its anionic form, perfluorohexanoate ($C_5F_{11}COO^-$), for the whole pH range in which the studied membranes are negatively charged. Thus, the electrostatic repulsion between the negatively charged membranes and perfluorohexanoate would be expected to contribute to the enhancement of PFHxA separation. Accordingly, of all the membranes studied, PFHxA rejection decreased by the most for the NF270 membrane in acidic (pH 3.5) conditions near the membrane's isoelectric point (Table 2.4). This is because this membrane has the lowest contribution of size exclusion to solute rejection. At neutral pH, the negatively charged NF270 membrane surface promotes strong solute-membrane electrostatic interactions that, in combination with the shrinking of the polymer matrix, noticeably increases PFHxA rejection. However, charge exclusion might still play an important role in solute separation by the RO membranes we studied. At a neutral pH, throughout the entire pressure range (2.5–20 bar), the PFHxA rejection values were the highest for the XLE membrane, whose surface is more negatively charged than the other two RO membranes (Table 2.4). In contrast, PFHxA rejection was lower for the slightly charged BW30 and SW30XLE RO membranes.

As shown in Table 2.4, the molecular weight cut off (MWCO) of the NF270 membrane is very close to the molecular weight of PFHxA (Table 2.3). On the other hand, the estimated molecular width of PFHxA (0.415 nm; Table 2.3) is very similar to the mean pore radius of the NF270 membrane (0.42 ± 0.02 nm [11]). Hence, the pore radius may also contribute to PFHxA rejection by tight NF membranes due to steric hindrance [22]. In addition, the calculated Stokes radius of the PFHxA molecule (0.349 nm; Table 2.3) is less than the mean pore radius of the NF270 membrane. Therefore, the absence of electrostatic repulsion between PFHxA and the NF270 membrane at pH values close to the membrane's isoelectric point would likely promote permeation of the solute through the pores, which might explain the lower PFHxA rejection by NF270 in acidic pH rather than in neutral pH conditions.

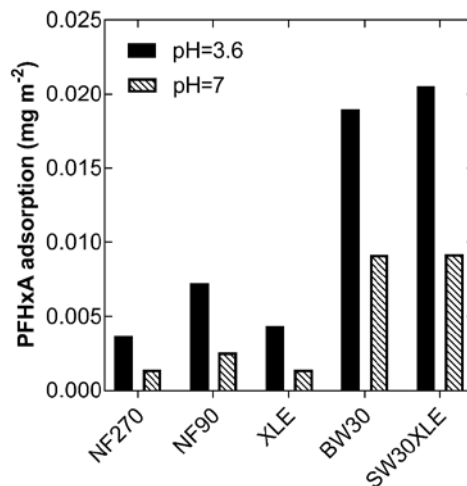


Figure 3.10. PFHxA adsorption on the different nanofiltration and reverse osmosis membranes under acid and neutral pH conditions.

The molecular weight of PFHxA was higher than the MWCO for the other membranes we studied, so in these cases, the separation mechanism was likely a combination of steric exclusion and charge repulsion. We also hypothesize that PFHxA might have been adsorbed at the membrane surfaces and subsequently diffused through them. Adsorption seemed to be slightly higher when the electrostatic repulsion was reduced at lower solution pH, close to the membranes isoelectric point. According to our data (Figure 3.10), that were obtained in adsorption tests working with aqueous solutions containing c.a. 100 mg L^{-1} of PFHxA, the PFHxA adsorption capacity of the SW30XLE membrane at acid pH ($0.021 \text{ mg of PFHxA. cm}^{-2}$ of membrane area) was higher than in neutral pH conditions (0.009 mg cm^{-2}). This could explain its lower PFHxA rejection at acid pH conditions. The PFHxA adsorption on the SW30XLE membrane would be higher than the adsorption observed by Steinle-Darling and Reinhard [6] on the NF270 surface for a wide range of PFCAs in concentrations of $150\text{-}400 \text{ ng L}^{-1}$, which is clearly justified by the different range of concentrations studied.

3.1.2.2. The influence of salt content on the performance of the NF270, NF90, and XLE membranes

Based on the PFHxA rejection and permeate flux results described in the previous sections, the performances of the NF270, NF90, and XLE membranes were compared in the treatment of process waters containing moderate amounts of salts (CaSO_4 , NaCl , and NaHCO_3), similar to the composition of effluents from the industrial production of perfluorinated compounds, as specified in Chapter 2. We used process design criterion to select membranes, considering the trade-off between membrane selectivity and permeate productivity. The NF270 was selected because it was the

most productive of all the five membranes and it had a moderate to high PFHxA rejection rate. The NF90 and XLE membranes were selected because their PFHxA rejection and productivities were high compared to the other membranes.

The presence of salts did not substantially modify the observed PFHxA rejection by the NF90 and XLE membranes but did slightly negatively affect the performance of the NF270 membrane (Figure 3.11). Observed PFHxA rejection with the XLE membrane was 99.0–99.4% while with the NF90 membrane it was 98.1–99.6%. According to different authors, adding Ca^{2+} could reduce the rejection of organic solutes by producing a shielding effect on the negatively charged surface of NF membranes. In agreement with our findings (Figure 3.11a), this would be especially noticeable in membranes with larger pores such as the NF270 [23]. Nghiem and coworkers [24] explained this behavior as a decrease of the length of the electrical double layer of the charged solutes and membrane surface (Debye length), which causes a screening effect and thus decreases the electrostatic interactions between the membrane and the charged solute, resulting in less rejection.

To a lesser extent, the addition of salts also impacted the NF90 and XLE permeate fluxes (Figure 3.11b). In our experiments, very high calcium (up to 99.6%) and sulfate (97.3%) rejections were obtained with the XLE membrane (Figure 3.12) and similar ion rejections were obtained with the NF90 membrane (up to 99.6% for Ca^{2+} and 99.2% for SO_4^{2-}).

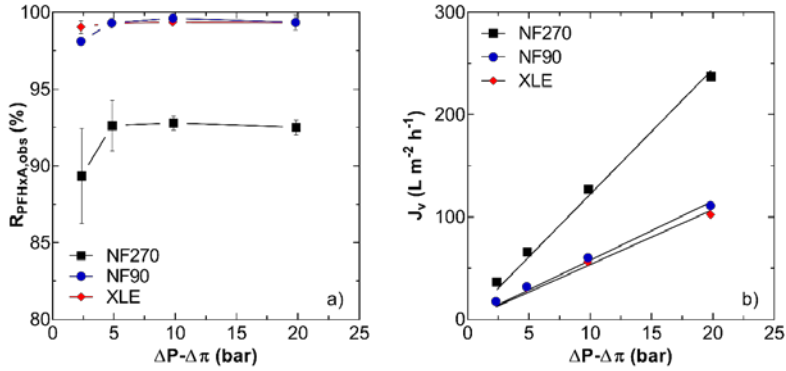


Figure 3.11. PFHxA observed rejection (R_{obs}) and water flux (J_v) versus the effective pressure gradient, for the NF270, XLE, and NF90 membranes. Synthetic process water feed solution: 100 mg L⁻¹ of PFHxA, 36 mg L⁻¹ of NaCl, 575 mg L⁻¹ of CaSO₄, and 98 mg L⁻¹ of NaHCO₃, at pH=7.8 ± 0.1.

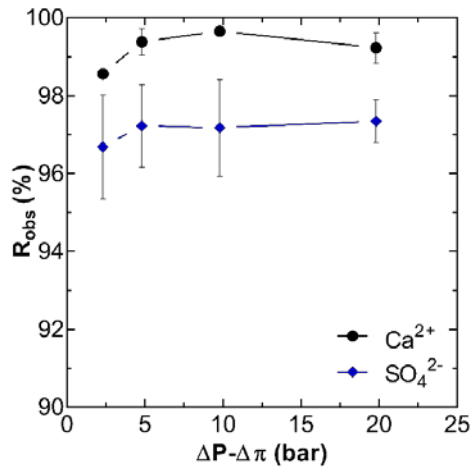


Figure 3.12. Calcium and sulfate rejection. XLE membrane. Synthetic process water feed solution: 100 mg L⁻¹ of PFHxA, 36 mg L⁻¹ of NaCl, 575 mg L⁻¹ of CaSO₄, and 98 mg L⁻¹ of NaHCO₃, at pH=7.8 ± 0.1.

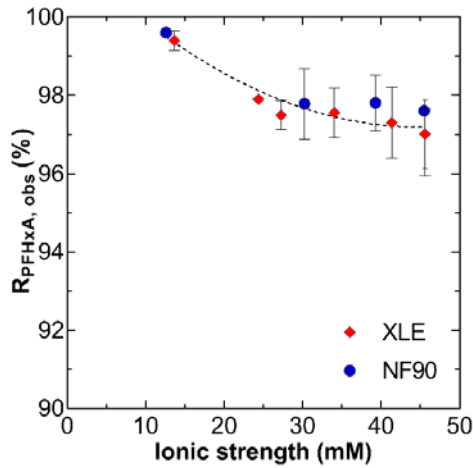


Figure 3.13. Effect of ionic strength on PFHxA rejection by the XLE and NF90 membranes. The plotted line is provided to guide the reader's eye.

In the presence of salts, the PFHxA concentration in the permeate at $\Delta P=10$ bar was $0.7 \pm 0.3 \text{ mg L}^{-1}$ for the XLE membrane, $0.4 \pm 0.3 \text{ mg L}^{-1}$ for the NF90 membrane, and $7.8 \pm 0.8 \text{ mg L}^{-1}$ for the NF270 membrane; both the NF90 and XLE membranes behaved similarly in terms of permeability and retention of ionic species. Thus, any of both membranes could be used for the integrated process proposed in this thesis.

To study the effect of the feed solution ionic strength, several solutions with different concentrations of PFHxA and salts were prepared: starting with the model solution described in section 2.2.1 (100 mg L^{-1} of PFHxA with salts), higher concentrations of each component were added varying the ionic strength of the solution from 13 mM to 45 mM. Experiments were conducted with the NF90 and the XLE membranes at $\Delta P=10$ bar and the effect of the ionic strength on PFHxA rejection by both membranes is

depicted in Figure 3.13. As the ionic strength of the solution increased, PFHxA rejection slightly decreased to 96.5% and 97.0% for the NF90 and XLE membranes, respectively.

Zhao and coworkers [25] recently reported an increase in PFOS rejection with increasing concentrations of cationic and anionic species when using the ESNA1-K1 NF membrane. Similarly, Wang and coworkers [26] found that PFOS rejection by a self-manufactured poly(piperazine-amide) ultrathin film NF membrane was favored by higher feed solution ionic strengths, while, on the contrary, perfluorobutane sulfonate (PFBS) rejection substantially decreased in the same study [26]. Authors claimed that the dissimilar membrane behavior observed in terms of PFOS and PFBS rejection was because of the different effects the predominant mechanisms of the NF membrane had on these two different molecular size PFASs. As the ionic strength increased, the electrostatic repulsion mechanism weakened and the size exclusion mechanism was enhanced, thus making NF membranes more permeable to short-chain PFBS compared to the PFOS molecule with its longer fluorinated chain. In the present study, PFHxA rejection was slightly reduced as the ionic strength increased, a behavior that can be attributed to the higher concentration of counter-ions which may promote the charge shielding effect on the membrane surface, as previously explained.

3.1.2.3. Additional experiments with ESNA-LF and ESNA-LF2 membranes

In addition to the experiments discussed above, some further experiments were carried out to test two nanofiltration membranes (ESNA-LF and ESNA-LF2) in the treatment of PFHxA impacted waters. The results from

this experiments were disseminated in the 12th European Congress of Chemical Engineering (September 2019), but not published in the scientific articles gathered in Chapter 5, and therefore will be discussed here.

Two types of feed samples were prepared: (i) 100 mg L⁻¹ PFHxA aqueous solutions at neutral pH, and (ii) model solutions to emulate the salts content of real process waters with 100 mg L⁻¹ of PFHxA, 36 mg L⁻¹ of NaCl, 575 mg L⁻¹ of CaSO₄, and 98 mg L⁻¹ of NaHCO₃, at pH=7.84 ± 0.1. Figure 3.14 shows the influence of the water matrix composition on the PFHxA observed rejection and the volumetric flux. For both membranes, PFHxA rejection was severely affected by the chemistry of the solution while the permeability remained reasonably constant. Whilst very high PFHxA rejection values were obtained when treating pure PFHxA aqueous solutions (ESNA1-LF: 96.1 – 99%; ESNA1-LF2: 95.4 – 97.9%), the presence of salts considerably reduced the rejection performance (ESNA1-LF: 67.2 – 70.4%; ESNA1-LF2: 70.2 – 76.5%).

Membrane permeability was not substantially affected by the background electrolyte, and ranged from 6.5 to 7.0 L m⁻² h⁻¹ bar⁻¹ for the ESNA-LF membrane and from 7.4 to 7.8 L m⁻² h⁻¹ bar⁻¹ for the ESNA-LF2 membrane. The negative effect of the presence of salts on PFHxA rejection by both membranes could be attributed to the high counter-ion concentration in the feed side of the membranes that could induce a shielding effect on the negatively-charged surface of the two NF membranes. Thus, the diminished electrostatic repulsion between the charged NF membranes surface and the perfluorohexanoate anion form of PFHxA in solution at neutral pH, would leave the steric-exclusion role as the dominant separation mechanism.

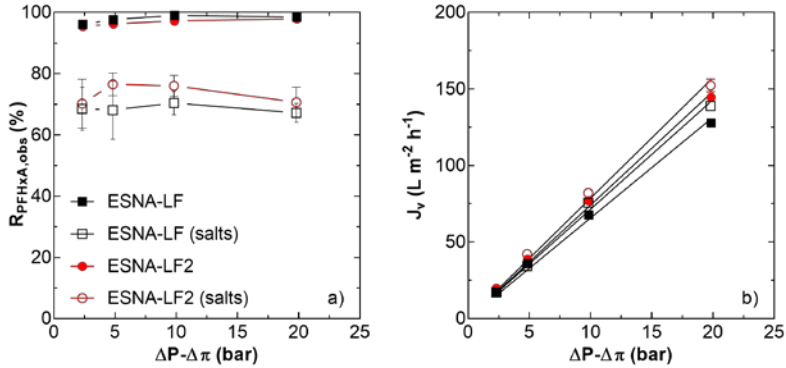


Figure 3.14. PFHxA observed rejection (R_{obs}) and water flux (J_v) versus the effective pressure gradient, for the ESNA-LF and ESNA-LF2 membranes.

The low rejection obtained under real water conditions is detrimental for the design of the integrated process proposed in this thesis. Decontamination of complex water matrixes impacted with PFHxA generated in the process industry needs of more selective nanofiltration or reverse osmosis membranes, as those discussed in the previous sections.

3.2. Electrochemical oxidation treatment

In this part of the thesis, the electrochemical oxidation of PFASs by means of commercial BDD anodes, was studied. On the one hand, the applicability of the electrochemical oxidation technology was investigated in the degradation of PFHxA from industrial real waters concentrated by NF membranes and, on the other hand, in the degradation and mineralization of 6:2 FTSA, a fluorotelomer compound currently implemented by the industry as alternative to long chain perfluorinated carboxylic and sulfonic acids.

3.2.1. Treatment of NF concentrates from real industrial streams

The results showed in this section correspond to the following published work: *Á. Soriano, D. Gorri, and A. Urtiaga, "Efficient treatment of perfluorohexanoic acid by nanofiltration followed by electrochemical degradation of the NF concentrate" Water Research, 112, pp. 147–156, 2017.*

3.2.1.1 Influence of the applied current density

Initial tests aimed at the selection of the applied current density were performed using model solutions (CM-S1) that were prepared with similar PFHxA concentrations and salts composition as the NF concentrates obtained from sample S1 (more information can be found in section 2.3.1 of Chapter 2).

Figure 3.15 depicts the PFHxA and TOC evolution with time at three different working current density values: $J=20, 50,$ and 100 A m^{-2} . The kinetics of PFHxA degradation and mineralization were clearly enhanced when the applied current density was increased from 20 to 50 A m^{-2} . Further increase in current density to 100 A m^{-2} provided an additional improvement in degradation kinetics, although less noticeable than the previous increment from 20 to 50 A m^{-2} . As stated in a widely proposed oxidation mechanism [27]–[30] the electrochemical oxidation of PFCAs involves electron transfer to the anode to form the highly reactive $\text{C}_n\text{F}_{2n+1}\text{COO}\cdot$ radical, which then reacts with electrogenerated hydroxyl radicals. According to this pathway, PFHxA degradation would include both direct and indirect electrochemical oxidation steps. BDD anodes are well known for their wide electrochemical window that allows the formation of hydroxyl radicals at lower electrode potentials than those

needed for the oxygen evolution reaction. However, their high reactivity confines hydroxyl radicals in the very near proximity of the anode surface.

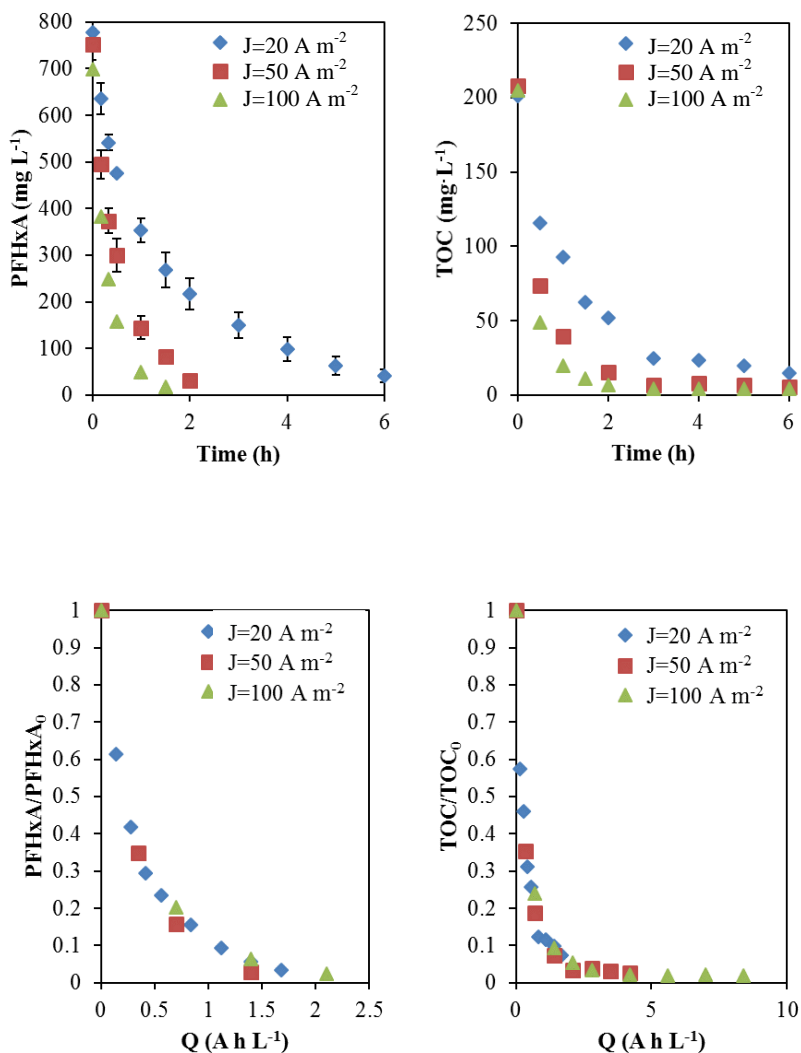


Figure 3.15. PFHxA and TOC evolution as function of time (t) and specific electrical charge (Q), using the NF concentrate of sample S1: CM-S1 [PFHxA]₀=774 mg·L⁻¹. Initial conductivity=2.31-2.48 mS·cm⁻¹.

Therefore, two different operating regimes can be defined for BDD oxidation: i) when the applied current density is below the limiting current density, the electrolysis is under current control and the concentration of organic compounds decreases linearly with time; ii) when the applied current density is above the limiting current density, the electrolysis is under mass transport control and the removal of organics follows a first-order exponential trend. In the present study, the limiting current density (J_{lim} , Equation 2.11) was calculated as $J_{lim}=48.1 \text{ A m}^{-2}$ at the initial PFHxA concentration in CM-S1. This means that when working at $J=20 \text{ A m}^{-2}$, the electrolysis was initially under current control, although it rapidly shifted to mass transfer control at $t=1 \text{ h}$ as the concentration of PFHxA decreased. At $J=50 \text{ A m}^{-2}$, the system was working under mass transfer control for the entire experiment.

The small but noticeable increase in the PFHxA removal rate observed at 100 A m^{-2} can be attributed to the oxidative effect of secondary strong oxidants such as sulfate radicals. This assumption is based on the results reported by Hori and coworkers [31], who found that the photolysis of persulfate anions produced highly oxidative sulfate radical anions, which efficiently decomposed PFOA and other PFCAs bearing $\text{C}_4\text{-C}_8$ perfluoroalkyl groups. At present, we are not able to definitely elucidate the rate limiting step of PFHxA degradation, although the experimental results that show only a minor kinetic enhancement when the applied current is doubled from 50 to 100 A m^{-2} , point to the predominance of indirect oxidation by means of electrogenerated oxidants.

To select the suitable operating conditions, it is also useful to look at the evolution of PFHxA and TOC as functions of the specific electrical charge passed (Q), also shown in Figure 3.15. An increase in the applied current

density did not significantly affect the efficacy of the process. The energy demand for a 90 % PFHxA degradation ratio was calculated using Equations 2.9 and 2.10. The calculated electrolysis time for a 90% reduction of the initial PFHxA concentration were obtained from the rate constant calculated using the fitting of concentration- Q data. Results are summarized in Table 3.3, where V is the experimental cell voltage under galvanostatic conditions. The energy consumption for $J=50 \text{ A m}^{-2}$ was 15.2 kWh m^{-3} , the lowest among the three current densities under consideration. It was also observed that the electrolysis time needed to reach 90 % degradation at 50 A m^{-2} was three times lower than when the applied current was 20 A m^{-2} . Accordingly, it was decided to select $J=50 \text{ A m}^{-2}$ as the working current density for the electrochemical treatment of the real industrial process concentrates.

The energy consumption for the electrochemical treatment of PFHxA, 15.2 kWh m^{-3} , is lower than previously reported values for the removal of different PFASs in waters. Zhuo and coworkers [32] and Niu and coworkers [33] reported the electrolysis of PFOA using tin oxide and lead dioxide electrodes with energy consumptions of 48 and 45 kWh m^{-3} . Similar values in the range 41.7-76.6 kWh m^{-3} have been gathered by Niu and coworkers [34] for the degradation of perfluorodecanoic and perfluorononanoic acids using BDD, SnO_2 , and PbO_2 electrodes. The energy consumption reported in the present study is the lowest of all the values reported so far, which shows evidence of the improvement of efficiency of the electrolysis treatment of PFASs using a preconcentration strategy.

Table 3.3. Energy consumption and electrolysis time required to achieve a 90% PFHxA degradation ratio in sample CM-S1.

J (A m^{-2})	Kinetic constant k_2 ($\text{L A}^{-1} \text{h}^{-1}$)*	V (V)	Q (A h L^{-1})	W (kWh m^{-3})	Electrolysis time (h)
20	1.859	12.9	1.24	16.0	4.42
50	2.252	14.9	1.02	15.2	1.47
100	1.814	16.8	1.27	21.3	0.90

3.2.1.2. Electrochemical mineralization of PFHxA in concentrates from industrial process waters

Figure 3.16 shows the evolution of PFHxA and TOC concentration with electrolysis time when treating the real industrial process waters preconcentrated by NF at the selected value of current density ($J=50 \text{ A m}^{-2}$). Linearized dimensionless values are presented, since the initial concentrations of PFHxA in the two samples were significantly different. The volume of sample is included in the linearization of data because of the lower feed water volume used in the C-S2 experiment (0.8 L) compared to C-S1 (1 L), due to the lack of available sample. After 90 minutes, the degradation of PFHxA concentration was 91% and 98% of the initial concentration in samples C-S1 and C-S2, respectively. It is also interesting to confirm the high removal of TOC, showing the mineralization of the organic compound. PFHxA removal was slightly faster for C-S2 than for C-S1. This behavior can be assigned to its higher initial PFHxA concentration ($C_{0,C-S1}=870 \text{ mg L}^{-1}$). During the experiments we detected degradation products such as perfluoropentanoic acid and perfluorobutanoic acid. In all cases, the observed amounts of secondary PFCAs were lower than the quantification limit of the HPLC-DAD analytical technique. It means that only small amounts of the shorter chain

PFCAs obtained upon PFHxA degradation diffused out of the proximity of the anode surface.

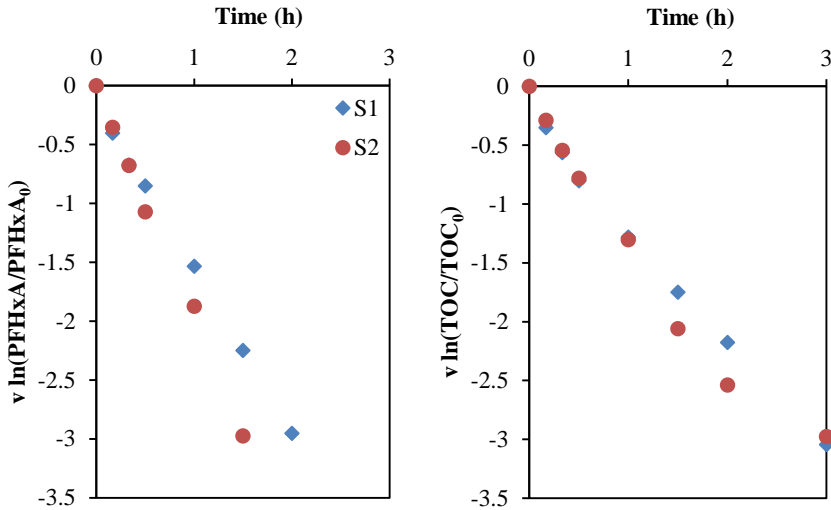


Figure 3.16. Linearized dimensionless PFHxA and TOC evolution with time using the real concentrates. $J=50 \text{ A}\cdot\text{m}^{-2}$. \blacklozenge :C-S1, $[\text{PFHxA}]_0=870 \text{ mg}\cdot\text{L}^{-1}$, initial conductivity = $2.48 \text{ mS}\cdot\text{cm}^{-1}$, volume= 1 L ; \bullet :C-S2, $[\text{PFHxA}]_0=344 \text{ mg}\cdot\text{L}^{-1}$, initial conductivity = $2.63 \text{ mS}\cdot\text{cm}^{-1}$, volume= 0.8 L .

Figure 3.17 shows the evolution of fluoride with the electrolysis time. The fluoride concentration reached a maximum at 90 min, and then started to decrease slowly. At the same time, the concentration of calcium decreased continuously, a clear indication that calcium fluoride was being formed from the beginning of the electrochemical test. As can be seen from Table 2.2, which summarizes the initial physico-chemical characterization of the feed waters, calcium was originally present in the industrial waters under study. Local pH variations at the anode and cathode surfaces and the

intense fluid turbulence gave rise to the supersaturated calcium fluoride solution and deposition of calcium fluoride on the cathode surface. For electrochemical treatment time longer than 2 h, the degradation of PFHxA was nearly completed and there was no further release of fluoride ions. Therefore, in the present application the defluorination ratio is not an appropriate indicator of PFHxA degree of mineralization, as this indicator considers the concentration of fluoride ions in the solution. Calcium fluoride scaling was easily removed from the cathode surface by acid cleaning using an HCl aqueous solution (1 M) at the end of each experimental run. This fouling formation could be detrimental to the performance of the system at larger scales, as it would require the implementation of a periodical cleaning procedure to avoid scaling on the electrode surface, as it was recently proposed by Schaefer and coworkers [35].

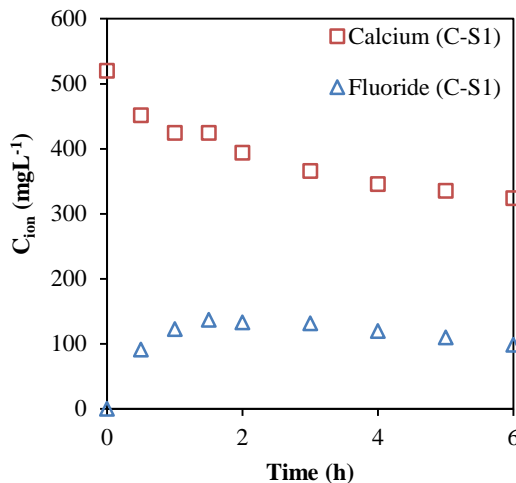


Figure 3.17. Calcium and fluoride evolution during the electrochemical treatment of sample C-S1.

The pseudo-first order kinetic constant for PFHxA degradation obtained from the experimental data in Figure 3.16, was $0.0021 \text{ m min}^{-1}$, after correcting for the volume treated and anode area. This value is ten times higher than the kinetic constant obtained by Niu and coworkers [33] for the degradation of PFHxA using a Ce-doped PbO_2 anode. Similarly, Zhuo and coworkers [36] reported the electrooxidation of a PFHxA synthetic aqueous solution (100 mg L^{-1}) using a small BDD anode (8.5 cm^2) in a laboratory-scale batch reactor at an applied current density of 232 A m^{-2} . In that work, the reported PFHxA degradation kinetic constant was $0.0016 \text{ m min}^{-1}$. The kinetic constant obtained in the present study surpasses the two previously reported values and validates the use of commercial BDD cells for the removal of PFASs from industrial process waters.

3.2.2. 6:2 FTSA electrochemical treatment. Evaluation of operating variables and by-product formation

The overall goal of this study was to evaluate and demonstrate the efficient electrochemical degradation of 6:2 FTSA with BDD electrodes. 6:2 FTSA is one of the alternative compounds to substitute PFOS in surface treatment operations and emulsion polymerization. Aqueous solutions prepared from 6:2 FTSA formulations, that are commercialized as surfactants, were investigated. Experiments examined the effects of the type of electrolyte, using sulfate, chloride and perchlorate salts, on 6:2 FTSA defluorination and mineralization, by means of the total organic carbon (TOC) removal. The influence of the main operation parameter, e.g.: the applied current density, from $5 - 600 \text{ A m}^{-2}$, on reaction rates and on the generation and degradation of shorter chain perfluorinated intermediate products was studied. Treatment of individual PFCAs was also assessed, in order to validate the proposal of kinetic regime.

The results showed in this section correspond to the following published article: A. Urtiaga, Á. Soriano, and J. Carrillo-Abad, “BDD anodic treatment of 6:2 fluorotelomer sulfonate (6:2 FTSA). Evaluation of operating variables and by-product formation” *Chemosphere*, 201, pp. 571–577, 2018.

3.2.2.1. Influence of the electrolyte and generation of oxidative byproducts

Initial experiments were aimed at evaluating the effect of the electrolyte on the 6:2 FTSA mineralization. Three electrolyte solutions were tested: Na_2SO_4 (5 g L^{-1}), NaCl (3.5 g L^{-1}), and NaClO_4 (9.4 g L^{-1}), working at $J=50 \text{ A m}^{-2}$. The concentration of each salt was selected to provide the electrolyte solution with a similar background conductivity (6.9 mS cm^{-1}).

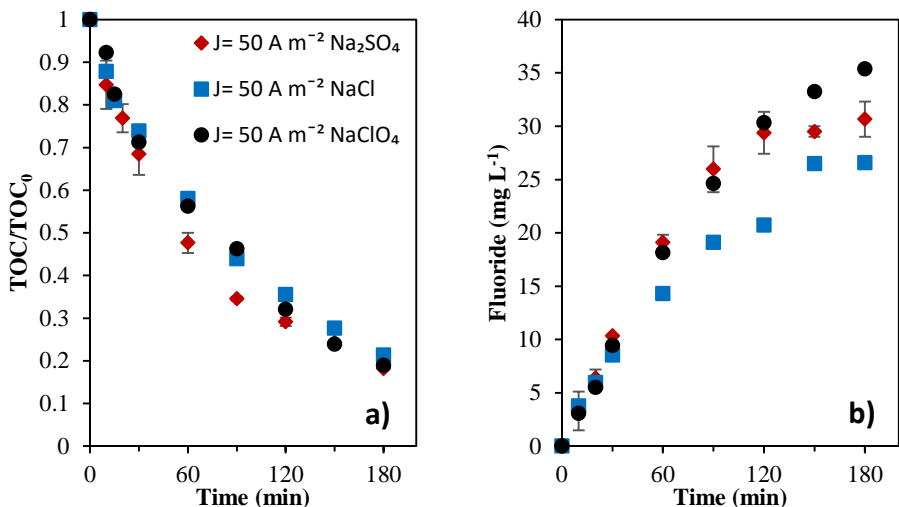


Figure 3.18. Effect of electrolyte on 6:2 FTSA mineralization and defluorination. (a) Fractional TOC (b) and fluoride release.

While perchlorate salts are known to behave as inert electrolytes in BDD electrooxidation [37], sulfate and chloride have been reported to act as promoters of secondary oxidants such as active chlorine, sulfate radical or persulfate anion [38]–[41]. Nevertheless, Figure 3.18a shows no significant influence of the type of electrolyte on TOC kinetics removal, for a 100 mg L⁻¹ 6:2 FTSA solution, revealing that the formation of secondary oxidants with potential ability to degrade 6:2 FTSA and its secondary degradation products did not occur at the low range of applied current density ($J=50 \text{ A m}^{-2}$) used in this group of experiments. Similarly, the release of fluoride anions observed in Figure 3.18b, that resulted from the cleavage of C-F bonds in the perfluorocarboxylic chain of 6:2 FTSA, supports the effective mineralization of the fluorotelomer sulfonate compound into CO₂ and fluoride. A slightly slower fluoride release is observed for NaCl electrolyte solution, in good correspondence with the TOC evolution. This behavior can be attributed to the partial use of the applied current for the anodic oxidation of chloride to chlorine [42], [43].

Using the NaCl electrolyte turned into free chlorine and chlorate generation, as Figure 3.19 depicts, although it is worth mentioning that perchlorate formation was not observed. Electrogenerated active chlorine did not have enough oxidative power to decompose perfluorinated compounds, as shown in Figure 3.18. These results contrast with previously reported BDD degradation of diazo dyes [40] and naphtenic acids [44], where active chlorine species formed upon chloride oxidation significantly enhanced the kinetics of the organic compounds removal.

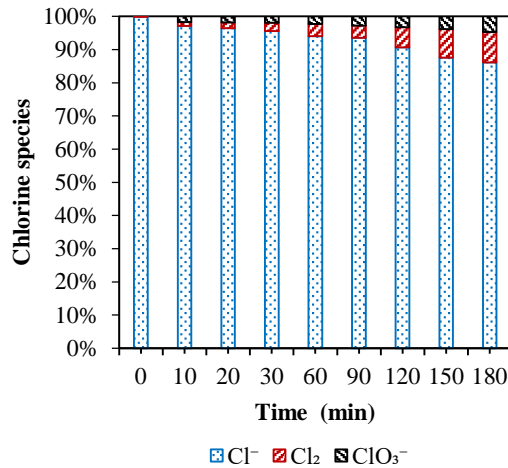


Figure 3.19. Distribution (mol%) of inorganic chlorine species during the ELOX treatment of 6:2 FTSA, when using NaCl as electrolyte. $[\text{NaCl}] = 3.5 \text{ g L}^{-1}$. $[\text{6:2 FTSA}]_0 = 100 \text{ mg L}^{-1}$, $J = 50 \text{ A m}^{-2}$. Total chlorine concentration, as sum of chloride, active chlorine and chlorate, was maintained constant along the experimental time.

Nevertheless, in line with the results of the present study, Schaefer and coworkers [45] proved that chloride had a minimal effect on BDD electrochemical removal of perfluorooctanoic acid and perfluorooctane sulfonic acid, showing that the electrogenerated active chlorine does not degrade perfluorinated compounds. Perchlorate formation by BDD anodic oxidation has been largely reported for sodium chloride electrolytes [37], [46], [47] although perchlorate generation is also known to be delayed at high chloride concentrations [48] and low applied current densities [49], [50]. The low current density ($J = 50 \text{ A m}^{-2}$) applied in the experiments of Figure 3.18 explains the low chlorate development and the absence of perchlorate generation.

Sulfate release was also observed in experiments performed using NaCl and NaClO₄ electrolytes. The C-S bond between the unfluorinated carbon of the alkyl chain and the sulfonic end group (-CH₂-SO₃⁻) makes 6:2 FTSA easily susceptible to oxidation. Results pointed to the total release of the sulfate group contained in the 6:2 FTSA molecule, although the quantitation of sulfate was adversely affected by the large sample dilution that was needed to avoid the saturation of the conductivity detector in the ion chromatography system. For example, using NaCl as electrolyte, the electrochemical treatment of 6:2 FTSA (100 mg L⁻¹, $J=50 \text{ A m}^{-2}$) gave rise to 24 mg L⁻¹ of sulfate in the treated water, that is equivalent to the total amount of oxidized sulfur contained in the initial feed.

3.2.2.2. Influence of the applied current density on 6:2 FTSA degradation and byproducts formation

The effect of the applied current density on 6:2 FTSA treatment is shown in Figures 3.20 and 3.21. Both TOC removal and fluoride release became progressively faster when increasing the applied current in the range 5 – 600 A m⁻². TOC removals at the low J range, 5 – 20 A m⁻², followed zeroth-order trends, although a remarkable enhancement of the TOC removal rate was observed when increasing the applied current in that range. Both features point to a current control regime of the removal kinetics in the low J range. In contrast, increasing the applied current to 50 – 600 A m⁻² modified the apparent TOC removal kinetics to first order, which is associated to a diffusion control kinetic regime. Moreover, increasing the applied current from 50 to 600 A m⁻² granted moderate improvements in the kinetic rates of TOC disappearance. It is worth mentioning that the effect of varying the applied current density had a stronger influence on the kinetics of fluoride release (Figure 3.20b).

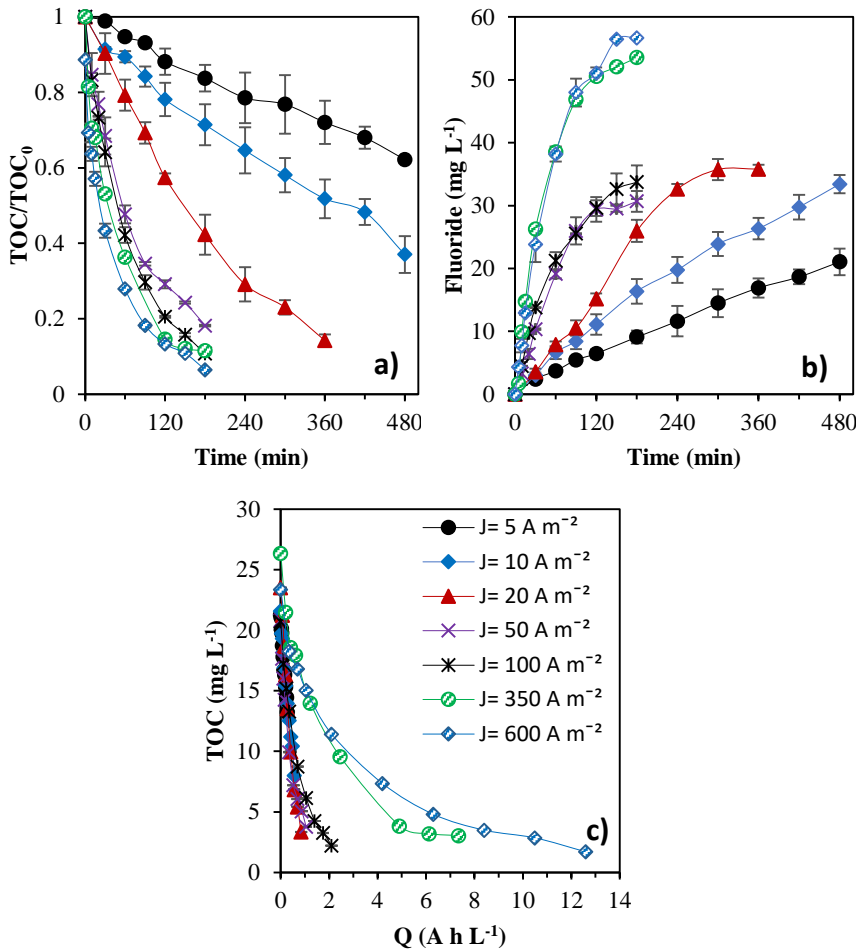


Figure 3.20. Effect of the applied current on the removal of fractional TOC with time (a), and as a function of the specific charge passed Q (b); Fluoride release (c). $[6:2 \text{ FTSA}]_0 = 100 \text{ mg L}^{-1}$, $[\text{TOC}]_0 = 22.5 \text{ mg L}^{-1}$.

This behavior could indicate a beneficial effect of the applied current on the removal of the secondary products, perfluorocarboxylic acids, that were obtained upon degradation of 6:2 FTSA, as it will be discussed later. In terms of energy consumption, the plot (Figure 3.20c) of TOC removal vs. the specific charge passed (Q , A h L⁻¹) indicates that the optimal range

of applied current for the BDD electrochemical treatment of 100 mg L^{-1} 6:2 FTSA solutions is between 20 and 100 A m^{-2} ; the upper value would imply a moderately higher energy consumption, but with the advantage of reducing the treatment time.

Figure 3.21 shows the progress of 6:2 FTSA during BDD electrooxidation at J values from 20 to 600 A m^{-2} . Three distinct zones can be distinguished. Increasing the applied current from 20 to 50 A m^{-2} produced an increase in the kinetics of 6:2 FTSA degradation, although further increase of J to 100 A m^{-2} did not provide any further improvement. Distinctively, the increase of the applied current to 350 and 600 A m^{-2} had a remarkable positive effect on the kinetics of 6:2 FTSA removal, a behavior that can be assigned to the oxidative action of electrogenerated secondary oxidants as a result of sulfate oxidation and reduction reactions to form sulfate radicals ($\text{SO}_4^{\cdot-}$) and peroxidisulfate ($\text{S}_2\text{O}_8^{4-}$), respectively [51], [52].

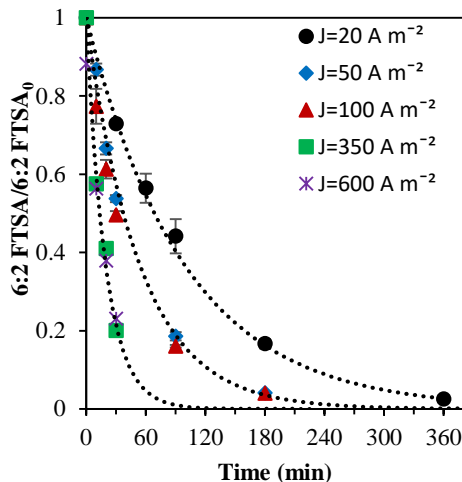


Figure 3.21. Effect of applied current density on fractional 6:2 FTSA removal. $[\text{6:2 FTSA}]_0 = 100 \text{ mg L}^{-1}$. Dotted lines are first order exponential fittings of experimental data.

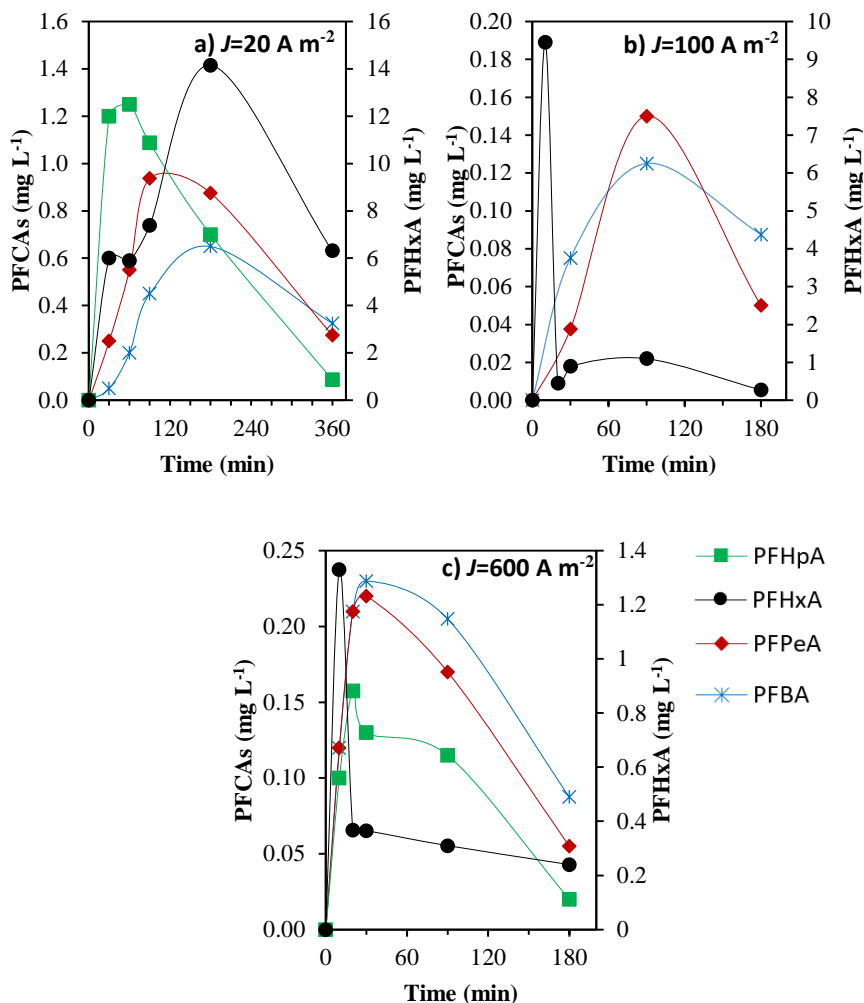


Figure 3.22. Short chain perfluorocarboxylic acids (PFHpA, PFHxA, PFPeA and PFBA) obtained as secondary products of 6:2 FTSA BDD electrooxidation. (a) $J=20 \text{ A m}^{-2}$; (b) $J=100 \text{ A m}^{-2}$; (c) $J=600 \text{ A m}^{-2}$. $[6:2 \text{ FTSA}]_0=100 \text{ mg L}^{-1}$.

Perfluorocarboxylic acids that were obtained as degradation products of 6:2 FTSA are plotted in Figure 3.22 (for conciseness, only data obtained at 20, 100 and 600 A m^{-2} is displayed). At any J , PFHxA was the product

observed at a highest concentration (PFHxA values are read in the right-hand side Y-axis). The maximum PFHxA concentration was observed at earlier treatment times as the applied current was increased. Other PFCAs (PFHpA, PFPeA and PFBA) were observed at lower concentrations than PFHxA, typically below 1 mg L^{-1} , and their content was clearly reduced as the applied current density was increased. PFCAs smaller than PFBA are volatile compounds and cannot be determined in the liquid samples. Remarkably, the formation of PFHpA is observed at much lower concentration than PFHxA, in good agreement with the observations reported by Park and coworkers [53] for heat activated persulfate oxidation of 6:2 FTSA. These results can be explained by the preferential attack of hydroxyl radicals to the $-\text{CH}_2-$ group attached to the perfluoroalkyl chain. Shorter chain PFPeA and PFBA are formed upon the loss of successive CF_2 units in consecutive steps [45], [50]. The results of analyzed PFASs also explains the faster kinetics of 6:2 FTSA disappearance compared to the TOC removal rate, related to the extra energy needed for the degradation of PFCAs obtained as secondary products.

3.2.2.3. Kinetics of the electrochemical oxidation of short-chain perfluorocarboxylic acids

The kinetics of the removal of perfluorocarboxylic acids PFHpA, PFHxA, PFPeA were further explored. In a trial to facilitate the observation of the oxidation by products, and to avoid the conditions needed for the formation of secondary oxidants, the applied current was intentionally maintained at a low value, $J=20 \text{ A m}^{-2}$. Experiments were performed starting with solutions of on single PFHpA, PFHxA or PFPeA, with an initial concentration of 100 mg L^{-1} in every case. 6:2 FTSA removal is included for comparison. Concentration data in Figure 3.23 show that the kinetics

of removal were only slightly faster as the molecular size decreased. These results can be explained by the diffusion control kinetic regime, that is moderately faster as the molecular size of the PFASs compound is reduced. It means that the degradation reaction occurring at the electrode is faster than the diffusion of the compounds moving from the liquid bulk towards the electrode vicinity. The high fast reactivity of the hydroxyl radical mediated oxidizing reactions and direct electron transfer at the anode surface prevents the intermediate compounds of diffusing from the proximity of the anode towards the liquid bulk, and therefore, the observed concentrations of degradation products are always much lower than those predicted from the apparent kinetic constants obtained in individual experiments.

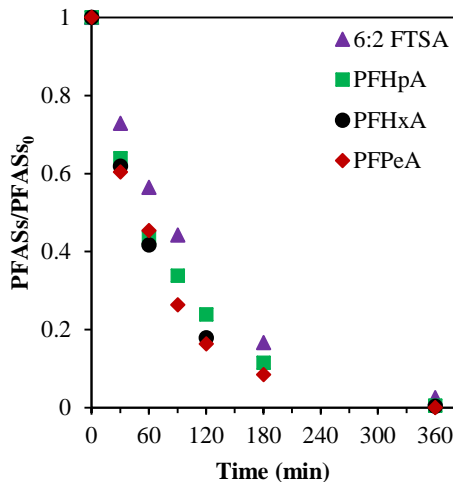


Figure 3.23. Removal of different PFASs. Initial concentration 100 mg L^{-1} for every perfluoroalkyl substance. $J=20 \text{ A m}^{-2}$.

3.3. Design, simulation and optimization of the integrated membrane – electrooxidation process

In this section, the main results of the process design, simulation and optimization of the integrated process described in section 2.5 of Chapter 2 are reported. First, a preliminary study was carried out with a single-stage NF pre-concentration coupled with electrooxidation layout. This study was focused on reducing the energy consumption of perfluorohexanoic acid electrochemical treatment, using simulation tools. The results from this preliminary study correspond to the following published work: *Á. Soriano, D. Gorri, and A. Urriaga, “Membrane pre-concentration as an efficient tool to reduce the energy consumption of perfluorohexanoic acid electrochemical treatment” Separation and Purification Technology, 208, pp. 160–168, 2019.*

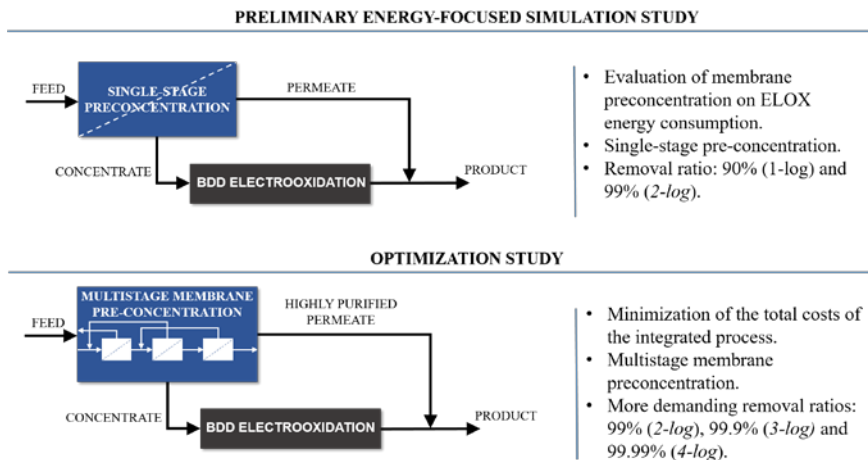


Figure 3.24. Main differences between the preliminary energy-focused analysis and the optimization study.

Then, a rigorous optimization study of the multistage membrane-electrooxidation integrated approach, described in section 2.5.1 of Chapter 2, considering the total economy of the process (capital and operating costs), was performed. The results from this study correspond to the following published work: *Á. Soriano, D. Gorri, L.T. Biegler and A. Urtiaga, "An optimization model for the treatment of perfluorocarboxylic acids considering membrane preconcentration and BDD electrooxidation" Water Research, 164, 114959.*

In both works, we evaluated two of the membranes studied in Section 3.1, the NF90 and the NF270. The results from the membrane characterization work showed in the that the NF90 membrane highly rejects PFHxA (overall, $R_{obs} > 99\%$) but its water permeability is about one-half the permeability of the NF270 membrane, although the latter one achieved PFHxA rejections up to 95%. Ideally, the PFHxA concentration in the permeate should be as low as possible, although the membrane should be highly water-permeable, to diminish preconcentration times and the costs related to the membrane system. Therefore, the evaluation of the NF90 and NF270 membranes in the different scenarios helped to identify the impact of the membrane selectivity/productivity trade-off on the costs of the integrated process.

Figure 3.24 shows the main differences of the two integration approaches. While the first study described in this section of the PhD thesis is focused on the evaluation of the energy consumption of the hybrid process and the influence of the membrane preconcentration on the ELOX energy consumption, the second study is focused on the minimization, by means of optimization tools, of the total costs of the integrated process. Another important difference between both studies is that in the first one it was

considered a single-stage membrane preconcentration layout, whilst in the optimization study it was considered a multistage preconcentration layout that allows to fulfill higher PFHxA abatement ratios at the end of the treatment train.

3.3.1. Preliminary study on PFHxA electrochemical treatment energy savings, through membrane preconcentration

This section summarizes the main results from the preliminary study aimed at studying the minimization of the energy consumption. The integration approach consisted of a basic single-membrane preconcentration stage coupled to electrooxidation layout described in section 2.5.1 of Chapter 2. Information about empirical input data such as empirically obtained parameters used can be found at *Á. Soriano, D. Gorri, and A. Urtiaga, “Membrane preconcentration as an efficient tool to reduce the energy consumption of perfluorohexanoic acid electrochemical treatment” Separation and Purification Technology, 208, pp. 160–168, 2019.*

Two different PFHxA target removal ratios (RR), RR=90% and RR=99%, were considered for the simulation runs of the electrooxidation stage and of the integrated NF-ELOX process. Figure 3.25 shows the total energy consumption of the combined process per cubic meter of treated water as a function of the VRF parameter. $VRF=1$ describes the situation in which no preconcentration is carried out, i.e., ELOX is the only applied treatment. It is important to note that the maximum VRF value that is feasible to apply in the membrane preconcentration stage differs for the different scenarios under study. According to the PFHxA mass balance at the mixing point, to meet a given C_{target} at the end of the treatment train, different C_{pt}^{PFHxA} and C_{ELOX} values are needed (Figure 2.6 of Chapter 2). With the increase of

VRF (or analogously, with the increase of the nanofiltration preconcentration operation time) the concentration in the permeate tank (C_{pt}^{PFHxA}) increases too, forcing the required C_{ELOX} at the exit of the electrooxidation stage to become lower, in order to meet C_{target} at the mixing point. Eventually C_{ELOX} will become equal to zero. At this point, VRF takes its maximum value.

For $RR=90\%$, the use of ELOX alone consumes 14.3 kWh m^{-3} , while the combination of NF270-ELOX minimizes the energy needs at a $VRF = 4.0$, with a specific energy consumption of 7.0 kWh m^{-3} . Further energy savings can be obtained by using the NF90 membrane, that allows 90% PFHxA removal at a $VRF=10$ with only 3.3 kWh m^{-3} .

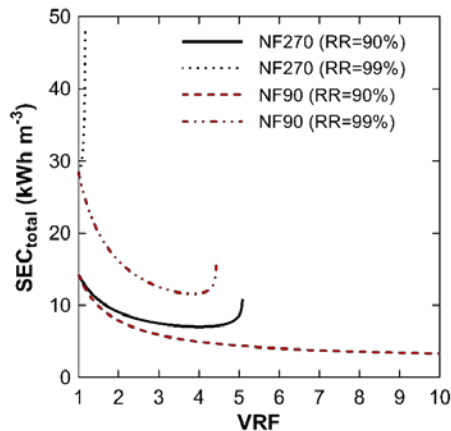


Figure 3.25. Specific energy consumption of the integrated NF-ELOX process as function of VRF for different PFHxA removal ratios at the end of the treatment train ($RR=90\%$ and $RR=99\%$). $V_{it}=5 \text{ m}^3$, $C_{i,0}=204 \text{ mgL}^{-1}$.

When the target RR is set at 99%, the appropriate selection of the membrane module appears to be more important. The integration with the NF270 does not bring any benefit in terms of energy reduction. In fact, the preconcentration step only contributes to increase the total energy demands of the system. In contrast, significant energy savings can be obtained with the NF90 –ELOX system. The energy consumption for the single electrooxidation system (28.4 kWh m^{-3}), is reduced to less than half (11.6 kWh m^{-3}) by the integrated system.

Then, the different PFHxA rejections of the NF90 and NF270 membranes are a key performance parameter for the design and optimization of the integrated NF-ELOX process. When a low target concentration is demanded, the concentration in the membrane permeate stream needs to be low, and the NF90 membrane fulfills this need at a much higher extent than the NF270 membrane. In the RR=99% scenario and due to the insufficient NF270 PFHxA rejection, the PFHxA concentration in the permeate tank (C^{PFHxA}_{pt}) at initial time (12.9 mg L^{-1}) is considerably higher than the objective C_{target} (2.0 mg L^{-1}) and keeps increasing with the increase of VRF . The required C_{ELOX} at the exit of the electrooxidation stage to meet the PFHxA mass balance is therefore progressively smaller as VRF gets higher. Thus, the ELOX energy requirements to treat the NF concentrate to such low C_{ELOX} values are very high and keeps increasing with the simulation run. Conversely, the NF90 allows to obtain much lower PFHxA concentration in the permeate tank due to its higher PFHxA retention. For this reason, the required C_{ELOX} to meet the C_{target} is much less demanding and the ELOX energy consumption is reduced.

Table 3.4. Optimal variables allowing maximum energy savings in the integrated process

Scenario	VRF	C^{PFHxA}_{ft} (mg L ⁻¹)	C^{PFHxA}_{pt} (mg L ⁻¹)	C_{ELOX} (kWh m ⁻³)	SEC_{NF} (kWh m ⁻³)	SEC_{ELOX} (kWh m ⁻³)
NF270 RR=90%	4	748	22.9	11.3	1.2	5.8
NF270 RR=99%	-	204	-	2	-	28.4
NF90 RR=90%	10	2014	3.4	169.6	2	1.3
NF90 RR=99%	3.9	779	2.4	0.7	1.6	10

The local minimum of the energy- VRF curve gives information on the optimal VRF value that allows maximum energy savings. When the target removal ratio is not so demanding (RR=90%) the benefits of the NF-ELOX integration strategy can be clearly seen, and it is possible to apply longer NF preconcentration times and thus higher VRF values with maximum energy savings in the process. For higher target removal ratios, only the NF90-ELOX combined strategy can reduce the energy consumption compared to the single electrooxidation process. Information about the optimal VRF for the different scenarios is gathered in Table 3.4. The reported energy consumption values of the ELOX treatment in all the studied scenarios are significantly lower than the previously reported energy consumption of the electrochemical degradation of long-chain PFASs, in the range of 41.7 – 76.6 kWh m⁻³ [34], especially when the integration with the NF90 is carried out (1.3 -10.0 kW m⁻³ for RR=90% and RR=99%, respectively).

Figure 3.26 shows the contribution of the ELOX and membrane technologies to the total energy consumption, in two situations: i) first, when no preconcentration is applied and only ELOX is considered for

PFHxA removal; and ii) when the integrated process is considered and NF pre-concentration is applied using the optimal *VRF*, that is, the *VRF* that allows minimizing the energy consumption for each target removal ratio, as given in Figure 3.25. For $RR=90\%$, the hybrid process consumes 50.6% (NF270) and 76.7% (NF90) less energy than the ELOX process alone. It is important to highlight that most of the energy consumption comes from the ELOX step. For $RR=99\%$, the integration with the NF90 membrane is able to reduce the ELOX energy consumption by 64.9%. As the optimal *VRF* is limited to 3.9, the nanofiltration contribution to the total energy consumption is noticeably reduced. In this case, the hybrid process consumes 59.2% less energy than the ELOX process alone.

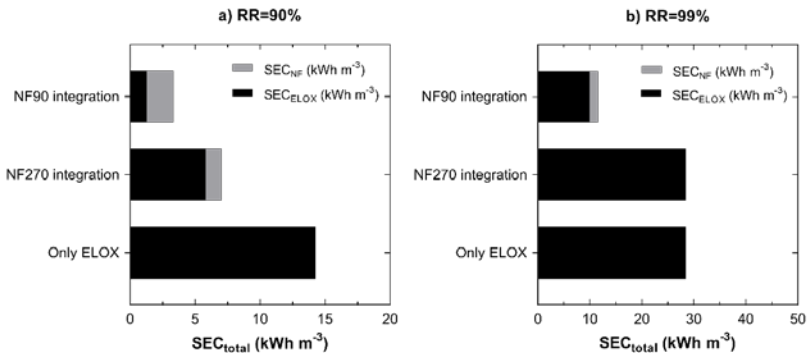


Figure 3.26. Comparison of specific energy consumption (SEC) when NF/ELOX are coupled at the optimal *VRF* and ELOX without previous NF pre-concentration are used, for the different PFHxA removal ratios. (a) $RR=90\%$; (b) $RR=99\%$.

Although the results from this preliminary integration study are quite promising, there are also certain limitations that must be solved in the design of the integrated process. Some of the most important are the following:

- The present study only takes into consideration the energy consumption of the integrated process. The design of the integrated process must be completed through a rigorous techno-economic assessment that takes into account the process modelling of the system and the economic evaluation of all the operating and capital costs.
- As discussed previously, demanding PFHxA abatement targets are only fulfilled by very selective membranes, working in a one-stage separation process. More demanding PFHxA targets may need of additional separation stages. Thus, the design of the integrated process must take into account the possibility of including a multistage membrane preconcentration layout.
- The simulation tools used in this study are not adequate to determine the optimal value of all the variables involved in the design of the integrated process. In this regard, optimization tools are useful to properly determine all the sizing and operation variables. In accordance with the first point, a rigorous study must design the integrated process by determining the optimal variables that minimizes the total costs (operating and capital costs) of the process.

Following the previous analysis, a more rigorous and insightful design work was carried out in the optimization study discussed in the next section, aimed at solving all these limitations and challenges.

3.3.2. Optimization of the multistage membrane preconcentration – electrooxidation integrated process

Finally, in this part of the PhD thesis, it was carried out a rigorous design and optimization of the multistage membrane-electrooxidation integrated process described in Section 2.5.1 (Chapter 2), considering the complete economy (capital and operating costs) of the process.

The design of this process is a complex issue as several variables regarding its sizing and operation should be considered. The most relevant are the following: the membrane area per stage, number of stages, the anode area, the preconcentration operating time, the electrolysis time, the concentrated volume to be electrolyzed as well as the input and output concentration of solutes to the ELOX system and output concentration of all solutes in the permeate and concentrate stream. They affect many other variables, as the flowrates of the membrane system, the pumping and ELOX system energy consumption, operating costs and capital investment costs. All these variables are strongly interrelated and a trade-off between them should be established. Additionally, the resulting hybrid process design must be less costly compared with the application of the individual ELOX process alone. To design such complex cost-optimal process it is necessary to use computer aided process engineering tools. The formulated optimization problem must be solved by minimizing the total costs of the integrated process, at the same time the optimal values of all the variables involved in the process are calculated.

The case of study dealt with the treatment of persistent short chain perfluorocarboxylic acids from the industrial process streams described in Chapter 2. More specifically, the objective was set at the *2-log*, *3-log* and

4-log reduction of PFHxA concentration in the treated water (equivalent to a 99%, 99.9% and 99.99% removal ratio, respectively). We developed a semi-empirical mathematical model describing PFHxA concentration by means of a cascade of membrane elements and the BDD electrolysis of the concentrate stream obtained as retentate in the membrane system. More information about the mathematical and economic model equations and process input parameters can be found in Chapter 5, in the publication *Á. Soriano, D. Gorri, L.T. Biegler and A. Urriaga, "An optimization model for the treatment of perfluorocarboxylic acids considering membrane preconcentration and BDD electrooxidation" in Water Research, 164, 114959.* A scheme of the proposed multistage membrane – electrooxidation process can be found in Figure 2.7 of Chapter 2. Results from this section are expressed in US dollars (\$). At the time this optimization study was carried out, 1 \$ \approx 0.90 €.

3.3.2.1 Hybrid preconcentration / electrooxidation process optimization results

Table 3.5 and Table 3.6 contain the optimal preconcentration and electrooxidation times, membrane area per stage, anode electrode area and total cost for the different scenarios and for two types of nanofiltration membranes (NF270 and NF90), which differ in their water permeability and solute selectivity properties.

We evaluated the use of 1, 2 and 3 preconcentration stages in the membrane system and compared the total cost of all the scenarios with the application of ELOX alone without any preconcentration stage. In Tables 3.5 and 3.6, a preconcentration time equal to zero means that the optimized solution eliminated the preconcentration stage.

Table 3.5. Integration with NF90 membrane optimization results

PFHxA removal	2-log			3-log			4-log		
	1	2	3	1	2	3	1	2	3
Number of stages in the membrane cascade									
Membrane stage 1 area, A_1 (m ²)	28.1	14.0	12.4	2.6	16.0	14.0	2.6	24.8	15.4
Membrane stage 2 area, A_2 (m ²)		10.4	9.2		11.8	10.4		14.4	11.4
Membrane stage 3 area, A_3 (m ²)			9.2			10.3			11.3
Anode electrode area, A_e (m ²)	3.9	1.3	1.4	13.7	1.9	2.0	18.3	2.9	2.6
Preconcentration time, t_{PC} (h)	4.0	12.6	14.2	0.0	11.0	12.6	0.0	9.0	11.5
Electrolysis time, t_{ELOX} (h)	36.0	27.4	25.8	40.00	29.0	27.4	40.0	31.0	28.5
Total annual cost, TC (\$ y ⁻¹)	2.6E+04	1.3E+04	1.4E+04	7.8E+04	1.7E+04	1.8E+04	1.0E+05	2.3E+04	2.2E+04
Total specific cost, TSC (\$ m ⁻³)	12.9	6.4	7.2	39.0	8.3	9.1	51.0	11.7	10.9
Savings (%)	51.3	75.8	72.7	-	78.5	76.3	-	76.9	78.4

Table 3.6. Integration with NF270 membrane optimization results

PFHxA removal	2-log			3-log			4-log		
Number of stages in the membrane cascade	1	2	3	1	2	3	1	2	3
Membrane stage 1 area, A_1 (m ²)	2.6	11.7	10.0	2.6	37.0	11.5	2.6	2.7	10.2
Membrane stage 2 area, A_2 (m ²)		9.4	8.0		10.2	9.2		2.6	36.9
Membrane stage 3 area, A_3 (m ²)			7.6			8.7			7.5
Anode electrode area, A_e (m ²)	9.1	1.5	1.4	13.7	11.4	2.0	18.3	18.3	3.2
Preconcentration time, t_{PC} (h)	0.0	10.4	12.9	0.0	4.1	11.2	0.0	0.0	13.0
Electrolysis time, t_{ELOX} (h)	40.0	29.6	27.1	40.0	35.9	28.8	40.0	40.0	27.1
Total annual cost, TC (\$ y ⁻¹)	5.4E+04	1.3E+04	1.3E+04	7.8E+04	7.0E+04	1.8E+04	1.0E+05	1.0E+05	2.7E+04
Total specific cost, TSC (\$ m ⁻³)	26.9	6.6	6.7	39.0	35.2	8.8	51.0	51.4	13.7
Savings (%)	-	75.0	74.7	-	8.9	77.2	-	-	72.9

For the different scenarios with NF270-1 stage integration for any target PFHxA removal ratio, and the NF90-1 stage integration for 3-*log* and 4-*log* PFHxA abatement, the preconcentration time is equal to zero. In these cases, the hybrid strategy does not bring any benefit from the point of view of total cost savings, since one membrane stage is not enough to obtain a high purity permeate. Since the required target concentration (C_{target}) is considerably lower than the permeate concentration (C_{pt}^{PFHxA}), the output ELOX concentration (C_{ELOX}) must be acutely low to meet the imposed mass balance at the exit of the treatment train. As a result, the ELOX energy costs are significantly higher, and the optimal solution eliminates the preconcentration stage ($t_{PC}=0$), as it only contributes to increase the total treatment costs.

The distribution of all the optimal capital and operating costs, expressed as total specific cost, for the different cases of study are shown in Figure 3.27 and Figure 3.28, using the NF90 and the NF270 membrane, respectively. In all scenarios, the most important contribution to the total costs are the capital costs related to the electrochemical reactor system (from a 47% contribution in the worst scenario to a 36% impact in the best scenario). Based on the optimization results, the costs of the ELOX reactor can be greatly reduced though its integration with the membrane preconcentration strategy, as the total anode area is significantly reduced. The membrane integration also managed to reduce all the operating costs related to the ELOX system, i.e., the lower the anode area, the lower are the costs related to the replacement of the anodes and maintenance. For the 2-*log* PFHxA abatement, the anode area can be reduced from 9.1 m² in the case of only-ELOX, to 3.9 m² with NF90-1 stage integration, and furthermore, to 1.3 m² with NF90-2 membrane stages and 1.4 m² with NF90-3 membrane stages.

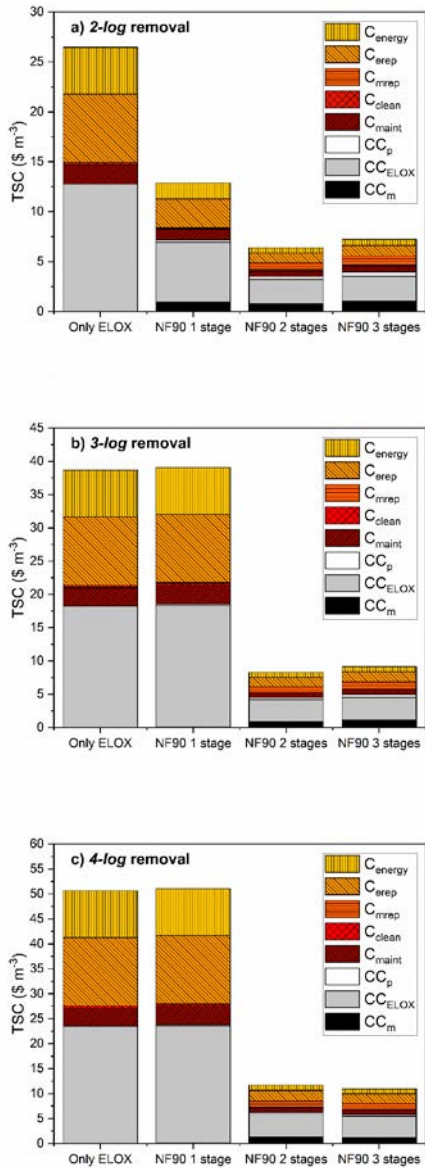


Figure 3.27. Comparison of the CAPEX (CC) and OPEX (C) costs distribution for the 1, 2 and 3 NF90 membrane stages coupled to ELOX, and application of ELOX without preconcentration for different PFHxA abatement targets: 2-log, 3-log and 4-log

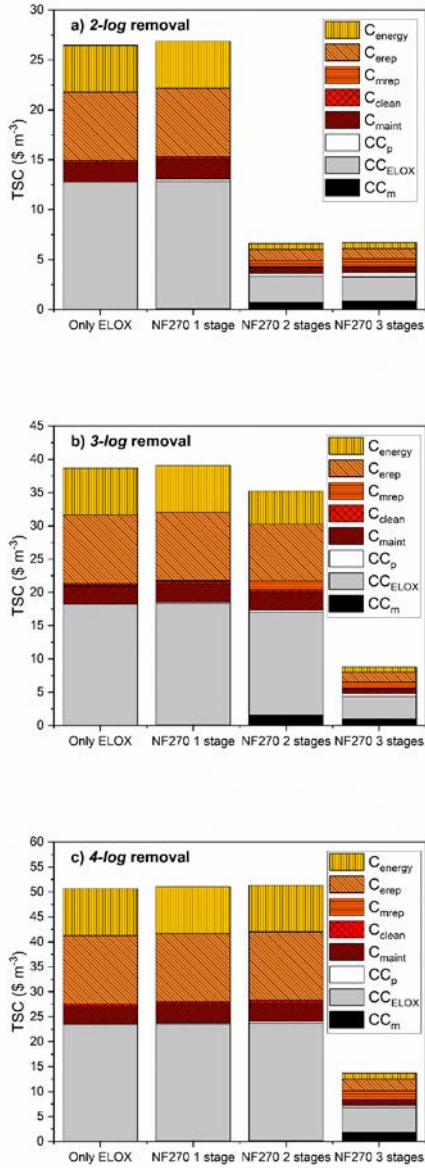


Figure 3.28. Comparison of the CAPEX (CC) and OPEX (C) costs distribution for the 1, 2 and 3 NF270 membrane stages coupled to ELOX, and application of ELOX without preconcentration for different PFHxA abatement targets: 2-log, 3-log and 4-log.

These results are translated into 51.3% savings of the total cost with the NF90-1 stage integration, compared to the application of the electrooxidation process alone. These savings are even higher with the use of two stages (75.8%) because of the lower optimal anode area capital and replacement costs. Overall, the integration results are slightly better when two membrane stages are used, since adding more membrane stages also increases the capital and operating costs related to the membrane system. On the other hand, cleaning costs only represents up to 0.9% of the total costs of the integrated process. In the case of cathode scaling promoters, such as calcium, being present at elevated concentrations, more frequent chemical cleanings will be needed. Nevertheless, due to the minor contribution of the cleaning costs to the total costs function the presence of scaling species would not have a great impact on the optimization results.

When an extremely demanding PFHxA abatement is required, as it is the *4-log* elimination scenario, the integration of a three stages membrane cascade provides better results, and the total savings increased to 78.4%, through the optimization of all the process variables. For the highly productive but more PFHxA permeable NF270 membrane, a *4-log* PFHxA abatement requires a three stages cascade preconcentration, although the total cost is slightly higher than for the NF90 integration. This is because the optimal output ELOX concentration in the NF270 integration scenario ($C_{ELOX}=0.02 \text{ mg L}^{-1}$) is more demanding than when using the NF90 ($C_{ELOX}=0.1 \text{ mg L}^{-1}$), which, as previously explained, is a consequence of the lower PFHxA rejection of the NF270 membrane. Therefore, the costs related to the ELOX energy consumption are higher. As the ELOX capital costs clearly overshadow the membrane system equipment costs, it is possible to add up to three membrane stages for a *4-log* abatement and still get a slight reduction of the total costs. (e.g., in the *4-log* NF90 case of

study). In general, the membrane equipment investment only represents 7% to 13% of the total costs in those scenarios in which the integration approach works, and the pump capital cost contributions are up to 7%.

The integration strategy is also able to accomplish important reductions on the operating costs related to the energy consumption of the process compared to the application of the electrolysis alone (Figure 3.29). Depending on the PFHxA elimination target, the energy specific costs of the only-ELOX scenario range from 4.7 \$ m⁻³ for a 2-log PFHxA removal to 9.4 \$ m⁻³ for a 4-log removal. Remarkably, the membrane coupling approach can reduce the energy costs to 0.6 \$ m⁻³, 0.7 \$ m⁻³ and 1.0 \$ m⁻³ for a 2-log, 3-log and 4-log PFHxA abatement, respectively. These energy savings (up to 89%) notably influence the total costs, as the energy cost contribution to the total costs is reduced from an 18% to only 8-9%.

The pathway for reducing the energy costs goes through the optimization of the electrolysis time, which is much lower in the membrane integrated system than in the approach with ELOX alone. The cutback on the electrolysis time is mainly due to (i) the much lower volume to be electrolyzed and, (ii) the less demanding PFHxA concentration at the exit of the ELOX system that is needed to meet the target concentration at the exit of the treatment train. This is also influenced by the very low PFHxA concentration obtained in the permeate tank of the membrane system at the end of the preconcentration run. Additionally, membrane separation also increases the concentration of salts in solution, to make the electrolyte more conductive, and therefore the cell voltage is also reduced, diminishing to a lesser degree the ELOX energy costs.

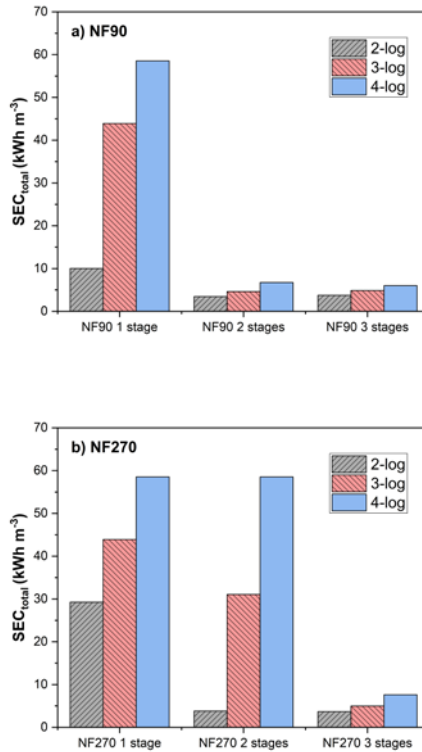


Figure 3.29. Optimal total specific energy consumption of the hybrid process using the NF90 and NF270 membranes for the different PFHxA abatement targets.

As Figure 3.29 shows, the ELOX energy savings have a huge impact on the overall energy consumption. Taking as a reference the estimated electrolysis energy consumptions of the ELOX-only scenario (29.3 kWh m⁻³, 43.9 kWh m⁻³ and 58.5 kWh m⁻³, for a *2-log*, *3-log* and *4-log* PFHxA abatement, respectively) the optimized hybrid process consumes 29.3% – 89.7% less energy, depending on the type of membrane used and on the number of membrane stages. In most cases, and except for the *2-log* NF90-

1 stage scenario, the use of a single membrane stage does not provide energy savings.

3.3.2.2. Parametric sensitivity analysis

The two commercial membranes considered in this work (NF90 and NF270) yielded excellent results in the integrated process through proper optimization of the process variables. However, it is interesting to determine if hypothetically more selective or more permeable membrane materials would achieve better results in terms of minimization of the total costs. It should be also highlighted that the rejection performance of the herein studied membranes can be affected by the increase of the solution ionic strength, pH acidification or due to the effect of concentration on the selectivity factor. Initial permeate flux might also be reduced because of organic and inorganic fouling. Hence, in this section, a sensitivity analysis is performed with the aim of getting a deeper understanding on the influence of the studied membrane properties on the total cost objective function. Additionally, we evaluated the influence of the kinetic constant of the electrochemical PFHxA degradation on the total costs objective function when using the NF90 membrane and different number of membrane stages.

The effect of the membrane hydraulic permeability (L_p) and the selectivity factor (defined as $\alpha^{PFHxA} = 1 - (R_{obs,PFHxA}/100)$) on the total specific cost for a 3-log PFHxA abatement is shown in Figure 3.30. Only two and three membrane stages are illustrated since the use of a single membrane stage did not provide any optimal TSC below the only-ELOX scenario.

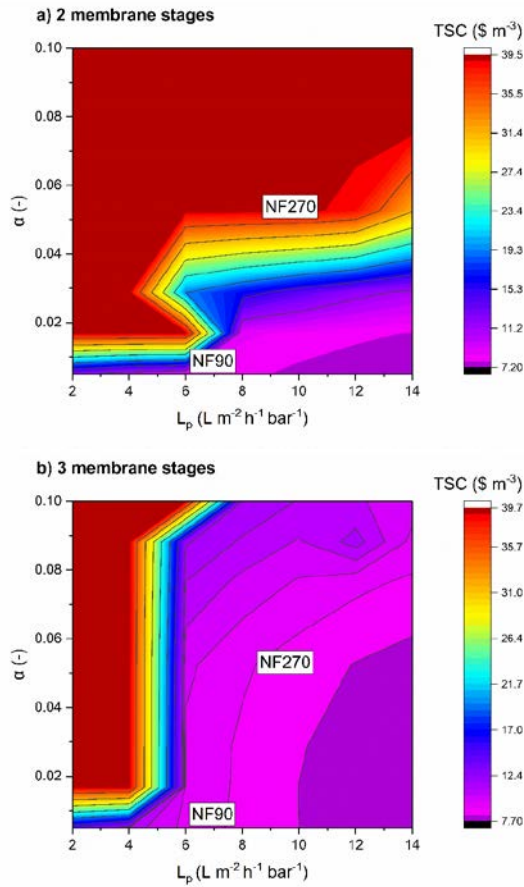


Figure 3.30. Influence of the membrane properties on the total cost objective function for a 3-log PFHxA abatement. (a) 2 membrane stages and (b) 3 membrane stages.

In Figure 3.30, the dark red area corresponds to TSC solutions in which the optimal scenario is to eliminate the pre-concentration process and therefore, the integration does not provide any advantage. For orientation purposes, the optimal results of the two commercial membranes studied in this work (NF90 and NF270) have been added to the figure, according to their PFHxA selectivity and hydraulic permeability data. In Figure 3.30, α^{PFHxA}

ranges from $\alpha^{PFHxA} = 0.1$ (equivalent to $R_{PFHxA} = 90\%$) to $\alpha^{PFHxA} = 0.005$ ($R_{PFHxA} = 99.5\%$), since the empirical values of PFHxA rejection ranged from 94.8% (NF270) and 99.4% (NF90).

In Figures 3.30a and 3.30b, the lower left hand corner would correspond to TSC solutions theoretically given by reverse osmosis membranes typically characterized by their low permeability and very high selectivity (low α^{PFHxA} value) [54]. With two membrane stages (Figure 3.30a), only membranes with very high PFHxA selectivity and medium-high water permeability would be able to accomplish significant total cost savings, as in the case of the NF90 membrane. However, as seen in Figure 3.30a the excellent results given by the NF90 membrane are subject to changes in the optimum TSC with any hypothetical reduction of the PFHxA rejection performance or by any decrease of the membrane permeate flux as a result of membrane fouling.

On the other hand, less selective but more water permeable membranes, such as the NF270, achieve similar total costs savings when three membrane stages are considered (Fig 3.30b). In contrast with the 2-stage integration scenario, any rejection decline in the 3-stage integration scenario would not severely affect the optimal TSC given by the two nanofiltration membranes. However, from a process operation viewpoint it is easier and more suitable to manage a process with fewer membrane stages. Also, according to Figure 3.30, more selective and more productive membranes would be able to reduce the TSC to a minimum of $7.2 \text{ \$ m}^{-3}$, which is very close to the best scenario obtained with the commercial NF90 membrane and by means of two membrane stages ($8.3 \text{ \$ m}^{-3}$). Finally, in any integration scenario the use of highly PFHxA selective but low water-permeable membranes, as in the case of some reverse osmosis membranes,

is not recommended, as any noticeable reduction of the PFHxA rejection performance would severally modify the optimal TSC, thus compromising the benefits of the integrated strategy. It is also worth mentioning that literature reports effective nanofiltration retentions of shorter-chained PFASs such as perfluorobutanoic acid (PFBA), perfluorobutanesulfonic acid (PFBS) and perfluoropentanoic acid (PFPeA), that are generally above 93-95% [5], [6]. From Figure 3.30, it can be seen that the use of the NF-ELOX strategy for the treatment of these substances may require up to 3 stages to bring benefits from the point of view of total costs savings.

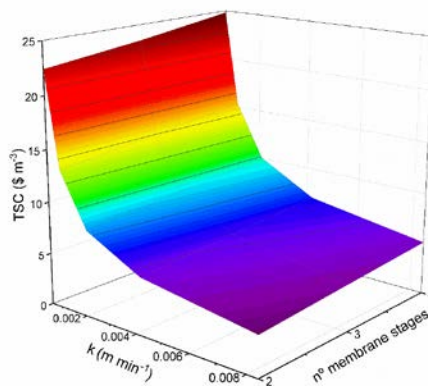


Figure 3.31. Influence of the PFHxA degradation constant (k_{PFHxA}) on the total cost objective function for a 3-log PFHxA abatement and different number of membrane stages. Integration with the NF90 membrane.

Figure 3.31 shows the sensibility of the optimized solution to variations of the kinetics of PFHxA electrolysis. Considering a 3-log PFHxA abatement and using the NF90, doubling the value of k_{PFHxA} ($k_{PFHxA} = 2.1 \times 10^{-3} \text{ m min}^{-1}$, empirically determined from experiments shown in Section 3.2.1.2) would reduce the total costs of the hybrid process from 8.3 \$ m^{-3} to 5.5 \$

m^{-3} , a consequence of the drastic 45% reduction of the optimal anode area. Conversely, halving the value of k_{PFHxA} has a greater impact on the objective function, as the total costs increases to $13.4 \text{ \$ m}^{-3}$. Yet, in this hypothetical scenario the integrated strategy would be still able to reduce the total costs a remarkable 65.3% compared to the application of the electrooxidation alone without previous preconcentration.

3.4. Nomenclature

A_e	Total anode electrode area (m^2)
A_k	Stage k membrane area (m^2)
$CAPEX$	Total capital expenses (\$)
CC_{ELOX}	Electrooxidation plant capital expenses (\$)
C_{clean}	Cleaning operating costs ($\text{\$ y}^{-1}$)
CC_M	Membrane equipment capital cost (\$)
CC_p	Preconcentration pumping capital cost (\$)
C_{ELOX}	Concentration in the ELOX reactor (mg L^{-1})
C_{energy}	Energy costs ($\text{\$ y}^{-1}$)
C_{eq}	Equivalent ion concentration (mol L^{-1})
C_{erep}	Electrode replacement costs ($\text{\$ y}^{-1}$)
$C_{P,k}^i$	Stage k permeate stream concentration (mg L^{-1})
C_{pt}^i	Permeate tank solute concentration (mg L^{-1})
$C_{R,k}^i$	Retentate stream solute concentration (mg L^{-1})
C_{maint}	Maintenance operating costs ($\text{\$ y}^{-1}$)
C_{mrep}	Membrane replacement costs ($\text{\$ y}^{-1}$)
C_{target}	PFHxA target concentration (mg L^{-1})

E_{ELOX}	ELOX energy consumption (kWh)
E_{PC}	NF energy consumption (kWh)
J	Applied current density ($A\ m^{-2}$)
J_{lim}	Limiting current density ($A\ m^{-2}$)
J_v	Volumetric permeate flux ($L\ m^{-2}\ h^{-1}$)
k_{PFHxA}	PFHxA degradation kinetic constant ($m\ min^{-1}$)
L_p	Membrane permeability ($L\ m^{-2}\ h^{-1}\ bar^{-1}$)
$L_{p,S1}$	Mem. permeability (feed water S1) ($L\ m^{-2}\ h^{-1}\ bar^{-1}$)
$L_{p,S2}$	Mem. permeability (feed water S2) ($L\ m^{-2}\ h^{-1}\ bar^{-1}$)
L_{pm}	Mem. permeability (model solution) ($L\ m^{-2}\ h^{-1}\ bar^{-1}$)
L_{pw}	Mem. permeability (pure water) ($L\ m^{-2}\ h^{-1}\ bar^{-1}$)
$MWCO$	Molecular weight cut-off (Da)
$OPEX$	Operating expenses ($\$ y^{-1}$)
Q	Specific charge ($A\ h\ L^{-1}$)
$R_{int,i}$	Intrinsic rejection of solute i
$R_{obs,i}$	Observed rejection of solute i
RR	Removal rate (%)
SEC_{ELOX}	ELOX specific energy consumption ($kWh\ m^{-3}$)
SEC_{NF}	NF specific energy consumption ($kWh\ m^{-3}$)
SEC_{total}	Total specific energy consumption ($kWh\ m^{-3}$)
TC	Total annual cost ($\$ y^{-1}$)
t_{ELOX}	ELOX operation time (h)
t_{PC}	Preconcentration time (h)
TSC	Total specific cost ($\$ m^{-3}$)

U	ELOX cell voltage (V)
V	Electrochemical cell voltage (V)
VRF	Volume reduction factor (-)
z^i	Ionic valence (-)
α^i	Solute partitioning empirical parameter (-)
ΔP	Effective pressure difference (bar)
$\Delta\pi$	Osmotic pressure difference (bar)

3.5. References

- [1] J. Wang, Z. Wang, Y. Liu, J. Wang, and S. Wang, "Surface modification of NF membrane with zwitterionic polymer to improve anti-biofouling property," *J. Memb. Sci.*, vol. 514, pp. 407–417, 2016.
- [2] L. D. Nghiem and S. Hawkes, "Effects of membrane fouling on the nanofiltration of pharmaceutically active compounds (PhACs): Mechanisms and role of membrane pore size," *Sep. Purif. Technol.*, vol. 57, no. 1, pp. 176–184, 2007.
- [3] A. Pérez-González, R. Ibáñez, P. Gómez, A. M. Urriaga, I. Ortiz, and J. A. Irabien, "Nanofiltration separation of polyvalent and monovalent anions in desalination brines," *J. Memb. Sci.*, vol. 473, pp. 16–27, 2015.
- [4] X. Hang, X. Chen, J. Luo, W. Cao, and Y. Wan, "Removal and recovery of perfluorooctanoate from wastewater by nanofiltration," *Sep. Purif. Technol.*, vol. 145, pp. 120–129, 2015.
- [5] T. D. Appleman, E. R. V Dickenson, C. Bellona, and C. P. Higgins, "Nanofiltration and granular activated carbon treatment of perfluoroalkyl acids," *J. Hazard. Mater.*, vol. 260, pp. 740–746, 2013.
- [6] E. Steinle-Darling and M. Reinhard, "Nanofiltration for trace organic contaminant removal: Structure, solution, and membrane fouling effects on the rejection of perfluorochemicals," *Environ. Sci. Technol.*, vol. 42, no. 14, pp. 5292–5297, 2008.
- [7] C. Bellona and J. E. Drewes, "Viability of a low-pressure nanofilter in treating recycled water for water reuse applications: A pilot-scale study," *Water Res.*, vol. 41, no. 17, pp. 3948–3958, 2007.
- [8] N. Hilal, V. Kochkodan, H. Al Abdulgader, and D. Johnson, "A combined ion

- exchange-nanofiltration process for water desalination: II. Membrane selection,” *Desalination*, vol. 363, pp. 51–57, 2015.
- [9] K. V. Plakas and A. J. Karabelas, “Membrane retention of herbicides from single and multi-solute media: The effect of ionic environment,” *J. Memb. Sci.*, vol. 320, no. 1–2, pp. 325–334, 2008.
- [10] J. Shen and A. I. Schäfer, “Factors affecting fluoride and natural organic matter (NOM) removal from natural waters in Tanzania by nanofiltration/reverse osmosis,” *Sci. Total Environ.*, vol. 527–528, pp. 520–529, 2015.
- [11] A. J. C. Semião and A. I. Schäfer, “Removal of adsorbing estrogenic micropollutants by nanofiltration membranes: Part B-Model development,” *J. Memb. Sci.*, vol. 431, pp. 257–266, 2013.
- [12] A. E. Childress and M. Elimelech, “Relating nanofiltration membrane performance to membrane charge (electrokinetic) characteristics,” *Environ. Sci. Technol.*, vol. 34, no. 17, pp. 3710–3716, 2000.
- [13] B. A. M. Al-Rashdi, D. J. Johnson, and N. Hilal, “Removal of heavy metal ions by nanofiltration,” *Desalination*, vol. 315, pp. 2–17, 2013.
- [14] M. J. López-Muñoz, A. Sotto, J. M. Arsuaga, and B. Van der Bruggen, “Influence of membrane, solute and solution properties on the retention of phenolic compounds in aqueous solution by nanofiltration membranes,” *Sep. Purif. Technol.*, vol. 66, no. 1, pp. 194–201, 2009.
- [15] A. L. Ahmad, L. S. Tan, and S. R. Abd. Shukor, “The role of pH in nanofiltration of atrazine and dimethoate from aqueous solution,” *J. Hazard. Mater.*, vol. 154, no. 1–3, pp. 633–638, 2008.
- [16] L. Huang, N. N. Bui, M. T. Meyering, T. J. Hamlin, and J. R. McCutcheon, “Novel hydrophilic nylon 6,6 microfiltration membrane supported thin film composite membranes for engineered osmosis,” *J. Memb. Sci.*, vol. 437, pp. 141–149, 2013.
- [17] The Dow Chemical Company, “Dow Water and Process Solutions.” [Online]. Available: <https://www.dow.com/en-us/water-and-process-solutions/products>. [Accessed: 28-Aug-2018].
- [18] S. Rayne and K. Forest, “Theoretical studies on the pKa values of perfluoroalkyl carboxylic acids,” *J. Mol. Struct. THEOCHEM*, vol. 949, no. 1–3, pp. 60–69, 2010.
- [19] Y. Kiso, K. Muroshige, T. Oguchi, M. Hirose, T. Ohara, and T. Shintani, “Pore radius estimation based on organic solute molecular shape and effects of pressure on pore radius for a reverse osmosis membrane,” *J. Memb. Sci.*, vol. 369, no. 1–2, pp. 290–298, 2011.

- [20] E. L. Cussler, *Diffusion: Mass Transfer in Fluid Systems*, 2nd ed. Cambridge, UK: Cambridge University Press, 1997.
- [21] R. H. Perry, D. W. Green, and J. O. Maloney, *Perry's Chemical Engineers' Handbook*, 7th ed. New York: McGraw-Hill, 1997.
- [22] C. Bellona, J. E. Drewes, P. Xu, and G. Amy, "Factors affecting the rejection of organic solutes during NF/RO treatment - A literature review," *Water Res.*, vol. 38, no. 12, pp. 2795–2809, 2004.
- [23] C. Bellona and J. E. Drewes, "The role of membrane surface charge and solute physico-chemical properties in the rejection of organic acids by NF membranes," *J. Memb. Sci.*, vol. 249, no. 1–2, pp. 227–234, 2005.
- [24] L. D. Nghiem, A. I. Schäfer, and M. Elimelech, "Role of electrostatic interactions in the retention of pharmaceutically active contaminants by a loose nanofiltration membrane," *J. Memb. Sci.*, vol. 286, no. 1–2, pp. 52–59, 2006.
- [25] C. Zhao *et al.*, "Study on the effects of cations and anions on the removal of perfluorooctane sulphonate by nanofiltration membrane," *Sep. Purif. Technol.*, vol. 202, pp. 385–396, 2018.
- [26] J. Wang *et al.*, "Perfluorooctane sulfonate and perfluorobutane sulfonate removal from water by nanofiltration membrane: The roles of solute concentration, ionic strength, and macromolecular organic foulants," *Chem. Eng. J.*, vol. 332, pp. 787–797, 2018.
- [27] Q. Zhuo *et al.*, "Degradation of perfluorinated compounds on a boron-doped diamond electrode," *Electrochim. Acta*, vol. 77, pp. 17–22, 2012.
- [28] Q. Zhuo, S. Deng, B. Yang, J. Huang, and G. Yu, "Efficient electrochemical oxidation of perfluorooctanoate using a Ti/SnO₂-Sb-Bi anode," *Environ. Sci. Technol.*, vol. 45, no. 7, pp. 2973–2979, 2011.
- [29] H. Lin, J. Niu, S. Ding, and L. Zhang, "Electrochemical degradation of perfluorooctanoic acid (PFOA) by Ti/SnO₂-Sb, Ti/SnO₂-Sb/PbO₂ and Ti/SnO₂-Sb/MnO₂ anodes," *Water Res.*, vol. 46, no. 7, pp. 2281–2289, 2012.
- [30] Q. Zhuo *et al.*, "Electrochemical oxidation of 1H,1H,2H,2H-perfluorooctane sulfonic acid (6:2 FTS) on DSA electrode: Operating parameters and mechanism," *J. Environ. Sci. (China)*, vol. 26, no. 8, pp. 1733–1739, 2014.
- [31] H. Hori *et al.*, "Efficient decomposition of environmentally persistent perfluorocarboxylic acids by use of persulfate as a photochemical oxidant," *Environ. Sci. Technol.*, vol. 39, no. 7, 2005.
- [32] Q. Zhuo, S. Deng, B. Yang, J. Huang, and G. Yu, "Efficient electrochemical

- oxidation of perfluorooctanoate using a Ti/SnO₂-Sb-Bi anode,” *Environ. Sci. Technol.*, vol. 45, no. 7, 2011.
- [33] H. Lin, J. Niu, S. Ding, and L. Zhang, “Electrochemical degradation of perfluorooctanoic acid (PFOA) by Ti/SnO₂-Sb, Ti/SnO₂-Sb/PbO₂ and Ti/SnO₂-Sb/MnO₂ anodes,” *Water Res.*, vol. 46, no. 7, pp. 2281–2289, 2012.
- [34] J. Niu, Y. Li, E. Shang, Z. Xu, and J. Liu, “Electrochemical oxidation of perfluorinated compounds in water,” *Chemosphere*, vol. 146, pp. 526–538, 2016.
- [35] C. E. Schaefer, G. M. Lavorgna, T. S. Webster, M. A. Deshusses, C. Andaya, and A. Urtiaga, “Pilot-scale electrochemical disinfection of surface water: assessing disinfection by-product and free chlorine formation,” *Water Sci. Technol. Water Supply*, Sep. 2016.
- [36] Q. Zhuo *et al.*, “Degradation of perfluorinated compounds on a boron-doped diamond electrode,” *Electrochim. Acta*, vol. 77, pp. 17–22, 2012.
- [37] O. Azizi, D. Hubler, G. Schrader, J. Farrell, and B. P. Chaplin, “Mechanism of perchlorate formation on boron-doped diamond film anodes,” *Environ. Sci. Technol.*, vol. 45, no. 24, pp. 10582–10590, 2011.
- [38] M. J. Martín de Vidales, M. Millán, C. Sáez, J. F. Pérez, M. A. Rodrigo, and P. Cañizares, “Conductive diamond electrochemical oxidation of caffeine-intensified biologically treated urban wastewater,” *Chemosphere*, vol. 136, pp. 281–288, 2015.
- [39] A. Uranga-Flores, C. De La Rosa-Júarez, S. Gutierrez-Granados, D. C. De Moura, C. A. Martínez-Huitle, and J. M. Peralta Hernández, “Electrochemical promotion of strong oxidants to degrade Acid Red 211: Effect of supporting electrolytes,” *J. Electroanal. Chem.*, vol. 738, pp. 84–91, 2015.
- [40] H. Jalife-Jacobo, R. Feria-Reyes, O. Serrano-Torres, S. Gutiérrez-Granados, and J. M. Peralta-Hernández, “Diazo dye Congo Red degradation using a Boron-doped diamond anode: An experimental study on the effect of supporting electrolytes,” *J. Hazard. Mater.*, vol. 319, pp. 78–83, 2016.
- [41] Y. Lan, C. Coetsier, C. Causserand, and K. Groenen Serrano, “On the role of salts for the treatment of wastewaters containing pharmaceuticals by electrochemical oxidation using a boron doped diamond anode,” *Electrochim. Acta*, vol. 231, pp. 309–318, 2017.
- [42] A. Cabeza, A. M. Urtiaga, and I. Ortiz, “Electrochemical treatment of landfill leachates using a boron-doped diamond anode,” *Ind. Eng. Chem. Res.*, vol. 46, no. 5, pp. 1439–1446, 2007.

- [43] A. Urriaga, I. Ortiz, A. Anglada, D. Mantzavinos, and E. Diamadopoulos, "Kinetic modeling of the electrochemical removal of ammonium and COD from landfill leachates," *J. Appl. Electrochem.*, vol. 42, no. 9, pp. 779–786, 2012.
- [44] N. Diban and A. Urriaga, "Electrochemical mineralization and detoxification of naphthenic acids on boron-doped diamond anodes," *Environ. Sci. Pollut. Res.*, pp. 1–8, 2018.
- [45] C. E. Schaefer *et al.*, "Electrochemical treatment of perfluorooctanoic acid and perfluorooctane sulfonate: insights into mechanisms and application to groundwater treatment," *Chem. Eng. J.*, vol. 317, pp. 424–432, 2017.
- [46] M. E. H. Bergmann, J. Rollin, and T. Iourtchouk, "The occurrence of perchlorate during drinking water electrolysis using BDD anodes," *Electrochim. Acta*, vol. 54, no. 7, pp. 2102–2107, 2009.
- [47] A. Urriaga, P. Fernandez-Castro, P. Gómez, and I. Ortiz, "Remediation of wastewaters containing tetrahydrofuran. Study of the electrochemical mineralization on BDD electrodes," *Chem. Eng. J.*, vol. 239, 2014.
- [48] G. Pérez, J. Saiz, R. Ibañez, A. M. Urriaga, and I. Ortiz, "Assessment of the formation of inorganic oxidation by-products during the electrocatalytic treatment of ammonium from landfill leachates," *Water Res.*, vol. 46, no. 8, pp. 2579–2590, 2012.
- [49] A. R. F. Pipi, I. Sirés, A. R. De Andrade, and E. Brillas, "Application of electrochemical advanced oxidation processes to the mineralization of the herbicide diuron," *Chemosphere*, vol. 109, pp. 49–55, 2014.
- [50] B. Gomez-Ruiz *et al.*, "Boron doped diamond electrooxidation of 6:2 fluorotelomers and perfluorocarboxylic acids. Application to industrial wastewaters treatment," *J. Electroanal. Chem.*, vol. 798, no. March, pp. 51–57, 2017.
- [51] J. Davis, J. C. Baygents, and J. Farrell, "Understanding persulfate production at boron doped diamond film anodes," *Electrochim. Acta*, vol. 150, pp. 68–74, 2014.
- [52] F. Sopaj, M. A. Rodrigo, N. Oturan, F. I. Podvorica, J. Pinson, and M. A. Oturan, "Influence of the anode materials on the electrochemical oxidation efficiency. Application to oxidative degradation of the pharmaceutical amoxicillin," *Chem. Eng. J.*, vol. 262, pp. 286–294, 2015.
- [53] S. Park, L. S. Lee, V. F. Medina, A. Zull, and S. Waisner, "Heat-activated persulfate oxidation of PFOA, 6:2 fluorotelomer sulfonate, and PFOS under conditions suitable for in-situ groundwater remediation," *Chemosphere*, vol. 145,

pp. 376–383, 2016.

- [54] Á. Soriano, D. Gorri, and A. Urriaga, “Selection of High Flux Membrane for the Effective Removal of Short-Chain Perfluorocarboxylic Acids,” *Ind. Eng. Chem. Res.*, vol. 58, no. 8, pp. 3329–3338, 2019.

4. Conclusions

4.1. Conclusions and perspective

This thesis aims to develop advanced technologies for the treatment of persistent short-chain per- and polyfluoroalkyl substances (PFASs), currently used in the industry as alternative to phased-out long-chain PFASs, from real industrial effluents. To fulfil this objective, it was evaluated the use of nanofiltration (NF) / reverse osmosis (RO) and electrooxidation (ELOX) technologies in the treatment of perfluorohexanoic acid and 6:2 fluortelomer sulfonic acid. Also, process systems engineering and optimization tools were used to design and evaluate an integrated membrane preconcentration/electrooxidation process to overcome the individual limitations of each of both processes. Specific conclusions drawn from the results of this thesis are listed below.

4.1.1. Nanofiltration and reverse osmosis

- i. The commercial NF270 membrane showed the highest water permeability among all the commercial NF and RO membranes at all pH conditions. However, it also showed a significant water flux decline when the pH shifted from acidic to neutral. For the rest of the membranes studied, including the other pure NF membranes (ESNA-LF, ESNA-LF2), the NF90 and the RO membranes (XLE, BW30 and SW30XLE), the water permeability was barely affected by changes in the solution pH.
- ii. Although the NF270 membrane effectively retained perfluorohexanoic acid (PFHxA) from industrial and model solutions streams at neutral pH conditions, the rejection severely declined at acidic conditions. Slight PFHxA rejection reductions were observed when using tighter membranes, such as the NF90

and the RO membranes. These findings suggest that size exclusion and electrostatic interactions between the deprotonated perfluorohexanoate and the membrane surface, may simultaneously occur. Electrostatic repulsion played an important role when the separation was carried out by NF membranes with similar pore size to the PFHxA molecular size. On the contrary, for smaller pore size membranes such as the NF90 and the RO membranes, pore size exclusion was the main separation mechanism.

- iii. The NF90 and XLE membranes provided very high PFHxA rejections in the treatment of process waters containing moderate amounts of salts ($R_{obs,PFHxA}=99.4\% - 99.6\%$). On the contrary, the PFHxA rejections by the NF270 and, especially the ESNA-LF and ESNA-LF2 membranes, were severely influenced by increasing salts concentration in the solution. These results suggest that the presence of counter-ions in the solution, such as calcium, may introduce a charge-shielding effect, diminishing the electrostatic repulsion between the membrane and the solute. This effect may also explain the slight decrease of PFHxA rejection by the NF90 and XLE when increasing the ionic strength of the solution.
- iv. Overall, is it possible to effectively separate and concentrate PFHxA from industrial streams. The use of low-pressure reverse osmosis (LPRO) membranes such as the XLE or tight NF membranes such as the NF90 membranes are generally preferred because of their good trade-off between water permeability and PFHxA rejection.

4.1.2. Electrooxidation

- i. PFHxA from real industrial water concentrates obtained by NF was effectively treated (>98% degradation ratio at 2 h), confirmed by its almost complete mineralization and defluorination (>95% reduction of the total organic carbon (TOC)). This results were obtained working at low current density ($J=50 \text{ A m}^{-2}$), a value that was chosen after an insightful study and selection of the optimal current density for the process waters under study. These results clearly confirm the outstanding oxidative power of boron doped diamond (BDD) anodes in the mineralization of persistent perfluorocarboxylic acids in real industrial water matrixes
- ii. The energy consumption of the electrochemical treatment of PFHxA from real industrial effluents concentrates was 15.2 kWh m^{-3} for a 90% degradation ratio, far below the previously reported energy consumption of PFASs electrooxidation in literature, based on similar experimental approaches. This result clearly confirms the benefits of using a preconcentration strategy from the energy consumption point of view.
- iii. The high oxidative power of BDD anodes was also confirmed in the treatment of 6:2 FTSA, as the attained removal ratios edged 100%, and TOC and defluorination ratios reached 90% at $J=50 \text{ A m}^{-2}$. 6:2 FTSA degradation kinetics were found to be diffusion-controlled in the low range of applied current density. However, the increase of the applied current density turned out in even faster removal rates. This behavior was assigned to the formation of

highly oxidative secondary oxidants as sulfate radicals and peroxydisulfate.

- iv. The main products of 6:2 FTSA electrochemical oxidation were perfluoroheptanoic acid (PFHpA), PFHxA, perfluoropentanoic acid (PFPeA) and perfluorobutanoic acid (PFBA), although PFHxA was found in a much higher proportion than the rest of perfluorocarboxylic acids (PFCAs). This results confirm the PFASs degradation pathway proposed in literature for advanced oxidation processes, that combine electron transfer and hydroxyl radical mediated oxidation. Short-chain PFCAs were detected at very low concentrations in the bulk of the solution, which suggest that very fast reactions happened at the proximity of the BDD surface. The set of byproducts compounds decreased with time up to become hardly detectable.

4.1.3. Design and optimization of an integrated membrane preconcentration / electrooxidation process

- i. Excellent results are obtained by the innovative integration methodology presented in this PhD thesis. Very important capital and operating costs savings can be achieved in the electrochemical treatment of PFCAs though its integration with membrane preconcentration (up to 78.4% of total costs savings compared to the application of electrooxidation alone).
- ii. The energy consumption of the ELOX process, together with the electrode replacement costs, were found to be the major contributions to the total operating costs of the integrated process. With the optimization of the required electrolysis time the ELOX

energy savings reached an 89% and its contribution to the total costs (operating and capital) was reduced from 18% to only 8 – 9%. The electrooxidation energy consumption, for a 99% removal ratio at the end of the treatment train, ranged from 10.0 kWh m⁻³ using a single NF90 membrane stage to 3.5 and 3.8 kWh m⁻³ using two and three NF90 membrane stages respectively. The electrode replacement costs were also greatly reduced by optimization of the required anode area which also contributed importantly to reduce the electrochemical reactor capital investment.

- iii. Through the use of a multistage membrane preconcentration layout and the rigorous optimization of all the operational and sizing variables, very high pollutant abatement requirements can be fulfilled in a much less costly way, if compared to the application of electrooxidation without previous preconcentration. Overall, most of the pollutant abatement targets can be fulfilled with a two-stages membrane preconcentration layout.
- iv. A sensitivity analysis aimed to evaluate the influence of membrane properties on the total costs objective function showed that, overall, when designing the integrated process, it is economically preferable to use NF membranes, characterized by their medium to high hydraulic permeability and medium to high PFHxA selectivity, in opposition to low permeable and highly selective reverse osmosis membranes.
- v. Even in the best-case optimal scenario, which allowed an 86% reduction of the required electrochemical reactor anode area, the costs related to investment, maintenance and replacement of the

electrodes clearly outweigh the rest of the process capital and operating costs. Hence, the high price of BDD electrodes still remains as an actual bottleneck in the implementation of large-scale electrochemical processes for wastewater remediation.

4.1.4. Future perspective

Future work on the development of innovative technologies for the treatment of PFASs, such as nanofiltration / reverse osmosis or electrooxidation, should continue exploring the capability of these technologies in the treatment of other real water matrixes with single or various PFASs at different concentration ranges. For example, it would be interesting to explore the applicability of these technologies in the treatment of real aqueous fire-fighting foams (AFFFs) impacted groundwater with very low PFASs concentrations. In that sense, the evaluation of the herein proposed integrated process and the optimization methodology proposed in this thesis could be extended to the treatment of these water matrixes or to the treatment of other persistent organic pollutants. Regarding the design of the integrated process, there is still room for improvement. Other design layouts could be explored, as different batch scheduling proposals or the possibility of introducing a continuous mode preconcentration process. Also, as previously mentioned, the high price of the BDD electrode is still a serious obstacle in the large-scale implementation of electrochemical oxidation processes. Research efforts may be focused on the optimization of its manufacturing process or the development of new and cheaper electrode materials able to efficiently mineralize highly recalcitrant PFASs.

4.2. Conclusiones y perspectiva futura

Esta tesis tiene como objetivo desarrollar tecnologías avanzadas para el tratamiento de sustancias per- and polifluoroalquílicas (PFASs) persistentes de cadena corta en efluentes industriales reales, utilizados en la industria como alternativa a los PFASs de cadena larga, actualmente desfasados. Para cumplir con este objetivo, se evaluó el uso de nanofiltración (NF)/ ósmosis inversa (OI) y electrooxidación en el tratamiento de ácido perfluorohexanoico (PFHxA) y 6:2 ácido fluorotelomero sulfónico. Además, se utilizaron herramientas de optimización e ingeniería de sistema de procesos para diseñar y evaluar un proceso integrado consistente en pre-concentración con membranas y electrooxidación, con el objetivo de superar las limitaciones individuales de cada una de las tecnologías. A continuación, se detallan las conclusiones específicas obtenidas de los resultados de esta tesis.

4.2.1. Nanofiltración y ósmosis inversa

- i. La membrana comercial NF270 mostró la mayor permeabilidad al agua de entre todas las membranas de NF y OI a todos los pH. Sin embargo, también experimentó una reducción significativa en el flujo de agua cuando se cambió las condiciones de pH de ácido a neutro. Para el resto de las membranas estudiadas, incluyendo las otras membranas puras de NF (ESNA-LF y ESNA-LF2), la membrana NF90 o las membranas de OI (XLE, BW30 y SW30XLE), la permeabilidad apenas se vio afectada por cambios de pH en la disolución.
- ii. Aunque la membrana NF270 retuvo de forma efectiva el ácido perfluorohexanoico (PFHxA) procedente de corrientes

industriales y disoluciones modelo bajo condiciones de pH neutras, el rechazo sí que se vio seriamente reducido en condiciones ácidas. Cuando se utilizaron membranas más densas, como la NF90 o las membranas de OI, solo se observaron pequeñas reducciones en los rechazos de PFHxA al acidificar el pH. Estos resultados sugieren que los mecanismos dominantes en la separación de PFHxA fueron la exclusión por tamaño molecular y las interacciones electrostáticas entre el ion perfluorohexanoato y la superficie de la membrana. Cuando la separación fue llevada a cabo por membranas NF con tamaño de poro similar al tamaño molecular del PFHxA, la repulsión electrostática fue el mecanismo que desempeñó el papel más importante. Por el contrario, la exclusión por tamaño de poro fue el mecanismo predominante cuando se utilizaron membranas de tamaño de poro más pequeño, como la NF90 o las membranas de OI.

- iii. Las membranas NF90 y XLE obtuvieron rechazos de PFHxA muy altos en el tratamiento de aguas de proceso que contenían cantidades moderadas de sales ($R_{obs,PFHxA}=99.4\% - 99.6\%$). Por el contrario, la presencia de estas sales sí que afectó severamente el rechazo de PFHxA obtenido con la membrana NF270, y especialmente con las membranas ESNA-LF y ESNA-LF2. Estos resultados sugieren que la presencia de contraiones en la disolución puede introducir un efecto de blindaje de la carga de la membrana, reduciendo el efecto de repulsión electrostática entre la membrana y el soluto. Este efecto también podría explicar la leve disminución de rechazo de PFHxA observado con las membranas NF90 y XLE cuando se aumentó la fuerza iónica de la disolución.

- iv. En general, es posible separar y concentrar de manera efectiva el PFHxA procedente de corrientes industriales. Generalmente, es preferible el uso de membranas de ósmosis inversa que operen a bajas presiones, como es el caso de la XLE, o el uso de membranas densas de nanofiltración como la NF90, ya que es posible obtener un buen balance entre la permeabilidad de agua y los rechazos de PFHxA obtenidos.

4.2.2. Electrooxidación

- i. Se trató de forma efectiva el PFHxA procedente de efluentes industriales concentrados con NF (ratio de eliminación >98% a las 2h de electrolisis), resultados que fueron confirmados por su casi completa mineralización y defluoración (>95% de eliminación del carbono orgánico total (COT)). Estos resultados fueron obtenidos operando a una densidad de corriente baja ($J=50 \text{ A m}^{-2}$), cuyo valor fue escogido después de un estudio y selección de la densidad de corriente óptima para el proceso bajo estudio. Estos resultados claramente confirman el excepcional poder oxidativo de los ánodos de diamante dopado con boro (DDB) en la mineralización de ácidos perfluorocarboxílicos persistentes en matrices acuosas industriales.
- ii. El consumo de energía en el tratamiento electroquímico de PFHxA procedente de efluentes industriales reales fue de 15.2 kWh m^{-3} para un 90% de ratio de degradación de PFHxA, muy por debajo del consumo energético previamente reportado en literatura relativo a la electrooxidación de PFASs, lo que, desde el punto de

vista de ahorros energéticos, claramente confirma los beneficios de usar una etapa de concentración previa.

- iii. Se confirmó el alto poder oxidativo de los ánodos de DDB cuando se trató electroquímicamente 6:2 FTSA, cuyas ratios de eliminación rozaron el 100%. Las ratios de eliminación de COT y de defluoración alcanzaron el 90% utilizando $J=50 \text{ A m}^{-2}$. Cuando se utilizó un rango de densidad de corriente bajo, la cinética de degradación del 6:2 FTSA estuvo controlada por la transferencia de materia. Sin embargo, cuando se aumentó la densidad de corriente aplicada, las cinéticas de degradación aumentaron. Este comportamiento puede atribuirse a la formación de especies secundarias altamente oxidantes, como los radicales sulfato o peroxidisulfato.

- iv. Los principales productos de degradación del 6:2 FTSA fueron el ácido perfluoroheptanoico (PFHpA), el PFHxA, el ácido perfluoropentanoico (PFPeA) y el ácido perfluorobutanoico (PFBA). Sin embargo, el PFHxA fue hallado en una proporción mucho mayor en comparación con el resto de ácidos perfluorocarboxílicos (PFCAs). Esto confirma la ruta de degradación de PFASs propuesta en la literatura. Los PFCAs fueron detectados a concentraciones muy bajas en el seno de la disolución, lo que sugiere que sucedieron reacciones muy rápidas en la proximidad del electrodo. El conjunto de subproductos disminuyó con el tiempo hasta volverse apenas detectable.

4.1.3. Diseño y optimización del proceso integrado de preconcentración con membranas y electrooxidación

- i. La metodología de integración presentada en esta tesis dio lugar a excelentes resultados. Se obtuvieron ahorros potenciales muy importantes de costes de capital y de operación en el tratamiento electroquímico de PFCAs a través del planteamiento de integración con preconcentración mediante membranas (hasta un 78.4% de ahorros de costes totales comparado con la aplicación de electrooxidación en solitario).
- ii. Se encontró que, los costes de reemplazo de electrodo junto al consumo energético de la electrooxidación, fueron los costes con mayor contribución en los costes de operación totales del proceso integrado. Debido a la optimización del tiempo de electrolisis requerido, se ahorró hasta un 89% de los costes de energía de electrooxidación y su contribución a los costes totales (costes de capital y de operación) fue reducido de un 18% a tan solo un 8 – 9 %. Los costes de reemplazo de electrodo fueron también reducidos en gran manera gracias a la optimización del área de ánodo requerido, que por otro lado también ayudó a reducir de forma importante los costes de inversión del reactor electroquímico.
- iii. Mediante el uso de un esquema de preconcentración de membranas consistente en múltiples etapas de separación y a través de la optimización rigurosa de todas las variables de dimensionamiento y operación, se logró cumplir con requisitos muy exigentes de eliminación de contaminante de una forma mucho menos costosa que la aplicación de electrooxidación sin

preconcentración previa. En general, la mayoría de requisitos de eliminación de contaminante puede ser satisfechos con un esquema de preconcentración de dos etapas.

- iv. Se llevó a cabo un análisis de sensibilidad con el objetivo de estudiar la influencia de las propiedades de membrana en la función objetivo de costes totales. Este estudio mostró que, en el diseño del proceso integrado, es económicamente preferible utilizar membranas de NF, caracterizadas por su selectividad media-alta y permeabilidad media-alta, en contraposición a membranas de OI altamente selectivas, pero poco permeables.
- v. Incluso en el escenario de integración más óptimo, que permitió hasta un 86% de reducción del área de electrodo requerido, los costes de inversión, mantenimiento y reemplazo de los electrodos claramente superan el resto de costes de capital y operación del proceso. Por lo tanto, el alto precio de los electrodos DDB sigue siendo un importante cuello de botella a superar de cara a la implementación de procesos electroquímicos a gran escala para el tratamiento de aguas residuales.

4.2.4. Perspectiva futura

El trabajo futuro relativo al desarrollo de tecnologías innovadoras para el tratamiento de PFASs, como es el caso de la nanofiltración / ósmosis inversa y la electrooxidación, debe continuar explorando las capacidades de estas tecnologías en el tratamiento de otro tipo de matrices acuosas reales contaminadas por una o varios PFASs en diferentes rangos de concentración. Por ejemplo, sería interesante explorar la aplicabilidad de estas tecnologías en el tratamiento de aguas subterráneas reales

contaminadas por espumas de extinción de incendios, con concentraciones de PFASs muy bajas. En ese sentido, podría evaluarse tanto el proceso integrado como la metodología de optimización del mismo propuesto en esta tesis, en el tratamiento de este tipo de matrices acuosas o incluso en el tratamiento de otros contaminantes orgánicos persistentes. En lo relativo al diseño del proceso integrado, hay todavía margen de mejora que explorar. Pueden evaluarse otros esquemas de diseño, como diferentes propuestas de programación por lotes o bien la posibilidad de introducir el proceso de pre-concentración trabajando en modo continuo. Además, como se ha mencionado anteriormente, el alto precio de los electrodos BBD supone todavía un serio obstáculo de cara a la implementación a gran escala de procesos de oxidación electroquímica. Los esfuerzos de investigación deben estar dirigidos a la optimización del proceso de fabricación de los electrodos DDB o bien al desarrollo de materiales electrocatalíticos más baratos capaces de mineralizar de forma efectiva los PFASs de carácter altamente recalcitrante.

5. Scientific publications

5.1. Scientific publication #1.

Efficient treatment of perfluorohexanoic acid by nanofiltration followed by electrochemical degradation of the NF concentrate

Authors:

Álvaro Soriano, Daniel Gorri, Ane Urriaga

Department of Chemical and Biomolecular Engineering. University of Cantabria. Av. de Los Castros 46. 39005 Santander. Spain

Accepted 20 January 2017

Water Research

Volume 112 (2017), Pages 147-156

DOI: 10.1016/j.watres.2017.01.043



Efficient treatment of perfluorohexanoic acid by nanofiltration followed by electrochemical degradation of the NF concentrate



Álvaro Soriano, Daniel Gorri, Ane Urtiaga*

Department of Chemical and Biomolecular Engineering, University of Cantabria, Av. de Los Castros s/n, 39005 Santander, Spain

ARTICLE INFO

Article history:

Received 20 August 2016

Received in revised form

4 January 2017

Accepted 20 January 2017

Available online 25 January 2017

Keywords:

Perfluorohexanoic acid

Perfluoroalkyl substances (PFASs)

Nanofiltration

Electrooxidation

Boron doped diamond electrode

ABSTRACT

The present study was aimed at the development of a strategy for removing and degrading perfluorohexanoic acid (PFHxA) from industrial process waters at concentrations in the range 60–200 mg L⁻¹. The treatment train consisted of nanofiltration (NF) separation followed by electrochemical degradation of the NF concentrate. Using a laboratory-scale system and working in the total recirculation mode, the DowFilm NF270 membrane provided PFHxA rejections that varied in the range 96.6–99.4% as the operating pressure was increased from 2.5 to 20 bar. The NF operation in concentration mode enabled a volume reduction factor of 5 and increased the PFHxA concentration in the retentate to 870 mg L⁻¹. Results showed that the increase in PFHxA concentration and the presence of calcium sulfate salts did not induce irreversible membrane fouling. The NF retentate was treated in a commercial undivided electrochemical cell provided with two parallel flow-by compartments separated by bipolar boron doped diamond (BDD) electrode, BDD counter anode, and counter cathode. Current densities ranging from 20 to 100 A m⁻² were examined. The electrochemical degradation rate of PFHxA reached 98% and was accompanied by its efficient mineralization, as the reduction of total organic carbon was higher than 95%. Energy consumption, which was 15.2 kWh m⁻³ of treated NF concentrate, was minimized by selecting operation at 50 A m⁻². While most of the previous research on the treatment of perfluoroalkyl substances (PFASs) focused on the removal of perfluorooctanoic acid (PFOA) and perfluorooctane sulfonate (PFOS), these compounds have been phased out by chemical manufacturers. Our findings are relevant for the treatment of PFHxA, which appears to be one of the present alternatives to long-chain PFASs thanks to its lower bioaccumulative potential than PFOA and PFOS. However, PFHxA also behaves as a persistent pollutant. Moreover, our results highlight the potential of combining membrane separation and electrochemical oxidation for the efficient treatment of PFAS-impacted waters.

© 2017 Elsevier Ltd. All rights reserved.

1. Introduction

Perfluoroalkyl substances (PFASs) are highly persistent organic compounds that contain a fluorinated alkyl chain and a hydrophilic end group (Arvaniti and Stasinakis, 2015). PFASs have been used in a wide variety of applications as part of surfactants, emulsifiers, aqueous film forming foams, additives for polymers, for paper and cardboard coatings used in food packaging products, and for stain and water repellency in textiles and leather, among others (Appleman et al., 2014; Rahman et al., 2014; Yu et al., 2009).

Long-chain PFASs are bioaccumulative and toxic to laboratory animals and wildlife (ECHA, 2014; Lin et al., 2014). Hence, environmental protection institutions have established limits to perfluoroalkyl carboxylic acids (PFCAs) and perfluoroalkane sulfonates with eight or more fluorinated carbons. Perfluorooctane sulfonate (PFOS) and its salts were added to Annex B of the list developed in 2009 as a result of the Stockholm Convention on Persistent Organic Pollutants (Ahrens and Bundschuh, 2014). PFOS and its derivatives were recently added as priority hazardous substances in Directive 2013/39/UE of the European water policy. The United States Environmental Protection Agency has recently set health advisory levels for perfluorooctanoic acid (PFOA) and PFOS in drinking water at 0.07 µg/L, both individually and combined (USEPA, 2016).

Nowadays, industry has phased out the use of PFOA, PFOS, and

* Corresponding author.

E-mail address: urtiaga@unican.es (A. Urtiaga).

longer chain homologues (USEPA, 2015). The alternatives are mostly short chain PFASs such as the 6:2 fluorotelomer alcohol (6:2 FTOH), which contains six fully fluorinated carbon atoms (ECHA, 2014). 6:2 FTOH is readily biodegradable, but it degrades into the persistent compounds perfluorohexanoic acid (PFHxA) and perfluoropentanoic acid (Zhao et al., 2013c). In general, shorter chain PFASs have been reported to be quickly eliminated in mammals (Wang et al., 2015b), although PFHxA is equally persistent and cannot be degraded under biotic or abiotic conditions.

Various technologies have been examined for the treatment of PFASs from aqueous media, although most of the previous studies were exclusively focused on the removal of PFOA and PFOS. The most widely studied techniques are adsorption, membranes, and oxidation processes (Arvaniti and Stasinakis, 2015). The use of activated carbon and anion exchange resins was successfully reported for the retention of PFOA and PFOS (Yu et al., 2009; Zaggia et al., 2016; Zhang et al., 2016). Nanofiltration (NF) and reverse osmosis (RO) processes are of special interest in the separation of PFASs from drinking water sources. Several works studied the rejection of PFASs by NF membranes, which ranged from 90% to 99%. Rejections were mainly dependent on the type of membrane, but also on a variety of other factors that included the properties of the solution and the effect of the operating variables (Appleman et al., 2013; Hang et al., 2015; Steinle-Darling and Reinhard, 2008; Tang et al., 2007; Wang et al., 2015a; Zhao et al., 2013a). Other studies reported that RO could achieve higher PFASs rejection than NF, which in most cases was better than 99%, but at the expense of significantly lower permeate fluxes (Baudequin et al., 2014; Tang et al., 2007, 2006). Only a few studies included data about PFHxA rejections by the NF270 membrane (Steinle-Darling and Reinhard, 2008). It is important to note that those studies used artificial or spiked mixtures of PFASs that included PFHxA in low concentrations ($1 \mu\text{g L}^{-1}$ and $100\text{--}400 \text{ ng L}^{-1}$), and thus may not reflect mechanisms that dominate at higher PFHxA concentrations similar to those usually found in industrial process streams. Moreover, PFHxA rejection values ($>95\%$) reported by Appleman et al. (2013) were estimations, as the permeate concentrations were not quantified due to limitations of the analytical technique in the low permeate concentration range.

The use of membrane processes alone is not enough for the overall treatment of PFASs because these compounds are retained in the concentrate stream, which must be treated before disposal. Although the concept of coupling membrane technology with advanced oxidation processes has been previously reported in the treatment of emerging micropollutants such as pharmaceutical compounds in a wide variety of water samples (Dialynas et al., 2008; Ioannou et al., 2013; Pérez et al., 2010; Radjenovic et al., 2011), we are unaware of any studies assessing the impact of its application to the treatment of PFASs.

The strength of the C–F bond makes PFASs resistant to traditional advanced oxidation processes (Sansotera et al., 2014). Electrochemical treatment by anodic oxidation has been examined by several research groups (Chaplin, 2014). Boron doped diamond (BDD) electrodes could satisfactorily decompose the PFOA and PFOS contained in synthetic water solutions (Carter and Farrell, 2008; Ochiai et al., 2011; Urtiaga et al., 2015). BDD electrodes have interesting properties that make their use advantageous for the treatment of organic pollutants. These are their high chemical inertness, hardness, extended lifetime, the ability to generate hydroxyl radicals ($\text{HO}\cdot$) from water oxidation, and the efficient use of electrical energy (Cañizares et al., 2005; Cabeza et al., 2007; Polcaro et al., 2009; Pérez et al., 2010). Most of the research effort is currently focused on the development of new electrode materials (Xue et al., 2015; Yang et al., 2015; Zhao et al., 2013b; Zhuo et al., 2014) and very little information is available about the

electrochemical degradation of PFASs in real polluted water matrices. Exceptions include the recent study by Schaefer et al. (2015), who demonstrated the electrochemical degradation of PFOA and PFOS in groundwater impacted by the use of aqueous film-forming foams. It is noted that the majority of previous studies have focused exclusively on the removal of PFOA and PFOS. One notable gap is the lack of knowledge about the electrochemical treatment of shorter-chain PFASs that are used in chemical manufacturing processes as alternatives to PFOA and PFOS.

The objective of this work was to study the removal of PFHxA from two process waters produced in an industrial manufacturing process in which the initial concentration of PFHxA was in the range $60\text{--}200 \text{ mg L}^{-1}$. The treatment train began with an initial nanofiltration separation that allowed concentration of PFHxA within the retentate stream. This was subsequently degraded by electrooxidation using BDD electrodes. A commercial BDD electrochemical cell was used. The study of the operating variables that affected the rejection of PFHxA and other salts contained in the process waters was assessed. The effect of the applied current and the mechanisms that govern the kinetics of the electrochemical process are also discussed.

2. Materials and methods

2.1. Water characteristics

Two different samples of process streams produced in an industrial manufacturing process were used in this experimental work. The samples were taken just before the PFHxA collecting facility that removed the contaminant before the general wastewater treatment was applied at the industrial plant. Table 1 displays the chemical characterization of the two samples, referred to as S1 and S2. The main difference lays in the content of PFHxA, which is about three times higher in S1 than in S2. Other components were common inorganic salts, which provided the samples the adequate conductivity for use as an electrolyte in the electrochemical experiments. It can be noticed that the values of total organic carbon (TOC) exceeded the theoretical TOC values calculated from the concentration of PFHxA. Therefore, the industrial waters contained other soluble organic compounds of unknown nature.

In addition to the real process waters described above, model solutions with salt contents equivalent to the real ones were prepared. All chemicals were of analytical grade and used as received without further purification. Perfluorohexanoic acid ($\geq 97\%$) was supplied by Sigma-Aldrich. Calcium sulfate dihydrate ($\geq 98\%$) was purchased from Scharlau. Sodium chloride ($\geq 99\%$) was obtained from Panreac. Sodium carbonate ($\geq 99.9\%$) was supplied by Merck Millipore.

Table 1

Main characteristics of the industrial process water samples used in the experimental study.

Parameter	Units	Sample	
		S1	S2
PFHxA	mg L^{-1}	204	64
TOC	mg L^{-1}	82	24
pH	–	7.7	7.4
Conductivity	mS cm^{-1}	1.05	1.02
Chloride	mg L^{-1}	19.8	16.9
Sulfate		321	360
Bicarbonate		98	92
Calcium		172	171
Sodium		24.9	28.7

2.2. Nanofiltration experiments

Nanofiltration experiments were carried out in a laboratory membrane cross-flow test cell (SEPA-CF, GE Osmonics). An NF270 flat membrane supplied by Dow Filmtec was used. It is a thin film composite of a polyester non-woven support matrix, a microporous polysulfone interlayer, and a semiaromatic piperazine-based aromatic polyamide barrier layer. At neutral pH, the NF270 membrane surface is negatively charged, a property that would improve the rejection of large negative species such as perfluorohexanoate, which is obtained by the dissociation of PFHxA at neutral pH (Wang et al., 2016).

The membrane area inside the cell was 155 cm². New membrane specimens were preconditioned by immersion in ultrapure water for 24 h–48 h. A back pressure valve (Swagelok, 0–40 bar), installed at the outlet port of the retentate stream, was used to control the operating pressure. The permeate chamber was maintained at atmospheric pressure. The feed was circulated using a diaphragm pump (Hydra-Cell D-03).

Fig. 1 shows the NF set-up. In the total recirculation experiments (Fig. 1a), both the retentate and the permeate streams were continuously recycled to the feed tank. Therefore, in the total recirculation NF experiments the feed composition was constant during the entire experiment. Initially, the NF system was pressurized with the feed solution at 20 bar for 1 h with total recirculation of the solution. After achieving stable permeate fluxes in consecutive measurements for at least 1 h, the pressure was sequentially reduced to 15, 10, 5, and 2.5 bar. At each pressure, the system was allowed to reach steady-state flux before the next reduction in operating pressure. In concentration mode experiments (Fig. 1b), only the rejection stream was recycled to the feed tank, while the permeate stream was collected in a separate tank. In concentration mode experiments, the concentration of PFHxA and salts in the feed continuously increased during the length of the experimental run. Concentration mode experiments were conducted until a volume reduction factor (VRF) approximately equal to 5 was obtained, where VRF is defined as the ratio between the initial feed volume and the concentrate final volume (Mulder, 1996). In concentration mode, the membrane was initially pressurized for 1 h at 35 bar using deionized water. The pressure was then fixed at 10 bar during the NF test. In all experiments, the permeate rejection and feed streams were sampled periodically. All experiments were conducted at room temperature.

2.3. Electrooxidation experiments

The retentate stream produced in the NF concentration mode tests, which accumulated PFHxA and soluble salts, was used as the feed solution in the electrooxidation experiments. The set-up consisted of an electrochemical cell (DiaCell 201 PP, Adamant

Technologies), a power supply (Vitecom 75-HY3005D), a jacketed feed tank, and a cooling bath (Polyscience 9510). The cell contained two parallel flow-by compartments made of a central bipolar p-Si/BDD electrode and p-Si/BDD anode and cathode, with an inter-electrode gap of 1 mm in each channel. Further details on the experimental system can be found elsewhere (Díaz et al., 2011; Urtiaga et al., 2014). The feed tank was filled with 1 L of the NF concentrate, unless otherwise stated. The experiments were carried out in batch mode, at a constant temperature of 20 °C. Three different current densities were applied: 20, 50, and 100 A m⁻². Model solutions representative of the NF concentrates were used in the experiments aimed at the selection of the optimum operating conditions for electrooxidation.

To determine the efficiency of the process, it is useful to calculate the specific electrical charge (Q , A h L⁻¹) and the energy consumption (W , kWh·m⁻³) as follows (Anglada et al., 2009):

$$Q = \frac{JAt}{v} \quad (1)$$

$$W = QV \quad (2)$$

where J is the current density (A m⁻²), A is the total anode area (m²), t is the time (h), v is the feed tank volume (L), and V is the cell voltage (V).

The limiting current density (J_{lim} , A m⁻²) at a given time t , can be calculated as follows (Martínez-Huitle et al., 2015; Panizza and Cerisola, 2009):

$$J_{lim} = 12Fk_m[PFHxA]_t \quad (3)$$

where F is the Faraday constant (C mol⁻¹), $[PFHxA]_t$ is the concentration of PFHxA (mol m⁻³) at a given experimental time, and k_m is the mass transport coefficient in the electrochemical reactor (m s⁻¹). The factor of 12 is the number of electrons exchanged during the oxidation of one PFHxA molecule. k_m was calculated following the work of Anglada et al. (2010), who analyzed the effect of hydrodynamics and scale-up for electrochemical cells with a similar geometry to the equipment used in the present study.

2.4. Analytical methods

The perfluorinated compounds were quantified using two different analytical methods. The appropriate method was selected according to the PFHxA concentration range and to the calcium and bicarbonate content in the samples:

1. The PFHxA concentration in the feed and retentate NF samples was generally within the range 5–900 mg L⁻¹. Moreover, these samples had high calcium, sulfate, and bicarbonate

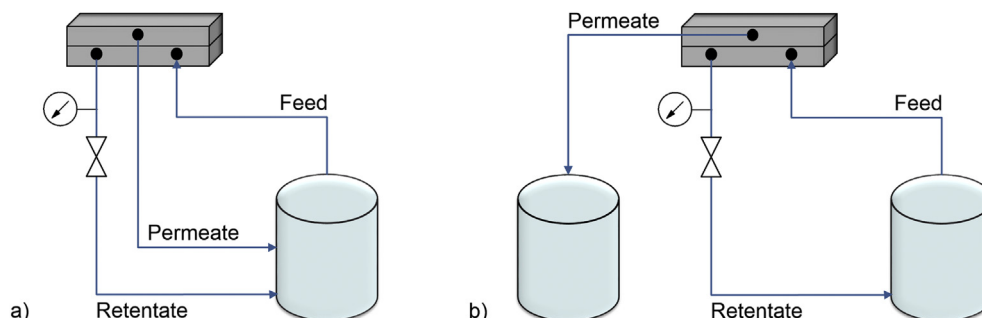


Fig. 1. Nanofiltration set-up in a) total recirculation mode, and b) concentration mode.

concentrations. High-performance liquid chromatography (HPLC) with a diode array UV–visible detector was employed (Waters 2695-DAD). The separation column was an X-Bridge C18 (5 μm , 250 \times 4.6 mm). The mobile phase was a solution of methanol (CH_3OH) and sodium dihydrogen phosphate ($\text{Na}_2\text{H}_2\text{PO}_4$, 20 mM) in the 65:35 vol ratio at a flow rate of 0.5 mL min^{-1} . The limit of quantification (LOQ) for PFHxA was 5 mg L^{-1} . The UV absorption at 205.4 nm was used for quantification.

2. HPLC (Waters 2690) equipped with a triple quadrupole mass spectrometer (TQD Detector Acquity, Waters) was used to analyze NF permeate samples, with PFHxA concentrations generally below 5 mg L^{-1} and with low salt content. The column was the X-Bridge BEH C18 (2.5 μm , 2.1 \times 75 mm). The eluents were: (i) an aqueous solution containing ammonium acetate ($\text{CH}_3\text{COONH}_4$) 2 mM and 5% of methanol, and (ii) pure methanol. The eluent flow rate was 0.15 mL min^{-1} . The LOQ for PFHxA was 1 $\mu\text{g L}^{-1}$.

It was checked that both analytical protocols provided analogous PFHxA quantification in the feed sample S1.

Conductivity was measured using a portable conductivity meter (Hach sensION 5). The pH was measured using a pH meter (GLP Crison 22). An automatic carbon analyzer (TOC-V CPH Shimadzu) was used to measure the total organic carbon (TOC). The determination of chloride, sulfate, and fluoride anions was carried out by ion chromatography (Dionex ICS-1100) using an ion exchange resin column (Dionex AS9-HC). The mobile phase was sodium carbonate (Na_2CO_3 , 9 mM) with a flow rate of 1 mL min^{-1} . Sodium and calcium cations were determined by ion chromatography (Dionex DX-120) using a Dionex IonPac TM CS12 column and methanesulfonic acid (18 mM at 1 mL min^{-1}) as eluent.

3. Results and discussion

3.1. Nanofiltration experiments

3.1.1. Total recirculation tests

The volumetric flux of permeate passing through the membrane, J_v , is defined by Darcy's law (Eq. (4)), which states that this variable is the product of the membrane permeability L_p ($\text{L m}^{-2} \text{h}^{-1} \text{bar}^{-1}$), which is an empirical constant, and the pressure gradient between the two sides of the membrane, defined as the difference between the effective pressure ΔP (bar) and the osmotic pressure gradient $\Delta\pi$ (bar) (Pérez-González et al., 2015):

$$J_v = L_p(\Delta P - \Delta\pi) \quad (4)$$

where $\Delta\pi$ is defined as:

$$\Delta\pi = \pi_0 - \pi_p \quad (5)$$

where π_0 and π_p are the feed and the permeate osmotic pressures, respectively. The osmotic pressure of the solutions was calculated from the concentration of the dissolved salts (Asano, 1998):

$$\pi = 1.19(T + 273) \sum m_i \quad (6)$$

where T is the temperature of the solution ($^{\circ}\text{C}$) and m_i is the molality of the constituent in the solution.

Fig. 2 shows the correlation between the permeate flux and the pressure gradient across the membrane. Three types of water samples were considered: ultrapure water, real industrial process waters, and the model solution. The last represents the salt composition of the real samples S1 and S2, according to Table 1, but

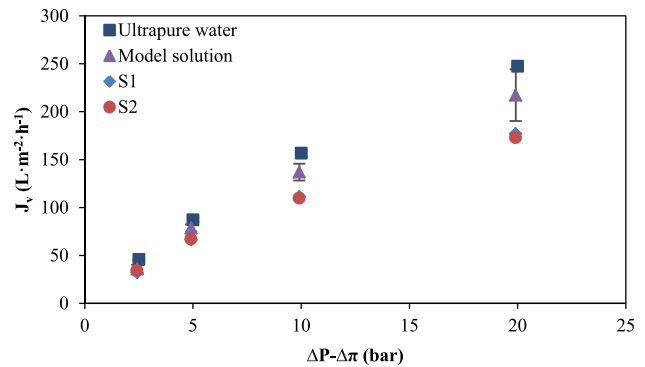


Fig. 2. Experimental permeate flux data as a function of the effective pressure gradient. Model solution composition: NaCl (60 mg L^{-1}), CaSO_4 (600 mg L^{-1}). Averages of duplicate experiments are reported for ultrapure water and the model solution.

without the addition of PFHxA. It was observed that the membrane permeability to ultrapure water was the highest, $L_{pw} = 13.3 \pm 0.04 \text{ L m}^{-2} \text{ h}^{-1} \text{ bar}^{-1}$, a value that is similar to previously reported water permeabilities for the same NF270 membrane (Nghiem and Hawkes, 2007). The presence of salts in solution decreased the membrane permeability, as was observed for the flux data obtained with the model solution, $L_{pm} = 11.7 \pm 1.2 \text{ L m}^{-2} \text{ h}^{-1} \text{ bar}^{-1}$. A similar trend was observed in previous studies dealing with the NF treatment of desalination brines, e.g., Pérez-González et al. (2015) found that solution permeability decreased exponentially when increasing the initial salt concentration. The membrane permeabilities of the two samples of real process water S1 and S2 (which contained PFHxA) were very similar to each other ($L_{p,S1} = 9.6 \text{ L m}^{-2} \text{ h}^{-1} \text{ bar}^{-1}$, and $L_{p,S2} = 9.4 \text{ L m}^{-2} \text{ h}^{-1} \text{ bar}^{-1}$), and lower than the values for pure water and the model salt solution. Hang et al. (2015) reported a similar observation after the nanofiltration of PFOA and suggested that such behavior could be attributed to adsorption of the molecule in the expanded membrane pores.

The effect of the effective pressure gradient on the rejection of PFHxA and ions was also studied. The observed rejection (R_{obs}) was calculated as follows (IUPAC, 1996):

$$R_{obs} = \left(1 - \frac{C_p}{C_r}\right) \times 100 \quad (7)$$

where C_p and C_r are the concentration of the species in the permeate and retentate streams, respectively.

Due to the high solvent flow through the membrane and the high rejection of the species, solutes accumulated on the membrane surface. Thus, the actual solute concentration at the membrane surface was higher than in the bulk solution, known as the concentration polarization phenomenon. In order to calculate the real membrane rejections (R_{real}) the equation of Fujioka et al. (2012) was employed:

$$R_{real} = \frac{R_{obs} \exp\left(\frac{J_v}{k}\right)}{1 + R_{obs} \left[\exp\left(\frac{J_v}{k}\right) - 1\right]} \times 100 \quad (8)$$

where k is the mass transfer coefficient of the considered species (m s^{-1}). k was calculated using Eq. (9), which is valid for laminar flow through rectangular closed channels (van den Berg et al., 1989):

$$Sh = \frac{2hk}{D_{AB}} = 0.664 \cdot Re^{0.5} Sc^{0.33} \left(\frac{2h}{L}\right)^{0.33} \quad (9)$$

In Eq. (9) Sh , Re , and Sc are the Sherwood, Reynolds, and Schmidt numbers, respectively; h is the NF cell channel height (1.7 mm) and L is the length of the path that follows the fluid inside the NF cell (0.13 m). D_{AB} is the diffusion coefficient of the species in water ($m^2 s^{-1}$). The diffusion coefficients reported by Samson et al. (2003) were applied for the ionic species (sulfate, calcium, sodium, and chloride). In the case of PFHxA, the Wilke-Chang equation (Perry et al., 1997) was used to estimate its diffusion coefficient in water, $D_{PFHxA,w} = 7.05 \times 10^{-10} m^2 s^{-1}$, at 25 °C.

The dependence of the PFHxA real rejection on the effective pressure is shown in Fig. 3. The PFHxA rejection increased from 97.3% to 99.1% for S1, and from 96.6% to 99.4% for S2 in the range of effective pressure gradient $2.4 < (\Delta P - \Delta \pi) < 19.9$ bar. Two main observations can be derived. First, the PFHxA real rejection remained high over the entire range of applied pressure. Secondly, the difference in the concentration of PFHxA, which was three times higher in S1 than in S2, did not significantly affect the rejection percentage. Appleman et al. (2013) reported PFHxA rejections higher than 95%, when using the same NF270 membrane for the treatment of spiked artificial groundwater with a feed PFHxA concentration of $1 \mu g L^{-1}$. The authors revealed that PFHxA was not detected in the permeate over the limit of quantification of the analytical technique used in that work. It can be argued that the differences in the feed concentration, which in the study of Appleman et al. (2013) was 200 times lower than in sample S1 of the present study, significantly reduced the concentration gradient across the membrane and thus the permeation flux of the species. Similar observations were reported by Steinle-Darling and Reinhard (2008) who studied the nanofiltration of synthetic mixtures of 15 perfluorochemicals in deionized water with concentrations in the range 150–400 $ng L^{-1}$. So far, to the best of our knowledge, the present study is the first one reporting the NF of PFHxA in real industrial process waters. Past research (Bellona and Drewes, 2007) demonstrated that NF membranes achieved a high rejection of negatively charged organic compounds through electrostatic exclusion. However, the detection of PFHxA in the permeate observed in the present work suggests that once the compound reached a partitioning equilibrium at the feed/membrane interface—which is enhanced by the high feed concentrations used in this work—the diffusion mechanism governs the overall solute transport through the membrane pores.

Fig. 4 shows the real rejection of ions (sulfate, chloride, sodium, and calcium) as a function of the operating pressure for the sample

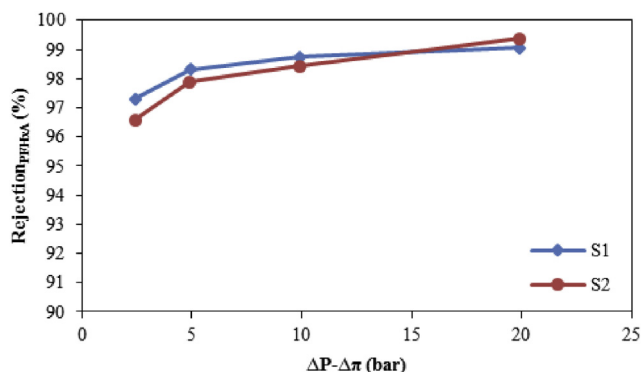


Fig. 3. PFHxA real rejection as a function of the effective pressure for process water samples S1 and S2 using an NF270 membrane.

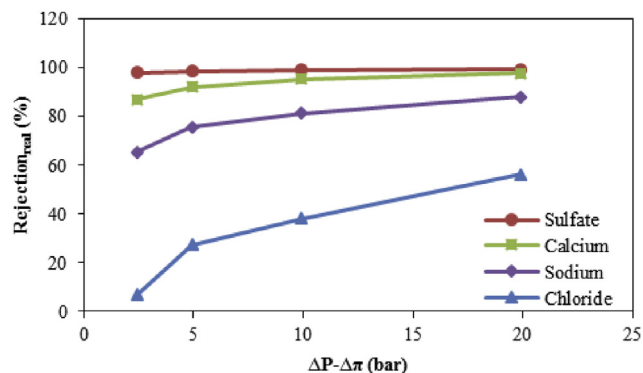


Fig. 4. Real rejection of ions as a function of the effective pressure. Data were obtained using sample S1 and an NF270 membrane. Similar results were observed for S2 sample and the model solution.

S1. Similar rejections were observed when NF was applied to S2 and to the model solutions (results not shown). In the range of operating pressures studied, chloride rejection increased from 6.8% to 56.4%, sodium rejection from 65.6% to 88.2%, calcium rejection from 87.3% to 97.9%, and sulfate rejection from 98.8% to 99.6%. The high values of sulfate rejection are very similar to those obtained for PFHxA because both are large negatively charged species that are easily rejected by the negatively charged membrane at neutral pH. The low value of chloride rejection can be explained by the Donnan ion distribution between the solution and the membrane. It means that sodium and calcium cations were attracted by the negatively charged membrane and were highly distributed from the liquid phase to the membrane phase. Chloride ions, which are much smaller than sulfate anions, tended to pass through the membrane together with the cations in order to preserve the electroneutrality (Hilal et al., 2015). Similar ion rejection behavior was observed by Pérez-González et al. (2015), who treated brackish water desalination brines in the pressure range of 5–20 bar using the same NF270 membrane. The observed ions rejections were beneficial for increasing the conductivity of the concentrate to be used as an electrolyte in the electrochemical treatment.

3.1.2. Concentration mode experiments

The purpose of the concentration mode experiments was to obtain a low volume of highly concentrated PFHxA solution. In addition, these experiments allowed the evaluation of the stability of membrane performance along the time of operation in terms of PFHxA rejection and permeate flux. Fig. 5 shows the evolution of the permeate flux over time (for samples S1 and S2) using a feed

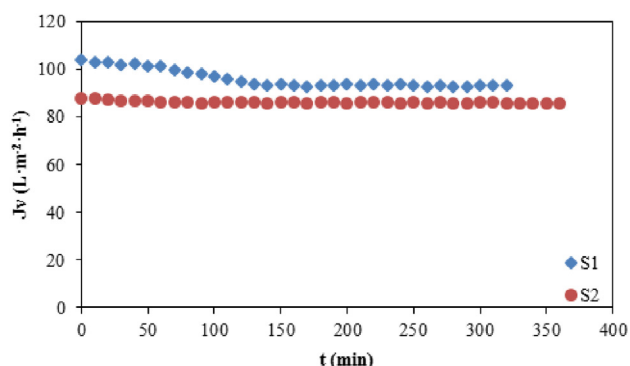


Fig. 5. Nanofiltration operation in concentration mode. Permeate flux evolution with time for samples S1 and S2. Feed pressure = 10 bar.

pressure of 10 bar. In both cases the flux slightly decreased in the first hours and then stabilized at a constant value. The membrane permeability values at constant flux were $L_{p,S1} = 9.4 \text{ L m}^{-2} \text{ h}^{-1} \text{ bar}^{-1}$ and $L_{p,S2} = 8.6 \text{ L m}^{-2} \text{ h}^{-1} \text{ bar}^{-1}$, which are similar or only slightly below those reported in the above section. At the end of each experiment, the membrane was tested again with ultrapure water to evaluate whether the observed loss of permeability corresponded to reversible or irreversible fouling. For example, after the NF test with S1, the membrane permeability to pure water was $12.8 \text{ L m}^{-2} \text{ h}^{-1} \text{ bar}^{-1}$, which was only 4% less than the initial value reported in Fig. 1. The difference is believed to be due to the variability of properties in different membrane specimens. It was concluded that the NF of PFHxA solutions did not generate irreversible fouling in the NF270 membrane.

In the concentration mode experiments, the NF270 membrane showed high PFHxA real rejections that were essentially constant over time: $98.2 \pm 0.2\%$, and $98.8 \pm 0.2\%$, for S1 and S2 respectively (real and observed PFHxA rejection values with time are compared in Fig. S1 of the supplementary material). The volume was reduced from the 10 L initially used as feed, to a final volume of approximately 2 L of concentrate. PFHxA concentrations of 870 mg L^{-1} and 344 mg L^{-1} were achieved in the final concentrates C-S1 and C-S2, respectively. The evolution with time of the PFHxA concentration in retentate and permeate streams is given in Fig. S2 of the supplementary material. Simultaneously, the conductivity of the concentrates reached 2.48 mS cm^{-1} and 2.63 mS cm^{-1} . These concentrates served as feed for the next electrooxidation step. PFHxA was detected in the permeates at concentrations of 21 mg L^{-1} for S1, and 8 mg L^{-1} for S2. These values corresponded to the composite permeates obtained throughout the duration of the tests. Moreover, Fig. 6 shows that under the conditions of the present study, PFHxA concentrations in the permeate and in the retentate matched a linear relationship ($r^2 = 0.97$), an observation that further supports diffusion as the predominant PFHxA transport mechanism through the NF270 membrane.

3.2. Electrooxidation experiments

3.2.1. Influence of the applied current density

Initial tests aimed at the selection of the applied current density were performed using model solutions (CM-S1) that were prepared with similar PFHxA concentrations and salts composition as the NF concentrates obtained from sample S1. Fig. 7 depicts the development of PFHxA and TOC with time at three applied current density values: $J_{app} = 20, 50, \text{ and } 100 \text{ A m}^{-2}$. The kinetics of PFHxA degradation and mineralization were clearly enhanced when the

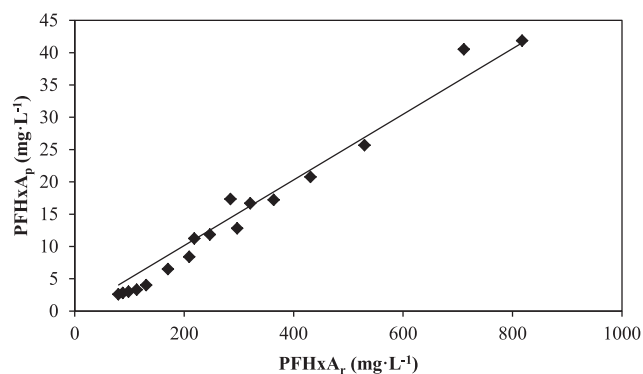


Fig. 6. Nanofiltration operation in concentration mode. PFHxA concentration in the permeate vs. PFHxA concentration in the retentate. The NF270 membrane was operated at a feed pressure of 10 bar.

applied current density was increased from 20 to 50 A m^{-2} . Further increase in current density to 100 A m^{-2} provided an additional improvement in degradation kinetics, although less noticeable than in the previous jump from 20 to 50 A m^{-2} .

The recent review by Niu et al. (2016) proposed that electrochemical oxidation mechanism of PFCAs involves electron transfer to the anode to form the highly reactive $\text{C}_n\text{F}_{2n+1}\text{COO}^\cdot$ radical, which then reacts with electrogenerated hydroxyl radicals. According to this pathway, PFHxA degradation would include both direct and indirect electrochemical oxidation steps. BDD anodes are well known for their wide electrochemical window that allows the formation of hydroxyl radicals at lower electrode potentials than those needed for the oxygen evolution reaction. However, as hydroxyl radicals are confined to the proximity of the anode surface, two different operating regimes can be defined for BDD oxidation: i) when the applied current density is below the limiting current density, the electrolysis is under current control and the concentration of organic compounds decreases linearly with time; ii) when the applied current density is above the limiting current density, the electrolysis is under mass transport control and the removal of organics follows a first-order exponential trend. In the present study, the limiting current density (J_{lim} , Eq. (3)) was calculated as $J_{lim} = 48.1 \text{ A m}^{-2}$ at the initial PFHxA concentration in CM-S1. This means that when working at $J_{app} = 20 \text{ A m}^{-2}$, the electrolysis was initially under current control but rapidly shifted to mass transfer control at $t = 1 \text{ h}$ as the concentration of PFHxA decreased. When $J_{app} = 50 \text{ A m}^{-2}$, the system was working under mass transfer control for the entire experiment. The small but noticeable increase in the PFHxA removal rate observed at 100 A m^{-2} can be assigned to the oxidative effect of secondary strong oxidants such as sulfate radicals. This assumption is based on the results reported by Hori et al. (2005), who found that the photolysis of persulfate anions produced highly oxidative sulfate radical anions, which efficiently decomposed PFOA and other PFCAs bearing $\text{C}_4\text{--C}_8$ perfluoroalkyl groups. At present, we are not able to definitely elucidate the rate limiting step of PFHxA degradation, although the experimental results that show only a minor kinetic enhancement when the applied current is doubled from 50 to 100 A m^{-2} , point to the predominance of indirect oxidation by means of electrogenerated oxidants.

To select the suitable operating conditions, it is also useful to look at the evolution of PFHxA and TOC as functions of the specific electrical charge passed (Q), also shown in Fig. 7. An increase in the applied current density did not significantly affect the efficacy of the process. The energy demand for 90% degradation of the initial PFHxA was calculated using Eqs. (1) and (2). The times for 90% PFHxA reduction were obtained from the rate constant calculated using the concentration- Q data. Results are summarized in Table 2, where V is the experimental cell voltage developed under galvanostatic conditions. The energy consumption for $J_{app} = 50 \text{ A m}^{-2}$ was 15.2 kWh m^{-3} , the lowest among the three current intensities under consideration. It was also observed that the electrolysis time needed to reach 90% degradation at 50 A m^{-2} was three times lower than when the applied current was 20 A m^{-2} . Accordingly, it was decided to select $J_{app} = 50 \text{ A m}^{-2}$ as the working current density for the electrochemical treatment of the real industrial process concentrates.

The energy consumption for the electrochemical treatment of PFHxA achieved in the present study, 15.2 kWh m^{-3} , is lower than previously reported values for the removal of different PFASs in waters. Zhuo et al. (2011) and Niu et al. (2012) reported the electrolysis of PFOA using tin oxide and lead dioxide electrodes with energy consumptions of 48 and 45 kWh m^{-3} . Similar values in the range $41.7\text{--}76.6 \text{ kWh m}^{-3}$ have been gathered by Niu et al. (2016) for the degradation of perfluorodecanoic and perfluorononanoic

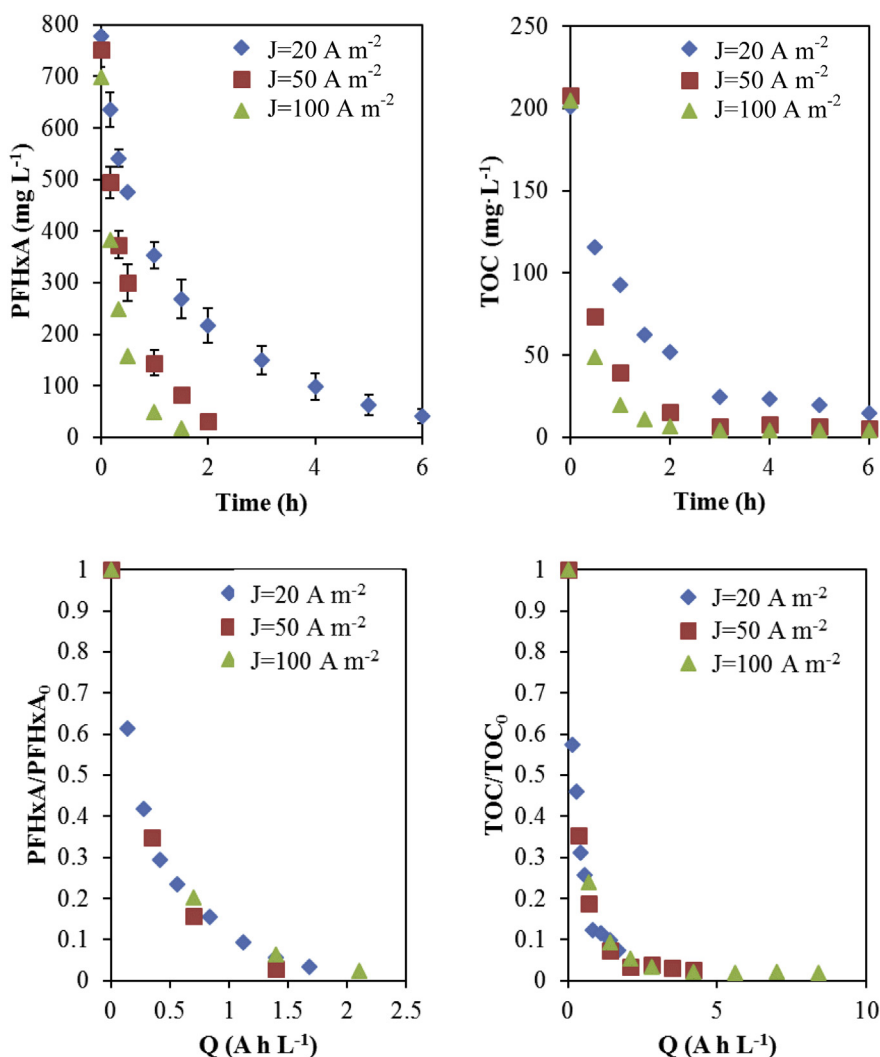


Fig. 7. PFHxA and TOC evolution as function of time (t) and specific electrical charge (Q), using the NF concentrate of sample S1: CM-S1 $[PFHxA]_0 = 774 \text{ mg L}^{-1}$; C-S1 $[PFHxA]_0 = 870 \text{ mg L}^{-1}$. Initial conductivity = $2.31\text{--}2.48 \text{ mS cm}^{-1}$ ◆: $J = 20 \text{ A m}^{-2}$; ■: $J = 50 \text{ A m}^{-2}$; ▲: $J = 100 \text{ A m}^{-2}$.

Table 2

Energy consumption and electrolysis time required to achieve 90% PFHxA degradation in sample CM-S1.

J_{app} (A m^{-2})	Kinetic constant k_2 ($\text{L A}^{-1}\text{h}^{-1}$) ^a	V (V)	Q (A h L^{-1})	W (kWh m^{-3})	Electrolysis time (h)
20	1.859	12.9	1.24	16.0	4.42
50	2.252	14.9	1.02	15.2	1.47
100	1.814	16.8	1.27	21.3	0.90

^a k_2 obtained from the fitting of experimental concentration vs. Q data to $[PFHxA]/[PFHxA]_0 = e^{-k_2 \cdot Q}$.

acids using BDD, SnO_2 , and PbO_2 electrodes. The energy consumption reported in the present study is the lowest of all the values reported so far, which shows evidence of the improvement of efficiency of the electrolysis treatment of PFASs using a pre-concentration strategy.

3.2.2. Electrochemical mineralization of PFHxA in concentrates from industrial process waters

Fig. 8 shows the development of PFHxA and TOC when treating the real industrial process waters pre-concentrated by NF at the selected value of current density ($J_{app} = 50 \text{ A m}^{-2}$). Linearized dimensionless values are presented, since the initial concentrations of PFHxA in the two samples were significantly different. The volume of sample is included in the linearization of data because of the

lower feed water volume used for C-S2 (0.8 L) than for C-S1 (1 L), due to the lack of sample. After 90 min, the degradation of PFHxA concentration was 91% and 98% of the initial in samples C-S1 and C-S2, respectively. It is also interesting to confirm the high removal of TOC, showing the mineralization of the organic compound. PFHxA removal was slightly faster for C-S2 than for C-S1. This behavior can be assigned to its higher initial PFHxA concentration ($C_{0,C-S1} = 870 \text{ mg L}^{-1}$). During the experiments we detected degradation products such as perfluoropentanoic acid and perfluorobutanoic acid. In all cases, the observed amounts of secondary PFCAs were lower than the quantification limit of the HPLC-DAD analytical technique. It means that only small amounts of the shorter chain PFCAs obtained upon PFHxA degradation diffused out of the proximity of the anode surface.

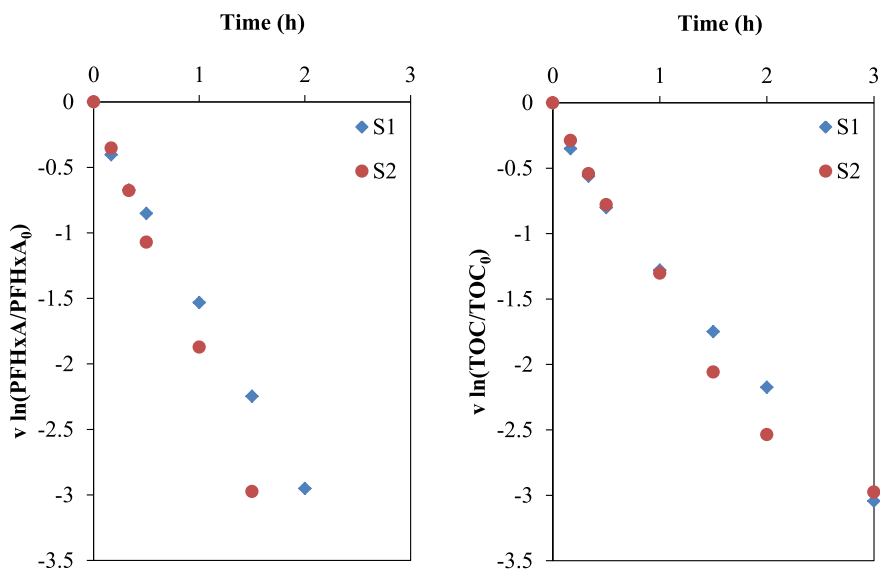


Fig. 8. Linearized dimensionless PFHxA and TOC evolution with time using the real concentrates. $J_{app} = 50 \text{ A m}^{-2}$ ◆:C-S1, $[\text{PFHxA}]_0 = 870 \text{ mg L}^{-1}$, initial conductivity = 2.48 mS cm^{-1} , volume = 1 L; ●:C-S2, $[\text{PFHxA}]_0 = 344 \text{ mg L}^{-1}$, initial conductivity = 2.63 mS cm^{-1} , volume = 0.8 L.

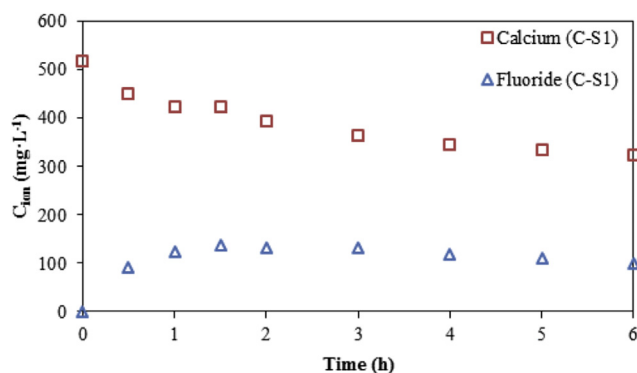


Fig. 9. Calcium and fluoride evolution during the electrochemical treatment of sample C-S1.

Fig. 9 shows the evolution of fluoride with electrochemical treatment. The fluoride concentration reached a maximum at $t = 90 \text{ min}$, and then started to decrease slowly. At the same time, the concentration of calcium decreased continuously, a clear indication that calcium fluoride was being formed from the beginning of the electrochemical test. Local pH variations at the anode and cathode surfaces and the intense fluid turbulence gave rise to the supersaturated calcium fluoride solution and deposition of calcium fluoride on the cathode surface. For electrochemical treatment longer than 2 h, the degradation of PFHxA was nearly completed and there was no further release of fluoride ions. The decrease of fluoride and calcium concentrations was contained showing the slow precipitation of calcium fluoride. Therefore, in the present application, defluorination rate is not an appropriate measurement of the degree of mineralization of PFHxA, as that parameter takes into account the concentration of fluoride ions in the solution. Calcium fluoride scaling was easily removed from the cathode surface by acid cleaning using an aqueous solution of HCl (3 M) at the end of each experimental run. This fouling formation could be detrimental to the performance of the system at larger-scales, which would require implementing a periodical cleaning procedure to avoid scaling on the electrode surface, as it was recently proposed by Schaefer et al. (2016).

The pseudo-first order kinetic constant for PFHxA degradation obtained from the experimental data in Fig. 8, was 0.0021 min^{-1} , after correcting for the volume treated and anode area. This value is ten times higher than the kinetic constant obtained by Niu et al. (2012) for the degradation of PFHxA using a Ce-doped PbO_2 anode. Similarly, Zhuo et al. (2012) reported the electrooxidation of a synthetic aqueous solution of PFHxA (100 mg L^{-1}) using a small BDD anode (8.5 cm^2) in a laboratory-scale batch reactor at an applied current of 232 A m^{-2} . In that work, the reported PFHxA degradation kinetic constant was 0.0016 min^{-1} . The kinetic constant obtained in the present study surpasses the two previously reported values, and validates the use of commercial BDD cells for the removal of PFASs from industrial process waters.

Fig. 10 shows an overview of the process that combines low pressure nanofiltration as the preconcentration step, and electro-oxidation as the degradation technique. This strategy was able to eliminate 90% of the initial PFHxA mass contained in the industrial process waters, at a moderate energy consumption, by increasing the concentration of organic compounds for the electrooxidation process (Sirés et al., 2014). Higher removal rates could be attained by using a more selective membrane system (such as reverse osmosis) that however operates at higher pressures and provides much lower permeate fluxes. Another option would be the electrochemical system alone, which would also be able to further reduce the final PFHxA concentration, at the expense of a higher energy consumption.

4. Conclusions

Results presented herein demonstrate that a combination of nanofiltration (NF) followed by the electrochemical oxidation (ELOX) of the NF concentrate is effective in removing per-fluorohexanoic acid (PFHxA) from industrial process waters. Very few previous studies have reported the treatment of PFHxA, and none of them addressed the NF/ELOX conjunction or the concentration range found in industrial streams, thus showing the novelty of the present study.

It is concluded that the NF270 (Dow/Filmtech) membrane provides high PFHxA rejections (reaching 99.6% when operating at a feed pressure of 20 bar), without any noticeable membrane fouling.

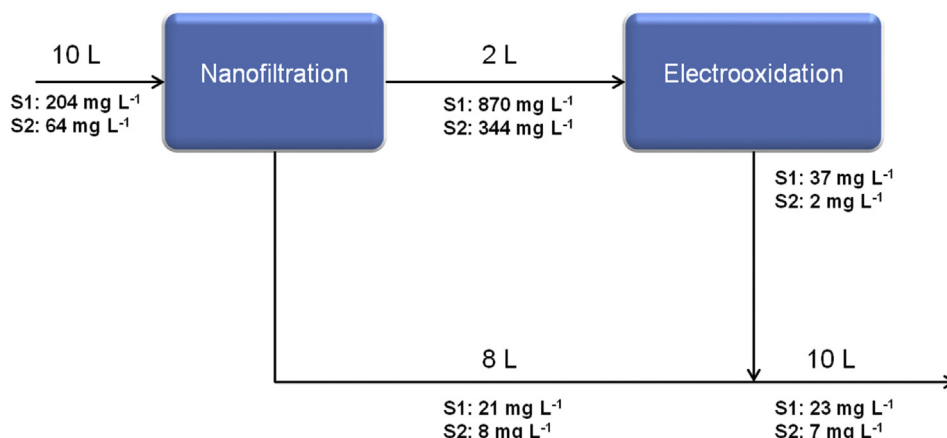


Fig. 10. Global scheme of the combined NF- electrooxidation process.

This performance improves on previously reported results with longer chain PFASs such as PFOA, which showed adhesion to the membrane that reduced the permeate flux. This implies that nanofiltration is a viable technical option for the separation of PFHxA from process water streams when compared to more extended adsorption practices. The presence of sulfate and the adequate rejection of divalent ions by the NF270 membrane provided adequate conductivity to the concentrate stream, which facilitated the subsequent application of electrochemical treatment without the further addition of electrolytes.

Electrooxidation with boron doped diamond electrodes, working at a current density of 50 A m^{-2} , easily degraded the PFHxA retained in the NF concentrate. Traces of shorter chain PFASs were observed in the early stages of the electrochemical process, which nevertheless were later degraded below the limit of quantification of the analytical technique. The possible adverse impact of fluoride ions obtained as a final degradation product was avoided by in situ precipitation as calcium fluoride, promoted by the incoming calcium contained in the industrial process stream. The observed kinetics of PFHxA oxidation was substantially faster than previously reported results using Ce-doped PbO_2 and BDD anodes, probably fostered by the optimal selection of operation variables achieved in this study.

Overall, these results suggest that the process integration of nanofiltration separation and BDD electrochemical degradation is a promising alternative for the treatment of PFHxA that could be extended to the treatment of waters impacted by other PFASs such as PFOA and PFOS.

Funding

Financial support from projects CTM2013-44081-R and CTM2016-75509-R (MINECO, SPAIN-FEDER 2014–2020) is gratefully acknowledged.

Appendix A. Supplementary data

Supplementary data related to this article can be found at <http://dx.doi.org/10.1016/j.watres.2017.01.043>.

References

Ahrens, L., Bundschuh, M., 2014. Fate and effects of poly- and perfluoroalkyl substances in the aquatic environment: a review. *Environ. Toxicol. Chem.* 33, 1921–1929.

Anglada, Á., Urriaga, A., Ortiz, I., 2009. Contributions of electrochemical oxidation to waste-water treatment: fundamentals and review of applications. *J. Chem.*

Technol. Biotechnol. 84, 1747–1755. <http://dx.doi.org/10.1002/jctb.2214>.

Anglada, Á., Urriaga, A.M., Ortiz, I., 2010. Laboratory and pilot plant scale study on the electrochemical oxidation of landfill leachate. *J. Hazard. Mater.* 181, 729–735. <http://dx.doi.org/10.1016/j.jhazmat.2010.05.073>.

Appleman, T.D., Dickenson, E.R.V., Bellona, C., Higgins, C.P., 2013. Nanofiltration and granular activated carbon treatment of perfluoroalkyl acids. *J. Hazard. Mater.* 260, 740–746.

Appleman, T.D., Higgins, C.P., Quiñones, O., Vanderford, B.J., Kolstad, C., Zeigler-Holady, J.C., Dickenson, E.R.V., 2014. Treatment of poly- and perfluoroalkyl substances in U.S. full-scale water treatment systems. *Water Res.* 51, 246–255. <http://dx.doi.org/10.1016/j.watres.2013.10.067>.

Arvaniti, O.S., Stasinakis, A.S., 2015. Review on the occurrence, fate and removal of perfluorinated compounds during wastewater treatment. *Sci. Total Environ.* 524–525, 81–92.

Asano, T., 1998. *Wastewater Reclamation and Reuse: Water Quality Management Library*. CRC Press, Florida.

Baudequin, C., Mai, Z., Rakib, M., Deguerly, I., Severac, R., Pabon, M., Couallier, E., 2014. Removal of fluorinated surfactants by reverse osmosis - role of surfactants in membrane fouling. *J. Memb. Sci.* 458, 111–119. <http://dx.doi.org/10.1016/j.memsci.2014.01.063>.

Bellona, C., Drewes, J.E., 2007. Viability of a low-pressure nanofilter in treating recycled water for water reuse applications: a pilot-scale study. *Water Res.* 41, 3948–3958. <http://dx.doi.org/10.1016/j.watres.2007.05.027>.

Cabeza, A., Urriaga, A.M., Ortiz, I., 2007. Electrochemical treatment of landfill leachates using a boron-doped diamond anode. *Ind. Eng. Chem. Res.* 46, 1439–1446. <http://dx.doi.org/10.1021/ie061373x>.

Cañizares, P., Lobato, J., Paz, R., Rodrigo, M.A., Sáez, C., 2005. Electrochemical oxidation of phenolic wastes with boron-doped diamond anodes. *Water Res.* 39, 2687–2703. <http://dx.doi.org/10.1016/j.watres.2005.04.042>.

Carter, K.E., Farrell, J., 2008. Oxidative destruction of perfluorooctane sulfonate using boron-doped diamond film electrodes. *Environ. Sci. Technol.* 42, 6111–6115. <http://dx.doi.org/10.1021/es703273s>.

Chaplin, B.P., 2014. Critical review of electrochemical advanced oxidation processes for water treatment applications. *Environ. Sci. Process. Impacts* 16, 1182–1203. <http://dx.doi.org/10.1039/c3em00679d>.

Dialynas, E., Mantzavinos, D., Diamadopoulos, E., 2008. Advanced treatment of the reverse osmosis concentrate produced during reclamation of municipal wastewater. *Water Res.* 42, 4603–4608. <http://dx.doi.org/10.1016/j.watres.2008.08.008>.

Díaz, V., Ibáñez, R., Gómez, P., Urriaga, A.M., Ortiz, I., 2011. Kinetics of electro-oxidation of ammonia-N, nitrites and COD from a recirculating aquaculture saline water system using BDD anodes. *Water Res.* 45, 125–134. <http://dx.doi.org/10.1016/j.watres.2010.08.020>.

ECHA, 2014. Candidate List of Substances of Very High Concern for Authorisation [WWW Document]. URL: <https://echa.europa.eu/candidate-list-table>.

Fujioka, T., Nghiem, L.D., Khan, S.J., McDonald, J.A., Poussade, Y., Drewes, J.E., 2012. Effects of feed solution characteristics on the rejection of N-nitrosamines by reverse osmosis membranes. *J. Memb. Sci.* 409–410, 66–74. <http://dx.doi.org/10.1016/j.memsci.2012.03.035>.

Hang, X., Chen, X., Luo, J., Cao, W., Wan, Y., 2015. Removal and recovery of perfluorooctanoate from wastewater by nanofiltration. *Sep. Purif. Technol.* 145, 120–129.

Hilal, N., Kochkodan, V., Al Abdulgader, H., Johnson, D., 2015. A combined ion exchange-nanofiltration process for water desalination: II. Membrane selection. *Desalination* 363, 51–57. <http://dx.doi.org/10.1016/j.desal.2014.11.017>.

Hori, H., Yamamoto, A., Hayakawa, E., Taniyasu, S., Yamashita, N., Kutsuna, S., Kiatagawa, H., Arakawa, R., 2005. Efficient decomposition of environmentally persistent perfluorocarboxylic acids by use of persulfate as a photochemical oxidant. *Environ. Sci. Technol.* 39 <http://dx.doi.org/10.1021/es0484754>.

- Ioannou, L.A., Michael, C., Vakondios, N., Drosou, K., Xekoukoulotakis, N.P., Diamadopoulos, E., Fatta-Kassinos, D., 2013. Winery wastewater purification by reverse osmosis and oxidation of the concentrate by solar photo-Fenton. *Sep. Purif. Technol.* 118, 659–669. <http://dx.doi.org/10.1016/j.seppur.2013.07.049>.
- IUPAC, 1996. Terminology for membranes and membrane processes (IUPAC Recommendation 1996). *J. Memb. Sci.* 120, 149–159. [http://dx.doi.org/10.1016/0376-7388\(96\)82861-4](http://dx.doi.org/10.1016/0376-7388(96)82861-4).
- Lin, A.Y.C., Panchangam, S.C., Tsai, Y.T., Yu, T.H., 2014. Occurrence of perfluorinated compounds in the aquatic environment as found in science park effluent, river water, rainwater, sediments, and biotissues. *Environ. Monit. Assess.* 186, 3265–3275. <http://dx.doi.org/10.1007/s10661-014-3617-9>.
- Martínez-Huitile, C.A., Rodrigo, M.A., Sirés, I., Scialdone, O., 2015. Single and coupled electrochemical processes and reactors for the abatement of organic water pollutants: a critical review. *Chem. Rev.* 115, 13362–13407. <http://dx.doi.org/10.1021/acs.chemrev.5b00361>.
- Mulder, M., 1996. Basic Principles of Membrane Technology. *Zeitschrift für Physikalische Chemie*. Springer, Netherlands. http://dx.doi.org/10.1524/zpch.1998.203.Part_1_2.263.
- Nghiem, L.D., Hawkes, S., 2007. Effects of membrane fouling on the nanofiltration of pharmaceutically active compounds (PhACs): mechanisms and role of membrane pore size. *Sep. Purif. Technol.* 57, 176–184. <http://dx.doi.org/10.1016/j.seppur.2007.04.002>.
- Niu, J., Li, Y., Shang, E., Xu, Z., Liu, J., 2016. Electrochemical oxidation of perfluorinated compounds in water. *Chemosphere* 146, 526–538. <http://dx.doi.org/10.1016/j.chemosphere.2015.11.115>.
- Niu, J., Lin, H., Xu, J., Wu, H., Li, Y., 2012. Electrochemical mineralization of perfluorocarboxylic acids (PFCAs) by Ce-doped modified porous nanocrystalline PbO₂ film electrode. *Environ. Sci. Technol.* 46, 10191–10198. <http://dx.doi.org/10.1021/es302148z>.
- Ochiai, T., Iizuka, Y., Nakata, K., Murakami, T., Tryk, D.A., Fujishima, A., Koide, Y., Morito, Y., 2011. Efficient electrochemical decomposition of perfluorocarboxylic acids by the use of a boron-doped diamond electrode. *Diam. Relat. Mater.* 20, 64–67. <http://dx.doi.org/10.1016/j.diamond.2010.12.008>.
- Panizza, M., Cerisola, G., 2009. Direct and mediated anodic oxidation of organic pollutants. *Chem. Rev.* 109, 6541–6569. <http://dx.doi.org/10.1021/cr9001319>.
- Pérez-González, A., Ibáñez, R., Gómez, P., Urriaga, A.M., Ortiz, I., Irbien, J.A., 2015. Nanofiltration separation of polyvalent and monovalent anions in desalination brines. *J. Memb. Sci.* 473, 16–27. <http://dx.doi.org/10.1016/j.memsci.2014.08.045>.
- Pérez, G., Fernández-Alba, A.R., Urriaga, A.M., Ortiz, I., 2010. Electro-oxidation of reverse osmosis concentrates generated in tertiary water treatment. *Water Res.* 44, 2763–2772. <http://dx.doi.org/10.1016/j.watres.2010.02.017>.
- Perry, R.H., Green, D.W., Maloney, J.O., 1997. *Perry's Chemical Engineers' Handbook, Chemical Engineering Series*. McGraw-Hill Professional Publishing, New York.
- Polcaro, A.M., Vacca, A., Mascia, M., Palmas, S., Rodriguez Ruiz, J., 2009. Electrochemical treatment of waters with BDD anodes: kinetics of the reactions involving chlorides. *J. Appl. Electrochem* 39, 2083–2092. <http://dx.doi.org/10.1007/s10800-009-9870-x>.
- Radjenovic, J., Bagastyo, A., Rozendal, R.A., Mu, Y., Keller, J., Rabaey, K., 2011. Electrochemical oxidation of trace organic contaminants in reverse osmosis concentrate using RuO₂/IrO₂-coated titanium anodes. *Water Res.* 45, 1579–1586. <http://dx.doi.org/10.1016/j.watres.2010.11.035>.
- Rahman, M.F., Peldszus, S., Anderson, W.B., 2014. Behaviour and fate of perfluoroalkyl and polyfluoroalkyl substances (PFASs) in drinking water treatment: a review. *Water Res.* 50, 318–340.
- Samson, E., Marchand, J., Snyder, K.A., 2003. Calculation of ionic diffusion coefficients on the basis of migration test results. *Mater. Struct. Constr.* 36, 156–165. <http://dx.doi.org/10.1617/14002>.
- Sansotera, M., Persico, F., Pirola, C., Navarrini, W., Di Michele, A., Bianchi, C.L., 2014. Decomposition of perfluorooctanoic acid photocatalyzed by titanium dioxide: chemical modification of the catalyst surface induced by fluoride ions. *Appl. Catal. B Environ.* 148, 29–35. <http://dx.doi.org/10.1016/j.apcatb.2013.10.038>.
- Schaefer, C.E., Andaya, C., Urriaga, A., McKenzie, E.R., Higgins, C.P., 2015. Electrochemical treatment of perfluorooctanoic acid (PFOA) and perfluorooctane sulfonic acid (PFOS) in groundwater impacted by aqueous film forming foams (AFFFs). *J. Hazard. Mater.* 295, 170–175. <http://dx.doi.org/10.1016/j.jhazmat.2015.04.024>.
- Schaefer, C.E., Lavorgna, G.M., Webster, T.S., Deshusses, M.A., Andaya, C., Urriaga, A., 2016. Pilot-scale electrochemical disinfection of surface water: assessing disinfection by-product and free chlorine formation. *Water Sci. Technol. Water Supply*. <http://dx.doi.org/10.2166/ws.2016.165>.
- Sirés, I., Brillas, E., Oturan, M.A., Rodrigo, M.A., Panizza, M., 2014. Electrochemical advanced oxidation processes: today and tomorrow. A review. *Environ. Sci. Pollut. Res.* 21, 8336–8367. <http://dx.doi.org/10.1007/s11356-014-2783-1>.
- Steinle-Darling, E., Reinhard, M., 2008. Nanofiltration for trace organic contaminant removal: structure, solution, and membrane fouling effects on the rejection of perfluorochemicals. *Environ. Sci. Technol.* 42, 5292–5297.
- Tang, C.Y., Fu, Q.S., Criddle, C.S., Leckie, J.O., 2007. Effect of flux (transmembrane pressure) and membrane properties on fouling and rejection of reverse osmosis and nanofiltration membranes treating perfluorooctane sulfonate containing wastewater. *Environ. Sci. Technol.* <http://dx.doi.org/10.1021/es062052f>.
- Tang, C.Y., Fu, Q.S., Robertson, A.P., Criddle, C.S., Leckie, J.O., 2006. Use of Reverse osmosis membranes to remove perfluorooctane sulfonate (PFOS) from semiconductor wastewater. *Environ. Sci. Technol.* <http://dx.doi.org/10.1021/es060831q>.
- Urriaga, A., Fernández-González, C., Gómez-Lavín, S., Ortiz, I., 2015. Kinetics of the electrochemical mineralization of perfluorooctanoic acid on ultrananocrystalline boron doped conductive diamond electrodes. *Chemosphere* 129, 20–26. <http://dx.doi.org/10.1016/j.chemosphere.2014.05.090>.
- Urriaga, A., Gómez, P., Arruti, A., Ortiz, I., 2014. Electrochemical removal of tetrahydrofuran from industrial wastewaters: anode selection and process scale-up. *J. Chem. Technol. Biotechnol.* 89, 1243–1250. <http://dx.doi.org/10.1002/jctb.4384>.
- USEPA, 2016. Drinking Water Health Advisories for PFOA and PFOS [WWW Document]. URL <https://www.epa.gov/ground-water-and-drinking-water/drinking-water-health-advisories-pfoa-and-pfos>.
- USEPA, 2015. Fact Sheet: 2010/2015 PFOA Stewardship Program [WWW Document]. URL <https://www.epa.gov/assessing-and-managing-chemicals-under-tsca/fact-sheet-20102015-pfoa-stewardship-program#meet>.
- van den Berg, G.B., Rácz, I.G., Smolders, C.A., 1989. Mass transfer coefficients in cross-flow ultrafiltration. *J. Memb. Sci.* 47, 25–51. [http://dx.doi.org/10.1016/S0376-7388\(00\)80858-3](http://dx.doi.org/10.1016/S0376-7388(00)80858-3).
- Wang, J., Wang, Z., Liu, Y., Wang, J., Wang, S., 2016. Surface modification of NF membrane with zwitterionic polymer to improve anti-biofouling property. *J. Memb. Sci.* 514, 407–417. <http://dx.doi.org/10.1016/j.memsci.2016.05.014>.
- Wang, T., Zhao, C., Li, P., Li, Y., Wang, J., 2015a. Fabrication of novel poly(m-phenylene isophthalamide) hollow fiber nanofiltration membrane for effective removal of trace amount perfluorooctane sulfonate from water. *J. Memb. Sci.* 477, 74–85. <http://dx.doi.org/10.1016/j.memsci.2014.12.038>.
- Wang, Z., Cousins, I.T., Scheringer, M., Hungerbuehler, K., 2015b. Hazard assessment of fluorinated alternatives to long-chain perfluoroalkyl acids (PFAAs) and their precursors: status quo, ongoing challenges and possible solutions. *Environ. Int.* 75, 172–179. <http://dx.doi.org/10.1016/j.envint.2014.11.013>.
- Xue, A., Yuan, Z.W., Sun, Y., Cao, A.Y., Zhao, H.Z., 2015. Electro-oxidation of perfluorooctanoic acid by carbon nanotube sponge anode and the mechanism. *Chemosphere* 141, 120–126. <http://dx.doi.org/10.1016/j.chemosphere.2015.06.095>.
- Yang, B., Jiang, C., Yu, G., Zhuo, Q., Deng, S., Wu, J., Zhang, H., 2015. Highly efficient electrochemical degradation of perfluoroalkyl acids (PFOA) by F-doped Ti/SnO₂ electrode. *J. Hazard. Mater.* 299, 417–424. <http://dx.doi.org/10.1016/j.jhazmat.2015.06.033>.
- Yu, Q., Zhang, R., Deng, S., Huang, J., Yu, G., 2009. Sorption of perfluorooctane sulfonate and perfluorooctanoate on activated carbons and resin: kinetic and isotherm study. *Water Res.* 43, 1150–1158. <http://dx.doi.org/10.1016/j.watres.2008.12.001>.
- Zaggia, A., Conte, L., Falletti, L., Fant, M., Chiorboli, A., 2016. Use of strong anion exchange resins for the removal of perfluoroalkylated substances from contaminated drinking water in batch and continuous pilot plants. *Water Res.* 91, 137–146. <http://dx.doi.org/10.1016/j.watres.2015.12.039>.
- Zhang, D., Luo, Q., Gao, B., Chiang, S.Y.D., Woodward, D., Huang, Q., 2016. Sorption of perfluorooctanoic acid, perfluorooctane sulfonate and perfluoroheptanoic acid on granular activated carbon. *Chemosphere* 144, 2336–2342. <http://dx.doi.org/10.1016/j.chemosphere.2015.10.124>.
- Zhao, C., Zhang, J., He, G., Wang, T., Hou, D., Luan, Z., 2013a. Perfluorooctane sulfonate removal by nanofiltration membrane the role of calcium ions. *Chem. Eng. J.* 233, 224–232. <http://dx.doi.org/10.1016/j.cej.2013.08.027>.
- Zhao, H., Gao, J., Zhao, G., Fan, J., Wang, Y., Wang, Y., 2013b. Fabrication of novel SnO₂-Sb/carbon aerogel electrode for ultrasonic electrochemical oxidation of perfluorooctanoate with high catalytic efficiency. *Appl. Catal. B Environ.* 136, 278–286. <http://dx.doi.org/10.1016/j.apcatb.2013.02.013>.
- Zhao, L., Folsom, P.W., Wolstenholme, B.W., Sun, H., Wang, N., Buck, R.C., 2013c. 6:2 Fluorotelomer alcohol biotransformation in an aerobic river sediment system. *Chemosphere* 90, 203–209. <http://dx.doi.org/10.1016/j.chemosphere.2012.06.035>.
- Zhuo, Q., Deng, S., Yang, B., Huang, J., Wang, B., Zhang, T., Yu, G., 2012. Degradation of perfluorinated compounds on a boron-doped diamond electrode. *Electrochim. Acta* 77, 17–22. <http://dx.doi.org/10.1016/j.electacta.2012.04.145>.
- Zhuo, Q., Deng, S., Yang, B., Huang, J., Yu, G., 2011. Efficient electrochemical oxidation of perfluorooctanoate using a Ti/SnO₂-Sb-Bi anode. *Environ. Sci. Technol.* 45, 2973–2979. <http://dx.doi.org/10.1021/es102454z>.
- Zhuo, Q., Li, X., Yan, F., Yang, B., Deng, S., Huang, J., Yu, G., 2014. Electrochemical oxidation of 1H,1H,2H,2H-perfluorooctane sulfonic acid (6:2 FTS) on DSA electrode: operating parameters and mechanism. *J. Environ. Sci.* 26, 1733–1739. <http://dx.doi.org/10.1016/j.jes.2014.06.014>.

Supplementary material

Efficient treatment of perfluorohexanoic acid by nanofiltration followed by electrochemical degradation of the NF concentrate

Álvaro Soriano, Daniel Gorri, Ane Urriaga*

Department of Chemical and Biomolecular Engineering, University of Cantabria

Av. de Los Castros s/n. 39005 Santander. Spain

*Corresponding author: urriaga@unican.es

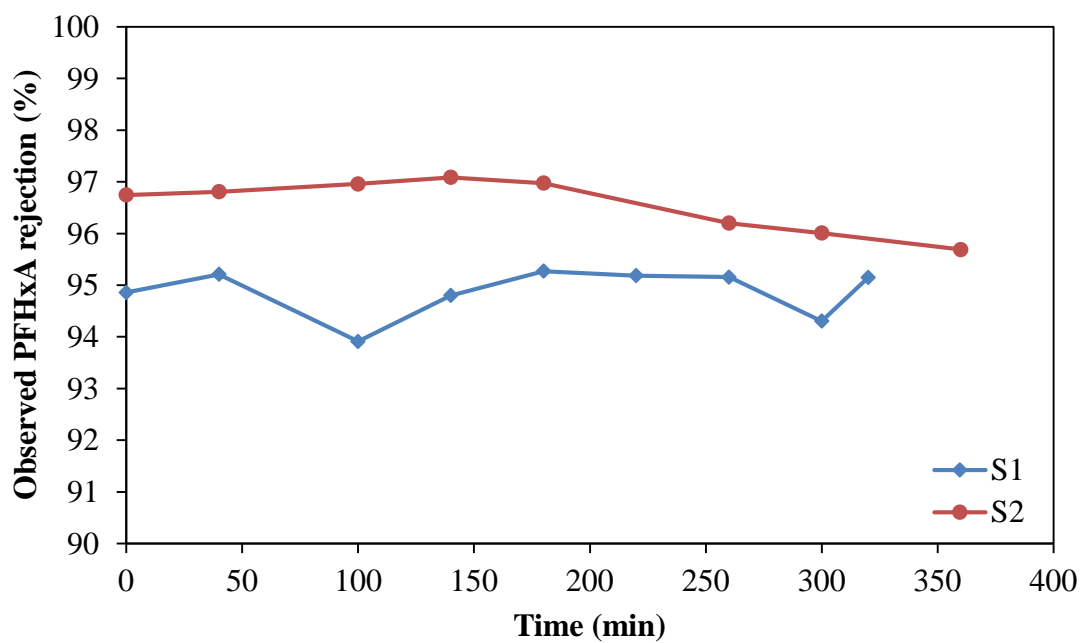
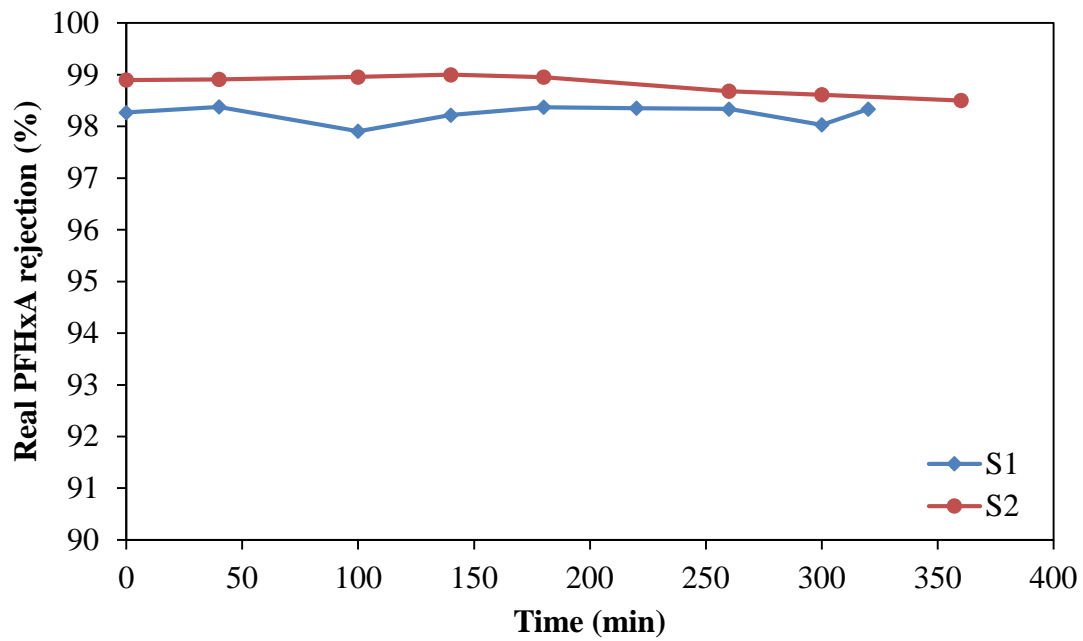


Figure S1. a) Real PFHxA rejection, and b) observed PFHxA rejection in concentration mode. NF270 membrane. Feed pressure: 10 bar.

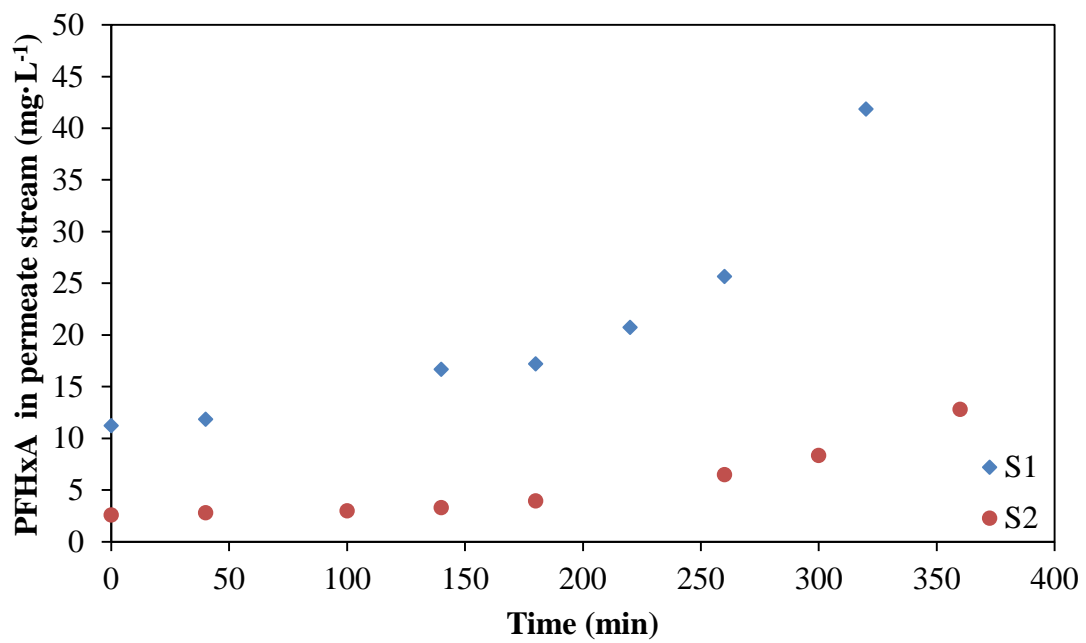
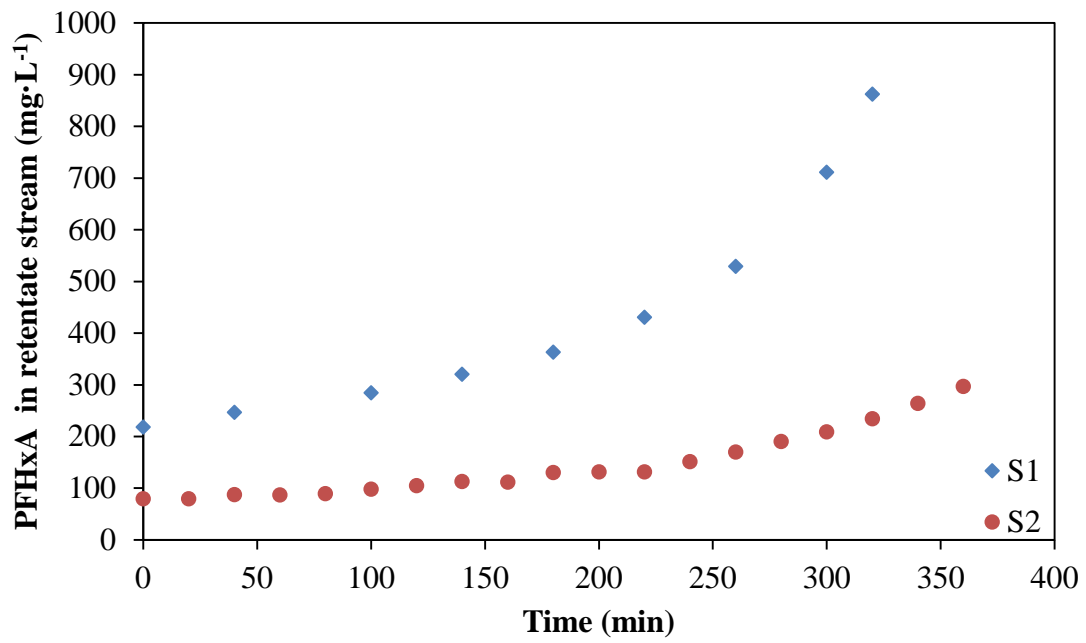


Figure S2. a) PFHxA concentration in the concentrate, and b) PFHxA concentration in the permeate in concentration mode. NF270 membrane. Feed pressure: 10 bar.

5.2. Scientific publication #2.

BDD anodic treatment of 6:2 fluorotelomer sulfonate (6:2 FTSA). Evaluation of operating variables and by-product formation

Authors:

Ane Urtiaga^a, Álvaro Soriano^a, Jordi Carrillo-Abad^{a,b}

^a Department of Chemical and Biomolecular Engineering. University of Cantabria. Av. de Los Castros 46. 39005 Santander. Spain

^b Dpto. Ingeniería Química y Nuclear, Universitat Politècnica de València, P.O. Box 22012, E-46023 Valencia, Spain

Accepted 4 March 2018

Chemosphere

Volume 201 (2018), Pages 571-577

DOI: 10.1016/j.chemosphere.2018.03.027



BDD anodic treatment of 6:2 fluorotelomer sulfonate (6:2 FTSA). Evaluation of operating variables and by-product formation

Ane Urriaga^{a,*}, Alvaro Soriano^a, Jordi Carrillo-Abad^{a,b}

^a Department of Chemical and Biomolecular Engineering, University of Cantabria, Av. de Los Castros s/n, 39005 Santander, Spain

^b Dpto. Ingeniería Química y Nuclear, Universitat Politècnica de València, P.O. Box 22012, E-46023 Valencia, Spain



HIGHLIGHTS

- 6:2 FTSA is completely removed by electrolysis with BDD anodes.
- 6:2 FTSA degradation results in the formation of PFHxA and shorter chain PFCAs.
- PFHxA is completely defluorinated and decarboxylated.
- Mineralization higher than 90% is attained after passing 2 kAh m⁻³.

ARTICLE INFO

Article history:

Received 15 December 2017

Received in revised form

27 February 2018

Accepted 4 March 2018

Available online 7 March 2018

Keywords:

6:2 FTSA

BDD

Electrolysis

Perfluorinated alkyl substances

PFHxA

Fluorochemicals

ABSTRACT

The concerns about the undesired impacts on human health and the environment of long chain perfluorinated alkyl substances (PFASs) have driven industrial initiatives to replace PFASs by shorter chain fluorinated homologues. 6:2 fluorotelomer sulfonic acid (6:2 FTSA) is applied as alternative to PFOS in metal plating and fluoropolymer manufacture. This study reports the electrochemical treatment of aqueous 6:2 FTSA solutions on microcrystalline BDD anodes. Bench scale batch experiments were performed, focused on assessing the effect of the electrolyte and the applied current density (5–600 A m⁻²) on the removal of 6:2 FTSA, the reduction of total organic carbon (TOC) and the fluoride release. Results showed that at the low range of applied current density ($J = 50$ A m⁻²), using NaCl, Na₂SO₄ and NaClO₄, the electrolyte exerted a minimal effect on removal rates. The formation of toxic inorganic chlorine species such as ClO₄⁻ was not observed. When using Na₂SO₄ electrolyte, increasing the applied current density to 350–600 A m⁻² promoted a notable enhancement of the 6:2 FTSA removal and defluorination rates, pointing to the positive contribution of electrogenerated secondary oxidants to the overall removal rate. 6:2 FTSA was transformed into shorter-chain PFCAs, and eventually into CO₂ and fluoride, as TOC reduction was >90%. Finally, it was demonstrated that diffusion in the liquid phase was controlling the overall kinetic rate, although with moderate improvements due to secondary oxidants at very high current densities.

© 2018 Elsevier Ltd. All rights reserved.

1. Introduction

There is an international recognition of long chain perfluorocarboxylic acids (PFCAs, C_nF_{2n+1}COOH, n ≥ 7) and perfluoroalkane sulfonic acids (PFASs, C_nF_{2n+1}SO₃H, n ≥ 7) as global contaminants, as a result of their high persistence and bioaccumulative properties (Stockholm Convention, 2009; ECHA, 2014). The concerns about the undesired impacts on human

health and the environment have driven industrial initiatives to phase out long chain perfluoroalkyl substances (USEPA, 2015) that are being substituted by products based on shorter perfluoroalkyl chains such as perfluorobutane sulfonate (PFBS) and fluorotelomer-based substances (Wang et al., 2013). 6:2 fluorotelomer sulfonic acid (6:2 FTSA, C₆F₁₃CH₂CH₂SO₃H) is applied as alternative to PFOS in the surface treatment of metal and plastic components, and as processing aid in emulsion polymerization of fluoropolymers (Brunn-Poulsen et al., 2011). 6:2 FTSA is also known to be the major degradation product from fluorotelomer sulfone and mercaptan chemistry used in telomer-based air fire fighting foams (AFFF) (Cheremisinoff, 2017). The C–C bonds of carbons substituted by

* Corresponding author.

E-mail address: urriaga@unican.es (A. Urriaga).

hydrogen and the C–S bond make 6:2 FTSA much more susceptible to biodegradation compared to refractory PFCAs and PFSA. Regarding the aquatic toxicity, a recent study concluded that 6:2 FTSA is not bioaccumulative, and that it poses minimal risk to aquatic organisms (Hoke et al., 2015). Even though, 6:2 FTSA may still pose risks as its aerobic biotransformation in wastewater treatment plants is slow and the main stable biodegradation product is perfluorohexanoic acid (PFHxA), a short chain PFCA that behaves as persistent in the environment as the long chain homologues (Wang et al., 2011). An annual average environmental quality standard (AA-EQS) of 1 mg L^{-1} for PFHxA in freshwaters has been recently proposed (Valsecchi et al., 2017).

Because of the persistence of its degradation products, 6:2 FTSA cannot be mineralized by conventional biological water treatments. Therefore, new advanced oxidation processes (AOPs) are being studied for the removal of this polyfluorinated substance from polluted waters. Fernandez et al. (2016) reported that less than 20% of fluoride was released in the sonolysis treatment of 6:2 FTSA (initial concentration $130 \mu\text{M}$). The use of ozone and hydrogen peroxide oxidation was investigated by Yang et al. (2014) who selected UV/H₂O₂ as the most effective technology among various AOPs investigated. Heat activated persulfate achieved fast 6:2 FTSA oxidation, with PFHxA being the dominant stable product (Park et al., 2016). Recent progress on electrochemical oxidation (ELOX) revealed the high efficiency of boron doped diamond (BDD) anodic electrolysis for the treatment of industrial wastewaters generated in the chemical manufacture of side-chain-fluorinated polymers and fluorotelomer based products for fire-fighting foams (Urtiaga et al., 2015; Gomez-Ruiz et al., 2017a). 6:2 FTSA and 8:2 fluorotelomer sulfonamide alkylbetaine (6:2 FTAB) were completely removed from the effluent of the wastewater treatment plant, and the group of PFCAs, PFHxA being the most abundant, were also progressively mineralized to achieve 99.74% of total poly and perfluoroalkyl substances (PFASs) removal. Similarly, Soriano et al. (2017) reported the significant reduction of energy consumption by means of membrane pretreatment followed by BDD electrochemical oxidation in the treatment of process waters containing high concentrations of PFHxA. To date, the electrochemical treatment of 6:2 FTSA on dimensionally stable anodes (DSA) has been reported to achieve low decomposition ratios of approximately 30%, and to yield increasing concentrations of PFHxA as final oxidation product (Zhuo et al., 2014). Therefore, DSA electro-oxidation did not achieve mineralization and defluorination of 6:2 FTSA.

The overall goal of this study was to evaluate and demonstrate the efficient electrochemical degradation of 6:2 FTSA with BDD electrodes. Aqueous solutions prepared from 6:2 FTSA formulations that are commercialized as surfactants for surface treatment operations and emulsion polymerization were investigated. Experiments examined the effects of the type of electrolyte, using sulfate, chloride and perchlorate salts, on 6:2 FTSA defluorination and mineralization, by means of the total organic carbon (TOC) removal. The influence of the main operation parameter, e.g.: the applied current density, from 5 to 600 A m^{-2} , on reaction rates and on the generation and degradation of shorter chain perfluorinated intermediate products was studied. Treatment of individual PFCAs was also assessed, in order to validate the proposal of kinetic regime.

2. Materials and methods

6:2 FTSA solutions were prepared from CAPSTONE FS-10[®] (Chemours), a commercial concentrated 6:2 FTSA aqueous solution. Perfluoroheptanoic acid (PFHpA, C₆F₁₃COOH), perfluorohexanoic acid (PFHxA, C₅F₁₁COOH) and perfluoropentanoic acid (PFPeA, C₄F₉COOH) were purchased from Sigma Aldrich Chemicals. All

perfluorocarboxylic acids were reagent grade or higher and were used as received without further purification. NaCl (Panreac), Na₂SO₄ (Panreac) and NaClO₄ (Sigma-Aldrich) were used to prepare the electrolyte solutions. All solutions were prepared using ultrapure water (Q-POD Millipore). Methanol (UHPLC-MS grade) was obtained from Scharlau.

The electrooxidation experimental set-up consisted of an electrochemical cell (DiaCell 201 PP, Adamant Technologies), a power supply (Vitecom 75-HY3005D), a jacketed feed tank, and a cooling bath (Polyscience 9510). The cell contained two parallel flow-by compartments made of a central bipolar p-Si/BDD electrode and p-Si/BDD anode and cathode, with an interelectrode gap of 1 mm in each channel. Each electrode had a surface area of 70 cm^2 , resulting in a total anodic area of 140 cm^2 . 2 L aqueous solutions of 6:2 FTSA (100 mg L^{-1}), or individual perfluorocarboxylic acids, were used as feed in the experiments that were conducted in batch mode at constant temperature of $20 \text{ }^\circ\text{C}$. The experiments were carried out in batch mode and galvanostatic conditions. Further details on the experimental system can be found elsewhere (Urtiaga et al., 2014; Soriano et al., 2017). The applied current density (J) was varied in the range $5\text{--}600 \text{ A m}^{-2}$. Treated samples were collected in polypropylene containers, and preserved at $4 \text{ }^\circ\text{C}$ until analysis.

Total organic carbon (TOC) analyses were performed using a TOC-V CPH (Shimadzu). Fluoride was analyzed by ion chromatography (Dionex 120 IC) provided with an IonPac As-HC column and using a $9 \text{ mM Na}_2\text{CO}_3$ solution as eluent, that was circulated at a flowrate of 1 mL min^{-1} , based on Standard Methods 4110 B (APHA, 1998). The limit of quantification (LOQ) for fluoride analysis was 0.03 mg L^{-1} .

The analyses of 6:2 FTSA and its degradation products PFHpA, PFHxA, PFPeA and PFBA were carried out by ultra-high performance liquid chromatography coupled to tandem mass spectrometry (UPLC-MS/MS). Prior to instrumental analysis samples were extracted by a solid-phase extraction (SPE) procedure in order to eliminate dissolved salts. Non-filtered samples were diluted prior to SPE in 2% formic acid in order to acidify samples. TELOS neo WAX SPE cartridges (200 mg, 6 mL; Kinesis, U.K.) were conditioned with methanol and subsequently equilibrated with ultrapure water (Milli-Q, Millipore) before sample loading. Two interference elution wash steps were carried out separately with 3 mL Milli-Q water each one to eliminate ionic interferences. Finally, target analytes were eluted with 2 mL of methanol: ammonium hydroxide (95:5 v/v). The extracts were further evaporated until dryness under a gentle stream of dry nitrogen gas. The final volume was adjusted to 1 mL Milli-Q water and filtered ($0.22 \mu\text{m}$) prior to injection. Recovery rates of the SPE procedure were determined by applying the detailed method to spiked Milli-Q water samples ($n=6$) with target analyte standard solutions (6:2 FTSA, 100 mg L^{-1} ; PFHpA, PFHxA, and PFPeA, 10 mg L^{-1} , each one) and Na₂SO₄, 5 g L^{-1} . Percent recovery rates were as followed: 6:2 FTSA, 91.4 ± 8.8 ; PFHpA, 93.4 ± 14.4 ; PFHxA, 118.1 ± 10.6 ; PFPeA, 92.5 ± 19.6 .

The purified sample extracts were analyzed using an UPLC-TQD system (Waters, Milford, MA, USA) with an electrospray ionization (ESI) interface operated in the negative ionization mode. An Acquity UPLC BEH C18 column ($50 \times 2.1 \text{ mm} \times 1.7 \mu\text{m}$) at $50 \text{ }^\circ\text{C}$ was used for the analytical separation. The mobile phase consisted of 5% methanol containing 2 mmol L^{-1} ammonium acetate (A) and methanol (B), at an operating flow rate of 0.4 mL min^{-1} in gradient mode.

Dilutions from the stock standard solutions were prepared in water at 7 concentration levels ranging from 1 ng mL^{-1} to 400 ng mL^{-1} and calibration curves were built in order to calculate the PFASs concentrations in real samples and to control the linear range of the instrumental response. Quality control and validation of the method were made using recovery rates, method blanks,

calibration linearity, mass detection limits and quantification limits. LOQs were 1 ng mL^{-1} in real samples.

3. Results and discussion

Initial experiments were aimed at the analysis of the effect of the electrolyte on the 6:2 FTSA mineralization. Three electrolyte solutions were tested: Na_2SO_4 (5 g L^{-1}), NaCl (3.5 g L^{-1}), and NaClO_4 (9.4 g L^{-1}), working at $J = 50 \text{ A m}^{-2}$. The concentration of each salt was selected to provide the electrolyte solution with a similar background conductivity (6.9 mS cm^{-1}). While perchlorate salts are known to behave as inert electrolytes in BDD electrooxidation (Chaplin et al., 2011), sulfate and chloride have been reported to act as promoters of secondary oxidizing species such as active chlorine, sulfate radical or persulfate anion (Martín de Vidales et al., 2015; Uranga-Flores et al., 2015; Jalife-Jacobo et al., 2016; Lan et al., 2017). Nevertheless, Fig. 1a shows no significant influence of the type of electrolyte on TOC kinetics removal, for a 100 mg L^{-1} 6:2 FTSA solution, revealing that the formation of secondary oxidants with potential ability to degrade 6:2 FTSA and its secondary degradation products did not occur at the low range of applied current density ($J = 50 \text{ A m}^{-2}$) used in this group of experiments. Similarly, the release of fluoride anions observed in Fig. 1b, that resulted from the cleavage of C–F bonds in the perfluorocarboxylic chain of 6:2 FTSA, supports the effective mineralization of the fluorotelomer sulfonate compound into CO_2 and fluoride. A slightly slower fluoride release is observed for NaCl electrolyte solution, in good correspondence with the TOC evolution. This behavior can be attributed to the partial use of the applied current for the anodic oxidation of chloride to chlorine (Cabeza et al., 2007; Urriaga et al., 2012).

Using the NaCl electrolyte turned into free chlorine and chlorate generation, as it is depicted in Fig. 2, although it is worth mentioning that perchlorate formation was not observed. Free chlorine did not have enough oxidative power to decompose perfluorinated compounds as shown in Fig. 1. These results contrast with previously reported BDD degradation of diazo dyes (Jalife-Jacobo et al., 2016) and naphthenic acids (Diban and Urriaga, 2018), where active chlorine species formed upon chloride oxidation significantly enhanced the kinetics of the organic compounds removal. Nevertheless, in accordance to the results of the present study, Schaefer et al. (2017) proved that chloride had a minimal

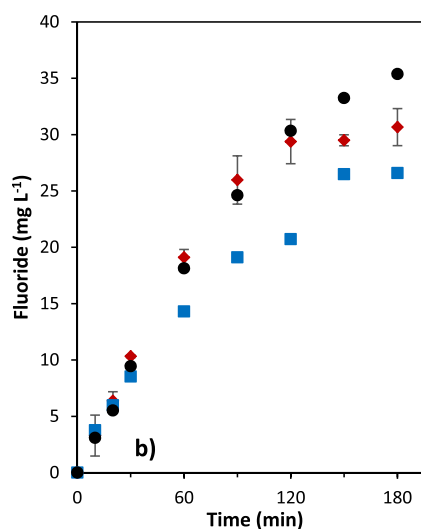
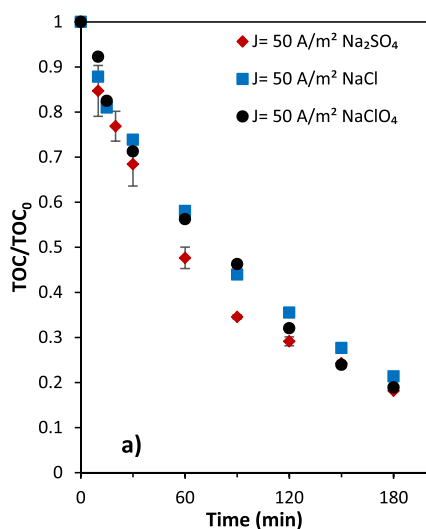


Fig. 1. Effect of electrolyte on 6:2 FTSA mineralization and defluorination. Fractional TOC (a) and fluoride release (b). Initial concentrations $[\text{6:2 FTSA}]_0 = 100 \text{ mg L}^{-1}$, $[\text{TOC}]_0 = 22.5 \text{ mg L}^{-1}$, $J = 50 \text{ A m}^{-2}$.

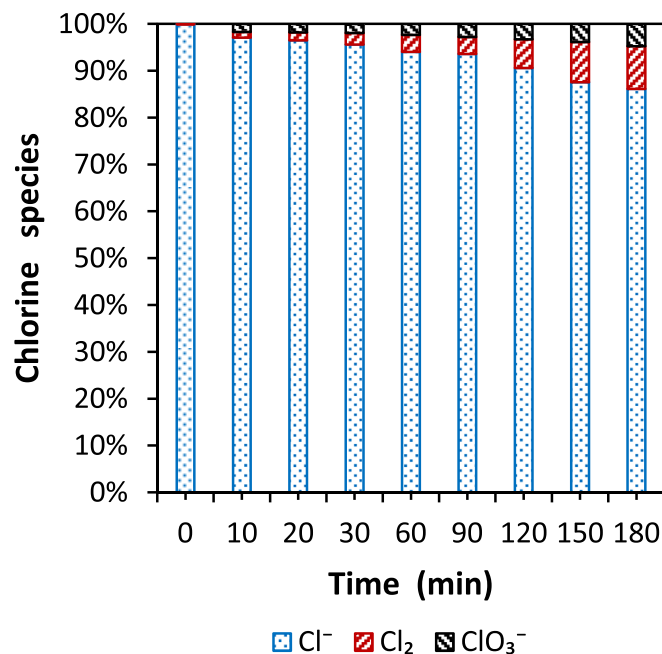


Fig. 2. Distribution (mol%) of inorganic chlorine species during the BDD electrochemical treatment of 6:2 FTSA, when using NaCl as electrolyte. $[\text{NaCl}] = 3.5 \text{ g L}^{-1}$, $[\text{6:2 FTSA}]_0 = 100 \text{ mg L}^{-1}$, $J = 50 \text{ A m}^{-2}$. Total chlorine was maintained constant along the experimental time.

effect on BDD electrochemical removal of perfluorooctanoic acid and perfluorooctane sulfonic acid, showing that the electro-generated active chlorine does not degrade perfluorinated compounds. Perchlorate formation by BDD anodic oxidation has been largely reported for sodium chloride electrolytes (Bergmann et al., 2009; Azizi et al., 2011; Urriaga et al., 2014), although perchlorate generation is also known to be delayed at high chloride concentrations (Perez et al., 2012) and low applied current densities (Pipi et al., 2014; Gomez-Ruiz et al., 2017a). The low current density ($J = 50 \text{ A m}^{-2}$) applied in the experiments of Fig. 1 explains the low chlorate development and the absence of perchlorate generation.

Sulfate release could be also observed in experiments

performed using NaCl and NaClO₄ electrolytes. The C–S bond between the unfluorinated carbon of the alkyl chain and the sulfonic end group (–CH₂–SO₃⁻) makes 6:2 FTSA easily susceptible to oxidation. Results pointed to the total release of the sulfate group contained in the 6:2 FTSA molecule, although the quantitation was adversely affected by the large sample dilution that was needed in order to avoid the saturation of the conductivity detector in the ion chromatography system. For example, using NaCl as electrolyte, the electrochemical treatment of 6:2 FTSA (100 mg L⁻¹, $J = 50 \text{ A m}^{-2}$) gave rise to 24 mg L⁻¹ of sulfate in the treated water, that is equivalent to the total amount of oxidized sulfur contained in the initial feed.

The effect of the applied current density on 6:2 FTSA treatment is shown in Fig. 3 and Fig. 4. Both TOC removal and fluoride release became progressively faster when increasing the applied current in the range 5–600 A m⁻². TOC removals at the low J range, 5–20 A m⁻², followed zeroth-order trends, although a remarkable enhancement of the TOC removal rate was observed when increasing the applied current in that range. Both features point to a current control regime of the removal kinetics in the low J range. In contrast, increasing the applied current to 50–600 A m⁻² modified the apparent TOC removal kinetics to first-order, which is associated to a diffusion control kinetic regime. Moreover, increasing the applied current from 50 to 600 A m⁻² granted moderate improvements in the kinetic rates of TOC disappearance. It is worth mentioning that the effect of varying the applied current density had a stronger influence on the kinetics of fluoride release (Fig. 3c).

This behavior could be indicating a beneficial effect of the applied current on the removal of the secondary products, perfluorocarboxylic acids, that were obtained upon degradation of 6:2 FTSA, as it will be discussed later on. In terms of energy consumption, the plot (Fig. 3b) of TOC removal vs. the specific charge passed ($Q, \text{ A h L}^{-1}$) indicates that the optimal range of applied current for the BDD electrochemical treatment of 100 mg L⁻¹ 6:2 FTSA solutions is between 20 and 100 A m⁻²; the upper value would imply a moderately higher energy consumption, but with the advantage of reducing the treatment time.

Fig. 4 shows the progress of 6:2 FTSA during BDD electro-oxidation at J values from 20 to 600 A m⁻². Three distinct zones can be distinguished. Increasing the applied current from 20 to 50 A m⁻² produced an increase in the kinetics of 6:2 FTSA degradation, although further increase of J to 100 A m⁻² did not provide any further improvement. Distinctively, increasing the applied current to 350 and 600 A m⁻² had a remarkable positive effect on the kinetics of 6:2 FTSA removal, a behavior that can be assigned to the oxidative action of electrogenerated secondary oxidants as a result of sulfate oxidation and reduction reactions to form sulfate radicals (SO₄^{-•}) and peroxodisulfate (S₂O₈⁴⁻), respectively (Davis et al., 2014; Sopaj et al., 2015).

Perfluorocarboxylic acids that were obtained as degradation products of 6:2 FTSA are plotted in Fig. 5 (for conciseness, only data obtained at 20, 100 and 600 A m⁻² are displayed). At any J , PFHxA was the product observed at a highest concentration (PFHxA values should be read in the right hand side Y-axis). The maximum PFHxA

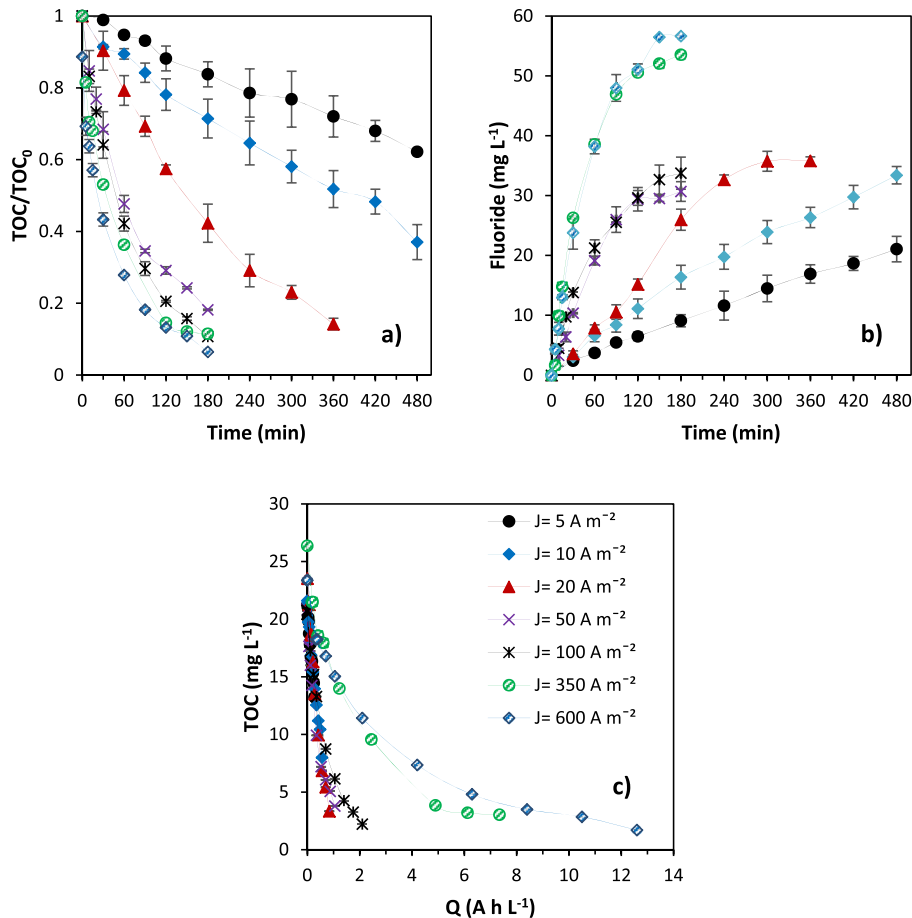


Fig. 3. Effect of the applied current on the removal of fractional TOC with time (a), Fluoride release (b), and TOC reduction as a function of the specific charge passed Q (c). [6:2 FTSA]₀ = 100 mg L⁻¹, [TOC]₀ = 22.5 mg L⁻¹.

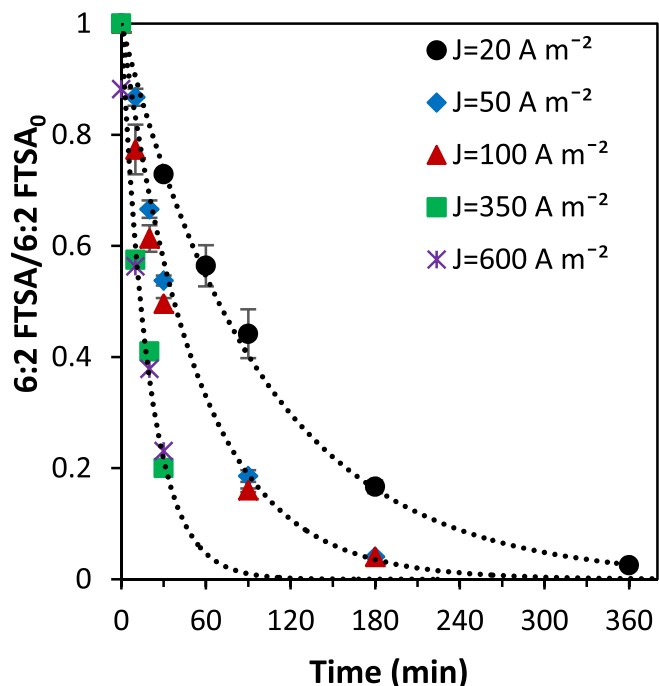


Fig. 4. Effect of applied current density on fractional 6:2 FTSA removal. $[6:2 \text{ FTSA}]_0 = 100 \text{ mg L}^{-1}$. Dotted lines are 1st-order exponential fittings of experimental data.

concentration was observed at earlier treatment times as the applied current was increased. Other PFCAs (PFHpA, PFPeA and PFBA) were observed at lower concentrations than PFHxA, typically below 1 mg L^{-1} , and their content was clearly reduced as the applied current density was increased. PFCAs smaller than PFBA are volatile compounds and cannot be determined in the liquid samples. Remarkably, the formation of PFHpA is observed at much lower concentration than PFHxA, in good agreement with the observations reported by Park et al. (2016) for heat activated persulfate oxidation of 6:2 FTSA. These results can be explained by the preferential attack of hydroxyl radicals to the $-\text{CH}_2-$ group attached to the perfluoroalkyl chain. Shorter chain PFPeA and PFBA are formed upon the loss of successive CF_2 units in consecutive steps (Gomez-Ruiz et al., 2017b; Schaefer et al., 2017). The results of analyzed PFASs also explains the faster kinetics of 6:2 FTSA disappearance compared to the TOC removal rate, related to the extra energy needed for the degradation of PFCAs obtained as secondary products.

The kinetics of the removal of perfluorocarboxylic acids PFHpA, PFHxA, PFPeA were further explored. In a trial to facilitate the observation of the oxidation by products, and also to avoid the conditions needed for the formation secondary oxidants, the applied current was intentionally maintained at a low value, $J = 20 \text{ A m}^{-2}$. Experiments were performed starting with solutions of one single PFCA: PFHpA, PFHxA or PFPeA, with an initial concentration of 100 mg L^{-1} in every case. 6:2 FTSA removal is included for comparison. Concentration data in Fig. 6 show that the kinetic removal was only slightly faster as the molecular size was

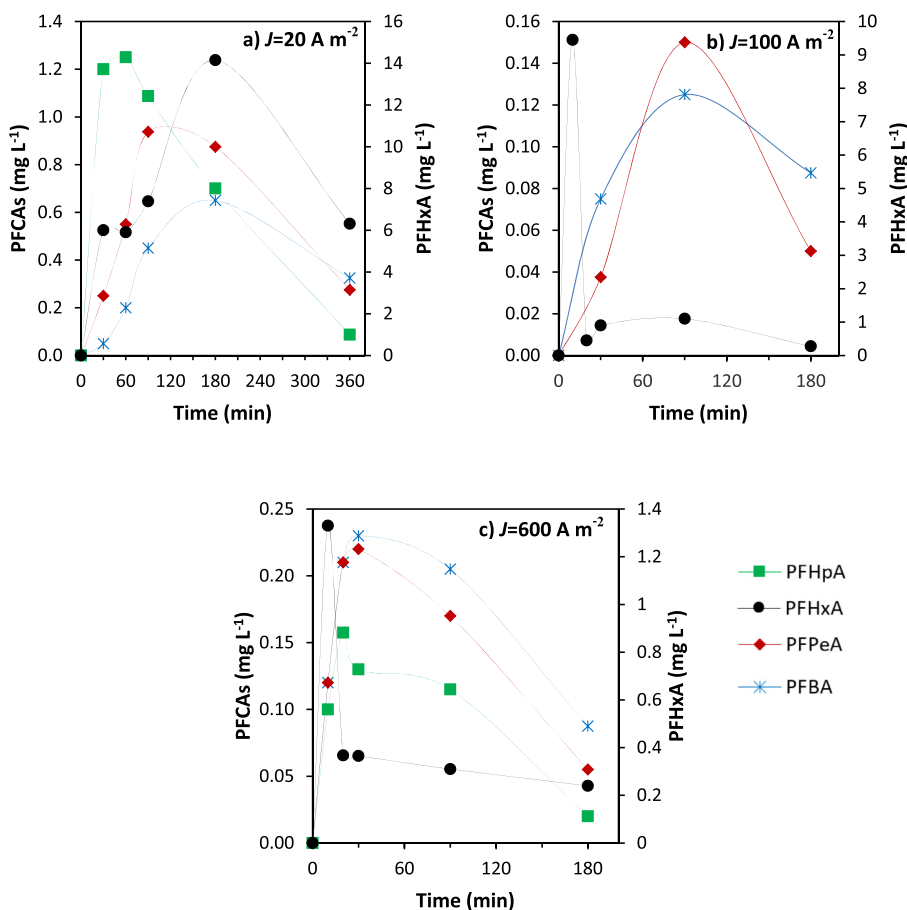


Fig. 5. Short chain perfluorocarboxylic acids (PFHpA, PFHxA, PFPeA and PFBA) obtained as secondary products of 6:2 FTSA BDD electrooxidation. (a) $J = 20 \text{ A m}^{-2}$; (b) $J = 100 \text{ A m}^{-2}$; (c) $J = 600 \text{ A m}^{-2}$. $[6:2 \text{ FTSA}]_0 = 100 \text{ mg L}^{-1}$.

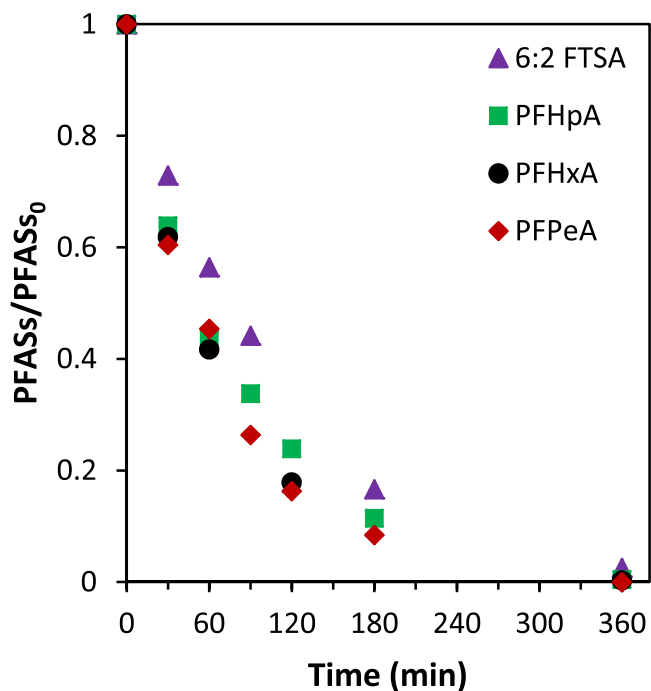


Fig. 6. Removal of different PFASs. Initial concentration 100 mg L^{-1} for every perfluoroalkyl substance. $J = 20 \text{ Am}^{-2}$.

decreasing. These results can be explained by the diffusion control kinetic regime, that is moderately faster as the molecular size of the PFASs compound is reduced. It means that the degradation reaction occurring at the electrode is faster than the diffusion of the compounds moving from the liquid bulk towards the electrode vicinity. The high fast reactivity of the hydroxyl radical mediated oxidizing reactions and the direct electron transfer at the anode surface prevent the intermediate compounds of diffusing from the proximity of the anode towards the liquid bulk, and therefore, the observed concentrations of degradation products are always much lower than those predicted from the apparent kinetic constants obtained in individual experiments.

4. Conclusions

The electrochemical treatment of 6:2 FTSA by means of microcrystalline boron doped diamond electrodes has been studied. Results herein presented demonstrated that 6:2 FTSA is electrochemically degraded, with removal rates that approach 100%. 6:2 FTSA was transformed into perfluorohexanoic acid (PFHxA) and perfluoroheptanoic acid (PFHpA), although PFHxA appeared at a much higher proportion than PFHpA. Effective mineralization was obtained, as demonstrated by the high TOC and defluorination rates achieved (>90%). The overall kinetics of 6:2 FTSA removal was controlled by the diffusion in the liquid phase in the low range of applied current density. However, increasing the applied current density resulted in faster removal rates, that were assigned to the role of strong electrogenerated oxidants from sulfate electrolyte. At any current density conditions, minority detection of perfluorocarboxylic acids in the liquid bulk was observed, showing that the secondary products were retained in the proximity of the anode surface to be rapidly degraded. Overall, this results poses BDD electrochemical treatment as effective technology for the treatment of 6:2 FTSA, used nowadays as substitute on perfluorooctane sulfonate (PFOS) in metal plating and fluorotelomer manufacture.

Acknowledgements

Support from MINECO and SPAIN-FEDER 2014–2020 to project CTM 2016-75509-R and to the Spanish Excellence Network E3TECH (CTQ 2015-71650-RDT) is acknowledged. J. Carrillo-Abad thanks the Generalitat Valenciana for granting a post-doctoral fellowship (APOSTD/2015/019). The authors are thankful to Dr. R. Buck (Chemours Co.) for kindly providing samples of Capstone FS10.

References

- APHA (American Public Health Association), 1998. Standard Methods for the Examination of Water and Wastewater, twentieth ed. Washington DC.
- Azizi, O., Hubler, D., Schrader, G., Farrell, J., Chaplin, B.P., 2011. Mechanism of perchlorate formation on boron-doped diamond film anodes. *Environ. Sci. Technol.* 45, 10582–10590.
- Bergmann, M.E.H., Rollin, J., Iourtchouk, T., 2009. The occurrence of perchlorate during drinking water electrolysis using BDD anodes. *Electrochim. Acta* 54, 2102–2107.
- Brunn-Poulsen, K., Gram, L.K., Jensen, A., Alsted-Rasmussen, A., Ravn, C., Moller, P., Jørgensen, C., Løkkegaard, K., 2011. Substitution of PFOS for Use in Non-decorative Hard Chrome Plating. Danish Ministry of Environment. Environmental Protection Agency. Environmental Project No. 1371 2011 Miljøprojekt. <https://www2.mst.dk/udgiv/publications/2011/06/978-87-92779-10-6.pdf>.
- Cabeza, A., Urtiaga, A.M., Ortiz, I., 2007. Electrochemical treatment of landfill leachates using a boron-doped diamond anode. *Ind. Eng. Chem. Res.* 46, 1439–1446.
- Chaplin, B.P., Wyle, I., Zeng, H., Carlisle, J.A., Farrell, J., 2011. Characterization of the performance and failure mechanisms of boron-doped ultrananocrystalline diamond electrodes. *J. Appl. Electrochem.* 41, 1329–1340.
- Cheremisinoff, N.P., 2017. Perfluorinated Chemicals (PFCs): Contaminants of Concern. Scivermer Publishing - Wiley & Sons, Hoboken.
- Davis, J., Baygents, J.C., Farrell, J., 2014. Understanding persulfate production at boron doped diamond film anodes. *Electrochim. Acta* 150, 68–74.
- Diban, N., Urtiaga, A., 2018. Electrochemical mineralization and detoxification of naphthenic acids on boron-doped diamond anodes. *Environ. Sci. Pollut. Res.* <https://doi.org/10.1007/s11356-017-1124-6>.
- ECHA, 2014. Candidate List of Substances of Very High Concern for Authorisation [WWW Document]. <https://echa.europa.eu/candidate-list-table>.
- Fernandez, N.A., Rodriguez-Freire, L., Keswani, M., Sierra-Alvarez, R., 2016. Effect of chemical structure on the sonochemical degradation of perfluoroalkyl and polyfluoroalkyl substances (PFASs). *Environ. Sci. Water Res. Technol.* 2, 975–983.
- Gomez-Ruiz, B., Gómez-Lavín, S., Diban, N., Boiteux, V., Colin, A., Dauchy, X., Urtiaga, A., 2017a. Efficient electrochemical degradation of poly- and perfluoroalkyl substances (PFASs) from the effluents of an industrial wastewater treatment plant. *Chem. Eng. J.* 322, 196–204.
- Gomez-Ruiz, B., Gómez-Lavín, S., Diban, N., Boiteux, V., Colin, A., Dauchy, X., Urtiaga, A., 2017b. Boron doped diamond electrooxidation of 6:2 fluorotelomers and perfluorocarboxylic acids. Application to industrial wastewaters treatment. *J. Electroanal. Chem.* 798, 51–57.
- Hoke, R.A., Ferrell, B.D., Ryan, T., Sloman, T.L., Green, J.W., Nabb, D.L., Mingoia, R., Buck, R.C., Korzeniowski, S.H., 2015. Aquatic hazard, bioaccumulation and screening risk assessment for 6:2 fluorotelomer sulfonate. *Chemosphere* 128, 258–265.
- Jalife-Jacobo, H., Feria-Reyes, R., Serrano-Torres, O., Gutiérrez-Granados, S., Peralta-Hernández, J.M., 2016. Diazo dye Congo Red degradation using a boron-doped diamond anode: an experimental study on the effect of supporting electrolytes. *J. Hazard. Mat* 319, 78–83.
- Lan, Y., Coetsier, C., Causserand, C., Groenen Serrano, K., 2017. On the role of salts for the treatment of wastewaters containing pharmaceuticals by electrochemical oxidation using a boron doped diamond anode. *Electrochim. Acta* 231, 309–318.
- Martín de Vidales, M.J., Millán, M., Sáez, C., Pérez, J.F., Rodrigo, M.A., Cañizares, P., 2015. Conductive diamond electrochemical oxidation of caffeine-intensified biologically treated urban wastewater. *Chemosphere* 136, 281–288.
- Park, S., Lee, L.S., Medina, V.F., Zull, A., Waisner, S., 2016. Heat-activated persulfate oxidation of PFOA, 6:2 fluorotelomer sulfonate, and PFOS under conditions suitable for in-situ groundwater remediation. *Chemosphere* 145, 376–383.
- Pérez, G., Saiz, J., Ibañez, R., Urtiaga, A.M., Ortiz, I., 2012. Assessment of the formation of inorganic oxidation by-products during the electrocatalytic treatment of ammonium from landfill leachates. *Water Res.* 46, 2579–2590.
- Pipi, A.R.F., Sirés, I., De Andrade, A.R., Brillas, E., 2014. Application of electrochemical advanced oxidation processes to the mineralization of the herbicide diuron. *Chemosphere* 109, 49–55.
- Schaefer, C.E., Andaya, C., Burant, A., Condee, C.W., Urtiaga, A., Strathmann, T.J., Higgins, C.P., 2017. Electrochemical treatment of perfluorooctanoic acid and perfluorooctane sulfonate: insights into mechanisms and application to groundwater treatment. *Chem. Eng. J.* 317, 424–432.
- Sopaj, F., Rodrigo, M.A., Oturan, N., Podvorica, F.I., Pinson, J., Oturan, M.A., 2015. Influence of the anode materials on the electrochemical oxidation efficiency. Application to oxidative degradation of the pharmaceutical amoxicillin. *Chem.*

- Eng. J. 262, 286–294.
- Soriano, A., Gorri, D., Urtiaga, A., 2017. Efficient treatment of perfluorohexanoic acid by nanofiltration followed by electrochemical degradation of the NF concentrate. *Water Res.* 112, 147–156.
- Stockholm Convention Secretariat, 2009. Decision SC-4/17: Listing of Perfluorooctane Sulfonic Acid, its Salts and Perfluorooctane Sulfonyl Fluoride.
- Uranga-Flores, A., Rosa-Júarez, C., Gutierrez-Granados, S., Chianca de Moura, D., Martínez-Huitile, C.A., Peralta Hernández, J.M., 2015. Electrochemical promotion of strong oxidants to degrade Acid red 211: effect of supporting electrolytes. *J. Electroanal. Chem.* 735, 84–91.
- Urtiaga, A., Ortiz, I., Anglada, A., Mantzavinos, D., Diamadopoulos, E., 2012. Kinetic modeling of the electrochemical removal of ammonium and COD from landfill leachates. *J. Appl. Electrochem.* 42, 779–786.
- Urtiaga, A., Fernández-Castro, P., Gómez, P., Ortiz, I., 2014. Remediation of wastewaters containing tetrahydrofuran. Study of the electrochemical mineralization on BDD electrodes. *Chem. Eng. J.* 239.
- Urtiaga, A., Fernández-González, C., Gómez-Lavín, S., Ortiz, I., 2015. Kinetics of the electrochemical mineralization of perfluorooctanoic acid on ultrananocrystalline boron doped conductive diamond electrodes. *Chemosphere* 129, 20–26.
- USEPA, 2015. Fact Sheet: 2010/2015 PFOA Stewardship Program [WWW Document]. URL <https://www.epa.gov/assessing-and-managing-chemicals-under-tsca/fact-sheet-20102015-pfoa-stewardship-program#meet>.
- Valsecchi, S., Conti, D., Crebelli, R., Polesello, S., Rusconi, M., Mazzoni, M., Preziosi, E., Carere, M., Lucentini, L., Ferretti, E., Balzamo, S., Simeone, M.G., Aste, F., 2017. Deriving environmental quality standards for perfluorooctanoic acid (PFOA) and related short chain perfluorinated alkyl acids. *J. Hazard Mater.* 323, 84–98.
- Wang, N., Liu, J., Buck, R.C., Korzeniowski, S.H., Wolstenholme, B.W., Folsom, P.W., Sulecki, L.M., 2011. 6:2 Fluorotelomer sulfonate aerobic biotransformation in activated sludge of waste water treatment plants. *Chemosphere* 82, 853–858.
- Wang, Z., Cousins, I.T., Scheringer, M., Hungerbühler, K., 2013. Fluorinated alternatives to long-chain perfluoroalkyl carboxylic acids (PFCAs), perfluoroalkane sulfonic acids (PFASs) and their potential precursors. *Environ. Int.* 60, 242–248.
- Yang, X., Huang, J., Zhang, K., Yu, G., Deng, S., Wang, B., 2014. Stability of 6:2 fluorotelomer sulfonate in advanced oxidation processes: degradation kinetics and pathway. *Environ. Sci. Pollut. Res.* 21, 4634–4642.
- Zhuo, Q., Li, X., Yan, F., Yang, B., Deng, S., Huang, J., Yu, G., 2014. Electrochemical oxidation of 1H,1H,2H,2H-perfluorooctane sulfonic acid (6:2 FTS) on DSA electrode: operating parameters and mechanism. *J. Environ. Sci.* 26, 1733–173.

5.3. Scientific publication #3.

Membrane preconcentration as an efficient tool to reduce the energy consumption of perfluorohexanoic acid electrochemical treatment

Authors:

Álvaro Soriano, Daniel Gorri, Ane Urriaga

Department of Chemical and Biomolecular Engineering. University of Cantabria. Av. de Los Castros 46. 39005 Santander. Spain

Accepted 23 March 2018

Separation & Purification Technology

Volume 208 (2019), Pages 160-168

DOI: 10.1016/j.seppur.2018.03.050



Membrane preconcentration as an efficient tool to reduce the energy consumption of perfluorohexanoic acid electrochemical treatment

Álvaro Soriano, Daniel Gorri, Ane Urtiaga*

Department of Chemical and Biomolecular Engineering, University of Cantabria, Av. de Los Castros s/n, 39005 Santander, Spain



ARTICLE INFO

Keywords:

BDD electrolysis
Energy minimization
Nanofiltration
Process integration
Perfluorohexanoic acid

ABSTRACT

One of the key points for the large-scale implementation of electrochemical water treatment technologies lies in the need of reducing the energy consumption. The present work analyzes the removal of persistent perfluorohexanoic acid (PFHxA, 204 mg L^{-1}) from industrial process waters using a strategy that combines membrane pre-concentration followed by electrooxidation of the concentrate. A mathematical model describing the nanofiltration (NF) system was developed and complemented with new and background experimental data of PFHxA and ion species rejections and total permeate flux through the NF270 and NF90 membranes. Similarly, the kinetics of PFHxA electrolysis on boron doped diamond anodes was determined at laboratory scale. Later, the model was used to simulate the NF-ELOX integrated process, where a commercial spiral wound unit (membrane area 7.6 m^2) was implemented and the electrooxidation unit was scaled-up to pilot plant (anode area 1.05 m^2). The obtained energy savings depended on a combination of the target PFHxA removal ratio at the end of the treatment train, the separation performance of the commercial membrane and the reduction of the electrolyte ohmic resistance in the electrooxidation stage, that was attained as a result of the increase of salts content in the concentrate. Only the tight NF90 membrane allowed to achieve high (99%) PFHxA removal ratios in the integrated NF-ELOX process, and the specific energy consumption was estimated at 11.6 kWh m^{-3} , 59.2% less than when electrolysis alone was applied. Still, the electrolysis is the most energy demanding step, with 85.9% contribution to the total energy consumption. The strategy of combining membrane pre-concentration with electrochemical degradation could be extended to the treatment of other highly persistent organic compounds.

1. Introduction

Perfluoroalkyl substances (PFASs) are persistent organic pollutants that are recalcitrant to traditional water treatment technologies [1,2]. There is a growing concern about these substances due to their high bioaccumulation potential and their possible harmful effects on living beings [3,4]. Perfluorooctane sulfonate (PFOS) and its derivatives were classified as priority hazardous substances by the European water policy [5]. Recently, the European Regulation concerning Registration, Evaluation and Authorization of Chemicals (REACH), has fixed restrictions in the manufacturing for perfluorooctanoic acid (PFOA), its salts and PFOA-related substances [6]. The high concern about the persistence of PFASs have forced chemical manufacturers to substitute long-chain PFASs by their shorter-chain homologues [7]. Some alternatives, such as 6:2 fluorotelomer sulfonate (6:2 FTSA) and 6:2 fluorotelomer sulfonamide alkylbetaine (6:2 FTAB) are easily biodegradable, but their degradation products, among them perfluorohexanoic acid (PFHxA) being the most abundant, are still highly persistent [7,8].

Recently, electrochemical oxidation is gaining attention as an effective technology for the removal of PFASs [9–13]. However, so far the research is generally focused on degradation of PFOA and PFOS in model solutions, and the application of this technology to the treatment of PFASs in industrial effluents and real environmental matrixes is still at its beginning [11,13,14]. The main advantages of boron doped diamond (BDD) electrochemical oxidation (ELOX) for the abatement of persistent pollutants includes its high removal efficacy, mild temperature and pressure operation conditions, ease of scale-up and automation [15–20]. Among the disadvantages, the high energy consumption stands as major drawback that hinder the large scale implementation of electrochemical technologies for water treatment. [16,18,19,21–23].

In search of innovations to achieve the energy optimization of environmental electrochemistry, this study is focused on the integration of pre-concentration strategies. The concentrations of PFASs in environmental media are usually very low [3,24], that leads to mass-transfer controlled electrooxidation kinetics, thus constraining the efficiency of the electrochemical process [21]. Pre-concentration strategies such as

* Corresponding author.

E-mail address: urtiaga@unican.es (A. Urtiaga).

Nomenclature			
A	active membrane area (m^2)	Q_f	feed volumetric flow rate to NF module ($m^3 h^{-1}$)
A_e	total anode area (m^2)	Q_p	permeate volumetric flow rate ($m^3 h^{-1}$)
C_c	PFHxA concentration in the concentrate ($mg L^{-1}$)	Q_r	retentate volumetric flow rate ($m^3 h^{-1}$)
C_{ELOX}	concentration in the ELOX reactor ($mg L^{-1}$)	SEC_{ELOX}	ELOX specific energy consumption ($kWh m^{-3}$)
C_{eq}	equivalent ion concentration ($mol L^{-1}$)	SEC_{NF}	NF specific energy consumption ($kWh m^{-3}$)
$C_{i,ft}$	feed tank concentration ($mg L^{-1}$)	SEC_{total}	total specific energy consumption ($kWh m^{-3}$)
$C_{i,p}$	permeate stream concentration ($mg L^{-1}$)	T	temperature of the solution ($^{\circ}C$)
$C_{i,pt}$	permeate tank concentration ($mg L^{-1}$)	t_{ELOX}	ELOX operation time (h)
$C_{i,r}$	retentate stream concentration ($mg L^{-1}$)	t_{NF}	NF operation time (h)
C_{target}	PFHxA target concentration ($mg L^{-1}$)	U	ELOX cell voltage (V)
E_{ELOX}	ELOX energy consumption (kWh)	V_c	concentrate volume (m^3)
E_{NF}	NF energy consumption (kWh)	V_{ft}	feed tank volume (m^3)
I	ELOX cell current intensity (A)	V_{pt}	permeate tank volume (m^3)
J	current density ($A m^{-2}$)	VRF	volume reduction factor (–)
k	kinetic constant ($m min^{-1}$)	z_i	ionic valence (–)
L_p	membrane permeability ($L m^{-2} h^{-1} bar^{-1}$)	ΔP	effective pressure difference (bar)
m_i	molality of the species dissolved ($mol kg^{-1}$)	$\Delta \pi$	osmotic pressure difference (bar)
		π	osmotic pressure (bar)

electrocoagulation [25] and membrane separation [14,26,27] have been proposed to overcome this limitation. Membrane separation such as nanofiltration (NF) and reverse osmosis could play a key role optimizing the electrochemical treatment of persistent PFASs due to the facts that: (i) it allows increasing PFASs concentration in the retentate whilst at the same time the volume to be electrolyzed is drastically reduced. In this way, higher feed concentrations promote the kinetics of diffusion controlled electrooxidation; (ii) not only PFASs, but also the concentration of salts naturally present in the water matrix will be increased, therefore decreasing the internal ohmic resistance of the electrolyte, which will make lower the cell voltage [28]; and (iii) higher concentration of dissolved ion species promotes the electrogeneration of oxidant species participating in indirect oxidation routes [29]. For example, the production of highly oxidative sulfate radical could contribute to the decomposition of PFCAs [30]. The first experimental attempt to integrate membrane separation and BDD electrolysis for PFHxA removal from industrial process waters showed that the energy consumption was reduced to $15.2 kWh m^{-3}$ for a 90% PFHxA removal ratio [14], a value that is significantly lower than energy requirements previously reported for PFASs electrochemical treatment, in the range $41.7\text{--}76.6 kWh m^{-3}$ [31]. The efficient PFHxA mineralization was confirmed by the high reduction ($> 95\%$) of the total organic carbon (TOC). The selected nanofiltration membrane, the NF270 from Dow/Filmtec, was characterized by its very high productivity and its medium to high salt passage but the PFHxA retention might be insufficient when higher PFHxA removal ratios at the exit of the treatment train are required. Tighter NF or RO membranes could be useful to achieve this goal, usually at the expense of lower permeate fluxes. Also, our previous

experimental work did not carry out any comprehensive assessment of the true impact of different membrane pre-concentration ratios on the energy consumption of the integrated process and on the contribution of each individual process on the overall energy demand. In this way, the modelling tools presented herein could help to quantitative select the appropriate operation variables thus providing knowledge that allows to move towards the definition of an optimized integrated process.

The aim of this study was to develop a methodology for the optimal integration of membrane separation and electrochemical oxidation for the treatment of waters impacted by persistent organic pollutants, with the objective of minimizing the energy consumption of the integrated NF-ELOX process. As a case of study, the removal and degradation of PFHxA will be analyzed. A global scheme of the proposed strategy is shown in Fig. 1. A mathematical model describing the membrane separation and the ELOX processes enabled the simulation of both technologies at pilot scale. Commercial spiral wound membrane modules and a battery of serial-parallel electrochemical cells were implemented in the simulations. The contribution of the two technologies to the total energy consumption was also analyzed.

2. Methods

2.1. Chemicals and materials

All chemicals were analytical grade. Perfluorohexanoic acid ($\geq 97\%$) was purchased from Sigma-Aldrich. Sodium chloride ($\geq 99\%$), sodium hydroxide solution (1 N) and hydrochloric acid solution (1 N) were purchased from Panreac. Calcium sulphate dihydrate ($\geq 98\%$) and

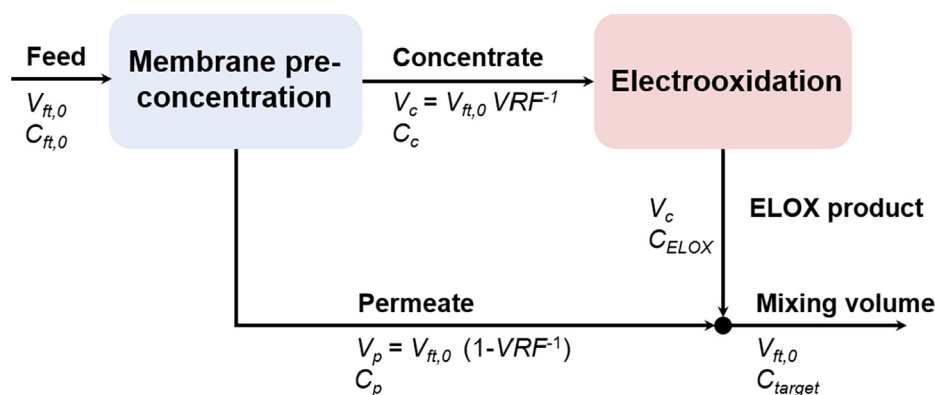


Fig. 1. Global scheme of the proposed NF-ELOX process.

Table 1
Feed water characteristics.

PFHxA	204 mg L ⁻¹
SO ₄ ²⁻	321 mg L ⁻¹
Cl ⁻	19.8 mg L ⁻¹
Ca ²⁺	172 mg L ⁻¹
Na ⁺	24.9 mg L ⁻¹

methanol, UHPLC-MS (≥99.9%) were purchased from Scharlau. All solutions were prepared using ultrapure water (Milli-Q, Millipore).

Model solutions were prepared emulating real process waters previously studied [14], which were process streams in an industrial manufacturing process. The main process water characteristics are summarized in Table 1.

2.2. Analytical methods

An ultra-performance liquid chromatography (UPLC) system (Acquity H-Class, Waters) coupled with a triple quadrupole mass spectrometer (Acquity TDQ detector, Waters) and a column Acquity UPLC BEH C18 (1.7 μm, 2.1 × 50 mm) were used for the analysis of PFHxA at experiments carried out for the characterization of the NF90 membrane. A 2 mM ammonium acetate and 5% methanol aqueous solution and pure methanol were used as mobile phases at a flow rate of 0.15 mL min⁻¹.

2.3. Background data

Previous NF experiments at laboratory-scale treating real industrial process streams [14] provided information about NF270 (Dow Filmtec) membrane permeability, rejections of PFHxA and ions in solution, as well as empirical correlations between PFHxA and ions concentrations in the retentate ($C_{r,i}$) and permeate ($C_{p,i}$) streams. The kinetic constant for the electrochemical degradation of PFHxA by means of BDD anodes at a working current density (J) of 50 A m⁻² was also obtained ($k = 2.1 \times 10^{-3} \text{ m min}^{-1}$).

In the present study, further experiments were conducted to characterize the tighter NF90 membrane (Dow Filmtec) using model

solutions emulating the process waters described in Table 1. PFHxA concentration was varied in the range 100–500 mg L⁻¹. Solutions were adjusted to neutral pH by adding sodium hydroxide 0.1 M and hydrochloric acid 0.1 M. Experiments were carried out in a laboratory membrane cross-flow test cell (SEPA-CF, GE Osmonics). Membrane coupons were cut with an effective membrane area of 155 cm². Feed solution was maintained at 20 °C and the operating pressure was varied from 2.5 bar to 20 bar.

2.4. System definition

A global scheme of the integrated process is sketched in Fig. 2. The technologies were simulated in batch mode. In the NF set-up, the retentate stream was recycled to the feed tank while the permeate stream was collected in the permeate tank, both open to the atmosphere. In this way, the concentration of PFHxA in the feed increased over time, whilst the feed volume decreased during the filtration run. Two commercial spiral-wound membrane modules (NF270-4040 and NF90-4040) were simulated and compared.

The composition of the resulting concentrate was considered as the feed properties in the ELOX simulation. For the ELOX simulations, the characteristics of an existing ELOX pilot plant previously used by our research group [18,32] were considered. The pilot plant is composed of a battery of serial-parallel electrochemical cells with a total BDD anode surface of 1.05 m², each one with similar characteristics to the cell used in the laboratory experiments. The current density was set at 50 A m⁻² since it had been previously determined to optimally degrade PFHxA from NF concentrates [14]. Table 2 collects information about the main characteristics and operating conditions considered for the simulation of both processes.

2.5. Process modelling

All streams are assumed to be dilute solutions with constant density. The change in the volume of the feed and permeate tanks and the mass balances for the PFHxA solute, assuming perfect mixing, are written as follows,

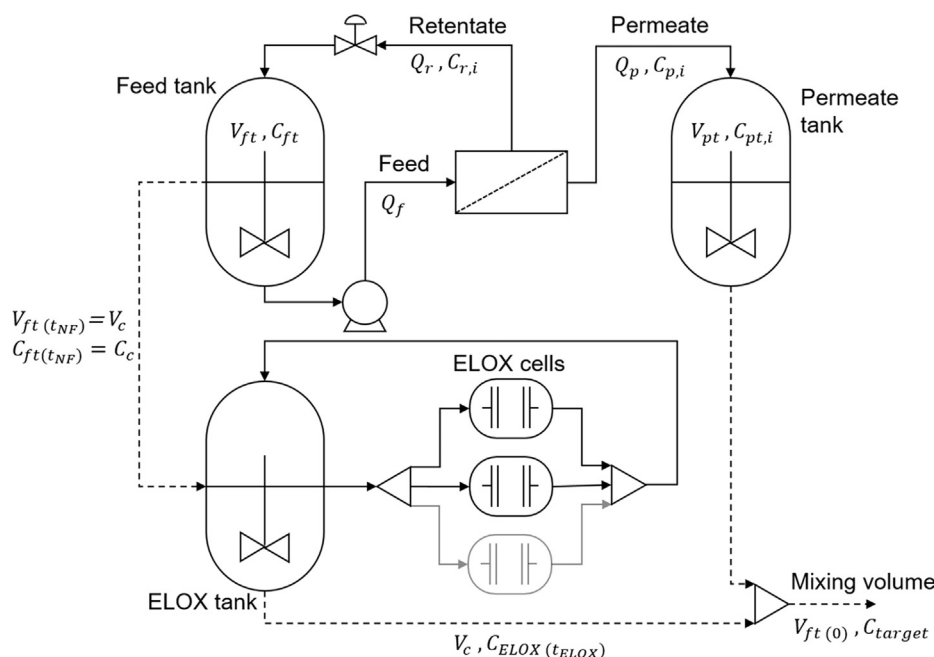


Fig. 2. Global scheme of the NF-ELOX integrated process. NF set-up with the commercial membrane module and ELOX of the NF concentrate using serial-parallel cells.

Table 2
Operating conditions and main characteristics of the system considered for the simulations.

<i>Nanofiltration pilot plant</i>	
Membrane area	7.6 m ²
Operating temperature	20 °C
Operating feed pressure	10 bar
Feed flow rate	3.6 m ³ h ⁻¹
Initial feed tank volume	5 m ³
<i>Electrooxidation pilot plant</i>	
Total anode surface	1.05 m ²
Current density	50 A m ⁻²

$$\frac{dV_{ft}}{dt} = Q_r - Q_f \quad (1)$$

$$\frac{dV_{pt}}{dt} = Q_p \quad (2)$$

$$\frac{d(V_{ft} C_{ft,i})}{dt} = Q_r C_{r,i} - Q_f C_{ft,i} \quad (3)$$

$$\frac{d(V_{pt} C_{pt,i})}{dt} = Q_p C_{p,i} \quad (4)$$

Additionally, mass balances in the membrane module are defined as follows,

$$Q_f = Q_p + Q_r \quad (5)$$

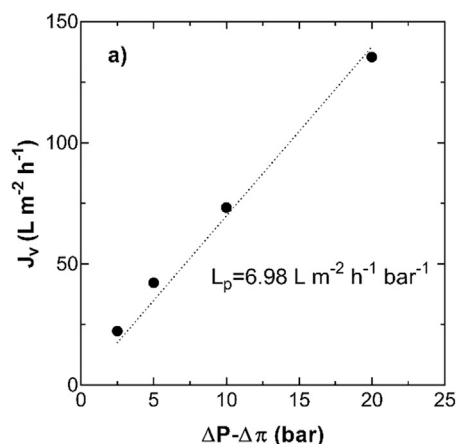
$$Q_f C_{ft,i} = Q_p C_{p,i} + Q_r C_{r,i} \quad (6)$$

To solve the system of Eqs. (1)–(6) and predict the transport of solute and solvent across the membrane could require the use of rigorous transport models such as the Nernst-Planck equation [33] or empirical data. In this work we have used empirical data from concentration-mode laboratory experiments. The permeate volumetric flow rate (Q_p) can be related to the pressure gradient across the membrane and the membrane area, according to the following modified version of the Darcy's law,

$$Q_p = 10^{-3} L_p A (\Delta P - \Delta \pi) \quad (7)$$

In Eq. (7), L_p symbolizes the membrane permeability to the feed process waters under study and was empirically obtained for each membrane. The osmotic pressure difference between the feed and permeate streams have been calculated from the concentration of the dissolved species, using Eq. (8) [34].

$$\pi = 1.19(T + 273) \sum m_i \quad (8)$$



Furthermore, the volume reduction factor (VRF) is defined as the ratio between the initial feed volume and the concentrate final volume, which in this case corresponds to the volume of the feed tank at the end of the experimental run. This is an important operational variable and will be used in this work to study the influence of the membrane pre-concentration on the behavior of the integrated NF-ELOX process.

$$VRF = \frac{V_{ft}}{V_c} \quad (9)$$

The following PFHxA mass balance in the ELOX tank is valid under the assumption of negligible residence time of the fluid in the electrochemical cell compared to its residence time in the recirculation tank,

$$\frac{dC_{ELOX}}{dt} = -k \left(\frac{A_e}{V_c} \right) C_{ELOX} \quad (10)$$

From Fig. 2, it must be noticed that the final volume obtained after the treatment train, which is the same as the initial feed volume (V_{ft}), is the result of mixing the final permeate volume from the nanofiltration step (V_{pt}) and the treated electrooxidation volume, which is the same as the final concentrate volume from NF (V_c), for a certain VRF . Therefore, the PFHxA mass balance at the mixing point is written as in Eq. (11).

$$V_{ft} C_{target} = V_c C_{ELOX} + V_{pt} C_{pt,PFHxA} \quad (11)$$

As VRF is used as operational variable, Eq. (11) can be rearranged for the calculation of the required PFHxA concentration and required electrolysis time in the ELOX treatment for meeting the target PFHxA concentration at the end of the treatment train under different VRF , after combining with Eq. (9),

$$C_{ELOX} = VRF [C_{target} - C_{pt,PFHxA} (1 - VRF^{-1})] \quad (12)$$

$$t_{ELOX} = \frac{\ln(C_{ELOX}/C_c) V_{ft}}{-k A_e VRF 60} \quad (13)$$

where 60 is a unit conversion factor (min h⁻¹). A simplified first approach to the NF energy consumption can be done by considering it equal to the work performed by the pump when it operates the time needed to reach a VRF value,

$$E_{NF} = \frac{Q_f \Delta P t_{NF}}{36 \eta} \quad (14)$$

where η is the global pumping system efficiency, including the pump and the electric motor efficiency, assumed to be 80% [35]. In Eq. (14), number 36 is a unit conversion factor and has units of bar W s Pa⁻¹ kW⁻¹ h⁻¹. On the other hand, the ELOX energy consumption was calculated as follows,

$$E_{ELOX} = 10^{-3} U I t_{ELOX} \quad (15)$$

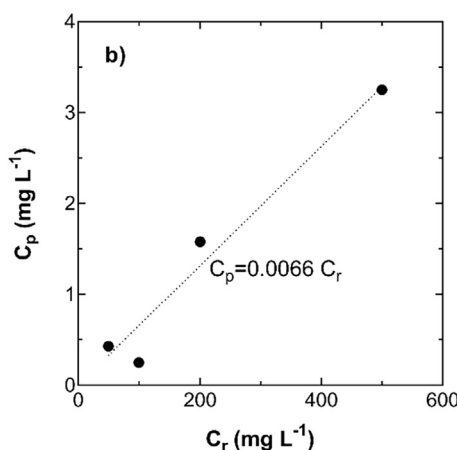


Fig. 3. (a) Volumetric permeate flux through the NF90 membrane. Membrane permeability (L_p) is obtained from the slope. Feed composition as in Table 1; (b) PFHxA concentration in the permeate vs. PFHxA in the retentate. $\Delta P = 10$ bar.

where 10^{-3} has units of kW W^{-1} . The specific energy consumption of the integrated process (SEC_{total}) is the result of the NF energy consumption plus the ELOX energy consumption, per m^3 treated, to treat the total inlet feed volume, which is the same as the outlet product volume. In this way, we also calculated the specific energy consumption of both individual processes (SEC_{NF} and SEC_{ELOX}) related the total product. All model equations were numerically solved using Scilab. The equations were solved using the following initial conditions; $V_{ft}(0) = 5 \text{ m}^3$; $V_{pt}(0) = 0 \text{ m}^3$; $C_{ft,PFHxA}(0) = 204 \text{ mg L}^{-1}$; $C_{ft,SO4^{2-}}(0) = 321 \text{ mg L}^{-1}$; $C_{ft,Ca^{2+}}(0) = 172 \text{ mg L}^{-1}$; $C_{ft,Na^+}(0) = 24.9 \text{ mg L}^{-1}$; $C_{ft,Cl^-}(0) = 19.8 \text{ mg L}^{-1}$; $C_{i,pt}(0) = 0 \text{ mg L}^{-1}$; $C_{ELOX}(0) = C_c$.

3. Results and discussion

3.1. Experimental systems characterization

In the present study, further experiments were conducted to characterize the tighter NF90 membrane (Dow Filmtec). Fig. 3a shows total permeate flux data as a function of the effective pressure gradient obtained for the NF90 membrane, using the feed process waters described in Table 1. The NF90 hydraulic permeability (L_p) was obtained from the slope of the linear regression. Fig. 3b provides the empirical correlation between the PFHxA concentrations in permeate and retentate streams at a fixed operating pressure of 10 bar, in experiments varying the feed concentration of PFHxA. In the same way, similar correlations were obtained for calcium, sulfate, chloride and sodium ions, all summarized in Table 3. For the NF90 membrane, these correlation equations correspond to the following average rejection factors [36]: $R_{PFHxA} = 99.4\%$, $R_{SO4} = 98.8 \pm 0.13\%$, $R_{Ca^{2+}} = 99.1 \pm 0.18\%$, $R_{Na^+} = 98.5 \pm 0.10\%$, $R_{Cl^-} = 93.6 \pm 0.67\%$. In the same way, for the NF270 the average rejection factors of all species are: $R_{PFHxA} = 95.7 \pm 0.01\%$, $R_{SO4} = 96.1 \pm 0.01\%$, $R_{Ca^{2+}} = 88.5 \pm 0.01\%$, $R_{Na^+} = 67.9 \pm 0.01\%$, $R_{Cl^-} = 41.7 \pm 0.05\%$.

Additionally, electrochemical experiments were carried out in galvanostatic conditions at $J = 50 \text{ A m}^{-2}$ to characterize the effect of increasing the electrolyte concentration on the cell voltage. The cell (DiaCell 201 PP, Adamant Technologies) was powered by two parallel flow-by compartments made of a central bipolar p-Si/BDD electrode and p-Si/BDD anode and cathode. The total anodic area was 140 cm^2 . 1 L saline feed solutions were prepared with calcium sulphate and sodium chloride with composition within the range of salts concentrations observed in the retentates of membrane experiments. The equivalent

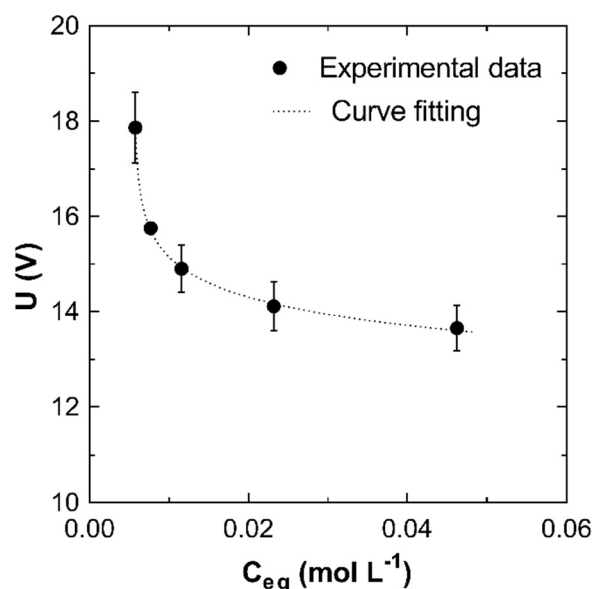


Fig. 4. Cell voltage as function of the electrolyte concentration (C_{eq}). A bipolar BDD DiaCell 201 PP was used in the experiments.

saline concentration (C_c) [33] was varied from $5.8 \times 10^{-2} \text{ mol L}^{-1}$ to $4.6 \times 10^{-2} \text{ mol L}^{-1}$. Fig. 4 shows how the cell voltage (U) can be moderately reduced as a result of the ohmic resistance decrease associated to the increase of the electrolyte concentration, although further reductions of the cell voltage are limited by the intrinsic resistances of the electrochemical cell. A good fit of the experimental data U vs. C_{eq} was obtained with a shifted power regression model, which was incorporated into the simulation runs (Table 3).

3.2. Membrane pre-concentration simulation

Fig. 5 shows the simulation of the NF system. Simulations were run until $VRF = 10$, considering an initial feed volume of 5 m^3 . As the feed volume V_{ft} keeps decreasing along the operation time, and as the NF270 and NF90 membranes are much more permeable to the solvent (water) than towards the solute (PFHxA), feed concentration C_{ft} and permeate tank concentration C_{pt} increases. The increase of salts concentration in the feed tank makes the osmotic pressure to increase too; as a result, the volumetric permeate flux Q_p decreases along the simulation run (Fig. 5e). With the NF270 membrane and at $VRF = 10$, PFHxA concentration in the feed tank increased from 204 mg L^{-1} to 1779 mg L^{-1} , after 6.7 h (Fig. 5a). On the other hand, when the NF90 membrane unit is simulated, the PFHxA concentration in the feed tank increased to 2014 mg L^{-1} at $VRF = 10$ after 9 h (Fig. 5b). Thus, when the NF90 membrane is used, more time is needed to achieve the same VRF , as a result of its lower permeability. Overall, this property will increase the energy consumption of the pre-concentration step, but with the benefit of getting much lower PFHxA concentrations in the permeate tank than when using the NF270 membrane. Fig. 5c and Fig. 5d show that at $VRF = 10$, the permeate tank PFHxA concentration with the NF90 membrane is 3.4 mg L^{-1} , while with the NF270 membrane its value is 30.7 mg L^{-1} . The higher PFHxA concentration that is achieved in the permeate tank by using the NF270 membrane could be a detrimental factor in attaining the essential energy minimization objective. Also, the operation up to long filtration times and high VRF could clog the membrane pores due to the progressively higher solutes concentration, thus decreasing the permeate flux in a greater way in a real large-scale process, forcing to include periodical cleaning procedures. Increasing chloride concentration in the concentrate volume could also facilitate the potential formation of chlorate in the subsequent BDD anodic oxidation treatment. Nevertheless, the process waters under study have a

Table 3

Empirical input data. NF270 and NF90 data determined at $\Delta P = 10 \text{ bar}$.

NF270 data	
Hydraulic permeability	$L_p = 9.40 \text{ L m}^{-2} \text{ h}^{-1} \text{ bar}^{-1}$
$C_{p,i}C_{r,i}$ correlation	$C_{p,PFHxA} = 5.1 \times 10^{-2} C_{r,PFHxA}$ $C_{p,SO4^{2-}} = 3.7 \times 10^{-2} C_{r,SO4^{2-}}$ $C_{p,Ca^{2+}} = 11.4 \times 10^{-2} C_{r,Ca^{2+}}$ $C_{p,Na^+} = 32.3 \times 10^{-2} C_{r,Na^+}$ $C_{p,Cl^-} = 1.3 \times 10^{-2} (C_{r,Cl^-})^2 - 5.2 \times 10^{-2} C_{r,Cl^-}$
NF90 data	
Hydraulic permeability	$L_p = 6.98 \text{ L m}^{-2} \text{ h}^{-1} \text{ bar}^{-1}$
$C_{p,i}C_{r,i}$ correlation	$C_{p,PFHxA} = 6.6 \times 10^{-3} C_{r,PFHxA}$ $C_{p,SO4^{2-}} = 4 \times 10^{-6} (C_{r,SO4^{2-}})^2 + 8.3 \times 10^{-3}$ $C_{r,SO4^{2-}}$ $C_{p,Ca^{2+}} = 5 \times 10^{-5} (C_{r,Ca^{2+}})^2 + 3.3 \times 10^{-3}$ $C_{r,Ca^{2+}}$ $C_{p,Na^+} = 2 \times 10^{-5} (C_{r,Na^+})^2 + 1.3 \times 10^{-2}$ C_{r,Na^+} $C_{p,Cl^-} = 6.1 \times 10^{-2} C_{r,Cl^-}$
Electrooxidation data	
$U - C_{eq}$ correlation	$U \text{ (V)} = 11.6 [C_{eq} \text{ (M)} - 5.8 \times 10^{-3}]^{-4.8 \times 10^{-2}}$
PFHxA degradation kinetic constant	$k = 2.1 \times 10^{-3} \text{ m min}^{-1}$ (for $J = 50 \text{ A m}^{-2}$)

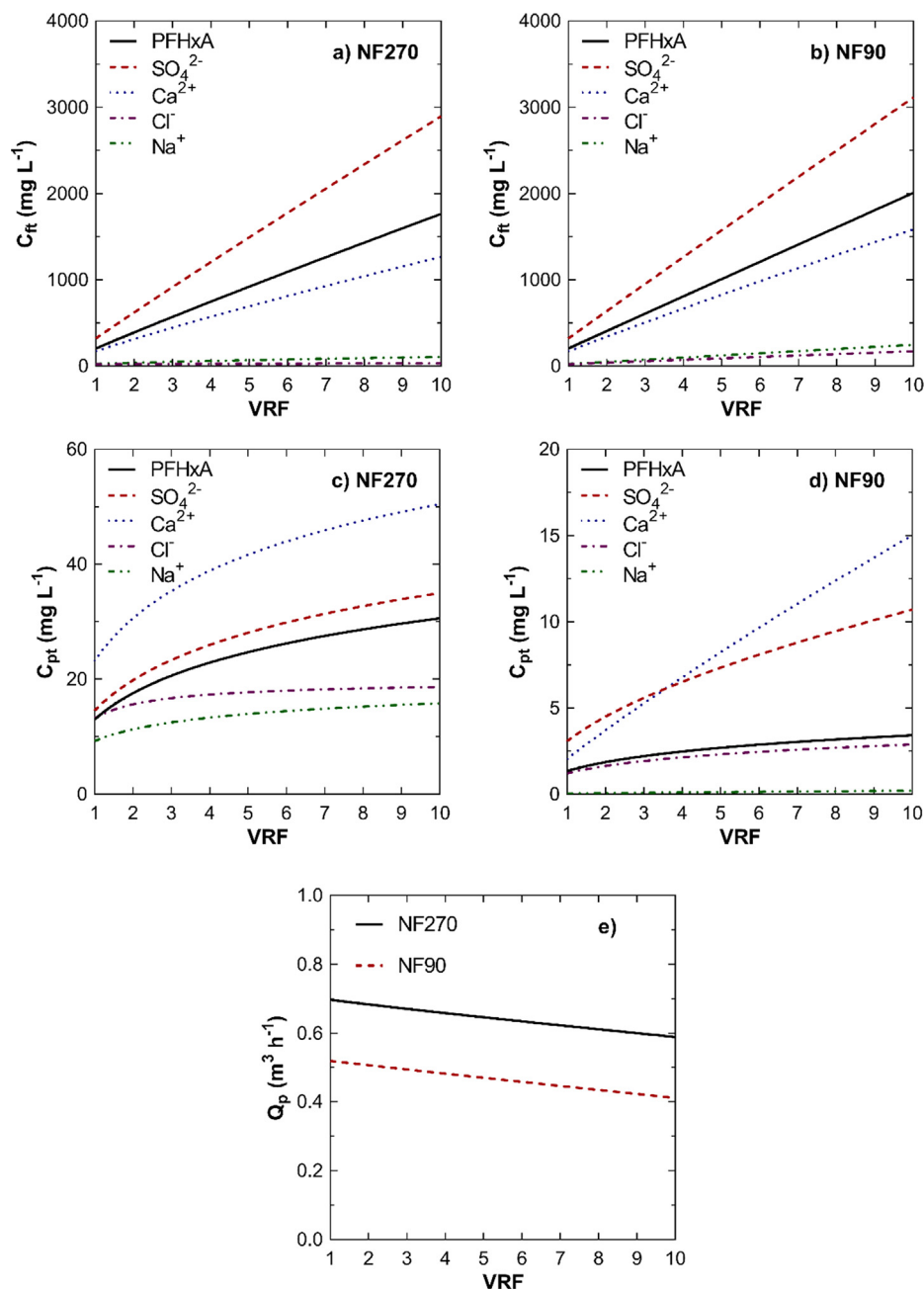


Fig. 5. Membrane pre-concentration simulations. PFHxA and ions concentration in the feed tank (a) and permeate tank (c) as a function of VRF with the NF270 membrane. PFHxA and ions concentration in the feed tank (b) and permeate tank (d) with the NF90 membrane. Permeate flux (e). Initial feed tank volume: 5 m^3 .

low chloride initial content (Table 1), being sulfate the major anion. On the other hand, nanofiltration membranes such as NF270 offer preferential retention of divalent anions (sulfate) over monovalent anions (chloride). As a result, Fig. 5 shows that chloride concentration in the retentate increased very little with the increase of VRF , also when working with the NF90 membrane. Additionally, the low current density ($J = 50 \text{ A m}^{-2}$) minimizes the potential chlorate formation in the electrolysis treatment [37].

3.3. Effect of the NF pre-concentration on the electrooxidation stage and global process behavior

Two different PFHxA target removal ratios (RR), $RR = 90\%$ and $RR = 99\%$, were considered for the simulation runs of the electrooxidation stage and of the integrated NF-ELOX process. Fig. 6 shows the

total energy consumption of the combined process per cubic meter of treated water as a function of the VRF parameter. $VRF = 1$ describes the situation in which no pre-concentration is carried out, i.e., ELOX is the only applied treatment. It is important to note that the maximum VRF value that is feasible to apply in the pre-concentration stage differs for the different scenarios under study. According to the PFHxA mass balance at the mixing point, Eq. (11), to meet a given C_{target} at the end of the treatment train, different C_{pt} and C_{ELOX} values are needed. With the increase of VRF (or analogously, with the increase of the nanofiltration pre-concentration operation time) the concentration in the permeate tank (C_{pt}) increases too, forcing the required C_{ELOX} at the exit of the electrooxidation stage to become lower, in order to meet C_{target} at the mixing point. Eventually C_{ELOX} will become equal to zero. At this point, VRF takes its maximum value.

For $RR = 90\%$, the use of ELOX alone consumes 14.3 kWh m^{-3} , while the combination of NF270-ELOX minimizes the energy needs at a

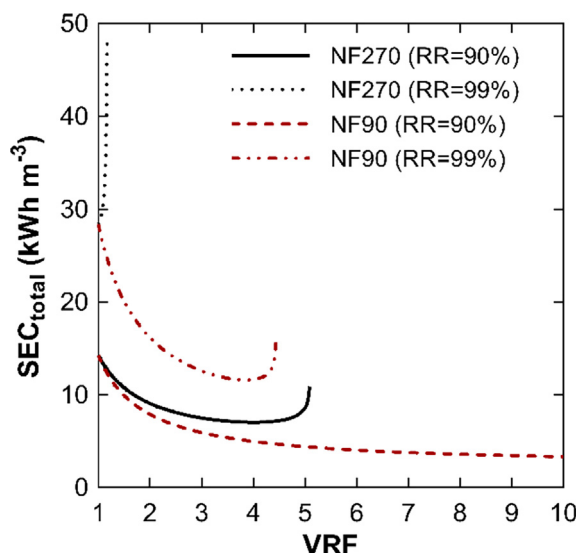


Fig. 6. Specific energy consumption of the integrated NF-ELOX process as function of *VRF* for different PFHxA removal ratios at the end of the treatment train (RR = 90% and RR = 99%). $V_{ft} = 5 \text{ m}^3$, $C_{f,0} = 204 \text{ mg L}^{-1}$.

$VRF = 4.0$, with a specific energy consumption of 7.0 kWh m^{-3} . Further energy savings can be obtained by using the NF90 membrane, that allows 90% PFHxA removal at a $VRF = 10$ with only 3.3 kWh m^{-3} . When the target RR is set at 99%, the appropriate selection of the membrane module appears to be more important. The integration with the NF270 does not bring any benefit in terms of energy reduction. In fact, the pre-concentration step only contributes to increase the total energy demands of the system. In contrast, significant energy savings can be obtained with the NF90–ELOX system. The energy consumption for the single electrooxidation system (28.4 kWh m^{-3}), is reduced to less than half (11.6 kWh m^{-3}) by the integrated system.

Then, the different PFHxA rejections of the NF90 and NF270 membranes are a key performance parameter for the design and optimization of the integrated NF-ELOX process. When a low target

concentration is demanded, the concentration in the membrane permeate stream needs to be low (Eq. (11)), and the NF90 membrane fulfills this need at a much higher extent than the NF270 membrane. In the RR = 99% scenario and due to the insufficient NF270 PFHxA rejection, the PFHxA concentration in the permeate tank (C_{pt}) at initial time (12.9 mg L^{-1}) is considerably higher than the objective C_{target} (2.0 mg L^{-1}) and keeps increasing with the increase of *VRF*. The required C_{ELOX} at the exit of the electrooxidation stage to meet the PFHxA mass balance is therefore progressively smaller as *VRF* gets higher. Thus, the ELOX energy requirements to treat the NF concentrate to such low C_{ELOX} values are very high and keeps increasing with the simulation run. Conversely, the NF90 allows to obtain much lower PFHxA concentration in the permeate tank due to its higher PFHxA retention. For this reason, the required C_{ELOX} to meet the C_{target} is much less demanding and the ELOX energy consumption is reduced. The local minimum of the energy-*VRF* curve gives information on the optimal *VRF* value that allows maximum energy savings. When the target removal ratio is not so demanding (RR = 90%) the benefits of the NF-ELOX integration strategy can be clearly seen, and it is possible to apply longer NF pre-concentration times and thus higher *VRF* values with maximum energy savings in the process. For higher target removal ratios, only the NF90-ELOX combined strategy is able to reduce the energy consumption compared to the single electrooxidation process. Information about the optimal *VRF* for the different scenarios is gathered in Table 4. The reported energy consumption values of the ELOX treatment in all the studied scenarios are significantly lower than the previously reported energy consumption of the electrochemical degradation of long-chain PFASs, in the range of $41.7\text{--}76.6 \text{ kWh m}^{-3}$ [31], especially when the integration with the NF90 is carried out ($1.3\text{--}10.0 \text{ kWh m}^{-3}$ for RR = 90% and RR = 99%, respectively).

Fig. 7 shows the contribution of the ELOX and membrane technologies to the total energy consumption, in two situations: (i) first, when no pre-concentration is applied and only ELOX is considered for PFHxA removal; and (ii) when the integrated process is considered and NF pre-concentration is applied using the optimal *VRF*, that is, the *VRF* that allows minimizing the energy consumption for each target removal ratio, as given in Fig. 6. For RR = 90%, the hybrid process consumes 50.6% (NF270) and 76.7% (NF90) less energy than the ELOX process

Table 4
Optimal variables allowing maximum energy savings in the integrated process.

Scenario	<i>VRF</i>	C_{fb} , NF (mg L^{-1})	C_{pt} , NF (mg L^{-1})	C_{ELOX} (mg L^{-1})	SEC_{NF} (kWh m^{-3})	SEC_{ELOX} (kWh m^{-3})
NF270 (RR = 90%)	4.0	748.0	22.9	11.3	1.2	5.8
NF270 (RR = 99%)	–	204.0	–	2.0	–	28.4
NF90 (RR = 90%)	10.0	2014.1	3.4	169.6	2.0	1.3
NF90 (RR = 99%)	3.9	778.7	2.4	0.7	1.6	10.0

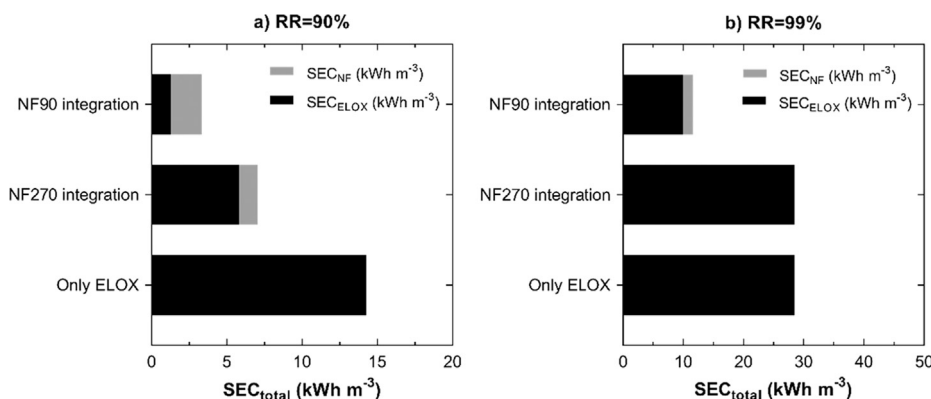


Fig. 7. Comparison of specific energy consumption when NF/ELOX are coupled at the optimal *VRF* and ELOX without previous NF pre-concentration are used, for the different PFHxA removal ratios. (a) RR = 90%; (b) RR = 99%.

alone. It is important to highlight that most of the energy consumption comes from the ELOX step. For RR = 99%, the integration with the NF90 membrane is able to reduce the ELOX energy consumption by 64.9%. As the optimal VRF is limited to 3.9, the nanofiltration contribution to the total energy consumption is noticeably reduced. In this case, the hybrid process consumes 59.2% less energy than the ELOX process alone.

4. Conclusions

The results presented herein stand out the integration of electrochemical technologies with membrane processes as a promising strategy to reduce the energy consumption of the electrochemical treatment of highly persistent organic pollutants in water. As a case of study, this work analyzed the removal of perfluorohexanoic acid from industrial process waters using a treatment train that combines nanofiltration and BDD electrochemical degradation of the concentrate stream obtained in the membrane separation unit. Mathematical simulation techniques, complemented by laboratory data of mass transfer parameters and electrolysis kinetics, were employed. In our case of study, the energy savings are clearly dependent on two factors: (i) the final target PFHxA concentration in the treated water, that is, the ratio of PFHxA removal and (ii) the permeability and rejection properties of the selected membrane. Thereof, the NF90 membrane followed by BDD electrooxidation allowed to achieve 76.7% and 59.2% energy savings for PFHxA removal ratios of 90% and 99%, compared to the direct BDD electrolysis. The use of a highly productive but less selective NF270 membrane provided 50.7% energy savings for a 90% removal ratio, although when the target removal ratio was raised to 99% the hybrid strategy did not bring any benefit. Also, it is relevant to point out that the contribution of NF to the process total energy consumption was the lowest in most cases. These results direct future research to the design of different membrane pre-concentration configurations. More sophisticated separations such as membrane cascade systems with multiple NF/RO stages and different recirculation and operation options could be useful to achieve higher purity in the permeate and lower electro-oxidation requirements in an integrated process. However, the trade-off between PFHxA and ions selectivity and productivity should be taken into account. In this way, further optimization studies are needed as the way to exploit the benefits of the integrated membrane separation-electrochemical treatment to reach high PFHxA removal ratios.

Acknowledgments

Financial support from projects CTM2013-44081-R, CTM2016-75509-R and CTQ2016-75158-R (MINECO, SPAIN-FEDER 2014–2020) and to the Spanish Excellence Network E3TECH (CTQ2015-71650-RDT) is gratefully acknowledged.

References

[1] O.S. Arvaniti, A.S. Stasinakis, Review on the occurrence, fate and removal of perfluorinated compounds during wastewater treatment, *Sci. Total Environ.* 524–525 (2015) 81–92, <http://dx.doi.org/10.1016/j.scitotenv.2015.04.023>.

[2] B. Gomez-Ruiz, P. Ribao, N. Diban, M.J. Rivero, I. Ortiz, A. Urriaga, Photocatalytic degradation and mineralization of perfluorooctanoic acid (PFOA) using a composite TiO₂–rGO catalyst, *J. Hazard. Mater.* 344 (2018) 950–957, <http://dx.doi.org/10.1016/j.jhazmat.2017.11.048>.

[3] I. Fuertes, S. Gómez-Lavín, M.P. Elizalde, A. Urriaga, Perfluorinated alkyl substances (PFASs) in northern Spain municipal solid waste landfill leachates, *Chemosphere* 168 (2017) 399–407, <http://dx.doi.org/10.1016/j.chemosphere.2016.10.072>.

[4] A.Y.C. Lin, S.C. Panchangam, Y.T. Tsai, T.H. Yu, Occurrence of perfluorinated compounds in the aquatic environment as found in science park effluent, river water, rainwater, sediments, and biotissues, *Environ. Monit. Assess.* 186 (2014) 3265–3275, <http://dx.doi.org/10.1007/s10661-014-3617-9>.

[5] The European Parliament and the Council of the European Union, Directive 2013/39/EU of the European Parliament and of the council of 12 August 2013 amending Directives 2000/60/EC and 2008/105/EC as regards priority substances in the field of water policy, *Off. J. Eur. Union. L* 226/1 (2013) 1–17. < <http://eur-lex.europa.eu/legal-content/EN/TXT/?uri=celex:32013L0039> > .

[6] The European Commission, Commission Regulation (EU) 2017/1000 of 13 June 2017: Amending Annex XVII to Regulation (EC) No 1907/2006 of the European Parliament and of the Council concerning the Registration, Evaluation, Authorisation and Restriction of Chemicals (REACH) as regard, *Off. J. Eur. Union. L* 150 (2017) 14–18. < <http://eur-lex.europa.eu/legal-content/EN/TXT/PDF/?uri=CELEX:32017R1000&from=EN> > .

[7] Z. Wang, I.T. Cousins, M. Scheringer, K. Hungerbuehler, Hazard assessment of fluorinated alternatives to long-chain perfluoroalkyl acids (PFAAs) and their precursors: Status quo, ongoing challenges and possible solutions, *Environ. Int.* 75 (2015) 172–179, <http://dx.doi.org/10.1016/j.envint.2014.11.013>.

[8] Z. Wang, I.T. Cousins, M. Scheringer, K. Hungerbuehler, Fluorinated alternatives to long-chain perfluoroalkyl carboxylic acids (PFCAs), perfluoroalkane sulfonic acids (PFASs) and their potential precursors, *Environ. Int.* 60 (2013) 242–248, <http://dx.doi.org/10.1016/j.envint.2013.08.021>.

[9] B. Yang, C. Jiang, G. Yu, Q. Zhuo, S. Deng, J. Wu, H. Zhang, Highly efficient electrochemical degradation of perfluorooctanoic acid (PFOA) by F-doped Ti/SnO₂ electrode, *J. Hazard. Mater.* 299 (2015) 417–424, <http://dx.doi.org/10.1016/j.jhazmat.2015.06.033>.

[10] H. Lin, J. Niu, S. Ding, L. Zhang, Electrochemical degradation of perfluorooctanoic acid (PFOA) by Ti/SnO₂-Sb, Ti/SnO₂-Sb/PbO₂ and Ti/SnO₂-Sb/MnO₂ anodes, *Water Res.* 46 (2012) 2281–2289, <http://dx.doi.org/10.1016/j.watres.2012.01.053>.

[11] C.E. Schaefer, C. Andaya, A. Burant, C.W. Condee, A. Urriaga, T.J. Strathmann, C.P. Higgins, Electrochemical treatment of perfluorooctanoic acid and perfluorooctane sulfonate: insights into mechanisms and application to groundwater treatment, *Chem. Eng. J.* (2017), <http://dx.doi.org/10.1016/j.cej.2017.02.107>.

[12] A. Urriaga, C. Fernández-González, S. Gómez-Lavín, I. Ortiz, Kinetics of the electrochemical mineralization of perfluorooctanoic acid on ultrananocrystalline boron doped conductive diamond electrodes, *Chemosphere* 129 (2015) 20–26, <http://dx.doi.org/10.1016/j.chemosphere.2014.05.090>.

[13] C.E. Schaefer, C. Andaya, A. Urriaga, E.R. McKenzie, C.P. Higgins, Electrochemical treatment of perfluorooctanoic acid (PFOA) and perfluorooctane sulfonic acid (PFOS) in groundwater impacted by aqueous film forming foams (AFFFs), *J. Hazard. Mater.* 295 (2015) 170–175, <http://dx.doi.org/10.1016/j.jhazmat.2015.04.024>.

[14] Á. Soriano, D. Gorri, A. Urriaga, Efficient treatment of perfluorohexanoic acid by nanofiltration followed by electrochemical degradation of the NF concentrate, *Water Res.* 112 (2017) 147–156, <http://dx.doi.org/10.1016/j.watres.2017.01.043>.

[15] M. Panizza, G. Cerisola, Direct and mediated anodic oxidation of organic pollutants, *Chem. Rev.* 109 (2009) 6541–6569, <http://dx.doi.org/10.1021/cr9001319>.

[16] C.A. Martínez-Huitle, M.A. Rodrigo, I. Sirés, O. Scialdone, Single and coupled electrochemical processes and reactors for the abatement of organic water pollutants: a critical review, *Chem. Rev.* 115 (2015) 13362–13407, <http://dx.doi.org/10.1021/acs.chemrev.5b00361>.

[17] J. Muff, Chapter 3 – Electrochemical Oxidation – A Versatile Technique for Aqueous Organic Contaminant Degradation, in: *Chem. Adv. Environ. Purif. Process. Water*, 2014: pp. 75–134. <http://doi.org/10.1016/B978-0-444-53178-0.00003-1>.

[18] Á. Anglada, A.M. Urriaga, I. Ortiz, Laboratory and pilot plant scale study on the electrochemical oxidation of landfill leachate, *J. Hazard. Mater.* 181 (2010) 729–735, <http://dx.doi.org/10.1016/j.jhazmat.2010.05.073>.

[19] A. Urriaga, P. Gómez, A. Arruti, I. Ortiz, Electrochemical removal of tetrahydrofuran from industrial wastewaters: Anode selection and process scale-up, *J. Chem. Technol. Biotechnol.* 89 (2014) 1243–1250, <http://dx.doi.org/10.1002/jctb.4384>.

[20] A. Urriaga, P. Fernandez-Castro, P. Gómez, I. Ortiz, Remediation of wastewaters containing tetrahydrofuran. Study of the electrochemical mineralization on BDD electrodes, *Chem. Eng. J.* 239 (2014), <http://dx.doi.org/10.1016/j.cej.2013.11.028>.

[21] J. Radjenovic, D.L. Sedlak, Challenges and opportunities for electrochemical processes as next-generation technologies for the treatment of contaminated water, *Environ. Sci. Technol.* 49 (2015) 11292–11302, <http://dx.doi.org/10.1021/acs.est.5b02414>.

[22] A. Anglada, D. Ortiz, A.M. Urriaga, I. Ortiz, Electrochemical oxidation of landfill leachates at pilot scale: evaluation of energy needs, *Water Sci. Technol.* 61 (2010) 2211–2217, <http://dx.doi.org/10.2166/wst.2010.130>.

[23] A. Anglada, A. Urriaga, I. Ortiz, Pilot scale performance of the electro-oxidation of landfill leachate at boron-doped diamond anodes, *Environ. Sci. Technol.* 43 (2009) 2035–2040, <http://dx.doi.org/10.1021/es802748c>.

[24] T.G. Schwanz, M. Llorca, M. Farré, D. Barceló, Perfluoroalkyl substances assessment in drinking waters from Brazil, France and Spain, *Sci. Total Environ.* 539 (2016) 143–152, <http://dx.doi.org/10.1016/j.scitotenv.2015.08.034>.

[25] J. Llanos, A. Raschitor, P. Cañizares, M.A. Rodrigo, Electrocoagulation as the key for an efficient concentration and removal of oxyfluorfen from liquid wastes, *Ind. Eng. Chem. Res.* 56 (2017) 3091–3097, <http://dx.doi.org/10.1021/acs.iecr.7b00347>.

[26] A.M. Urriaga, G. Pérez, R. Ibáñez, I. Ortiz, Removal of pharmaceuticals from a WWTP secondary effluent by ultrafiltration/reverse osmosis followed by electrochemical oxidation of the RO concentrate, *Desalination* 331 (2013) 26–34, <http://dx.doi.org/10.1016/j.desal.2013.10.010>.

[27] H.T. Madsen, E.G. Søgaard, J. Muff, Reduction in energy consumption of electrochemical pesticide degradation through combination with membrane filtration, *Chem. Eng. J.* 276 (2015) 358–364, <http://dx.doi.org/10.1016/j.cej.2015.04.098>.

[28] Á. Anglada, A. Urriaga, I. Ortiz, Contributions of electrochemical oxidation to waste-water treatment: fundamentals and review of applications, *J. Chem. Technol. Biotechnol.* 84 (2009) 1747–1755, <http://dx.doi.org/10.1002/jctb.2214>.

- [29] G. Pérez, A.R. Fernández-Alba, A.M. Urtiaga, I. Ortiz, Electro-oxidation of reverse osmosis concentrates generated in tertiary water treatment, *Water Res.* 44 (2010) 2763–2772, <http://dx.doi.org/10.1016/j.watres.2010.02.017>.
- [30] H. Hori, A. Yamamoto, E. Hayakawa, S. Taniyasu, N. Yamashita, S. Kutsuna, H. Kiatagawa, R. Arakawa, Efficient decomposition of environmentally persistent perfluorocarboxylic acids by use of persulfate as a photochemical oxidant, *Environ. Sci. Technol.* 39 (2005), <http://dx.doi.org/10.1021/es0484754>.
- [31] J. Niu, Y. Li, E. Shang, Z. Xu, J. Liu, Electrochemical oxidation of perfluorinated compounds in water, *Chemosphere* 146 (2016) 526–538, <http://dx.doi.org/10.1016/j.chemosphere.2015.11.115>.
- [32] A. Anglada, R. Ibañez, A. Urtiaga, I. Ortiz, Electrochemical oxidation of saline industrial wastewaters using boron-doped diamond anodes, *Catal. Today* 151 (2010) 178–184, <http://dx.doi.org/10.1016/j.cattod.2010.01.033>.
- [33] A. Pérez-González, R. Ibañez, P. Gómez, A.M. Urtiaga, I. Ortiz, J.A. Irabien, Nanofiltration separation of polyvalent and monovalent anions in desalination brines, *J. Memb. Sci.* 473 (2015) 16–27, <http://dx.doi.org/10.1016/j.memsci.2014.08.045>.
- [34] T. Asano, *Wastewater Reclamation and Reuse: Water Quality Management Library*, CRC Press, Florida, 1998.
- [35] F. Vince, F. Marechal, E. Aoustin, P. Bréant, Multi-objective optimization of RO desalination plants, *Desalination* 222 (2008) 96–118, <http://dx.doi.org/10.1016/j.desal.2007.02.064>.
- [36] IUPAC, Terminology for membranes and membrane processes (IUPAC Recommendation 1996), *J. Memb. Sci.* 120 (1996) 149–159. [http://doi.org/10.1016/0376-7388\(96\)82861-4](http://doi.org/10.1016/0376-7388(96)82861-4).
- [37] A.R.F. Pipi, I. Sirés, A.R. De Andrade, E. Brillas, Application of electrochemical advanced oxidation processes to the mineralization of the herbicide diuron, *Chemosphere* 109 (2014) 49–55, <http://dx.doi.org/10.1016/j.chemosphere.2014.03.006>.

5.4. Scientific publication #4.

**Selection of High Flux Membrane for the Effective Removal of
Short-Chain Perfluorocarboxylic Acids**

Authors:

Álvaro Soriano, Daniel Gorri, Ane Urtiaga

Ind. Eng. Chem. Res. 2019, 58, 8, 3329-3338

<https://doi.org/10.1021/acs.iecr.8b05506>

Department of Chemical and Biomolecular Engineering. University
of Cantabria. Av. de Los Castros 46. 39005 Santander. Spain

Accepted 25 January 2019

Industrial & Engineering Chemistry Research

Volume 58, Issue 8, (2019), Pages 3329-3338

DOI: 10.1021/acs.iecr.8b05506

Supporting information

Selection of high flux membrane for the effective removal of short-chain perfluorocarboxylic acids

*Álvaro Soriano, Daniel Gorri, Ane Urtiaga**

Department of Chemical and Biomolecular Engineering, University of Cantabria

Av. de Los Castros s/n. 39005 Santander. Spain

*Corresponding author: urtiaga@unican.es

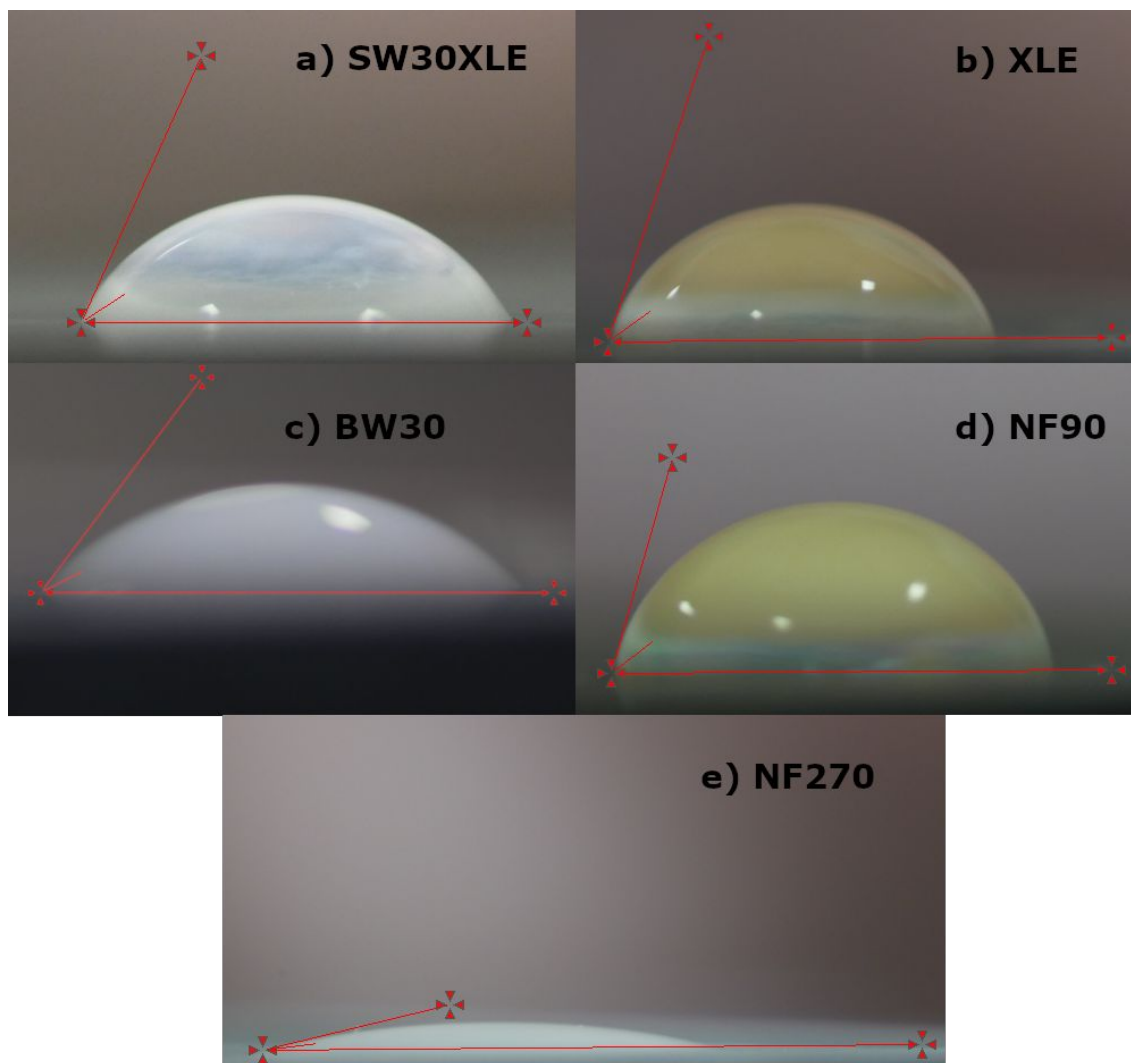


Figure S1. Captured images for measurement of contact angle of different nanofiltration and reverse osmosis membranes. Contact angle was measured from the images captured using the software Measure© 2.0 (C Thing Software 2001-2004, US) .

Adsorption tests

Tests with the three aromatic polyamide RO membranes (XLE, BW30, and SW30XLE) and two NF membranes (NF90 and NF270) were carried out in order to evaluate PFHxA sorption. For each membrane, two membrane coupons summing an area of 6.2 cm², and 40 mL of a PFHxA/water solution were placed in capped polypropylene tubes. Two types of PFHxA solutions were prepared: (i) 100 mg L⁻¹ of PFHxA in ultrapure water, with pH 3.6, as a result of PFHxA dissociation in water; and (ii) 100 mg L⁻¹ of PFHxA in water and neutral pH, that was adjusted by adding sodium hydroxide 0.1 M. The closed tubes with the membrane coupons and the PFHxA solution were gently stirred for 24 h at room temperature. All experiments were performed in duplicate. The mass of PFHxA adsorbed on the membranes was obtained from the difference of PFHxA concentrations in solution at the beginning and at the end of the adsorption tests.

The adsorbed mass was calculated as follows:

$$PFHxA_{mass}(mg\ m^{-2}) = \frac{V(C_0 - C_f)}{A_t} \quad (1)$$

where V is the volume of the solution, C_0 is the PFHxA concentration at the beginning of the tests, C_f is the PFHxA concentration in solution at the end and A_t is the total membrane area.

Figure S2 shows the PFHxA adsorption tests results at both neutral and acid pH conditions.

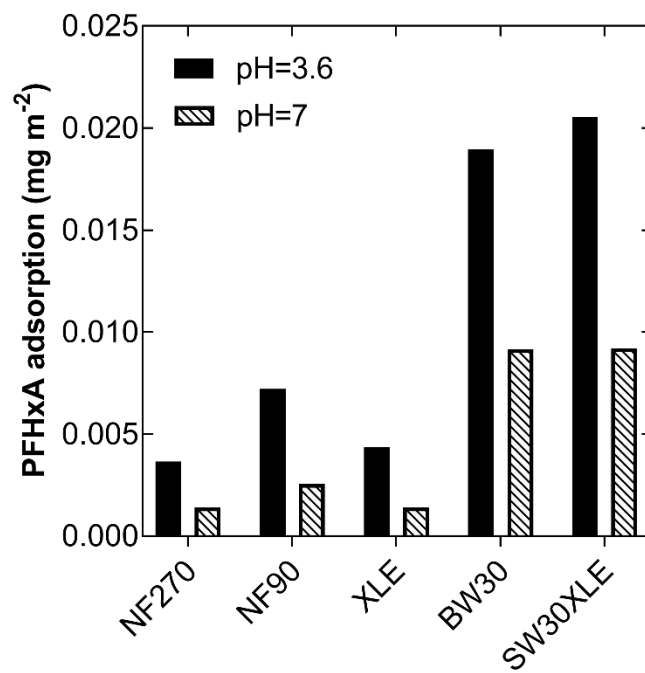


Figure S2. PFHxA adsorption on the different nanofiltration and reverse osmosis membranes under acid and neutral pH conditions.

5.5. Scientific publication #5.

An optimization model for the treatment of perfluorocarboxylic acids considering membrane preconcentration and BDD electrooxidation

Authors:

Álvaro Soriano^a, Daniel Gorri^a, Lorenz. T. Biegler^b, Ane Urtiaga^a

^a Department of Chemical and Biomolecular Engineering. University of Cantabria. Av. de Los Castros 46. 39005 Santander. Spain

^b Department of Chemical Engineering, Carnegie-Mellon University, Pittsburgh, PA, 15213-3890, USA

Accepted 3 August 2019

Water Research

Volume 164 (2019), Number: 114954

DOI: 10.1016/j.watres.2019.114



An optimization model for the treatment of perfluorocarboxylic acids considering membrane preconcentration and BDD electrooxidation

Álvaro Soriano ^a, Daniel Gorri ^a, Lorenz T. Biegler ^b, Ane Urriaga ^{a,*}

^a Department of Chemical and Biomolecular Engineering, University of Cantabria, Av. de Los Castros s/n, 39005, Santander, Spain

^b Department of Chemical Engineering, Carnegie-Mellon University, Pittsburgh, PA, 15213-3890, USA

ARTICLE INFO

Article history:

Received 17 May 2019

Received in revised form

17 July 2019

Accepted 3 August 2019

Available online 5 August 2019

Keywords:

Electrooxidation

Membrane technology

Process optimization

Economic evaluation

Perfluoroalkyl substances (PFAS)

Perfluorohexanoic acid (PFHxA)

ABSTRACT

Treatment of persistent perfluorocarboxylic acids in water matrixes requires of strong oxidation conditions, as those achieved by boron doped diamond (BDD) electrooxidation (ELOX). However, large scale implementation of ELOX is still hindered by its high energy consumption and economical investment. In this work, we used process systems engineering tools to define the optimal integration of a membrane pre-concentration stage followed by the BDD electrolysis of the concentrate, to drastically reduce the costs of treatment of perfluorohexanoic acid (PFHxA, 100 mg L⁻¹) in industrial waste streams. A multi-stage membrane cascade system using nanofiltration (NF90 and NF270 membranes) was considered to achieve more sophisticated PFHxA separations. The aim was to minimize the total costs by determining the optimal sizing of the two integrated processes (membrane area per stage and anode area) and the optimal process variables (pre-concentration operating time, electrolysis time, input and output concentrations). The non-linear programming model (NLP) was implemented in the General Algebraic Modelling System (GAMS). The results showed that for a 2-log PFHxA abatement (99% removal), the optimal two membrane stages using the NF90 membrane obtains a 75.8% (6.4 \$ m⁻³) reduction of the total costs, compared to the ELOX alone scenario (26.5 \$ m⁻³). The optimized anode area and the energy savings, that were 85.3% and 88.2% lower than in ELOX alone, were the major contributions to the costs reduction. Similar results were achieved for a 3-log and 4-log PFHxA abatement, pointing out the promising benefits of integrating electrochemical oxidation with membrane pre-concentration through proper optimization for its large-scale application to waters impacted by perfluorocarboxylic acids.

© 2019 Elsevier Ltd. All rights reserved.

1. Introduction

The growing presence of non-biodegradable and recalcitrant compounds in the environmental media and the inability of traditional wastewater treatment plants to remove this type of pollutants have forced researchers around the globe to find alternative treatment technologies (Sáez et al., 2013). Among them, electrochemical oxidation (ELOX) has gained a lot of attention as a promising technology for the mineralization or partial conversion of recalcitrant organic pollutants in wastewater (Anglada et al., 2009). ELOX may occur by two different mechanisms, direct oxidation and indirect oxidation, or a combination of both. Direct oxidation involves the diffusion of pollutants from the bulk of the liquid phase to the anode surface, followed by the direct electron

transfer from the absorbed compounds. In indirect oxidation, the pollutant reacts in the liquid phase with electrogenerated oxidizing species, typically hydroxyl radicals (•OH), sulfate radicals and chlorine (Panizza and Cerisola, 2009).

The outstanding degradation capability of the ELOX technology is extended to the elimination of extremely recalcitrant perfluoroalkyl substances (Gomez-Ruiz et al., 2017). Per- and polyfluoroalkyl substances (PFASs) are a family of persistent man-made organic compounds that have been extensively used for the last half century in the manufacturing of a wide variety of products (Ross et al., 2018; Valsecchi et al., 2017). The growing concern about their bioaccumulation potential and ubiquitous presence in the environment, especially of long-chain PFASs (number of C ≥ 7), have led to limitations in their production and use, and extensive research is currently being performed about their treatment (Arvaniti and Stasinakis, 2015). Perfluorooctanesulfonic acid (PFOS) and perfluorooctanoic acid (PFOA) were incorporated into the European Union REACH regulation (The European Commission, 2017,

* Corresponding author.

E-mail address: urriaga@unican.es (A. Urriaga).

2010), with restrictions to their use and manufacture. Additionally, the USEPA has established PFOA and PFOS health advisory levels at 70 ng L^{-1} in drinking water (USEPA, 2016). Manufacturers are progressively phasing-out long-chain PFASs with their short-chain homologues and 6:2 fluorotelomers (Wang et al., 2013), also with high persistence properties (Brendel et al., 2018). Besides, 6:2 FTSA biodegradation pathways lead to short-chain perfluorocarboxylic acids, being PFHxA a major product (Zhang et al., 2016). Thus, growing concentrations of PFHxA in the environment are expected in the next years.

PFASs degradation by means of boron doped diamond (BDD) electrodes has been successfully applied at laboratory scale, achieving excellent defluorination and mineralization ratios in different concentration ranges and water matrixes, including industrial wastewater and groundwaters impacted by soil pollution (Gomez-Ruiz et al., 2018, 2017; Schaefer et al., 2017, 2015; Soriano et al., 2017; Urriaga et al., 2015; Zhuo et al., 2012). However, a major drawback of electrochemical oxidation is the slow overall kinetics that results from mass transfer limitations in the low concentration range of PFASs (Pan et al., 2019). BDD electrodes also have the disadvantage of high chlorate and perchlorate generation, that, however, can be diminished working at low current densities (Urriaga et al., 2018). Also, low concentration of organics usually leads to low current efficiency, promoting undesirable secondary reactions such as the O_2 evolution reaction (Panizza et al., 2001). As a consequence, the high energy consumption of the ELOX technology (Anglada et al., 2010a; Gomez-Ruiz et al., 2017; Madsen et al., 2015) and the high economic investment when large electrode areas are needed (He et al., 2018; Radjenovic and Sedlak, 2015), make the large-scale practical implementation of electro-oxidation for PFASs treatment an actual challenge.

The use of membrane separation processes could solve these limitations through the previous concentration of PFASs. On the one-hand, the higher concentration of organic compounds will boost the mass-transfer controlled kinetics of the electrolysis. Also, the natural content of dissolved salts will achieve higher concentrations, and the electrolyte will increase its electrical conductivity. As a result, the cell voltage of the electrochemical reactor will decrease, making the process less energy consuming (Bagastyo et al., 2012; Pérez et al., 2010). The higher concentration of electrolytes could also help to promote the electrochemical generation of oxidant species involved in degradation routes. Our previous experimental work (Soriano et al., 2017) reported the concentration of PFHxA from industrial process waters by means of nanofiltration, that was followed by the electrochemical degradation using BDD electrodes. The energy consumption of the electrolysis stage was estimated at 15.2 kWh m^{-3} for a 90% PFHxA abatement, a value that is significantly lower than the energy consumptions previously reported (Niu et al., 2016) for PFASs electrolysis. However, when more demanding PFHxA removals are needed, more sophisticated separations will be required, such as membrane cascade systems. Besides, a more rigorous and not only energy-focused evaluation of the total economy of the integrated process is also needed.

The rigorous design of a single-stage or multistage membrane pre-concentration integrated to the ELOX process is a complex issue, as several variables regarding its sizing and operation should be considered. The most relevant are the following: the membrane area per stage, number of stages, the anode area, the pre-concentration operating time, the electrolysis time, the concentrated volume to be electrolyzed as well as the input and output concentration of solutes to the ELOX system and output concentration of all solutes in the permeate and concentrate stream. They affect many other variables, as the flowrates of the membrane system, the pumping and ELOX system energy consumption, operating costs and capital investment costs. All these variables are

strongly interrelated and a trade-off between them should be established. Additionally, the resulting hybrid process design must be less costly compared with the application of the individual ELOX process alone. To design such complex cost-optimal process it is necessary to use computer aided process engineering tools. The formulated optimization problem must be solved by minimizing the total costs of the integrated process, at the same time the optimal values of all the variables involved in the process are calculated. To the best of our knowledge, this is the first time that optimization models are used for the optimal integration of membrane and electrochemical oxidation systems.

The novel approach proposed in this work is aimed at solving some of the challenges for the implementation of ELOX technology. The case of study deals with the treatment of persistent short chain perfluorocarboxylic acids. More specifically, the objective was set at the 2-log, 3-log and 4-log reduction of PFHxA concentration in the treated water. We developed a semi-empirical mathematical model describing PFHxA concentration by means of a cascade of membrane elements and the BDD electrolysis of the concentrate stream obtained as retentate in the membrane system. We used optimization tools to determine the minimum total costs of the hybrid process, considering both the capital costs and the operating costs. To that end, optimal process sizing parameters and process variables were obtained for different target PFHxA concentrations at the end of the treatment train.

2. Methodology

2.1. Description of the integrated process including membrane pre-concentration coupled to electrooxidation

A schematic chart of the proposed membrane pre-concentration coupled to electrolysis system is illustrated in Fig. 1a. Both processes will be designed to work in sequential batch mode. First, the feed is sent to the pre-concentration (PC) membrane unit. At the end of the pre-concentration run time (t_{PC}), the volume of retentate that remains in the feed tank is used to feed the ELOX system. After the required electrolysis time (t_{ELOX}), the electrolyzed volume is mixed with the volume of permeate that was obtained in the membrane pre-concentration, resulting in the product volume. Transfer times are neglected. Each batch is processed once the precedent one has been completed.

The proposed membrane separation consists of a multistage cascade of membrane units where the permeate stream of the k stage is pressurized to become the feed to the $k+1$ stage (Fig. 1b). The successive filtration stages will allow to reduce the concentration of pollutants in the permeate, that is finally collected in the permeate tank. The retentate stream of each stage is recycled to the previous stage, except the retentate from the first stage, that is recycled to the feed tank. In this way, the PFHxA concentration in the feed tank will increase over time. This multistage cascade design has been previously proposed for the separation of various chemicals when very high purities are demanded (Abejón et al., 2014, 2012; Caus et al., 2009). The characteristics of two nanofiltration membranes, NF90 and NF270 commercialized by Dow Filmtec, were considered for this study. Both membranes were previously tested at laboratory scale (Soriano et al., 2019a, 2019b) for the separation of PFHxA. The results showed that the NF90 membrane highly rejects PFHxA (rejection $R > 99\%$) but its water permeability is about one-half the permeability of the NF270 membrane, although the latter one achieved PFHxA rejections up to 95%. Ideally, the PFHxA concentration in the permeate should be as low as possible, although the membrane should be highly water-permeable, to diminish pre-concentration times and the costs related to the membrane system. Therefore, the evaluation of the

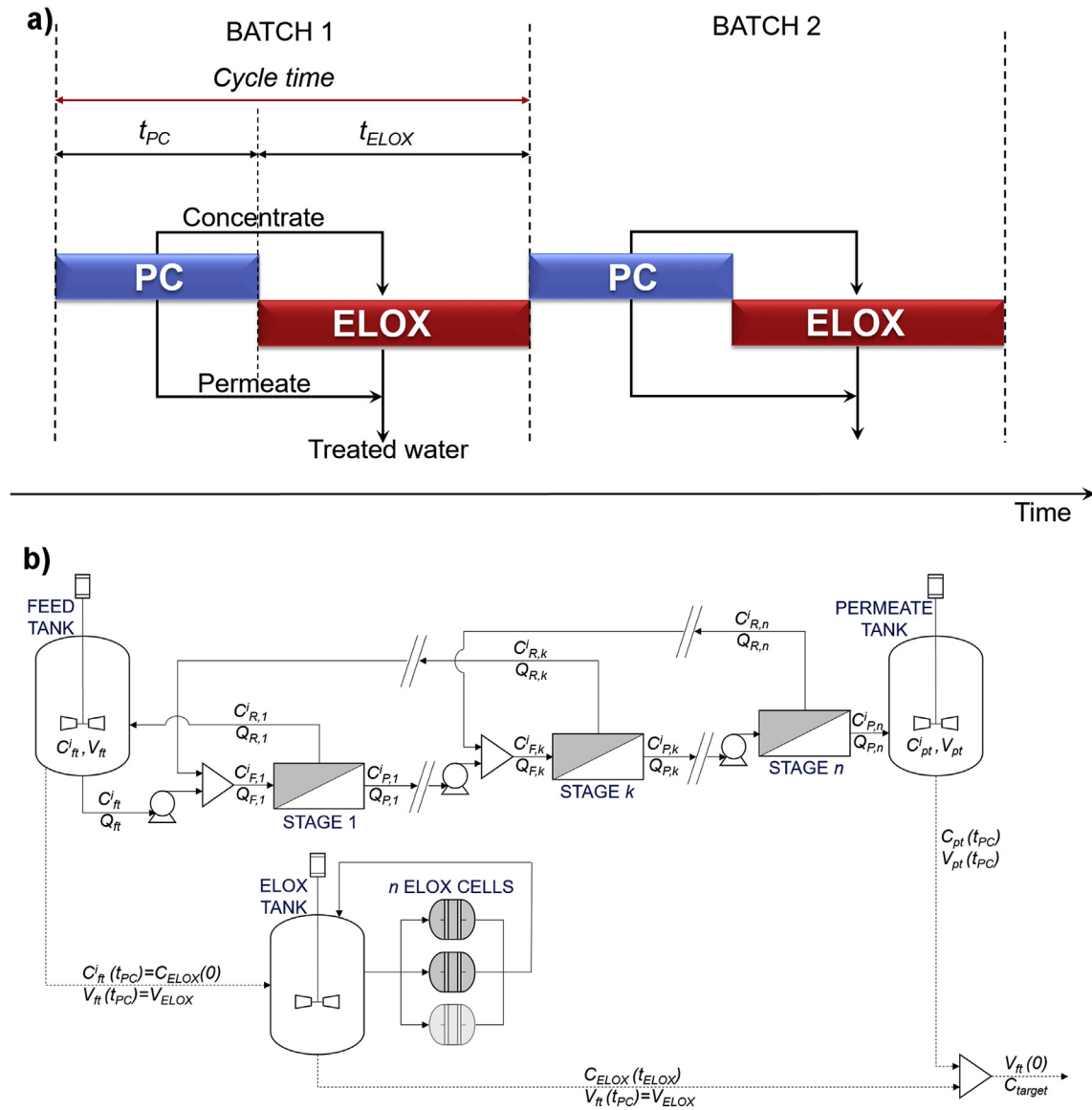


Fig. 1. Global scheme of the multistage countercurrent cascade membrane pre-concentration (PC) coupled to electrooxidation (ELOX) system. (a) Gantt-based chart for batch scheduling, (b) detailed process flowsheet.

NF90 and NF270 membranes in the different scenarios will help to identify the impact of the membrane selectivity/productivity trade-off on the optimal total cost of the hybrid process. Furthermore, the ELOX system is designed as a battery of n electrochemical reactors disposed in serial-parallel arrangement, all provided with boron-doped diamond electrodes (BDD). The design is based in the pilot plant that was built and tested by Anglada and coworkers (Anglada et al., 2010b) for the on-site treatment of landfill leachates.

Table 1 collects information about the problem input parameters such as operating conditions, main characteristics of the hybrid process, and empirically obtained parameters used to solve the optimization problem. We considered the PFHxA and salts concentration in the feed water to be analogous to real industrial process waters (Soriano et al., 2017).

2.2. Process modelling

The following assumptions were made when modelling the process.

- In the cascade membrane separation process, friction losses at the feed side of the membrane element are neglected and, consequently, feed and retentate pressure are the same. Therefore, the retentate is not pressurized when it is recycled to the previous stage; however, the membrane permeate side is at atmospheric pressure, and its pressure must be increased before feeding it to the next membrane stage (Melin and Rautenbach, 2007).
- Membrane fouling was not considered and therefore membrane permeability and the selectivity factor (α^i) will be used as constant parameters in the range of concentration studied.
- All process streams are dilute aqueous solutions with the same constant density.
- The residence time of the fluid inside the stack of electrochemical reactors is negligible compared to its residence time in the recirculation tank.

Modelling of the multistage membrane system: Overall and component mass balances for PFHxA and saline solutes in the feed

Table 1
Process model input parameters.

Initial conditions	
Initial concentration of solutes in the feed tank, C_{ft}^i	
PFHxA	100 mg L ⁻¹
SO ₄ ²⁻	338 mg L ⁻¹
Na ⁺	162 mg L ⁻¹
Feed and permeate tanks volume	
$V_{ft}^i(0)$	10 m ³
$V_{pt}^i(0)$	0 m ³
Operating conditions and process parameters	
Operating feed pressure at each membrane stage k	10 bar
Flow rate from feed tank to cascade membrane system, Q_{ft}	3.2 m ³ h ⁻¹
Solution temperature, T	293 K
ELOX current density, J_{app}	50 A m ⁻²
Empirical parameters (Soriano et al., 2019b, 2019a, 2017)	
Membrane hydraulic permeability	
NF90 permeability, L_p , NF90	6.98 L m ⁻² h ⁻¹ bar ⁻¹
NF270 permeability, L_p , NF270	9.40 L m ⁻² h ⁻¹ bar ⁻¹
NF90 solute transport correlation factor	
α^{PFHxA}	0.0066
$\alpha^{SO_4^{2-}}$	0.0129
α^{Na^+}	0.0152
NF270 solute transport correlation factor	
α^{PFHxA}	0.0520
$\alpha^{SO_4^{2-}}$	0.0369
α^{Na^+}	0.3228
ELOX cells empirical data	
PFHxA degradation kinetic constant at $J_{app} = 50$ A m ⁻² , k_{PFHxA}	0.0021 m min ⁻¹

and permeate tanks, assuming perfect mixing, are written as follows,

$$\frac{dV_{ft}}{dt} = Q_{R,1} - Q_{ft} \quad (1)$$

$$\frac{dV_{pt}}{dt} = Q_{p,n} \quad (2)$$

$$\frac{d(V_{ft} C_{ft}^i)}{dt} = Q_{R,1} C_{R,1}^i - Q_{ft} C_{ft}^i \quad (3)$$

$$\frac{d(V_{pt} C_{pt}^i)}{dt} = Q_{p,n} C_{p,n}^i \quad (4)$$

The subscript $k = 1, 2, \dots, n$ refers to the number of the membrane stage. The superscript i refers to the different compounds. The group of ordinary differential equations given by Eqs (1)–(4) were discretized by Lagrange interpolation polynomials using Runge-Kutta collocation methods in order to be solved as algebraic equations by GAMS (Biegler, 2010).

The equivalent saline concentration in the feed tank was calculated according to Eq. (5) (Pérez-González et al., 2015):

$$C_{eq} = 0.5 \sum_{i=1}^S |z^i| C_{ft}^i \quad (5)$$

The overall and solute mass balances in the mixers are written as follows:

Stage 1

$$Q_{ft} + Q_{R,2} = Q_{F,1} \quad (6)$$

$$Q_{ft} C_{ft}^i + Q_{R,2} C_{R,2}^i = Q_{F,1} C_{F,1}^i \quad (7)$$

Stage k

$$Q_{P,k-1} + Q_{R,k+1} = Q_{F,k} \quad (8)$$

$$Q_{P,k-1} C_{P,k-1}^i + Q_{R,k+1} C_{R,k+1}^i = Q_{F,k} C_{F,k}^i \quad (9)$$

Stage n

$$Q_{P,n-1} = Q_{F,n} \quad (10)$$

$$Q_{P,n-1} C_{P,n-1}^i = Q_{F,n} C_{F,n}^i \quad (11)$$

The overall and component i mass balances in the membrane modules are the following:

$$Q_{F,k} = Q_{R,k} + Q_{P,k} \quad (12)$$

$$Q_{F,k} C_{F,k}^i = Q_{R,k} C_{R,k}^i + Q_{P,k} C_{P,k}^i \quad (13)$$

The solute rejection factor at each membrane stage is defined as follows:

$$R^i = \left(1 - \frac{C_{P,k}^i}{C_{F,k}^i} \right) \times 100 \quad (14)$$

This equation can be rearranged to solve the solute mass transport across the membrane. Defining $\alpha^i = 1 - (R^i/100)$, we obtain the following relationship between the feed and the permeate solute concentration:

$$C_{P,k}^i = \alpha^i C_{F,k}^i \quad (15)$$

where α^i are empirically obtained selectivity parameters that are specific from each membrane and for every solute i (Table 1).

The permeate flowrate from membrane stage k is calculated using the modified Darcy's law expression, which considers the effective pressure gradient ($\Delta P - \Delta \pi$) across the membrane:

$$Q_{P,k} = 10^{-3} L_p A_k (\Delta P - \Delta \pi) \quad (16)$$

where L_p is the empirically determined membrane permeability (Soriano et al., 2019a, 2019b). The osmotic pressure difference (in psi) between both sides of the membrane is calculated according to Eq. (17) (Asano, 1998):

$$\pi = 1.19 T \sum m^i \quad (17)$$

Modelling of the electrochemical reactor: The PFHxA mass balance in the ELOX recirculation tank is defined as follows,

$$\frac{dC_{ELOX}}{dt} = -k_{PFHxA} C_{ELOX} \frac{A_a}{V_{ELOX}} \quad (18)$$

where k_{PFHxA} is the PFHxA electrochemical degradation kinetic constant. Table 1 contains the empirically determined k_{PFHxA} value at 50 A m⁻² in laboratory scale experiments (Soriano et al., 2017) using the BDD cell that is replicated in the design of the pilot plant. It should be noted that in Eq. (18) V_{ELOX} is the electrolyzed volume, which is equal to the volume of concentrate that was obtained in the membrane system at the end of the pre-concentration run ($V_{ELOX} = V_{ft}(t_{PC})$) and at $t_{ELOX} = 0$, C_{ELOX} is equal to $C_{PFHxA}^{ft}(t_{PC})$.

From the mass balance at the mixing point we can calculate the

required ELOX output concentration to meet the required PFHxA target concentration at the exit of the treatment train (Eq. (19)). Here, the target concentration will be defined by the desired PFHxA total abatement of the initial PFHxA concentration of fresh feed entering the process. In this work, we evaluated a 2-log (99%), 3-log (99.9%) and 4-log (99.99%) reduction of the initial PFHxA concentration $C_{ft}^{PFHxA}(0)$.

$$C_{ELOX} = VRF \left[C_{target} - C_{ft}^{PFHxA} \left(1 - VRF^{-1} \right) \right] \quad (19)$$

In Eq. (19), *VRF* symbolizes the volume reduction factor in the pre-concentration run. *VRF* is the ratio between the initial feed volume and the final concentrate volume in the feed tank, at the end of the pre-concentration run. In the same way, we integrated Eq. (18) to define the required electrooxidation time to meet the demanded C_{ELOX} , Eq. (19), as a function of the pre-concentration time:

$$t_{ELOX} = \frac{\ln \left[C_{ELOX} / C_{ft}^{PFHxA}(t_{PC}) \right] V_{ELOX}}{-k_{PFHxA} A_a 60} \quad (20)$$

Where 60 is a factor (min h⁻¹) for the unit conversion of k_{PFHxA} .

2.3. Process economics

The hybrid process was optimized by determining the minimum total annual cost (TC), accounting for the capital expenditures (CAPEX) and the operating expenditures (OPEX):

$$TC = CAPEX \frac{r(1+r)^t}{(1+r)^t - 1} + OPEX \quad (21)$$

In Eq. (21), the operating costs are on annual basis and the total capital investment is annualized taking into account the time value of money, being *T* the period of time and *r* the investment rate (Biegler et al., 1997). The fully detailed list of equations used for the estimation of capital and operating expenditures in Eq. (21) can be found in Table 2. The main parameters used in the process economics model are listed in Table 3.

We can also define the total specific cost (*TSC*) as the total annual cost related to the annual treated volume production (*AP*), the latter being defined as:

$$AP = \frac{OF}{t_{cycle}} V_{ft}(0) \quad (22)$$

with *OF* being the annual operation factor (Table 3) and t_{cycle} the cycle time needed to treat a single batch volume,

$$t_{cycle} = t_{PC} + t_{ELOX} \quad (23)$$

2.4. Process optimization

The full model described in Sections 2.2 and 2.3 can be formulated as the following optimization problem statement:

$$\begin{aligned} \min & TC(x) \\ \text{s.t.} & h(x) = 0 \\ & g(x) \geq 0 \\ & L \leq x \leq U \end{aligned} \quad (37)$$

being *x* the vector of decision variables, *h* the vector of algebraic equations, *g* the model constraints and *L* and *U* the lower and upper

Table 2

Process economics equations used for the estimation of capital and operating costs in Eq. (21).

Capital costs
Total capital costs
$CAPEX = CC_M + CC_{ELOX} + CC_P(24)$
Membrane equipment capital costs including membrane housing (Abejón et al., 2012; USEPA, 2006)
$CC_M = (MMP \sum_{k=1}^n A_k) + V_{pt}(t_{PC}) 14.85 \frac{24}{t_{cycle}}(25)$
Electrooxidation equipment capital costs (Cañizares et al., 2009)
$CC_{ELOX} = 19216(A_e^{0.7857}) + 9000A_e + 0.25P_{ELOX}(26)$
Pump capital costs (Sethi and Wiesner, 2000)
$CC_P = 81.27 UF f_1 f_2 L [(Q_{ft} \Delta P)^{0.39} + (\sum_{k=1}^{n-1} Q_{p,k} \Delta P)^{0.39}](27)$
Operating costs
Total operating costs
$OPEX = C_{clean} + C_{maint} + C_{mrep} + C_{erep} + C_{energy}(28)$
Cleaning costs (Arkell et al., 2013; USEPA, 2006)
$C_{clean} = 50 \times A_e + 2.63 \times 10^{-3} V_{pt}(t_{PC}) \frac{OF}{t_{cycle}}(29)$
Maintenance costs (Arkell et al., 2013)
$C_{maint} = 0.02 CAPEX(30)$
Membrane replacement costs (Abejón et al., 2012)
$C_{mrep} = \frac{MMP}{ML} \sum_{k=1}^n A_k(31)$
Electrode replacement costs
$C_{erep} = \frac{EP}{EL} A_e(32)$
Energy costs (Zarca et al., 2018)
$C_{energy} = EIP(E_{ELOX} + E_{PC}) \frac{OF}{t_{cycle}}(33)$
Electrooxidation process energy consumption (Martínez-Huitle et al., 2015)
$E_{ELOX} = 10^{-3} U J_{app} A_e t_{ELOX}(34)$
Equivalent saline concentration – ELOX cell voltage empirical correlation (Soriano et al., 2019b)
$U = 11.649(C_{eq} - 5.65 \times 10^{-3})^{-4.84 \times 10^{-2}}(35)$
Pre-concentration process pumping energy consumption
$E_{PC} = \frac{\Delta P t_{PC}}{36 \eta} (\sum_{k=1}^{n-1} Q_{p(k)} + Q_{ft})(36)$

limits of the set of decision variables.

We impose a *VRF* restriction, since reducing more than ten times the initial volume in the pre-concentration process is not a technically realistic scenario:

$$VRF \leq 10 \quad (38)$$

We also restrict the membrane area per stage (A_k), by defining lower and upper bounds to this variable based on the smallest and largest NF90 and NF270 membrane modules that are commercialized (2.6 m² (4'') and 37 m² (8'')) (The Dow Chemical Company, 2013):

$$2.6 \leq A_k \leq 37 \quad (39)$$

Finally, and for the sake of comparison between different cases of study, we evaluated the scenario in which the annual demand of volume of treated water (Eq. (22)), is equal to 2000 m³ y⁻¹.

Thus, the herein presented optimization model is aimed at the minimization of the total annual cost (Eq. (21)) of the hybrid pre-concentration/electrooxidation process, for a required PFHxA abatement at the end of the treatment train and for a demanded annual volume production. For each abatement scenario, the optimal individual operating pre-concentration and electrooxidation times are obtained, as well as the sizing of each individual processes (i.e. the optimal total anode area and the membrane area per stage) and the output concentrations at the exit of the pre-concentration process, input and output concentrations at the ELOX system, energy consumption of both processes and capital

Table 3
Economic model process parameters.

Parameter	Value
Investment rate, r (Zarca et al., 2018)	10%
Period, T (Zarca et al., 2018)	15 y
Pump construction material factor, f_1 (ductile iron) (Sethi and Wiesner, 2000)	1
Suction pressure range factor, f_2 (suction pressures up to 150 psi) (Sethi and Wiesner, 2000)	1
Labor factor, L (Sethi and Wiesner, 2000)	1.4
Membrane equipment price, MMP	500 \$ m ⁻²
Membrane module life, ML	8 y
BDD anode electrode price, EP (Cañizares et al., 2009; Sabatino et al., 2017)	9000 \$ m ⁻²
BDD anode electrode expected life, EL (Kraft, 2007)	6 y
EU-28 electricity price for non-household consumers, second half 2017, EIP (Eurostat, 2018)	0.16 \$ kWh ⁻¹
Annual operation factor, OF (Zarca et al., 2018)	8000 h y ⁻¹
Global pumping system efficiency, η (Vince et al., 2008)	80%

Table 4
Integration with NF90 membrane optimization results.

PFHxA removal	2-log			3-log			4-log		
	1	2	3	1	2	3	1	2	3
Number of stages in the membrane cascade	1	2	3	1	2	3	1	2	3
Membrane stage 1 area, A_1 (m ²)	28.1	14.0	12.4	2.6	16.0	14.0	2.6	24.8	15.4
Membrane stage 2 area, A_2 (m ²)		10.4	9.2		11.8	10.4		14.4	11.4
Membrane stage 3 area, A_3 (m ²)			9.2			10.3			11.3
Anode electrode area, A_e (m ²)	3.9	1.3	1.4	13.7	1.9	2.0	18.3	2.9	2.6
Pre-concentration time, t_{PC} (h)	4.0	12.6	14.2	0.0	11.0	12.6	0.0	9.0	11.5
Electrolysis time, t_{ELOX} (h)	36.0	27.4	25.8	40.00	29.0	27.4	40.0	31.0	28.5
Total annual cost, TC (\$ y ⁻¹)	2.6E+04	1.3E+04	1.4E+04	7.8E+04	1.7E+04	1.8E+04	1.0E+05	2.3E+04	2.2E+04
Total specific cost, TSC (\$ m ⁻³)	12.9	6.4	7.2	39.0	8.3	9.1	51.0	11.7	10.9
Savings (%)	51.3	75.8	72.7	–	78.5	76.3	–	76.9	78.4

and operating costs distributions. The dynamic nonlinear programming problem (NLP) was implemented in the General Algebraic Modelling System (GAMS) and solved using the IPOPTH solver on a 3.20 GHz Intel® Core™ i5-6500 processor.

3. Results and discussion

3.1. Hybrid pre-concentration/electrooxidation process optimization results

Table 4 and Table 5 show the optimal pre-concentration and electrooxidation times, membrane area per stage, anode electrode area and total cost for the different scenarios and for two types of nanofiltration membranes (NF270 and NF90), which differ in their water permeability and solute selectivity properties. We evaluated a 2-log, 3-log and 4-log PFHxA elimination ratios at the exit of the process. We also evaluated 1, 2 and 3 pre-concentration stages in the membrane system and compared the total cost of all the scenarios with the application of ELOX alone without any pre-concentration stage. In Tables 4 and 5, a pre-concentration time equal to zero means that the optimized solution eliminated the pre-concentration stage. This is the case of the NF270-1 stage

integration for any target PFHxA removal ratio, and the NF90-1 stage integration for 3-log and 4-log PFHxA abatement. In these cases, the hybrid strategy does not bring any benefit from the point of view of total cost savings, since one membrane stage is not enough to obtain a high purity permeate. Since the required target concentration (C_{target}) is considerably lower than the permeate concentration (C_{PFHxA}^{pt}), the output ELOX concentration (C_{ELOX}) must be acutely low to meet the imposed mass balance at the exit of the treatment train. As a result, the ELOX energy costs are significantly higher, and the optimal solution eliminates the pre-concentration stage ($t_{PC}=0$), as it only contributes to increase the total treatment costs.

The distribution of all the optimal capital and operating costs, expressed as total specific cost, for the different cases of study are shown in Fig. 2 and Fig. 3, using the NF90 and the NF270 membrane, respectively. In all scenarios, the most important contribution to the total costs are the capital costs related to the electrochemical reactor system (from a 47% contribution in the worst scenario to a 36% impact in the best scenario). Based on the optimization results, the costs of the ELOX reactor can be greatly reduced though its integration with the membrane pre-concentration strategy, as the total anode area is significantly

Table 5
Integration with NF270 membrane optimization results.

PFHxA removal	2-log			3-log			4-log		
	1	2	3	1	2	3	1	2	3
Number of stages in the membrane cascade	1	2	3	1	2	3	1	2	3
Membrane stage 1 area, A_1 (m ²)	2.6	11.7	10.0	2.6	37.0	11.5	2.6	2.7	10.2
Membrane stage 2 area, A_2 (m ²)		9.4	8.0		10.2	9.2		2.6	36.9
Membrane stage 3 area, A_3 (m ²)			7.6			8.7			7.5
Anode electrode area, A_e (m ²)	9.1	1.5	1.4	13.7	11.4	2.0	18.3	18.3	3.2
Pre-concentration time, t_{PC} (h)	0.0	10.4	12.9	0.0	4.1	11.2	0.0	0.0	13.0
Electrolysis time, t_{ELOX} (h)	40.0	29.6	27.1	40.0	35.9	28.8	40.0	40.0	27.1
Total annual cost, TC (\$ y ⁻¹)	5.4E+04	1.3E+04	1.3E+04	7.8E+04	7.0E+04	1.8E+04	1.0E+05	1.0E+05	2.7E+04
Total specific cost, TSC (\$ m ⁻³)	26.9	6.6	6.7	39.0	35.2	8.8	51.0	51.4	13.7
Savings (%)	–	75.0	74.7	–	8.9	77.2	–	–	72.9

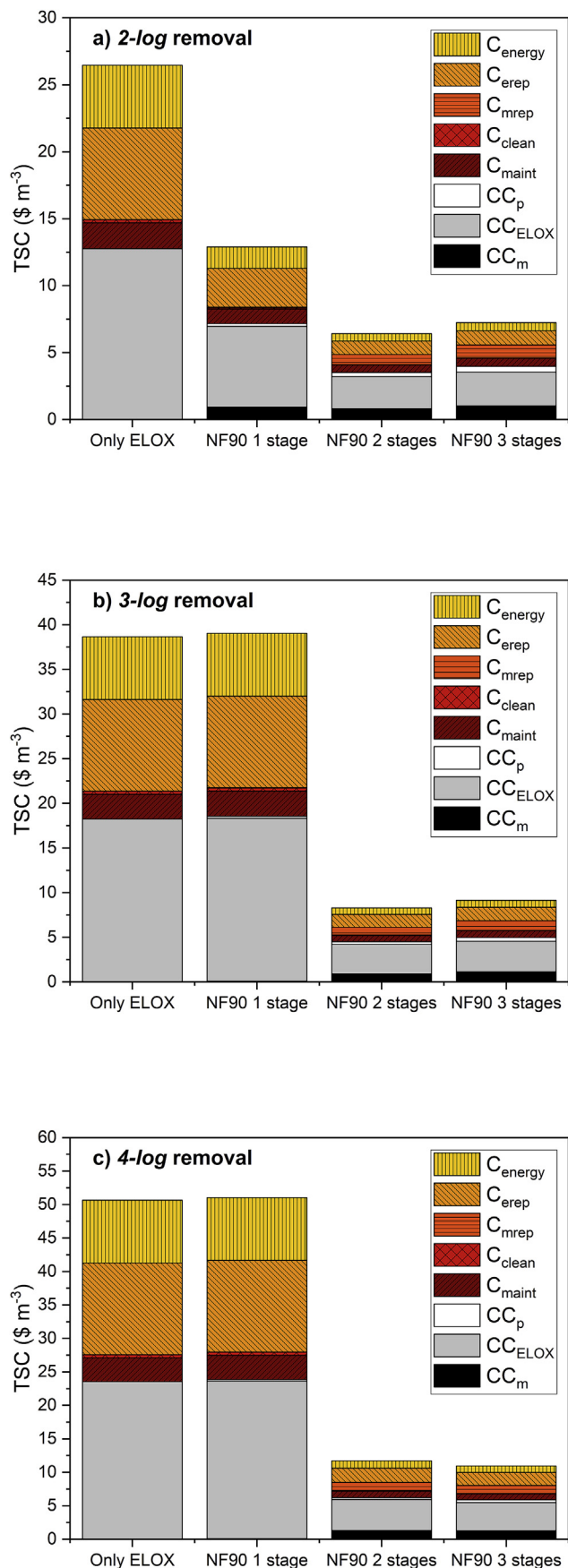
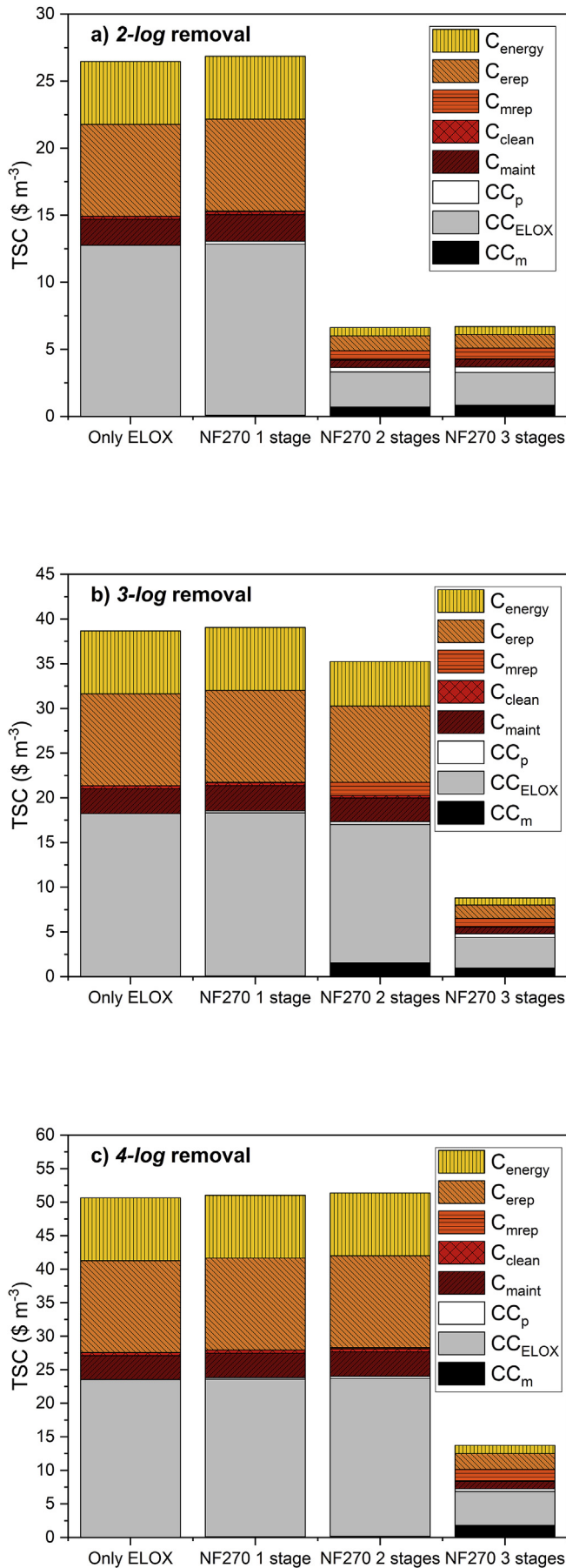


Fig. 2. Comparison of the CAPEX (CC) and OPEX (C) costs distribution for the 1, 2 and 3 NF90 membrane stages coupled to ELOX and the application of ELOX without pre-concentration for different PFHxA abatement targets: 2-log, 3-log and 4-log.

reduced. The membrane integration also managed to reduce all the operating costs related to the ELOX system, i.e., the lower the anode area, the lower are the costs related to the replacement of the anodes and maintenance. For the 2-log PFHxA abatement, the anode area can be reduced from 9.1 m² in the case of only-ELOX, to 3.9 m² with NF90-1 stage integration, and furthermore, to 1.3 m² with NF90-2 membrane stages and 1.4 m² with NF90-3 membrane stages. This is translated into 51.3% savings of the total cost with the NF90-1 stage integration, compared to the application of the electrooxidation process alone. These savings are even higher with the use of 2 stages (75.8%) because of the lower optimal anode area capital and replacement costs. Overall, the integration results are slightly better when two membrane stages are used, since adding more membrane stages also increases the capital and operating costs related to the membrane system. On the other hand, cleaning costs only represent up to 0.9% of the total costs of the integrated process. In the case of cathode scaling promoters, such as calcium, being present at elevated concentrations, more frequent chemical cleanings will be needed. Nevertheless, due to the minor contribution of the cleaning costs to the total costs function the presence of scaling species would not have a great impact on the optimization results.

When an extremely demanding PFHxA abatement is required, as it is the 4-log elimination scenario, the integration of a three stages membrane cascade provides better results, and the total savings increased to 78.4%, through the optimization of all the process variables. For the highly productive but more PFHxA permeable NF270 membrane, a 4-log PFHxA abatement requires a three stages cascade pre-concentration, although the total cost is slightly higher than for the NF90 integration. This is because the optimal output ELOX concentration in the NF270 integration scenario ($C_{ELOX} = 0.02 \text{ mg L}^{-1}$) is more demanding than when using the NF90 ($C_{ELOX} = 0.1 \text{ mg L}^{-1}$), which, as previously explained, is a consequence of the lower PFHxA rejection of the NF270 membrane. As a consequence, the costs related to the ELOX energy consumption are higher. As the ELOX capital costs clearly overshadow the membrane system equipment costs, it is possible to add up to three membrane stages for a 4-log abatement and still get a slight reduction of the total costs. (e.g. in the 4-log NF90 case of study). In general, the membrane equipment investment only represents 7%–13% of the total costs in those scenarios in which the integration approach works, and the pump capital cost contributions are up to 7%.

The integration strategy is also able to accomplish important reductions on the operating costs related to the energy consumption of the process compared to the application of the electrolysis alone. Depending on the PFHxA elimination target, the energy specific costs of the only-ELOX scenario range from 4.7 \$ m⁻³ for a 2-log PFHxA removal to 9.4 \$ m⁻³ for a 4-log removal. Remarkably, the membrane coupling approach can reduce the energy costs to 0.6 \$ m⁻³, 0.7 \$ m⁻³ and 1.0 \$ m⁻³ for a 2-log, 3-log and 4-log PFHxA abatement, respectively. These energy savings (up to 89%) notably impact the total costs, as the energy cost contribution to the total costs is reduced from a 18% to only 8–9%. The pathway for reducing the energy costs goes through the optimization of the electrolysis time, which is much lower in the membrane integrated system than in the approach with ELOX alone. The cutback on the electrolysis time is mainly due to (i) the much lower volume to be electrolyzed and, (ii) the less demanding PFHxA concentration at the exit of the ELOX system that is needed to meet the target concentration at the exit of the treatment train (Eq. (19)). This is also influenced by the very low PFHxA concentration obtained in the permeate tank of the membrane system at the end of the pre-concentration run. Additionally, membrane separation also increases the concentration of salts in solution, to make the electrolyte more conductive, and therefore the cell voltage is also reduced,



diminishing to a lesser degree the ELOX energy costs. As Fig. 4 shows, the ELOX energy savings have a huge impact on the overall energy consumption. Taking as a reference the estimated electrolysis energy consumptions of the ELOX-only scenario (29.3 kWh m^{-3} , 43.9 kWh m^{-3} and 58.5 kWh m^{-3} , for a 2-log, 3-log and 4-log PFHxA abatement, respectively) the optimized hybrid process consumes 29.3%–89.7% less energy, depending on the type of membrane used and on the number of membrane stages. In most cases, and except for the 2-log NF90-1 stage scenario, the use of a single membrane stage does not provide energy savings.

3.2. Parametric sensitivity analysis

The two commercial membranes considered in this work (NF90 and NF270) yielded excellent results in the integrated process through proper optimization of the process variables. However, it is interesting to determine if hypothetically more selective or more permeable membrane materials would achieve better results in terms of minimization of the total costs. It should be also highlighted that the rejection performance of the herein studied membranes can be affected by the increase of the solution ionic strength, pH acidification or due to the effect of concentration on the selectivity factor. Initial permeate flux might also be reduced as a consequence of organic and inorganic fouling. Hence, in this section, a sensitivity analysis is performed with the aim of getting a deeper understanding on the influence of the studied membrane properties on the total cost objective function. Additionally, we evaluated the influence of the kinetic constant of the electrochemical PFHxA degradation on the total costs objective function when using the NF90 membrane and different number of membrane stages.

The effect of the membrane hydraulic permeability (L_p) and the selectivity factor (α^{PFHxA}) on the total specific cost for a 3-log PFHxA abatement is shown in Fig. 5. Only two and three membrane stages are illustrated since the use of a single membrane stage did not provide any optimal TSC below the only-ELOX scenario. In Fig. 5, the dark red area corresponds to TSC solutions in which the optimal scenario is to eliminate the pre-concentration process and therefore, the integration does not provide any advantage. For orientation purposes, the optimal results of the two commercial membranes studied in this work (NF90 and NF270) have been added to the figure, according to their PFHxA selectivity and hydraulic permeability data (Table 1). In Fig. 5, α^{PFHxA} ranges from $\alpha^{\text{PFHxA}} = 0.1$ (equivalent to $R_{\text{PFHxA}} = 90\%$) to $\alpha^{\text{PFHxA}} = 0.005$ ($R_{\text{PFHxA}} = 99.5\%$), since the empirical values of PFHxA rejection ranged from 94.8% (NF270) and 99.4% (NF90).

In Fig. 5a and b, the lower left hand corner would correspond to TSC solutions theoretically given by reverse osmosis membranes typically characterized by their low permeability and very high selectivity (low α^{PFHxA} value) (Soriano et al., 2019a). With two membrane stages (Fig. 5a), only membranes with very high PFHxA selectivity and medium-high water permeability would be able to accomplish significant total cost savings, as in the case of the NF90 membrane. However, as seen in Fig. 5a the excellent results given by the NF90 membrane are subject to changes in the optimum TSC with any hypothetical reduction of the PFHxA rejection performance or by any decrease of the membrane permeate flux as a result of membrane fouling.

On the other hand, less selective but more water permeable membranes, such as the NF270, achieve similar total costs savings

Fig. 3. Comparison of the CAPEX (CC) and OPEX (C) costs distribution for the 1, 2 and 3 NF270 membrane stages coupled to ELOX, and application of ELOX without pre-concentration for different PFHxA abatement targets: 2-log, 3-log and 4-log.

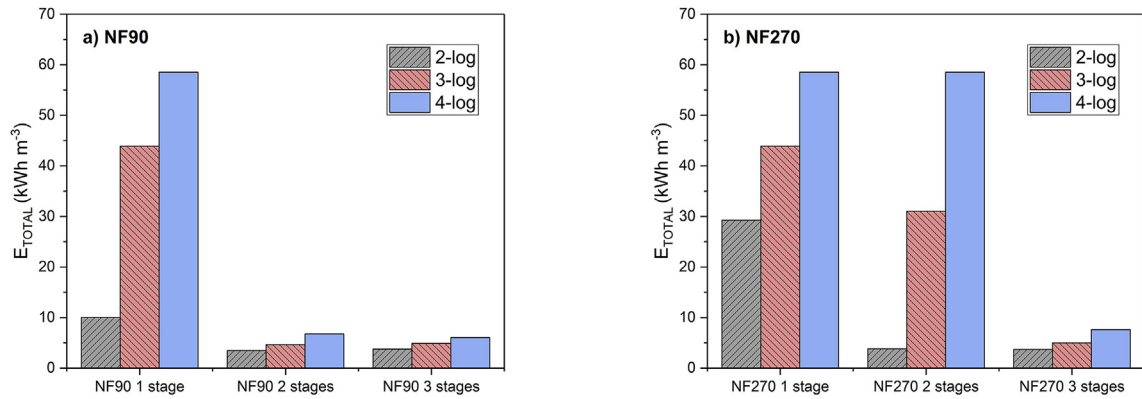


Fig. 4. Optimal total energy consumption of the hybrid process using the NF90 and NF270 membranes for the different PFHxA abatement targets.

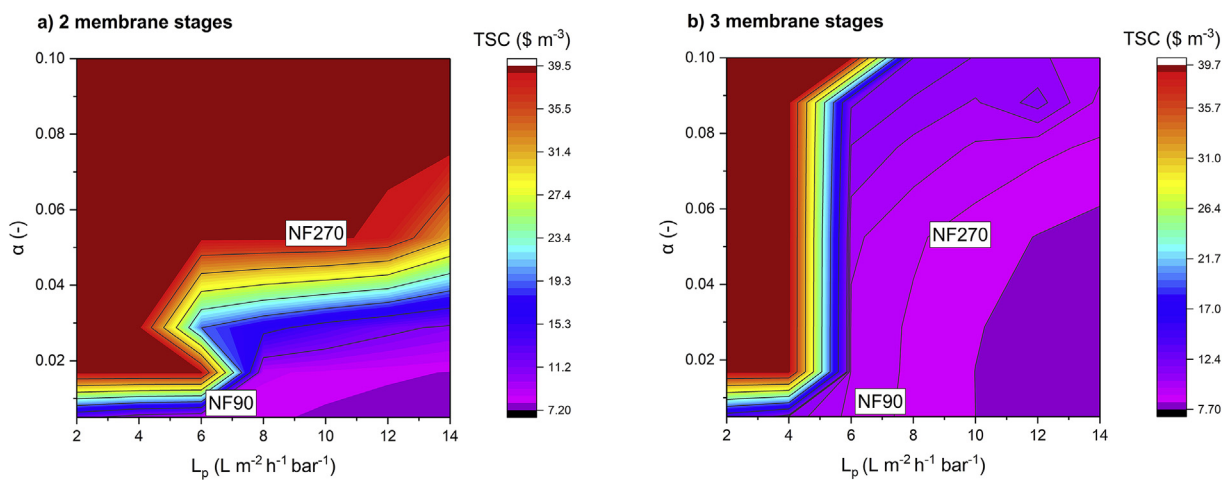


Fig. 5. Influence of the membrane properties on the total cost objective function for a 3-log PFHxA abatement. (a) 2 membrane stages and (b) 3 membrane stages.

when three membrane stages are considered (Fig. 5b). In contrast with the 2-stage integration scenario, any rejection decline in the 3-stage integration scenario would not severely affect the optimal TSC given by the two nanofiltration membranes. However, from a process operation viewpoint it is easier and more suitable to manage a process with fewer membrane stages. Also, according to Fig. 5, more selective and more productive membranes would be able to reduce the TSC to a minimum of 7.2 \$ m^{-3} , which is very close to the best scenario obtained with the commercial NF90 membrane and by means of two membrane stages (8.3 \$ m^{-3}). Finally, in any integration scenario the use of highly PFHxA selective but low water-permeable membranes, as in the case of some reverse osmosis membranes, is not recommended, as any noticeable reduction of the PFHxA rejection performance would severely modify the optimal TSC, thus compromising the benefits of the integrated strategy. It is also worth mentioning that literature reports effective nanofiltration retentions of shorter-chained PFASs such as perfluorobutanoic acid (PFBA), perfluorobutanesulfonic acid (PFBS) and perfluoropentanoic acid (PFPeA), that are generally above 93–95% (Appleman et al., 2013; Steinle-Darling and Reinhard, 2008). From Fig. 5, it can be seen that the use of the NF-ELOX strategy for the treatment of these substances may require up to 3 stages to bring benefits from the point of view of total costs savings.

Fig. 6 shows the sensibility of the optimized solution to variations of the kinetics of PFHxA electrolysis. Considering a 3-log

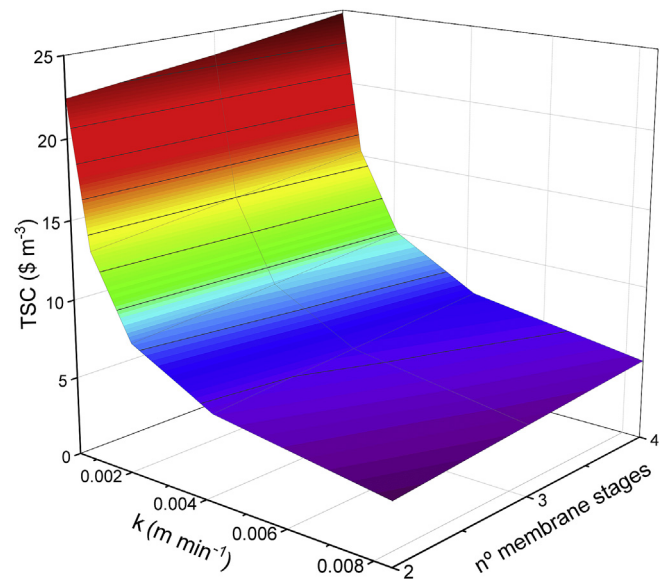


Fig. 6. Influence of the PFHxA degradation constant (k_{PFHxA}) on the total cost objective function for a 3-log PFHxA abatement and different number of membrane stages. Integration with the NF90 membrane.

PFHxA abatement and using the NF90, doubling the value of k_{PFHxA} (Table 1) would reduce the total costs of the hybrid process from 8.3 \$ m⁻³ to 5.5 \$ m⁻³, a consequence of the drastic 45% reduction of the optimal anode area. Conversely, halving the value of k_{PFHxA} has a greater impact on the objective function, as the total costs are elevated to 13.4 \$ m⁻³. Yet, in this hypothetical scenario the integrated strategy would be still able to reduce the total costs a remarkable 65.3% compared to the application of the electro-oxidation alone without previous pre-concentration.

4. Conclusions

This work demonstrates the advantages of integrating membrane separation with electrochemical oxidation for the treatment of short chain perfluorocarboxylic acids (PFCAs) in polluted waters. This novel approach uses process systems engineering tools to optimize the process variables in order to minimize the total costs of the process. Particularly, we studied the treatment of perfluorohexanoic acid at concentration levels that are found in industrial process waters (100 mg L⁻¹).

The results from this work shows that it is possible to achieve important savings in the total costs of the electrochemical treatment of persistent PFCAs through its integration with membrane pre-concentration. Moreover, through rigorous optimization, the integrated membrane separation-electrooxidation process is able to fulfil highly demanding pollutant abatement requirements, in a much less costly way compared to the application of electro-oxidation alone. Overall, elimination objectives are satisfied just with a two-stage membrane pre-concentration layout, achieving excellent savings of the process total costs (up to 78.4%). Overall, it is economically preferable to use nanofiltration membranes, characterized by their medium to high hydraulic permeability and medium to high PFHxA selectivity, in opposition to low permeable and highly selective reverse osmosis membranes. Still, even in the best optimal integration scenarios, which allow 86% reduction of the electrochemical reactor anodic area, the costs related to investment, replacement and maintenance of the electrodes, clearly outweigh the rest of the process capital and operating costs. BDD electrodes achieves outstanding performance for degradation, mineralization, and defluorination of perfluorinated compounds. Despite the excellent results achieved by the integrated process, the high price of the BDD electrodes remains as a bottleneck in the actual implementation of large-scale electrochemical processes. Thus, research efforts should be directed towards the optimization of the BDD manufacturing process or towards the development of new cheaper but equally effective electrocatalytic materials.

Declaration of competing interest

The authors declare that they have no known competing financial interests or personal relationships that could have appeared to influence the work reported in this paper.

Acknowledgments

Financial support by the Spanish Ministry of Economy and Competitiveness through the projects CTM2016-75509-R and CTQ2016-75158-R (MINECO, SPAIN-FEDER 2014–2020) is gratefully acknowledged.

Nomenclature

A_e	Total anode electrode area (m ²)
A_k	Stage k membrane area (m ²)
CAPEX	Total capital expenses (\$)

C_{ELOX}^C	Electrooxidation plant capital expenses (\$)
C_{clean}	Cleaning operating costs (\$ y ⁻¹)
CC_M	Membrane equipment capital cost (\$)
CC_p	Pre-concentration pumping capital cost (\$)
C_{ELOX}	Concentration in the ELOX reactor (mg L ⁻¹)
C_{energy}	Energy costs (\$ y ⁻¹)
C_{eq}	Equivalent ion concentration (mol L ⁻¹)
C_{erep}	Electrode replacement costs (\$ y ⁻¹)
$C_{F,k}^i$	Feed stream to stage k solute concentration (mg L ⁻¹)
C_{ft}^i	Solute concentration in the feed tank (mg L ⁻¹)
C_{maint}	Maintenance operating costs (\$ y ⁻¹)
C_{mrep}	Membrane replacement costs (\$ y ⁻¹)
$C_{P,k}^i$	Stage k permeate stream solute concentration (mg L ⁻¹)
C_{pt}^i	Permeate tank solute concentration (mg L ⁻¹)
$C_{R,k}^i$	Retentate stream solute concentration (mg L ⁻¹)
C_{target}	PFHxA target concentration (mg L ⁻¹)
E_{ELOX}	ELOX energy consumption (kWh)
EL	Electrode material life (y)
EP	Electrode material price (\$ m ⁻²)
E_{PC}	NF energy consumption (kWh)
f_1	Material pump factor
f_2	Suction pressure factor
J_{app}	Current density (A m ⁻²)
k_{PFHxA}	PFHxA degradation kinetic constant (m min ⁻¹)
L	Pumps labor factor
L_p	Membrane permeability (L m ⁻² h ⁻¹ bar ⁻¹)
m^i	Molality of the species dissolved (mol kg ⁻¹)
ML	Membrane module life (y)
MMP	Membrane module price (\$ m ⁻²)
OF	Operating factor (h y ⁻¹)
$OPEX$	Operating expenses (\$ y ⁻¹)
P_{ELOX}	Electrooxidation power supply (kW)
$Q_{F,k}$	Feed flow rate to stage k (m ³ h ⁻¹)
Q_{ft}	Volumetric flow rate from feed tank (m ³ h ⁻¹)
$Q_{P,k}$	Permeate volumetric flow rate from stage k (m ³ .h ⁻¹)
$Q_{R,k}$	Retentate volumetric flow rate from stage k (m ³ h ⁻¹)
r	Investment rate (%)
R^i	Rejection of solute i
T	Temperature of the solution (K)
t	Period (y)
TC	Total annual cost (\$ y ⁻¹)
TSC	Total specific cost (\$ m ⁻³)
t_{cycle}	Cycle time (h)
t_{ELOX}	ELOX operation time (h)
t_{PC}	Pre-concentration time (h)
U	ELOX cell voltage (V)
V_{ft}	Feed tank volume (m ³)
V_{pt}	Permeate tank volume (m ³)
VRF	Volume reduction factor (–)
z^i	Ionic valence (–)
α^i	Solute partitioning empirical parameter (–)
ΔP	Effective pressure difference (bar)
$\Delta \pi$	Osmotic pressure difference (bar)
η	Pump efficiency (%)
π	Osmotic pressure (bar)

References

- Abejón, R., Garea, A., Irabien, A., 2014. Analysis and optimization of continuous organic solvent nanofiltration by membrane cascade for pharmaceutical separation. *AIChE J.* 60, 931–948. <https://doi.org/10.1002/aic.14345>.
- Abejón, R., Garea, A., Irabien, A., 2012. Integrated countercurrent reverse osmosis cascades for hydrogen peroxide ultrapurification. *Comput. Chem. Eng.* 41, 67–76. <https://doi.org/10.1016/j.compchemeng.2012.02.017>.
- Anglada, A., Ortiz, D., Urriaga, A.M., Ortiz, I., 2010a. Electrochemical oxidation of landfill leachates at pilot scale: evaluation of energy needs. *Water Sci. Technol.* 61, 2211–2217. <https://doi.org/10.2166/wst.2010.130>.

- Anglada, A., Urtiaga, A., Ortiz, I., 2009. Contributions of electrochemical oxidation to waste-water treatment: fundamentals and review of applications. *J. Chem. Technol. Biotechnol.* 84, 1747–1755. <https://doi.org/10.1002/jctb.2214>.
- Anglada, A., Urtiaga, A.M., Ortiz, I., 2010b. Laboratory and pilot plant scale study on the electrochemical oxidation of landfill leachate. *J. Hazard Mater.* 181, 729–735. <https://doi.org/10.1016/j.jhazmat.2010.05.073>.
- Appleman, T.D., Dickenson, E.R.V., Bellona, C., Higgins, C.P., 2013. Nanofiltration and granular activated carbon treatment of perfluoroalkyl acids. *J. Hazard Mater.* 260, 740–746.
- Arkell, A., Krawczyk, H., Thuvander, J., Jönsson, A.S., 2013. Evaluation of membrane performance and cost estimates during recovery of sodium hydroxide in a hemicellulose extraction process by nanofiltration. *Separ. Purif. Technol.* 118, 387–393. <https://doi.org/10.1016/j.seppur.2013.07.015>.
- Arvaniti, O.S., Stasinakis, A.S., 2015. Review on the occurrence, fate and removal of perfluorinated compounds during wastewater treatment. *Sci. Total Environ.* 524 (525), 81–92. <https://doi.org/10.1016/j.scitotenv.2015.04.023>.
- Asano, T., 1998. *Wastewater Reclamation and Reuse: Water Quality Management Library*. CRC Press, Florida.
- Bagastyo, A.Y., Batstone, D.J., Kristiana, I., Gernjak, W., Joll, C., Radjenovic, J., 2012. Electrochemical oxidation of reverse osmosis concentrate on boron-doped diamond anodes at circumneutral and acidic pH. *Water Res.* 46, 6104–6112. <https://doi.org/10.1016/j.watres.2012.08.038>.
- Biegler, L.T., 2010. *Nonlinear Programming: Concepts, Algorithms and Applications to Chemical Processes*. Society for Industrial and Applied Mathematics, Philadelphia.
- Biegler, L.T., Grossmann, I.E., Westerberg, A.W., 1997. *Systematic Methods of Chemical Process Design*. Prentice Hall PTR, New Jersey.
- Brendel, S., Fetter, E., Staude, C., Vierke, L., Biegel-Engler, A., 2018. Short-chain perfluoroalkyl acids: environmental concerns and a regulatory strategy under REACH. *Environ. Sci. Eur.* 30, 9. <https://doi.org/10.1186/s12302-018-0134-4>.
- Cañizares, P., Paz, R., Sáez, C., Rodrigo, M.A., 2009. Costs of the electrochemical oxidation of wastewaters: a comparison with ozonation and Fenton oxidation processes. *J. Environ. Manag.* 90, 410–420. <https://doi.org/10.1016/j.jenvman.2007.10.010>.
- Caus, A., Braeken, L., Boussu, K., Van der Bruggen, B., 2009. The use of integrated countercurrent nanofiltration cascades for advanced separations. *J. Chem. Technol. Biotechnol.* 84, 391–398. <https://doi.org/10.1002/jctb.2052>.
- Eurostat, 2018. Electricity price statistics [WWW Document]. URL https://ec.europa.eu/eurostat/statistics-explained/index.php/Electricity_price_statistics. accessed 10.29.18.
- Gomez-Ruiz, B., Dibán, N., Urtiaga, A., 2018. Comparison of microcrystalline and ultrananocrystalline boron doped diamond anodes: influence on perfluorooctanoic acid electrolysis. *Separ. Purif. Technol.* 208, 169–177. <https://doi.org/10.1016/j.seppur.2018.03.044>.
- Gomez-Ruiz, B., Gómez-Lavín, S., Dibán, N., Boiteux, V., Colin, A., Dauchy, X., Urtiaga, A., 2017. Efficient electrochemical degradation of poly- and perfluoroalkyl substances (PFASs) from the effluents of an industrial wastewater treatment plant. *Chem. Eng. J.* 322, 196–204. <https://doi.org/10.1016/j.cej.2017.04.040>.
- He, Y., Lin, H., Guo, Z., Zhang, W., Li, H., Huang, W., 2018. Recent developments and advances in boron-doped diamond electrodes for electrochemical oxidation of organic pollutants. *Separ. Purif. Technol.* 212, 802–821. <https://doi.org/10.1016/j.seppur.2018.11.056>.
- Kraft, A., 2007. Doped diamond: a compact review on a new, versatile electrode material. *Int. J. Electrochem. Sci.* 2, 335–338.
- Madsen, H.T., Søgaard, E.G., Muff, J., 2015. Reduction in energy consumption of electrochemical pesticide degradation through combination with membrane filtration. *Chem. Eng. J.* 276, 358–364. <https://doi.org/10.1016/j.cej.2015.04.098>.
- Martínez-Huitle, C.A.C.A., Rodrigo, M.A.M.A., Sirés, I., Scialdono, O., 2015. Single and coupled electrochemical processes and reactors for the abatement of organic water pollutants: a critical review. *Chem. Rev.* 115, 13362–13407. <https://doi.org/10.1021/acs.chemrev.5b00361>.
- Melin, T., Rautenbach, R., 2007. *Membranverfahren. Grundlagen der Modul- und Anlagenauslegung*. Springer, Berlin.
- Niu, J., Li, Y., Shang, E., Xu, Z., Liu, J., 2016. Electrochemical oxidation of perfluorinated compounds in water. *Chemosphere* 146, 526–538. <https://doi.org/10.1016/j.chemosphere.2015.11.115>.
- Pan, Z., Song, C., Li, L., Wang, H., Pan, Y., Wang, C., Li, J., Wang, T., Feng, X., 2019. Membrane technology coupled with electrochemical advanced oxidation processes for organic wastewater treatment: recent advances and future prospects. *Chem. Eng. J.* <https://doi.org/10.1016/j.cej.2019.01.188>.
- Panizza, M., Cerisola, G., 2009. Direct and mediated anodic oxidation of organic pollutants. *Chem. Rev.* 109, 6541–6569. <https://doi.org/10.1021/cr9001319>.
- Panizza, M., Michaud, P.A., Cerisola, G., Cominellis, C., 2001. Anodic oxidation of 2-naphthol at boron-doped diamond electrodes. *J. Electroanal. Chem.* 507, 206–214. [https://doi.org/10.1016/S0022-0728\(01\)00398-9](https://doi.org/10.1016/S0022-0728(01)00398-9).
- Pérez-González, A., Ibáñez, R., Gómez, P., Urtiaga, A.M., Ortiz, I., Irabien, J.A., 2015. Nanofiltration separation of polyvalent and monovalent anions in desalination brines. *J. Membr. Sci.* 473, 16–27. <https://doi.org/10.1016/j.memsci.2014.08.045>.
- Pérez, G., Fernández-Alba, A.R., Urtiaga, A.M., Ortiz, I., 2010. Electro-oxidation of reverse osmosis concentrates generated in tertiary water treatment. *Water Res.* 44, 2763–2772. <https://doi.org/10.1016/j.watres.2010.02.017>.
- Radjenovic, J., Sedlak, D.L., 2015. Challenges and opportunities for electrochemical processes as next-generation technologies for the treatment of contaminated water. *Environ. Sci. Technol.* 49, 11292–11302. <https://doi.org/10.1021/acs.est.5b02414>.
- Ross, I., McDonough, J., Miles, J., Storch, P., Thelakkat Kochunaryanan, P., Kalve, E., Hurst, J., Dasgupta, S., Burdick, S.J., 2018. A review of emerging technologies for remediation of PFASs. *Remediat. J.* 28, 101–126. <https://doi.org/10.1002/rem.21553>.
- Sabatino, S., Galia, A., Saracco, G., Scialdono, O., 2017. Development of an electrochemical process for the simultaneous treatment of wastewater and the conversion of carbon dioxide to higher value products. *ChemElectroChem* 4, 150–159. <https://doi.org/10.1002/celec.201600475>.
- Sáez, C., Cañizares, P., Llanos, J., Rodrigo, M.A., 2013. The treatment of actual industrial wastewaters using electrochemical techniques. *Electrocatalysis* 4, 252–258. <https://doi.org/10.1007/s12678-013-0136-3>.
- Schaefer, C.E., Andaya, C., Burant, A., Condee, C.W., Urtiaga, A., Strathmann, T.J., Higgins, C.P., 2017. Electrochemical treatment of perfluorooctanoic acid and perfluorooctane sulfonate: insights into mechanisms and application to groundwater treatment. *Chem. Eng. J.* 317, 424–432. <https://doi.org/10.1016/j.cej.2017.02.107>.
- Schaefer, C.E., Andaya, C., Urtiaga, A., McKenzie, E.R., Higgins, C.P., 2015. Electrochemical treatment of perfluorooctanoic acid (PFOA) and perfluorooctane sulfonic acid (PFOS) in groundwater impacted by aqueous film forming foams (AFFFs). *J. Hazard Mater.* 295, 170–175. <https://doi.org/10.1016/j.jhazmat.2015.04.024>.
- Sethi, S., Wiesner, M.R., 2000. Cost modelling and estimation of crossflow membrane filtration processes. *Environ. Eng. Sci.* 17, 61–79.
- Soriano, A., Gorri, D., Urtiaga, A., 2019a. Selection of high flux membrane for the effective removal of short-chain perfluorocarboxylic acids. *Ind. Eng. Chem. Res.* 58, 3329–3338. <https://doi.org/10.1021/acs.iecr.8b05506>.
- Soriano, A., Gorri, D., Urtiaga, A., 2019b. Membrane preconcentration as an efficient tool to reduce the energy consumption of perfluorohexanoic acid electrochemical treatment. *Separ. Purif. Technol.* 208, 160–168. <https://doi.org/10.1016/j.seppur.2018.03.050>.
- Soriano, A., Gorri, D., Urtiaga, A., 2017. Efficient treatment of perfluorohexanoic acid by nanofiltration followed by electrochemical degradation of the NF concentrate. *Water Res.* 112, 147–156. <https://doi.org/10.1016/j.watres.2017.01.043>.
- Steinle-Darling, E., Reinhard, M., 2008. Nanofiltration for trace organic contaminant removal: structure, solution, and membrane fouling effects on the rejection of perfluorochemicals. *Environ. Sci. Technol.* 42, 5292–5297.
- The Dow Chemical Company, 2013. *Water & process solutions*. In: FILMTEC™ Reverse Osmosis Membranes: Technical Manual.
- The European Commission, 2017. Commission regulation (EU) 2017/1000 of 13 June 2017: amending annex XVII to regulation (EC) No 1907/2006 of the European Parliament and of the Council concerning the registration, evaluation, authorisation and restriction of chemicals (REACH) as regard. *Off. J. Eur. Union L* 150, 14–18.
- The European Commission, 2010. Commission regulation (EU) No 757/2010 of 24 August 2010 amending regulation (EC) No 850/2004 of the European Parliament and of the Council on persistent organic pollutants as regards annexes I and III text with EEA relevance. *Off. J. Eur. Union L* 223, 29–36.
- Urtiaga, A., Fernández-González, C., Gómez-Lavín, S., Ortiz, I., 2015. Kinetics of the electrochemical mineralization of perfluorooctanoic acid on ultrananocrystalline boron doped conductive diamond electrodes. *Chemosphere* 129, 20–26. <https://doi.org/10.1016/j.chemosphere.2014.05.090>.
- Urtiaga, A., Soriano, A., Carrillo-Abad, J., 2018. BDD anodic treatment of 6:2 fluorotelomer sulfonate (6:2 FTSA). Evaluation of operating variables and by-product formation. *Chemosphere* 201, 571–577. <https://doi.org/10.1016/j.chemosphere.2018.03.027>.
- USEPA, 2016. Drinking water health advisories for PFOA and PFOS [WWW Document]. URL <https://www.epa.gov/ground-water-and-drinking-water/drinking-water-health-advisories-pfoa-and-pfos>. accessed 3.16.18.
- USEPA, 2006. Technology and cost document for the final ground water rule [WWW Document]. URL <https://nepis.epa.gov/Exe/ZyPDF.cgi/P1002Y6I.PDF?DockKey=P1002Y6I.PDF>. accessed 5.6.19.
- Valsecchi, S., Conti, D., Crebelli, R., Polesello, S., Rusconi, M., Mazzoni, M., Preziosi, E., Carere, M., Lucentini, L., Ferretti, E., Balzamo, S., Simeone, M.G., Aste, F., 2017. Deriving environmental quality standards for perfluorooctanoic acid (PFOA) and related short chain perfluorinated alkyl acids. *J. Hazard Mater.* 323, 84–98. <https://doi.org/10.1016/j.jhazmat.2016.04.055>.
- Vince, F., Marechal, F., Aoustin, E., Bréant, P., 2008. Multi-objective optimization of RO desalination plants. *Desalination* 222, 96–118. <https://doi.org/10.1016/j.desal.2007.02.064>.
- Wang, Z., Cousins, I.T., Scheringer, M., Hungerbühler, K., 2013. Fluorinated alternatives to long-chain perfluoroalkyl carboxylic acids (PFCA), perfluoroalkane sulfonic acids (PFSA) and their potential precursors. *Environ. Int.* 60, 242–248. <https://doi.org/10.1016/j.envint.2013.08.021>.
- Zarca, G., Urtiaga, A., Biegler, L.T., Ortiz, I., 2018. An optimization model for assessment of membrane-based post-combustion gas upcycling into hydrogen or syngas. *J. Membr. Sci.* 563, 83–92. <https://doi.org/10.1016/j.memsci.2018.05.038>.
- Zhang, S., Lu, X., Wang, N., Buck, R.C., 2016. Biotransformation potential of 6:2 fluorotelomer sulfonate (6:2 FTSA) in aerobic and anaerobic sediment. *Chemosphere* 154, 224–230. <https://doi.org/10.1016/j.chemosphere.2016.03.062>.
- Zhuo, Q., Deng, S., Yang, B., Huang, J., Wang, B., Zhang, T., Yu, G., 2012. Degradation of perfluorinated compounds on a boron-doped diamond electrode. *Electrochim. Acta* 77, 17–22. <https://doi.org/10.1016/j.electacta.2012.04.145>.

Appendices

A1. Contributions to scientific meetings

1. Eliminación de ácido perfluorohexanoico (PFHxA) mediante un proceso integrado de nanofiltración y oxidación electroquímica con electrodos BDD, A. Soriano, D. Gorri, A. Urtiaga. XXXVII Reunión del Grupo de Electroquímica de la Real Sociedad Española de Química. Alicante (Spain), 17-20 July 2016. *Oral presentation*.
2. Removal of Perfluorohexanoic Acid (PFHxA) from Industrial Effluents by Nanofiltration Followed by Electrochemical Oxidation of the NF Concentrate, A. Soriano, D. Gorri, A. Urtiaga. 2° E3 Mediterranean Symposium: Electrochemistry for Environment and Energy. Gargnano, Brescia (Italy), 14-16 September 2016. *Oral presentation*.
3. Integration of electrochemical oxidation and nanofiltration for a more efficient treatment of perfluorohexanoic acid. A. Soriano, D. Gorri, A. Urtiaga. 11th European Symposium on Electrochemical Engineering, Prague (Czech Republic), 4-8 June 2017. *Oral presentation*.
4. Electrochemical technology for the abatement of Poly- and Perfluoroalkyl substances (PFASs) water pollution. A. Urtiaga, S. Gómez-Lavín, B. Gómez-Ruiz, A. Soriano, J. Carrillo-Abad, N. Diban. V Reunión Nacional de Dioxinas, Furanos y Compuestos Orgánicos Persistentes Relacionados. Barcelona (Spain), 12-16 June 2017. *Oral presentation*.
5. Design of a hybrid nanofiltration/electrooxidation process for the removal of perfluorohexanoic acid (PFHxA). A. Soriano, D. Gorri, A. Urtiaga. 27th European Symposium on Computer-Aided Process Engineering. Barcelona (Spain), 1-5 October 2017. *Poster presentation*.

6. Energy optimization of the electrochemical degradation of perfluorohexanoic acid by its integration with NF/RO membrane technology. A. Soriano, D. Gorri, A. Urriaga 10th World Congress of Chemical Engineering. Barcelona (España), 1-5 October 2017. *Oral presentation.*
7. Membrane selection for the removal of water priority pollutants. NF/RO separation of perfluorinated compounds. A. Soriano, D. Gorri, A. Urriaga. Euromembrane 2018. Valencia (Spain), 9 – 13 July 2018. *Oral presentation.*
8. Towards and efficient electrolysis of perfluorocarboxylic acids through integration with membrane separation using process system engineering tools. A. Soriano, D. Gorri, L.T. Biegler, A. Urriaga. 3rd Workshop of the Excellence Network on Environmental and Energy Applications of the Electrochemical Technology - Sustainable electrochemical technology. Toledo (Spain), 14 – 15 May 2019. *Oral presentation.*
9. BDD Anodic Oxidation of 6:2 Fluorotelomer Sulfonate and Short-chain Perfluorocarboxylic Acids Products. A. Soriano, J. Carrillo - Abad, A. Urriaga. 25th Topical Meeting of the International Society of Electrochemistry. Toledo (Spain), 10 – 15 May 2019. *Oral presentation.*
10. Minimization of electrooxidation total costs through its integration with membrane pre-concentration. Perfluorohexanoic acid removal as a case study. A. Soriano, D. Gorri, L.T. Biegler, A. Urriaga. ANQUE-ICCE-CIBIQ 2019. Santander (Spain), 19 – 21 June 2019. *Oral presentation.*

11. Optimization approach to the integration of electrochemical advanced oxidation and nanofiltration for treatment of fluorinated micropollutants in water. A. Soriano, D. Gorri, L.T. Biegler, A. Urtiaga. 6th European Conference on Environmental Applications of Advanced Oxidation Processes. Portoroz – Portorose (Slovenia), 26 – 30 June 2019. *Oral presentation*.

12. Nanofiltration removal of perfluorohexanoic acid: the role of salts concentration and pH. A. Soriano, D. Gorri, A. Urtiaga. 12th European Congress of Chemical Engineering. Florence (Italy), 15 – 19 September 2019. *Poster presentation*.

A2. GAMS codes for the optimization of the integrated process

A.2.1. Single-stage membrane pre-concentration / electrooxidation

```

$title: Optimization of a single batch membrane module coupled with ELOX

$OFFUPPER
$OFFSYMREF OFFSYMLIST

*-----
*This file implements the optimization of a single NF/RO stage + ELOX for the
*treatment of short-chain PFCASs in a saline water matrix. Model
*discretization allows to be solved as an NLP.

*More detail on the model can be found in:

*A. Soriano, D. Gorri, L.T. Biegler and A. Urtiaga,
*"An optimization model for the treatment of perfluorocarboxylic acids
*considering membrane preconcentration and BDD electrooxidation"
*Water Research, 164, 114959
*https://doi.org/10.1016/j.watres.2019.114954
*-----

*nfe number of finite elements
*ncp number of collocation points

$set nfe 50
$set ncp 3

Sets      i          number of finite elements          /1*nfe%/
            j          number of internal collocation points /1*ncp%/
            comp        compounds                          /PFH,SF,NA/      ;

Alias (j,k);

Scalar

*Process 1 (NF/RO) parameters

qfeed      feed flow rate to module          [m3 h-1]          /3.6/
dpress     effective pressure at membrane module [bar]            /10/
*empirical permeability for each membrane
perm       membrane permeability            [l m-2 h-1 bar-1] /6.98/
temp       solution temperature              [°C]              /20/
ctarget    target concentration              [mg L-1]          /1/
vfini      initial feed tank volume          [m3]              /10/
vpini      initial permeate tank volume      [m3]              /1e-4/
eta        pump efficiency                   [-]               /0.8/
*empirical alfa coefficient specific for each membrane
alfa       Cp-Cf correlation coef.           [-]               /0.0066/
pot_pump_feed feed pump power                [kWh]

*Process 2 (ELOX) parameters

pot        power                             [kW]
kapp       PFHxA kinetic constant            [m min-1]         /0.0021/
japp       current density                   [m2]              /50/

*Economic evaluation

r          interest rate                     [1e2*%]           /0.1/
T          plant lifetime                     [y]               /15/
MR         membrane replacement factor       [$ y-1 module-1]
MMP        membrane system price            [$ m2]            /500/
ML         membrane module life              [y]               /8/

```

```

ER      electrode replacement factor      [$ m-2 y-1]
ElP    electrode price                    [$ m-2]           /9000/
EL      electrode life                    [y]             /6/
EP      electricity price                 [$ kWh]         /0.16/
OF      operation factor                  [h y-1]        /8000/;

```

```
pot_pump_feed=(qfeed*(dpress-1.013))/36*eta;
```

```
MR=MMP/ML;
```

```
ER=ElP/EL;
```

```

Parameter MW(comp) value [g mol-1]           /PFH 314.05
                                                SF 96.05
                                                NA 22.99/;

```

```

Parameter cfinit(comp) value [mg L-1]       /PFH 100
                                                SF 338.15
                                                NA 161.85/;

```

```

Parameter cpinit(comp) value [mg L-1]       /PFH 0
                                                SF 0
                                                NA 0/;

```

```

Table 1(j,j) Lagrange basis collocation matrix
      1      2      3
1 1      0      0
2 0      1      0
3 0      0      1;

```

```

Table ldot(j,j) Lagrange basis first derivs collocation matrix
      1      2      3
1 -5.999997202501304 -3.464098384864128 3.464098384864127
2 6.464099408820847 2.999996178544585 -6.464099408820847
3 -0.464102206319543 0.464102206319543 3.000001023956719;

```

```

Parameter lfinal(j) value /1 1
                                                2 -1.732051615138131
                                                3 1.732051615138131/;

```

```

Parameter
cffinal(comp,i)
cpfinal(comp,i)
vffinal(i)
vpfinal(i)

```

positive variables

**Process 1 (NF/RO)*

```

area      membrane stage area
earea     electrode area
tf        final membrane time
dt        time step
mol(comp,i,j) molality
osm(i,j)  osmotic pressure in the feed side of membrane
qp(i,j)   permeate flowrate
qr(i,j)   retentate flowrate
cps(comp,i,j) permeate stream concentration
cr(comp,i,j) retentate concentration
cf(comp,i,j) feed tank species concentration
cp(comp,i,j) permeate species tank concentration
vf(i,j)   feed tank volume
vp(i,j)   permeate tank volume

```

**Process 2 (ELOX)*

```

pot_elox  Elox power
ceq       equivalent saline concentration
volt      voltage in the ELOX cells
VRF       volume reduction factor

```

```

celox                elox exit concentration
telox                electrooxidation time
*Economic evaluation
NPVcost              net present value cost
CAPEX                capital expenses
OPEX                 operating expenses
CCm                  membrane capex
CCelox               elox capex
CCp                  pumps capex
labman               labour and maintenance cost
clean                cleaning cost
mrep                 membrane replacement cost
erep                 electrode replacement cost
energy               energy cost
EPC                  preconcentration energy consumption
EELOX                electrooxidation energy consumption
;

```

variables

```

phi                  objective function (Energy [kWh])
cfdot (comp,i,j)    cf first order derivative
cpdot (comp,i,j)    cp first order derivative
vfdot (i,j)          vf first order derivative
vpdot (i,j)          vp first order derivative;

```

Equations

```

*Objective function
fobj                 criterion definition
*Process 1 (NF/RO)
annvol
Eq_dt
molality (comp,i,j)
osmoti (i,j)
perflowrate (i,j)
retflowrate (i,j)
cpcorrPF (i,j)
cpcorrSF (i,j)
cpcorrNA (i,j)
membmassbal (comp,i,j)
FECOLcf (comp,i,j)
FECOLcp (comp,i,j)
FECOLvf (i,j)
FECOLvp (i,j)
CONcf (comp,i)
CONcp (comp,i)
CONvf (i)
CONvp (i)
ODEcf (comp,i,j)
ODEcp (comp,i,j)
ODEvf (i,j)
ODEvp (i,j)
*Process 2 (ELOX)
equivc
voltage
eloxpower
vrfdef
celoxcal
teloxcal
eloxenergy
*Economic evaluation
capcosts
cmembrane
cceloxplant
ccpumps
opcconst
labmancost
cleancost

```

```

mrepcost
erepcost
energycost
PCenergy
ELOXenergy
;

*-----
*OBJECTIVE FUNCTION
*-----
fobj..
phi =e= CAPEX*((r*(1+r)**T))/(((1+r)**T)-1))+ OPEX;

*-----
*PROCESS 1 (NF/RO) EQUATIONS
*-----

annvol..                vfinit*(OF/(telox+tf)) =e= 2000;

Eq_dt..                dt =E= tf/card(i);

molality(comp,i,j)..   mol(comp,i,j) =e= cf(comp,i,j)/(MW(comp)*1e3);

osmoticp(i,j)..        osm(i,j) =e=
(1.19*(temp+273)*sum(comp,mol(comp,i,j)))*0.068948;

permflowrate(i,j)..   qp(i,j) =e= perm*area*1e-3*(dpress-osm(i,j));

retflowrate(i,j)..    qr(i,j) =e= qfeed-qp(i,j);

cpcorrPF(i,j)..       cps('PFH',i,j) =e= alfa*cf('PFH',i,j);

cpcorrSF(i,j)..       cps('SF',i,j) =e= 0.0129*cf('SF',i,j);

cpcorrNA(i,j)..       cps('NA',i,j) =e= 0.0152*cf('NA',i,j);

membmassbal(comp,i,j).. cr(comp,i,j)*qr(i,j) =e= qfeed*cf(comp,i,j)-
qp(i,j)*cps(comp,i,j);

*Lagrange basis collocation equations
FECOLcf(comp,i,j)$ord(j) gt 1).. dt*cfdot(comp,i,j) =e=
sum(k,ldot(k,j)*cf(comp,i,k)) ;

FECOLcp(comp,i,j)$ord(j) gt 1).. dt*cpdot(comp,i,j) =e=
sum(k,ldot(k,j)*cp(comp,i,k)) ;

FECOLvf(i,j)$ord(j) gt 1).. dt*vfdot(i,j) =e= sum(k,ldot(k,j)*vf(i,k)) ;

FECOLvp(i,j)$ord(j) gt 1).. dt*vpdot(i,j) =e= sum(k,ldot(k,j)*vp(i,k)) ;

*Continuity Equations
CONcfc(comp,i)$ord(i) gt 1)..
cf(comp,i,'1') =e= sum(j, cf(comp,i-1,j)*lfinal(j));

CONcpc(comp,i)$ord(i) gt 1)..
cp(comp,i,'1') =e= sum(j, cp(comp,i-1,j)*lfinal(j));

CONvfi(i)$ord(i) gt 1)..
vf(i,'1') =e= sum(j, vf(i-1,j)*lfinal(j));

CONvpi(i)$ord(i) gt 1)..
vp(i,'1') =e= sum(j, vp(i-1,j)*lfinal(j));

*Differential Equations
ODEcfc(comp,i,j)$ord(j) gt 1)..
cfdot(comp,i,j) =e= ((qr(i,j)*(cr(comp,i,j)-cf(comp,i,j))))/vf(i,j);

```

```

ODEcp(comp,i,j)$ord(j) gt 1)..
cpdot(comp,i,j) =e= ((qp(i,j)*(cps(comp,i,j)-cp(comp,i,j)))/vp(i,j);

ODEvf(i,j)$ord(j) gt 1)..
vfdot(i,j) =e= qr(i,j)-qfeed;

ODEvp(i,j)$ord(j) gt 1)..
vpdot(i,j) =e= qp(i,j);

*-----
*PROCESS 2 (ELOX) EQUATIONS
*-----

equivc(i,j)$ord(i) eq %nfe% and ord(j) eq %ncp%)..
ceq =e= 0.5*(2*mol('SF',i,j)+1*mol('NA',i,j));

voltage..
volt =e= 11.649*(ceq-5.65e-3)**(-4.84e-2);

vrfdef(i,j)$ord(i) eq %nfe% and ord(j) eq %ncp%)..
VRF*vf(i,j) =e= vfinit;

celoxcal(i,j)$ord(i) eq %nfe% and ord(j) eq %ncp%)..
celox =e= VRF*(ctarget-cp('PFH',i,j)*(1-(1/(VRF))));

teloxcal(i,j)$ord(i) eq %nfe% and ord(j) eq %ncp%)..
telox =e= (log(celox/cf('PFH',i,j))*vfinit)/(-kapp*earea*VRF*60);

*-----
*ECONOMIC EVALUATION
*-----

*Capital costs
capcosts..
CAPEX =e= Ccm + CCelox + CCp;

cmembrane..
Ccm =e= MMP*area+
vp('%nfe%', '%ncp%')*(264.162/1e6)*(24/(telox+tf))*1100*51.1;

cceloxplant..
CCelox =e= 19216*(earea**0.7857)+9000*earea+0.28*(japp*earea*20);

ccpumps..
CCp =e= (567.5/269.9)*1.4*81.27*(qfeed*(1/3600)*(dpress-1.013)*(1e5))**0.39;

*Operating costs

opcosts..
OPEX =e= labman + clean + mrep + erep + energy;

labmancost..
labman =e= 0.02*CAPEX;

cleancost..
clean =e= 50*earea +
(0.01/1000)*(1/0.0038)*vp('%nfe%', '%ncp%')*(OF/(telox+tf));

mrepcost..
mrep =e= MR;

erepcost..
erep =e= earea*ER;

energycost..
energy =e= EP*(EPC+EELOX)*(OF/(telox+tf));

```

```

eloxpower..
pot_elox=e*volt*japp*earea*1e-3;

PCenergy..
EPC=e*pot_pump_feed*tf;

ELOXenergy..
EELOX=e*pot_elox*telox;

Model membelox /all/;

*-----
*VARIABLE LIMITS AND INITIAL GUESSES
*-----
cf.lo(comp,i,j) = cfinit(comp);
cp.lo(comp,i,j) = cpinit(comp);
vf.lo(i,j) = 0;
vf.up(i,j)=vfinit;
vp.lo(i,j) = vpinit;
VRF.lo=1;
VRF.up=10;
*tf.lo=0;
*tf.up=7.5;
celox.lo=1e-9;
*cf.lo('PFH',i,j)=1e-9;

earea.l=18;
tf.l=1;
*tf.up=60;

area.lo=2.6;
area.up=37;

*dt.l=tf.l/card(i);
cf.l(comp,i,j)= cfinit(comp);
cp.l(comp,i,j) = cpinit(comp);
vf.l(i,j) = vfinit;
vp.l(i,j) = vpinit;
mol.l(comp,i,j)=cf.l(comp,i,j)/(MW(comp)*1e3);

loop((i,j)$(ord(i) eq %nfe% and ord(j) eq %ncp%),
      ceq.l=(0.5*(2*mol.l('SF',i,j)+1*mol.l('NA',i,j)));
) ;

loop((i,j)$(ord(i) eq %nfe% and ord(j) eq %ncp%),
      VRF.l=vfinit/vf.l(i,j);
) ;

loop((i,j)$(ord(i) eq %nfe% and ord(j) eq %ncp%),
      celox.l=(VRF.l*(ctarget-cp.l('PFH',i,j))-(ctarget-cp.l('PFH',i,j)));
) ;

*-----
*INITIAL CONDITIONS
*-----
cf.FX(comp,'1','1')=cfinit(comp);
cp.FX(comp,'1','1')=cpinit(comp);
vf.FX('1','1')=vfinit;
vp.FX('1','1')=vpinit;

Option nlp=ipopath;

Solve membelox minimizing phi using nlp;

execute_unload "results.gdx"

```

A.2.2. Multistage membrane pre-concentration / electrooxidation

```

$title: Optimization of a multistage membrane preconc coupled with ELOX

$OFFUPPER
$OFFSYMREF OFFSYMLIST

*-----
*This file implements the optimization of a multistage NF/RO pre-
*concentration + ELOX for the treatment of short-chain PFCASs in a saline
*water matrix. Model discretization allows to be solved as an NLP.

*More detail on the model can be found in:

*Á. Soriano, D. Gorri, L.T. Biegler and A. Urriaga,
*"An optimization model for the treatment of perfluorocarboxylic acids
*considering membrane preconcentration and BDD electrooxidation"
*Water Research, 164, 114959
*https://doi.org/10.1016/j.watres.2019.114954
*-----

$set nfe 50
$set ncp 3

*nms set number of membrane stages

$set nms 3

Sets      i      number of finite elements           /1*%nfe%/
            j      number of internal collocation points /1*%ncp%/
            comp    compounds                /PFH,SF,NA/
            n      number of membrane stages           /1*%nms%/      ;

Alias (j,k);

Scalar

*Process 1 (NF/RO) parameters

qfeed      feed flow rate from feed tank           [m3 h-1]           /3.2/
dpres      effective pressure at membrane module [bar]              /10/
*empirical permeability for each membrane
perm       membrane permeability                 [1 m-2 h-1 bar-1] /6.98/
temp       solution temperature                   [°C]               /20/
ctarget    target concentration                   [mg L-1]           /0.1/
vpinit     initial permeate tank volume           [m3]               /1e-4/
vfinit     initial feed tank volume               [m3]               /10/
eta        pump efficiency                         [-]                /0.8/
*empirical alfa coefficient specific for each membrane
alfa       Cp-Cf correlation coef.                [-]                /0.0066/
pot_pump_feed feed pump power                     [kWh]

*Process 2 (ELOX) parameters

pot        power                                   [kW]
kapp       PFHxA kinetic constant                 [m min-1]          /0.0021/
japp       current density                         [m2]               /50/

*Economic evaluation

r          interest rate                           [1e2*%]            /0.1/
T          plant lifetime                           [y]                /15/
UF         update factor (CEPCI 2017)              [-]                /4.93/
MR         membrane replacement factor             [$ y-1 module-1]
MMP        membrane system price                  [$ m2]              /500/

```

```

ML      membrane module life           [y]           /8/
ER      electrode replacement factor    [$ m-2 y-1]
ElP     electrode price                 [$ m-2]       /9000/
EL      electrode life                  [y]           /6/
EP      electricity price               [$ kWh]       /0.16/
pdrop   pressure drop in membrane module [bar]         /0.5/
OF      operation factor                [h y-1]      /8000/;

```

```
pot_pump_feed=(qfeed*(dpress-1.013))/36*eta;
```

```
MR=MMP/ML;
```

```
ER=ElP/EL;
```

```

Parameter MW(comp) value [g mol-1]           /PFH 314.05
                                                SF 96.05
                                                NA 22.99/;

```

```

Parameter cfini(comp) value [mg L-1]         /PFH 100
                                                SF 338.15
                                                NA 161.85/;

```

```

Parameter cpini(comp) value [mg L-1]         /PFH 0
                                                SF 0
                                                NA 0/;

```

```

Table 1(j,j) Lagrange basis collocation matrix
      1      2      3
1 1 0 0
2 0 1 0
3 0 0 1;

```

```

Table ldot(j,j) Lagrange basis first derivs collocation matrix
      1      2      3
1 -5.999997202501304 -3.464098384864128 3.464098384864127
2 6.464099408820847 2.999996178544585 -6.464099408820847
3 -0.464102206319543 0.464102206319543 3.000001023956719;

```

```

Parameter lfinal(j) value /1 1
                          2 -1.732051615138131
                          3 1.732051615138131/;

```

```

Parameter
cfinal(comp,i)
cpfinal(comp,i)
vfinal(i)
vpfinal(i)

```

positive variables

```
*Process 1
```

```

area(n)      membrane stage n area [m2]
earea       electrode area [m2]
tf          final membrane time [h]
dt          time step [h]
pot_pump(i,j)
mol(comp,i,j)      molality feed tank solution
moln(n,comp,i,j)  molality stage n feed stream
osm(n,i,j)         osmotic pressure in the feed side of membrane
qf(n,i,j)         feed flow rate to stage n
qp(n,i,j)         permeate flowrate
qp_stn(n,i,j)    permeate flowrate last stage
qr(n,i,j)         retentate flowrate from stage n
cfs(n,comp,i,j)  feed stream to stage n concentration
cps(n,comp,i,j)  permeate stream concentration
cr(n,comp,i,j)   retentate concentration

```

```

cf(comp,i,j)          feed tank species concentration
cp(comp,i,j)         permeate species tank concentration
vf(i,j)              feed tank volume
vp(i,j)              permeate tank volume

```

**Process 2*

```

pot_elox             Elox power
ceq                  equivalent saline concentration
volt                 voltage in the ELOX cells
VRF                  volume reduction factor
celox                elox exit concentration
telox                electrooxidation time

```

**Economic evaluation*

```

CAPEX
OPEX
CCm
CCelox
CCp
CCt
labman
clean
mrep
erep
pot_pump_perm(i,j)
energy
EPC
EELOX
;

```

variables

```

phi                  objective function (Energy [kWh])
cfdot(comp,i,j)    cf first order derivative
cpdot(comp,i,j)    cp first order derivative
vfdot(i,j)         vf first order derivative
vpdot(i,j)         vp first order derivative;

```

Equations

fobj criterion definition

**Process 1*

```

annvol
Eq_dt
pumppower(i,j)
molality(comp,i,j)
mixerl(n,i,j)
mixerk(n,i,j)
mixern(n,i,j)
mixerl_mass(n,comp,i,j)
mixerk_mass(n,comp,i,j)
mixern_mass(n,comp,i,j)
molalityn(n,comp,i,j)
osmoticp(n,i,j)
permflowrate(n,i,j)
permflowrestric(n,i,j)
retflowrate(n,i,j)
cpcorrPF(n,i,j)
cpcorrSF(n,i,j)
cpcorrNA(n,i,j)
membmassbal(n,comp,i,j)
FECOLcf(comp,i,j)
FECOLcp(comp,i,j)
FECOLvf(i,j)
FECOLvp(i,j)
CONcf(comp,i)
CONcp(comp,i)

```

```

CONvf (i)
CONvp (i)
ODEcf (comp, i, j)
ODEcp (comp, i, j)
ODEvf (i, j)
ODEvp (i, j)
*Process 2
equivc
voltage
eloxpower
vrfdef
celoxcal
teloxcal
*Economic evaluation
capcosts
ccmembrane
cceloxplant
ccpumps
opcosts
labmancost
cleancost
mrepcost
erepcost
energycost
permpumpwork (i, j)
PCenergy
ELOXenergy
;

*-----
*OBJECTIVE FUNCTION
*-----
fobj..
phi =e= CAPEX*(((r*(1+r)**T))/(((1+r)**T)-1)) + OPEX;

*-----
*PROCESS 1 (NF/RO) EQUATIONS
*-----

pumppower (i, j) ..
pot_pump (i, j) =e= sum (n, (qp (n, i, j) * (dpress-1.013)) / 36 * eta)
- (qp ('%nms%', i, j) * (dpress-1.013)) / 36 * eta;

*Feed tank solution molality

molality (comp, i, j) ..
mol (comp, i, j) =e= cf (comp, i, j) / (MW (comp) * 1e3);

*MIXERS

*Stage 1 Mixer

mixer1 (n, i, j) $(ord (n) eq 1) ..
qfeed + qr (n+1, i, j) =e= qf (n, i, j);

mixer1_mass (n, comp, i, j) $(ord (n) eq 1) ..
qfeed * cf (comp, i, j) + qr (n+1, i, j) * cr (n+1, comp, i, j) =e= qf (n, i, j) * cfs (n, comp, i, j);

*Stage 2-(n-1)

mixerk (n, i, j) $(ord (n) > 1 and ord (n) < %nms%) ..
qp (n-1, i, j) + qr (n+1, i, j) =e= qf (n, i, j);

mixerk_mass (n, comp, i, j) $(ord (n) > 1 and ord (n) < %nms%) ..
qp (n-1, i, j) * cps (n-1, comp, i, j) + qr (n+1, i, j) * cr (n+1, comp, i, j) =e= qf (n, i, j) * cfs (n, comp, i, j);

```

```

*Stage n

mixern(n,i,j)$ (ord(n) eq %nms%) ..
qp(n-1,i,j)=e= qf(n,i,j);

mixern_mass(n,comp,i,j)$ (ord(n) eq %nms%) ..
qp(n-1,i,j)*cps(n-1,comp,i,j)=e= qf(n,i,j)*cfs(n,comp,i,j);

*MEMBRANE MODULES EQUATIONS

molalityn(n,comp,i,j) ..
moln(n,comp,i,j) =e= cfs(n,comp,i,j)/(MW(comp)*1e3);

osmoticip(n,i,j) ..
osm(n,i,j) =e= (1.19*(temp+273)*sum(comp,moln(n,comp,i,j)))*0.068948;

permflowrate(n,i,j) ..
qp(n,i,j) =e= perm*area(n)*1e-3*(dpress-osm(n,i,j));

permflowrestric(n,i,j)$ (ord(n) gt 1) ..
qp(n,i,j) =l= qf(n,i,j);

retflowrate(n,i,j) ..
qr(n,i,j) =e= qf(n,i,j)-qp(n,i,j);

cpcorrPF(n,i,j) ..
cps(n,'PFH',i,j) =e= alfa*cfs(n,'PFH',i,j);

cpcorrSF(n,i,j) ..
cps(n,'SF',i,j) =e= 0.0129*cfs(n,'SF',i,j);

cpcorrNA(n,i,j) ..
cps(n,'NA',i,j) =e= 0.0152*cfs(n,'NA',i,j);

membmassbal(n,comp,i,j) ..
cr(n,comp,i,j)*qr(n,i,j) =e= qf(n,i,j)*cfs(n,comp,i,j)-
qp(n,i,j)*cps(n,comp,i,j);

*Lagrange basis collocation equations
FECOLcf(comp,i,j)$ (ord(j) gt 1) ..
dt*cfdot(comp,i,j) =e= sum(k,ldot(k,j)*cf(comp,i,k) );

FECOLcp(comp,i,j)$ (ord(j) gt 1) ..
dt*cpdot(comp,i,j) =e= sum(k,ldot(k,j)*cp(comp,i,k) );

FECOLvf(i,j)$ (ord(j) gt 1) ..
dt*vfdot(i,j) =e= sum(k,ldot(k,j)*vf(i,k) );

FECOLvp(i,j)$ (ord(j) gt 1) ..
dt*vpdot(i,j) =e= sum(k,ldot(k,j)*vp(i,k) );

*Continuity Equations
CONcf(comp,i)$ (ord(i) gt 1) ..
cf(comp,i,'1') =e= sum(j, cf(comp,i-1,j)*lfinal(j));

CONcp(comp,i)$ (ord(i) gt 1) ..
cp(comp,i,'1') =e= sum(j, cp(comp,i-1,j)*lfinal(j));

CONvf(i)$ (ord(i) gt 1) ..
vf(i,'1') =e= sum(j, vf(i-1,j)*lfinal(j));

CONvp(i)$ (ord(i) gt 1) ..
vp(i,'1') =e= sum(j, vp(i-1,j)*lfinal(j));

*Differential Equations
ODEcf(comp,i,j)$ (ord(j) gt 1) ..
cfdot(comp,i,j) =e= ((qr('1',i,j)*(cr('1',comp,i,j)-cf(comp,i,j)))/vf(i,j);

```

```

ODEcp(comp,i,j)$(ord(j) gt 1)..
cpdot(comp,i,j) =e= ((qp('%nms%',i,j)*(cps('%nms%',comp,i,j)-
cp(comp,i,j)))/vp(i,j);

ODEvf(i,j)$(ord(j) gt 1)..
vfdot(i,j) =e= qr('1',i,j)-qfeed;

ODEvp(i,j)$(ord(j) gt 1)..
vpdot(i,j) =e= qp('%nms%',i,j);

*-----
*PROCESS 2 (ELOX) EQUATIONS
*-----

equivc(i,j)$(ord(i) eq %nfe% and ord(j) eq %ncp%)..
ceq =e= 0.5*(2*mol('SF',i,j)+1*mol('NA',i,j));

voltage..
volt =e= 11.649*(ceq-5.65e-3)**(-4.84e-2);

eloxpower..
pot_elox=e=volt*japp*earea*1e-3;

vrfdef(i,j)$(ord(i) eq %nfe% and ord(j) eq %ncp%)..
VRF*vf(i,j) =e= vfinit;

celoxcal(i,j)$(ord(i) eq %nfe% and ord(j) eq %ncp%)..
celox =e= VRF*(ctarget-cp('PFH',i,j)*(1-(1/(VRF))));

teloxcal(i,j)$(ord(i) eq %nfe% and ord(j) eq %ncp%)..
(-kapp*telox*earea*VRF*60)/vfinit =e= log(celox)-log(cf('PFH',i,j));

*-----
*ECONOMIC EVALUATION
*-----

*CAPITAL COSTS

capcosts..
CAPEX =e= CCm + CCelox + CCp;

ccmembrane..
CCm =e= MMP*sum(n,area(n))+
vp('%nfe%', '%ncp%')*(264.162/1e6)*(24/(telox+tf))*1100*51.1;

cceloxplant..
CCelox =e= 19216*(earea**0.7857)+9000*earea+0.25*(japp*earea*20);

ccpumps..
CCp =e= (567.5/269.9)*1.4*81.27*(qfeed*(1/3600)*(dpress-1.013)*(1e5))**0.39
+('%nms%-1)*(567.5/269.9)*1.4*81.27*(0.5*(1/3600)*(dpress-1.013)*(1e5))**0.39;

*OPERATING COSTS

opcosts..
OPEX =e= labman + clean + mrep + erep + energy;

labmancost..
labman =e= 0.02*CAPEX;

cleancost..
clean =e= 50*earea +
(0.01/1000)*(1/0.0038)*vp('%nfe%', '%ncp%')*(OF/(telox+tf));

mrepcost..
mrep =e= MR*sum(n,area(n));

```

```

erepcost..
erep =e= earea*ER;

energycost..
energy =e= EP*(EPC+EELOX)*(OF/(telox+tf));

permpumpwork(i,j)..
pot_pump_perm(i,j)=e=sum(n,(qp(n,i,j)*(dpress-1.013))/36*eta
-(qp('%nms%',i,j)*(dpress-1.013))/36*eta);

PCenergy..
EPC=e=pot_pump_feed*tf+sum((i,j),pot_pump_perm(i,j)*(dt/%ncp%));

ELOXenergy..
EELOX=e=pot_elox*telox;

*-----
*ADDITIONAL EQUATIONS
*-----

annvol..
vfinit*(OF/(telox+tf)) =e= 2000;

Eq_dt..
dt =E= tf/card(i);

Model membelox /all/;

*-----
*VARIABLE LIMITS AND INITIAL GUESSES
*-----

cf.lo(comp,i,j) = cfinit(comp);
cp.lo(comp,i,j) = cpinit(comp);
vf.lo(i,j) = 0;
vf.up(i,j)=vfinit;
vp.lo(i,j) = vpinit;
celox.lo=1e-9;

VRF.lo=1;
VRF.up=10;

area.lo(n)=2.6;
area.up(n)=37;

earea.l=1;
tf.l=10;
tf.up=40;

cf.l(comp,i,j)= cfinit(comp);
cp.l(comp,i,j) = cpinit(comp);
vf.l(i,j) = vfinit;
vp.l(i,j) = vpinit;
mol.l(comp,i,j)=cf.l(comp,i,j)/(MW(comp)*1e3);

loop((i,j)$ (ord(i) eq %nfe% and ord(j) eq %ncp%),
      ceq.l=(0.5*(2*mol.l('SF',i,j)+1*mol.l('NA',i,j)));
) ;

loop((i,j)$ (ord(i) eq %nfe% and ord(j) eq %ncp%),
      VRF.l=vfinit/vf.l(i,j);
) ;

loop((i,j)$ (ord(i) eq %nfe% and ord(j) eq %ncp%),
      celox.l=(VRF.l*(ctarget-cp.l('PFH',i,j)))-(ctarget-cp.l('PFH',i,j)));
) ;

```

```
*-----  
*INITIAL CONDITIONS  
*-----  
cf.FX(comp,'1','1')=cfinit(comp);  
cp.FX(comp,'1','1')=cpinit(comp);  
vf.FX('1','1')=vfinit;  
vp.FX('1','1')=vpinit;  
  
Option nlp=ipopth;  
  
Solve membelox minimizing phi using nlp;  
  
execute_unload "resultados.gdx"
```


NOTES

NOTES

NOTES

NOTES